

UNIVERSITY OF TRENTO - Italy
Department of Civil, Environmental
and Mechanical Engineering



Doctoral School in Civil, Environmental and Mechanical Engineering
Topic 1. Civil and Environmental Engineering - XXXII cycle 2017/2019

Doctoral Thesis - January 2020

Moritz Wenzel

Development of a Metamaterial-Based Foundation System for the Seismic Protection of Fuel Storage Tanks

Supervisors

Oreste S. Bursi, University of Trento, Italy
Günter Fischbach, IGF, Germany

To my family

Acknowledgements

Above all, I would like to thank my supervisor, Oreste Salvatore Bursi, for investing his time and knowledge into my education and our conjoint research. His help and guidance were invaluable to my work. Secondly, but of no less importance, I wish to thank the European Union for funding my work through the XP-Resilience project (EU Horizon 2020 grant agreement no. 721816) and enabling young researchers to find cross border collaborations. Last but not least, my family and friends have my deepest gratitude for supporting me during stressful as well as joyful times.

Abstract

Metamaterials are typically described as materials with 'unusual' wave propagation properties. Originally developed for electro-magnetic waves, these materials have also spread into the field of acoustic wave guiding and cloaking, with the most relevant of these 'unusual' properties, being the so called band-gap phenomenon. A band-gap signifies a frequency region where elastic waves cannot propagate through the material, which in principle, could be used to protect buildings from earthquakes. Based on this, two relevant concepts have been proposed in the field of seismic engineering, namely: metabarriers, and metamaterial-based foundations.

This thesis deals with the development of the Metafoundation, a metamaterial-based foundation system for the seismic protection of fuel storage tanks against excessive base shear and pipeline rupture. Note that storage tanks have proven to be highly sensitive to earthquakes, can trigger severe economic and environmental consequences in case of failure and were therefore chosen as a superstructure for this study. Furthermore, when tanks are protected with traditional base isolation systems, the resulting horizontal displacements, during seismic action, may become excessively large and subsequently damage connected pipelines. A novel system to protect both, tank and pipeline, could significantly augment the overall safety of industrial plants.

With the tank as the primary structure of interest in mind, the Metafoundation was conceived as a locally resonant metamaterial with a band gap encompassing the tanks critical eigenfrequency. The initial design comprised a continuous concrete matrix with embedded resonators and rubber inclusions, which was later reinvented to be a column based structure with steel springs for resonator suspension. After investigating the band-gap phenomenon, a parametric study of the system specifications showed that the horizontal stiffness of the overall foundation is crucial to its functionality, while the superstructure turned out to be non-negligible when tuning the resonators.

Furthermore, storage tanks are commonly connected to pipeline system, which can be damaged by the interaction between tank and pipeline during seismic events. Due to the complex and nonlinear response of pipeline systems, the coupled tank-pipeline behaviour becomes increasingly difficult to represent through numerical models, which lead to the experimental study of a foundation-tank-pipeline setup. Under the aid of a hybrid simulation, only the pipeline needed to be represented via a physical substructure, while both tank and Metafoundation were modelled as numerical substructures and coupled to the pipeline. The results showed that the foundation can effectively reduce the stresses in the tank and, at the same time, limit the displacements imposed on the pipeline.

Leading up on this, an optimization algorithm was developed in the frequency domain, under the consideration of superstructure and ground motion spectrum. The advantages of optimizing in the frequency domain were on the one hand the reduction of computational effort, and on the other hand the consideration of the stochastic nature of the earthquake. Based on this, two different performance indices, investigating interstory drifts and energy dissipation, revealed that neither superstructure nor ground motion can be disregarded when designing a metamaterial-based foundation. Moreover, a 4 m tall optimized foundation, designed to remain elastic when verified with a response spectrum analysis at a return period of 2475 years (according to NTC 2018), reduced the tanks base shear on average by 30%. These results indicated that the foundation was feasible and functional in terms of construction practices and dynamic response, yet unpractical from an economic point of view.

In order to tackle the issue of reducing the uneconomic system size, a negative stiffness mechanism was invented and implemented into the foundation as a periodic structure. This mechanism, based on a local instability, amplified the metamaterial like properties and thereby enhanced the overall system performance. Note that due to the considered instability, the device exerted a nonlinear force-displacement relationship, which had the interesting effect of reducing the band-gap instead of increasing it. Furthermore, time history analyses demonstrated that with 50% of the maximum admissible negative stiffness, the foundation could be reduced to 1/3 of its original size, while maintaining its performance.

Last but not least, a study on wire ropes as resonator suspension was conducted. Their nonlinear behaviour was approximated with the Bouc Wen model, subsequently linearized by means of stochastic techniques and finally optimized with the algorithm developed earlier. The conclusion was that wire ropes could be used as a more realistic suspension mechanism, while maintaining the high damping values required by the optimized foundation layouts.

In sum, a metamaterial-based foundation system is developed and studied herein, with the main findings being: (i) a structure of this type is feasible under common construction practices; (ii) the shear stiffness of the system has a fundamental impact on its functionality; (iii) the superstructure cannot be neglected when studying metamaterial-based foundations; (iv) the complete coupled system can be tuned with an optimization algorithm based on calculations in the frequency domain; (v) an experimental study suggests that the system could be advantageous to connected pipelines; (vi) wire ropes may serve as resonator suspension; and (vii) a novel negative stiffness mechanism can effectively improve the system performance.

Publications

Journal articles

- V. La Salandra, **M. Wenzel**, G. Carta, O. S. Bursi and A. B. Movchan, (2017). "Conception of a 3D Metamaterial- Based Foundation for static and seismic Protection of Fuel storage Tanks", *Frontiers in Materials*, 4:30.
- **M. Wenzel**, F. Basone and O. S. Bursi, (2020). "Design of a Metamaterial-Based Foundation for Fuel Storage Tanks and Experimental Evaluation of Its Effect on a Connected Pipeline System", *Journal of Pressure Vessel Technology*, in press.
- F. Basone, **M. Wenzel**, O. S. Bursi and M. Fossetti, (2019). "Finite locally resonant Metafoundations for the seismic protection of fuel storage tanks", *Earthquake Engineering and Structural Dynamics*, 48:2, pp. 1-21.
- **M. Wenzel**, O. S. Bursi and I. Antoniadis, (2020). "Optimal finite locally resonant metafoundations enhanced with nonlinear negative stiffness elements for seismic protection", *Journal of Sound and Vibration*, (under revision).
- F. Basone, O. Bursi and **M. Wenzel**, (2020). "Optimal design of finite locally resonant metafoundations with linear and nonlinear devices for seismic isolation of fuel storage tanks", (article in preparation).

Publications at international conferences

- **M. Wenzel**, F. Basone, O.S. Bursi, (2018). "Novel Metamaterial-Based Foundation Concept Applied to a Coupled Tank-Pipeline System", ASME 2018 Pressure Vessels and Piping Conference. Awarded with the Rudy Scavuzzo Price.
- H. Crowley, D. Rodrigues, V. Silva, V. Despotaki, X. Romao, J.M. Castro, S. Akkar, U. Hancilar, K. Ptilakis, D. Ptilakis, M. Belvaux, S. Wiemer, L. Danciu, A.A. Correia, O.S. Bursi, **M. Wenzel**. (2018). "Towards a Uniform Earthquake Risk Model for Europe", 16th European Conference on Earthquake Engineering, Thessaloniki, Greece.
- **M. Wenzel**, O.S. Bursi, (2018). "Metamaterial-Based Foundation System for the Seismic Isolation of Fuel Storage Tanks", 16th European Conference on Earthquake Engineering, Thessaloniki, Greece.

- **M. Wenzel**, R. Andreotti, O.S. Bursi, (2019). "Metamaterial-Based Foundation System Endowed with Non-Linear Oscillators for the Protection of Fuel Storage Tanks", International Workshop on Multiscale Innovative Materials and Structures - MIMS19, Cetara, Amalfi Coast, Italy.
- **M. Wenzel**, O.S. Bursi, (2019). "Seismische Metamaterialien - Ein neuer Trend im Erdbebeningenieurwesen und die Entwicklung eines auf Metamaterialien Basierenden Fundaments" [Seismic Metamaterials - A new trend in seismic engineering and the development of a Metamaterial-Based Foundation], 16. D-A-CH Tagung Erdbebeningenieurwesen & Baudynamik (D-A-CH 2019), Innsbruck, Austria.
- G. Karagiannakis, **M. Wenzel**, P. Kowalczyk, M. Farhan, A. Zhelyazkov, F. Celano, S. Caprinuzzi, M. Pedot, B. Kalemi, H. K. Bennani, N. Graine, L. E. Vasquez Munoz, J. Randaxhe, M. J. Mahesh, (2020). "Seismic Risk and Resilience Assessment of Industrial Facilities: Case Study on a Black Carbon Plant", 17th World Conference on Earthquake Engineering 17WCEE, Sendai, Japan.

Open source software uploads

- Optimization algorithm for the optimal tuning of 1D linear dynamic structures [Python]: <https://github.com/moritz343/Optimization>

Contents

Contents	ix
1 Introduction	1
1.1 Metamaterials and Phononics	1
1.1.1 Dispersion analysis	2
1.2 Seismic-metamaterials	5
1.3 Fuel storage tanks and seismic engineering	7
1.4 Hybrid simulation	9
1.5 Scope, objective and structure of the thesis	11
1.5.1 Objective and novelty	11
1.5.2 Scope	11
1.5.3 Structure of the thesis	13
2 Conception of the Metafoundation	17
2.1 Introduction	18
2.2 Materials and methods	20
2.2.1 Floquet-Bloch theorem and Brillouin zone	20
2.2.2 Static analysis	22
2.2.3 Materials	23
2.2.4 Functionality evaluation of the original design	24
2.2.5 Optimization of the unit cell	25
2.3 Results	28
2.3.1 Modal analysis of a coupled broad-tank-foundation system	28
2.3.2 Unit cell design of the original smart foundation	28
2.3.3 Static analysis	29
2.3.4 Functionality evaluation	31
2.3.5 Results for the optimized unit cell	32
2.3.6 Influence of small cracks	34
2.4 Discussion	34
2.4.1 Conclusion	36

3	Metafoundation development and Experimental Study on a coupled Pipeline	39
3.1	Introduction	40
3.2	Design of the Foundation	41
3.2.1	Materials	41
3.2.2	Fuel storage tank modelling	41
3.2.3	Description of the structure and dynamic system . . .	43
3.2.4	Analytical model and Floquet-Bloch theorem	45
3.2.5	Results for the uncoupled foundation	47
3.2.6	Frequency response analysis of the coupled system . .	48
3.2.7	Seismic response analysis for the coupled system . . .	52
3.2.8	Validation of the 1D model through FE-modelling . .	53
3.3	Experimental Study	57
3.3.1	Experimental performance of the coupled tank-foundation-pipeline system	57
3.3.2	Physical substructure PS	58
3.3.3	Numerical Substructure	60
3.3.4	Results of the experimental study	62
3.4	Conclusion	63
4	Optimization of Locally Resonant Metafoundations	65
4.1	Introduction	66
4.1.1	Background and motivations	66
4.1.2	Scope	68
4.2	Description of the coupled system	68
4.2.1	Fuel storage tank modelling	69
4.2.2	Modelling of the coupled foundation-tank system . . .	71
4.2.3	Seismic design of the Metafoundation	72
4.2.4	Site-specific seismic hazard and accelerogram selection	73
4.3	Uncoupled system properties	74
4.3.1	Properties of a periodic lattice	74
4.3.2	Concept of seismic isolation and negative apparent mass	77
4.4	Optimization procedure of the Metafoundation	78
4.4.1	Ground motion modelling	79
4.4.2	Optimization procedures in the frequency domain . .	79
4.4.3	Optimization parameters	81
4.5	Results of Metafoundation optimizations	83
4.6	Time history analysis	85
4.6.1	Results for the coupled foundation-slender tank system	88
4.6.2	Results for the coupled foundation-broad tank system	90
4.7	Conclusion	90
4.8	Appendix: Non-stationary power spectral density	92
5	Negative Stiffness Element for Periodic Foundations	95

5.1	Introduction	96
5.1.1	Scope	98
5.2	Description of the structure	98
5.2.1	Negative stiffness element NSE	100
5.2.2	Dynamic system	103
5.2.3	Stability condition of the system	105
5.3	Band-gaps and wave propagation	107
5.3.1	Band gaps of the linear system	107
5.3.2	Band gaps in the nonlinear system	110
5.4	Optimization of the coupled system	114
5.4.1	Ground motion models	116
5.4.2	Optimization algorithm	117
5.5	Behaviour of the coupled system	119
5.5.1	Behaviour of the system in the frequency domain	119
5.5.2	System response in the time domain	120
5.6	Conclusion	123
6	Wire Ropes for Resonator Suspension	127
6.1	Introduction	127
6.1.1	Scope	129
6.2	Metamaterial concept and dynamic system	130
6.2.1	Metamaterial concept and negative apparent mass	131
6.2.2	System modelling and reduction	133
6.2.3	Modelling of wire ropes	136
6.2.4	Accelerogram selection and seismic input model	137
6.3	Optimization of the Metafoundation endowed with linear devices	138
6.3.1	Definition of optimization problem	139
6.3.2	Results of optimization	140
6.4	Results of time history analyses	141
6.5	Optimization of the Metafoundation endowed with nonlinear devices	143
6.5.1	Stochastic linearisation technique	144
6.5.2	Optimization of linearised devices	146
6.5.3	Definition of optimization problem	146
6.6	Hysteretic dampers, Bouc-Wen parameters and optimization results	147
6.6.1	Hysteretic dampers and Bouc-Wen parameters	147
6.6.2	Optimization results and time history analyses	147
6.7	Conclusion and future developments	152
6.8	Appendix: Obtaining the transmission matrix after SLT	153
7	Summary, conclusion and future developments	155
7.1	Summary	155

CONTENTS

7.2	Conclusions	156
7.3	Future developments	160
	Bibliography	163
	List of Figures	177
	List of Tables	182

Chapter 1

Introduction

1.1 Metamaterials and Phononics

Metamaterials are materials with '*unusual*' properties. This very broad definition, given by Solymar and Shamonina [1] in their book 'Waves in metamaterials', does not give insight in what properties those may be. But as the title of their book already promises, metamaterials are classically related to the propagation of waves. Originally, the term was coined by Smith et al. [2], who developed a material with negative permittivity and permeability in the electro-magnetic regime. However, as pointed out by Zouhdi et al. [3] the word metamaterial never got defined properly, but can be used to describe materials with unconventional wave propagation behaviour. Besides electro-magnetic waves [4], also phononic waves, which are characterized by mechanical vibrations, can be manipulated with metamaterial like structures. A comprehensive review of the recent advances in phononic waves was given by Maldovan [5], who highlighted that the main distinction between different types of metamaterials is the frequency range of application. Electromagnetic waves for example are widely used in modern technology, have a typical frequency range from 10^6 Hz (e.g. analogue Radio) up to 10^{20} Hz (PET-scan) and are characterized by the movement of photons and electrons. Phononic waves on the other hand, range from practically 0 Hz, where infra-sound and acoustic waves start; and reach up into the Terra-Hz scale, where thermal waves are located. The frequency range of seismic waves is, of course, located at the lower end of the phononic wave spectrum and can be regarded as part of the acoustic wave regime, as illustrated in Figure 1.1. The first to demonstrate that acoustic waves could be manipulated analogously to electromagnetic waves was Liu et al. [6]. They arranged centimeter sized lead balls coated with silicon rubber in a periodic array and showed numerically as well as experimentally that a structured material of this type can produce interesting wave propagation properties. Of particular

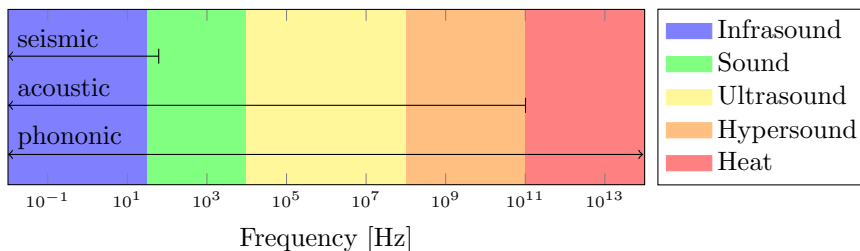


Figure 1.1: Frequency spectra of phononic waves.

interest, is the so called band-gap property, which prohibits elastic waves to propagate in a specific frequency region [7].

Band-gaps in acoustic materials can essentially be achieved through Bragg scattering or local resonance [8]. In particular, Bragg scattering relies on the obtainable phase shift through arranging unit cells, while local resonance depends on the local frequency of embedded resonators [9, 10]. For Bragg scattering, this entails that the frequency region where band gaps can be achieved is primarily dependent on the unit cell dimension of the structured medium. Note that the unit cell of a structured medium is the smallest identifiable component that, when arranged in a periodic manner, constitutes the overall material. For Bragg scattering the unit cell size can be estimated with,

$$R = \frac{\lambda}{2} \quad (1.1)$$

where, R is the lattice constant, or the size of the unit cell, while λ denotes the wave length. For seismic waves, the wave length can reach far beyond 100 m, which renders the application of metamaterials based on Bragg scattering nearly impossible. Local resonance, however, can produce band-gap like properties with unit cells much smaller than the wave length of the target waves. Therefore, locally resonant materials are of primary interest to seismic-metamaterials and, hence, also this thesis. The band-gaps of the proposed foundations will be calculated with dispersion analyses and discussed in the relevant chapters where applicable. In order to provide the reader with a better understanding of what kind of information can be read from the resulting dispersion diagrams, a short introduction to dispersion analysis follows here.

1.1.1 Dispersion analysis

The dispersion analysis sheds light on the wave propagation properties of periodic lattices and is elaborated here on the simplest case, the monoatomic chain. In order to obtain the dispersion diagram, the classical equations of

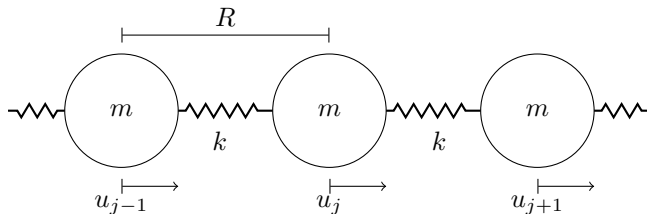


Figure 1.2: Monoatomic lattice.

motion (of one unit cell) need to be subjected to the Floquet-Bloch boundary condition [11–13]. Figure 1.2 displays a simple chain where, m describes the mass of the unit cell, in this case an atom, k represents the stiffness of the connection between the masses, R is the lattice constant as described above, and u_j , u_{j-1} , and u_{j+1} are the displacements of the unit cell under study, the previous unit cell, and the subsequent unit cell, respectively. The relevant equation of motion reads,

$$m\ddot{u}_j + k(u_{j-1} - u_j) + k(u_{j+1} - u_j) = 0 \quad (1.2)$$

According to the Floquet-Bloch theory, the previous and subsequent displacements can be related to the unit cell under study with,

$$u_{j+n} = u_0 e^{i(qnR - \omega t)} \quad (1.3)$$

Here u_0 is the amplitude of the wave, q is the angular wave number, which is defined as the inverse of the wavelength ($2\pi/\lambda$), while ω is the angular frequency of the propagating wave, and t denotes time. Furthermore, n relates to other unit cells with -1 for the previous and +1 for the subsequent unit cell. For a lattice constant of $R = 1$, the term qnR degenerates to $\pm q$, which can range from $-\pi \leq q \leq \pi$.

To highlight the meaning of this relationship, the oscillation of the central unit cell and the neighboring ones is demonstrated in Figure 1.3 via the complex plain. Note that the displacement of the unit cells develops over time as the real part of the expressions $e^{i(-q-\omega t)}$, $e^{-i\omega t}$, and $e^{i(q-\omega t)}$ multiplied with u_0 from (1.3), for the previous, central, and subsequent unit cell, respectively. After applying this relationship (1.3) to the equation of motion (1.2), and solving the system for the angular frequency ω , the dispersion relation reads,

$$\omega = \sqrt{\frac{2k(\cos(q) - 1)}{m}} \quad (1.4)$$

This equation essentially maps traveling waves to their propagation frequency. Figure 1.4 schematically depicts the dispersion branch of the monoatomic lattice with normalized mass $m = 1$ and stiffness $k = 1$. From Figure

1.3 it can be deduced that the dispersion relation has to be 2π periodic for q , since this will include all possible positions on the unit circle in the complex plain. This further entails that only a finite magnitude of wave number q can be studied for a specific system, which in turn depends on the unit cell dimension given by R . Moreover, the group and phase velocity v_p and v_g , for any given wave, can be studied from Figure 1.4, with the following relationships,

$$v_p = \frac{\omega_i}{q_i}, \quad v_g = \frac{d\omega_i}{dq_i} \quad (1.5)$$

Here, the subscript i corresponds to a generic point on the dispersion branch, for which the values of q_i , ω_i and the derivatives dq_i and $d\omega_i$ can be read from the diagram. Note that the phase velocity gives the speed at which features of the wave travel through the system, such as peaks and troughs, while the group velocity is the speed at which energy is transported. Of particular interest is the fact that at the end of the dispersion branch at values π and $-\pi$ the group velocity tends towards zero and waves become standing waves which do not propagate through the system, but remain localized. Furthermore, with the introduction of additional degrees of freedom more dispersion branches appear, which represent different modes of vibration. These, of course, depend on the system under study and will be discussed for various Metafoudation layouts in the respective chapters. But before diving into the peculiarities of the proposed foundation, a look at other technologies and research projects may give an idea about what is being investigated in the field of seismic metamaterials.

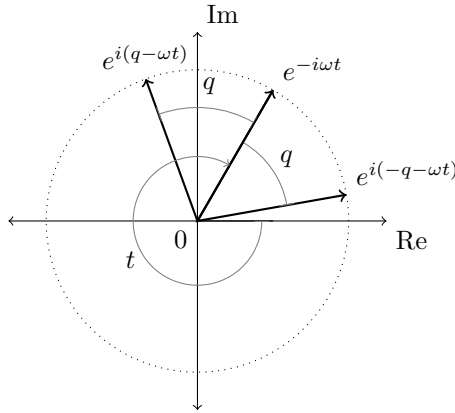


Figure 1.3: Oscillation of neighbouring unit cells in the imaginary plane.

1.2 Seismic-metamaterials

Two ideas are dominating the field of seismic metamaterials, namely, metamaterial based foundations and seismic metabarriers. Metabarriers essentially consist of resonators that are placed on or in the soil and target the attenuation of surface waves, while metamaterial-based foundations need to be placed under the building and have the capacity of attenuating bulk waves.

In terms of metabarriers, Brule et al. [14] studied the wave propagation through periodic bore holes in soil, by means of full scale dynamic testing, and showed that seismic metamaterials are indeed feasible to obtain. Besides this, Huang and Shi [15] showed how periodic pile barriers could be applied to produce attenuation zones for plane wave reduction. This concept was later improved by Achaoui et al. [16], who were able to achieve a much lower band-gap frequency range (≤ 10 Hz) by clamping pile foundations to the bedrock. These investigations were primarily oriented around the concept of Bragg scattering, which is limited in terms of feasibility due to the required unit cell dimensions.

Exploiting the concept of local resonance, [17, 18] proposed resonators embedded in the soil to further improve the obtainable band-gap for surface wave attenuation. Along these lines, Palermo et al. [19] then studied a realistic setup with steel resonators supported by rubber bearings that would be buried in the soil around a building of interest. The used resonators were designed as cylindrical units with approximate radius and height of 0.4 m and 1.7 m, which were then placed in concrete shells to protect them from the surrounding soil and potential damage. Arranged in a periodic grid, these resonators effectively reflected Rayleigh waves back into the ground and subsequently attenuated the seismic action affecting a building. Furthermore, the necessary equations to design a functional metabarrier dependent on soil type and desired band-gap were provided in their work.

Another interesting approach to seismic barriers was proposed by Colombi et al. [20], who studied a forest as a natural array of resonators for the

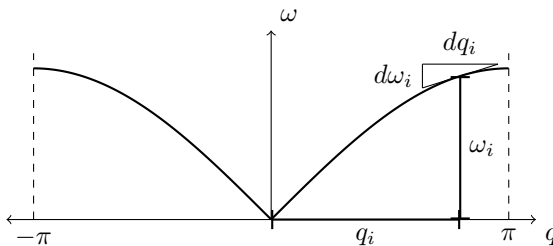


Figure 1.4: Dispersion relation of the Monoatomic lattice.

attenuation of Rayleigh waves. Through numerical simulations and the instrumentation of a forest, they found that band-gaps in a frequency range of tens of Hz can be obtained. More precisely, two band gaps were discovered for the studied forest ranging from about 30 - 45 Hz and 90 - 110 Hz, where incoming Rayleigh waves were attenuated. A further study on forests as metamaterials, namely the metaforest project, confirmed these findings by means of a large scale experiment, where 1000 seismic sensors instrumented an area of $120m \times 120m$ [21]. Building up on these developments [22] then proposed the metawedge, which essentially represented an array of vertical resonators that, due to the varying resonant frequencies, widened the achievable band-gap.

The clear advantage of metabarriers is that they can be placed next to the structure of interest, and may therefore be applied to existing structures. This is particularly interesting for the protection of cultural heritage sites where other types of seismic mitigation strategies can only be installed through extensive construction efforts. However, since surface waves are only one part of the seismic action that may damage a structure, metabarriers can only be applied in combination with other measures or at far field locations where primary and secondary body waves have already been attenuated.

Metamaterial-based foundations, on the other hand, have the advantage of covering any type of plane wave, since they represent the connection of the superstructure with the ground. Some of the first works in this regard were carried out by Xiang et al. [23] and Bao et al. [24]. Both studied layered foundations with alternating stiffness and mass properties and found that waves propagating inside the frequency regime of the designed band-gap would be attenuated.

Furthermore Cheng and Shi [25] and Jia and Shi [26] came up with 2D foundation systems for the seismic protection of nuclear power plants and traditional buildings, respectively. In their designs they used 1 and 2 component cylindrical inclusions consisting of steel and rubber, which provided low frequency band-gaps in the harmful frequency range of incoming earthquakes. Cheng and Shi [27] further developed their foundation concept to show different band-gaps for orthogonal wave propagation directions. Of particular interest was the attenuation of the vertical component of the earthquake, which usually has a different frequency content with respect to the horizontal one and has proven to be damaging to structures such as nuclear power plants. By arranging two different asymmetric unit cells in a periodic manner they showed how the vertical as well as the horizontal component of a seismic event could be attenuated through their foundation. However, in their study the foundation was considered as a filtering medium for the nuclear power plant, which entailed that they neglected the feedback from the power plant on the foundation. Besides this, also Yan et al. [28] studied the efficacy of periodic foundations for horizontal as well as vertical ground motions, and found that metamaterial-based foundations are indeed

able to address both components.

A seismic metamaterial endowed with isochronous oscillators was proposed by Finocchio et al. [29], where steel balls would roll on cycloidal surfaces inside a concrete matrix. Casablanca et al. [30] later developed a similar system comprised of concrete slabs separated by low damping teflon-steel surfaces; where the concrete slabs housed steel masses held in place with rubber inclusions, in order to add local resonance to the system. This composite foundation exerted the band-gap property in a low frequency range of 3.5 Hz - 13 Hz and was analyzed analytically as well as experimentally with a specimen size of approximately $1 \times 1m$. They effectively obtained an attenuation zone where the predicted band-gap was located. But also in this research effort, the feedback of the superstructure was neglected.

As shown in [31], which constitutes Chapter 4 of this thesis, the superstructure cannot be neglected, due to the feedback it imposes on the foundation. Furthermore, it was found that the horizontal stiffness is of critical importance to the effectiveness of the foundation [32], which in turn is constrained by the engineering design of the foundation according to common construction practice [31]. Besides this, the size of the resonators play a vital role for the functionality of the foundation, while at the same time are a major cost driving factor, due to the amount of required material.

Furthermore, it is worth mentioning that cracks are expected to occur in concrete structures and that those cracks can have an impact on the wave propagation [33]. The authors of [32] were inspired by the work of Mishuris, Movchan and Slepyan [34–36] to investigate the potential effect of such cracks on the wave propagation. Therefore, In Chapter 2, which comprises the publication [32], the effect of static cracks on the developed foundation is investigated. The results show that due to the location and small size of the expected cracks, no noticeable shift can be expected for the particular structure discussed herein.

1.3 Fuel storage tanks and seismic engineering

Since fuel storage tanks represent highly sensitive infrastructures that can have a sever impact on the community and the environment if damaged, they were chosen as a superstructure for this study. In 1999 the Kocaeli earthquake damaged several fuel storage tanks, which caused fires that couldn't be extinguished for 3 days [37]. Furthermore, the 2011 Tohoku earthquake and tsunami, which triggered the Fukushima accident [38, 39], destroyed 30% of the Japanese oil industry and initiated fires that took 10 days to extinguish [40–42]. These scenarios can be described as Natural Technological Events (NaTech events) [43, 44], where a natural disaster causes an technological accident, which subsequently increases the severity of the consequences significantly. Krausmann et al. [45] showed that storage tanks with connected

pipelines represent the most vulnerable equipment when it comes to NaTech events, triggered through earthquakes, floods or lightning.

Besides the consequence intensity of storage tanks, they also show varying fluid levels over their lifetime time, which significantly alters their fundamental periods [46, 47]. This is particularly problematic for seismic protection, since the protective measure has to be effective at every fluid level, and therefore, at varying eigenfrequencies. To date traditional seismic protection is still scarce for fuel storage tanks, due to the cost of seismic isolation and the difficulty of applying other means such as tuned mass dampers (TMD).

Traditional seismic protection can be split into passive and active control mechanisms, where active mechanisms require electric power for e.g. the excitation of hydraulic actuators, while passive devices are independent from external power sources [48]. For this work, only the passive control mechanisms are of interest, which essentially consist, but are not limited to the following 3 subgroups: (i) seismic isolation; (ii) energy dissipative devices [49]; and (iii) Tuned Mass Dampers (TMDs). Concerning the Metafoundation discussed herein, seismic isolation as well as TMD concepts are of interest, since the foundation exerts traits from both fields. Regarding seismic isolation two main technologies come to mind, firstly lead rubber bearings [50] and secondly the concave sliding bearings [51]. The underlying concept is to build a foundation that decouples the superstructure from the ground and thereby shifts the fundamental frequency of the overall structure to a frequency regime, where the seismic action causes less damage. This, however, is usually accompanied with large horizontal displacements, which can be particularly damaging to connected structures such as pipelines. TMDs on the other hand, represent resonators that are placed at critical locations of the building and oscillate in counter-phase with the eigenmodes of the structure. The downside of TMDs is that they need to be tuned to the correct frequency, can detune over time, and are not generally effective at attenuating seismic action, due to the wide frequency spectrum of earthquakes [52].

Besides horizontal ground excitations, also the vertical component of earthquakes has proven to have a great damage potential [53]. Particularly for structures that can cause severe consequences when failing, such as nuclear power plants, the vertical component should be taken seriously [54]. Also for fuel storage tanks, vertical accelerations can induce significant forces, due to the increased hydrostatic pressure deriving from the breathing mode [55, 56]. Note that classical isolation systems such as lead rubber bearings are particularly stiff, and therefore, not able to reduce the vertical excitation [57]. While in the present work, only the horizontal component is treated, it shall be mentioned here that in future studies, also the vertical component could be addressed by metamaterial-based foundations.

1.4 Hybrid simulation

As mentioned earlier, connected pipelines can experience significant damages due to the horizontal displacement of base isolated tanks during a seismic event. Since the correct response of pipelines, due to their strongly nonlinear behavior, is difficult to predict by means of numerical simulations, an experimental study is conducted in Chapter 3. More precisely, a hybrid simulation (HS) is carried out on a 15 m long pipeline system, where a tank protected by the Metafoundation and a tank protected by concave sliding bearings (CSB) serve as numerical substructures. While the experiment itself will be discussed in detail in the relevant chapter, an introduction to the used hybrid simulation setup follows here.

In principle, a HS setup splits a system into multiple substructures, of numerical or experimental nature and couples them via an appropriate time integration algorithm [58, 59]. Under the aid of this technique, complex engineering systems can be split up into multiple components, where the highly nonlinear ones, such as pipelines, are tested in the laboratory; while typically linear components, such as steel frame structures, are modelled numerically. The substructures are then coupled by means of a transfer system which enforces equilibrium and compatibility at their interfaces, which allows the HS method to accurately represent complex systems with economical testing setups.

The HS time integration algorithm used in Chapter 3 is based on the work done by Abbiati et al. [60] and relies on localized Lagrange multipliers for the coupling of the individual substructures. For instance, let's imagine 3 different substructures as shown in Figure 1.5, which could be of numerical or experimental nature, and let them share the generalized interface DOFs u_1^g and u_2^g . These substructures are then coupled to their interface DOFs via localized Lagrange multipliers denoted with λ , which allow the system of EOMs to be formulated as,

$$\mathbf{M}^{(l)}\ddot{\mathbf{u}}^{(l)} + \mathbf{R}^{(l)}(\mathbf{u}^{(l)}, \dot{\mathbf{u}}^{(l)}) = \mathbf{L}^{(l)T} \boldsymbol{\Lambda}^{(l)} - \mathbf{M}^{(l)}\mathbf{T}^{(l)}\mathbf{a}_g \quad (1.6)$$

$$\forall l \in 1, 2, 3$$

Here, \mathbf{M} , and \mathbf{R} are the mass matrix and the restoring force vector of the l -th substructure, while \mathbf{u} , $\dot{\mathbf{u}}$ and $\ddot{\mathbf{u}}$ denote the displacement, velocity and acceleration vectors, respectively. Besides this, \mathbf{a}_g denotes the applied ground acceleration, whereas $\mathbf{T}^{(l)}$ denotes a Boolean vector that determines the direction of the ground motion. Note that for linear subsystems, \mathbf{R} can be formulated as,

$$\mathbf{R}(\mathbf{u}, \dot{\mathbf{u}}) = \mathbf{K}\mathbf{u} + \mathbf{C}\dot{\mathbf{u}} \quad (1.7)$$

Furthermore, $\boldsymbol{\Lambda}$ describes the localized Lagrange multiplier vectors, containing the Lagrange multipliers (λ) of the substructures as depicted in Figure

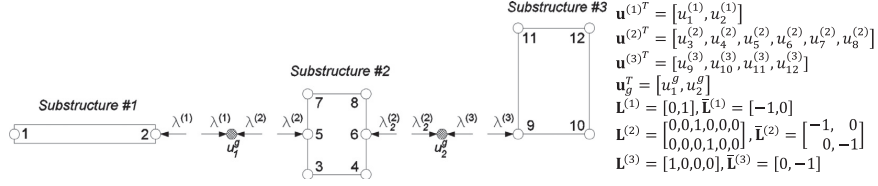


Figure 1.5: Three different substructures coupled via localized Lagrange multipliers (figure from [60]).

1.5. In order to enforce compatibility on the various subsystems, the following two conditions must be satisfied,

$$\mathbf{L}^{(l)} \dot{\mathbf{u}}^{(l)} + \bar{\mathbf{L}}^{(l)} \dot{\mathbf{u}}_g^{(l)} = \mathbf{0}$$

or

$$\mathbf{L}^{(l)} \mathbf{u}^{(l)} + \bar{\mathbf{L}}^{(l)} \mathbf{u}_g^{(l)} = \mathbf{0}$$

and

$$\sum_{l=1}^m \bar{\mathbf{L}}^{(l)T} \mathbf{\Lambda}^{(l)} = \mathbf{0}$$

here, the single substructure DOF vector $\mathbf{u}^{(l)}$ and the generalized interface DOF vector \mathbf{u}_g are collocated by the Boolean signed matrices \mathbf{L} and $\bar{\mathbf{L}}$. To put the matter more plainly, expression (1.6) contains the system of EOMs of all substructures, which need to be solved under the constraints of eqs. (1.8) and (1.9). Here, eq. (1.8) makes sure that either the displacements or the velocities of the coupled DOFs are equal, while eq. (1.9) imposes the force equilibrium at the interface nodes. The equations (1.6)-(1.9) can then be solved according to the time stepping algorithms shown in [60] and are able to couple any number of numerical or experimental substructures in a HS environment. Note that for the experiment presented in Chapter 3 this will be done for a pipeline as an experimental substructure, and two different numerical models containing a storage tank isolated with CSBs and a storage tank clamped to the Metafoundation. This setup has the advantage of yielding realistic results for the coupled foundation-tank-pipeline system under full consideration of the dynamic interaction between the substructures, while only the pipeline has to be physically tested in the laboratory. Additionally, some comparisons between the Metafoundation and traditional isolation devices can be drawn.

1.5 Scope, objective and structure of the thesis

1.5.1 Objective and novelty

The objective of this thesis is to conceive a new type of seismic protection based on metamaterial concepts for the safety of fuel storage tanks. This essentially consists of the following two tasks: designing a foundation that reduces the dynamic effects of an earthquake arriving at a tank; and developing a system that functions under standard civil engineering requirements. In pursuit of these goals, a column based foundation layout is developed, as depicted in Figure 1.6. Note that the tank is separated from the ground via the foundation, which forces the earthquake to travel through the metamaterial, thus experiencing filtering effects. In order to design this foundation an optimization algorithm, for the optimal tuning of the resonators, is established, which takes the ground motion and superstructure into account. While the foundation is targeted at the protection of storage tanks, an experimental study on the interaction between Metafoundation tank and a connected pipeline sheds light on the complete coupled behaviour. It is demonstrated that this type of foundation may have positive effects on connected pipelines, since both tank base shear and horizontal displacement can be limited. Furthermore, in order to improve the seismic isolation efficiency, an NSE is developed that effectively reduces the necessary foundation height. Note that the size reduction of metamaterial inspired seismic structures is highly desirable, since most proposals in the literature still show excessive system dimensions. Finally, in order to make the foundation design more practical, wire ropes are used as resonator suspension devices. It is worth mentioning that wire ropes can act in all 3 spatial directions and, in future, may be used to attenuate the vertical component of the earthquake.

In sum, the following original scientific contributions to the field of seismic metamaterials are obtained: (i) conception of a new column based foundation designed under common construction requirements; (ii) development of an optimization algorithm for the optimal tuning of the localized resonators, under consideration of ground motion and superstructure; (iii) experimental demonstration of the potential effects the foundation may have on a connected pipeline; (iv) design and study of a novel NSE targeted at the implementation in periodic foundations; and (v) study of wire ropes for a more practical resonator suspension.

1.5.2 Scope

Chapters 2-4 are devoted to conceiving a foundation that exerts the band-gap phenomenon and complies with common construction standards. In particular, Chapter 2 shows the initial design of the continuous concrete matrix with embedded resonators and demonstrates that the shear stiffness plays a

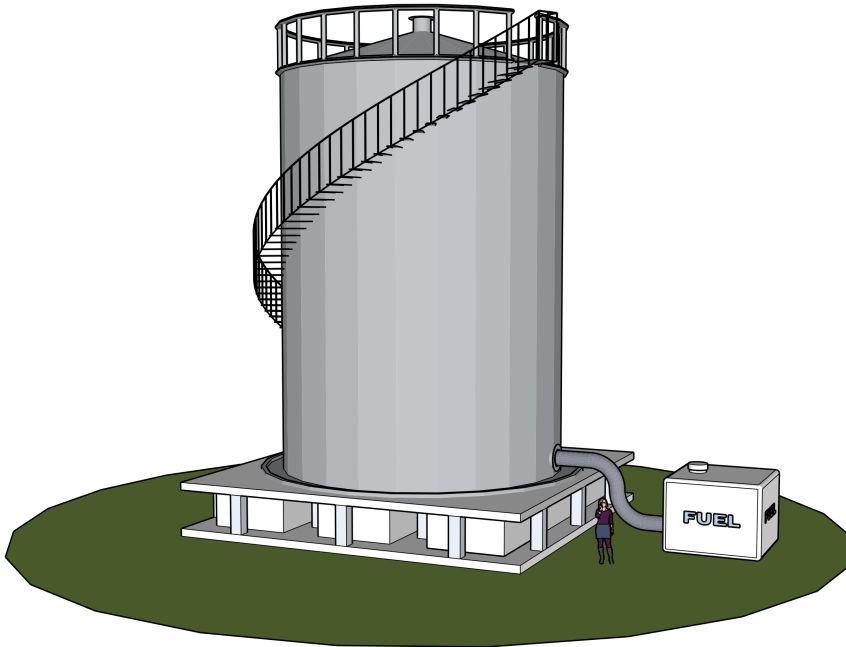


Figure 1.6: View of the Metafoundation placed under a tank.

vital role for locally resonant foundations. Based on these findings a column based foundation is proposed, which represents the basis for all future developments in the later chapters. Furthermore, a static analysis on the system ensures the structural integrity under gravity loading and reveals potential cracks in the periodic structure, which are then analyzed on their impact on the dispersion relation. As indicated in the introduction, the protection of pipelines connected to tanks represents an ongoing issue for petrochemical plants, and is therefore studied experimentally in Chapter 3. By means of a hybrid simulation setup, the coupled tank-foundation system is simulated numerically and coupled to a 15 m long pipeline. The Metafoundation setup is compared to a classical isolation setup with concave sliding bearings and the advantages and disadvantages are pointed out. Additionally, Chapter 3 also investigates the coupled foundation tank behaviour for varying fluid levels in the frequency domain and shows a 3D finite element model to test the representativeness of the discretized analytical model. Following up on these studies, Chapter 4 treats the engineering design and the optimization of the foundation. After dimensioning the components of the foundation according to Italian and European standards, the foundation is optimized

in the frequency domain under consideration of the ground motion and the superstructure. More precisely, the complete dynamic system is represented via its transmission matrix, while the ground motion is approximated with a Kanai-Tajimi filtered power spectral density fitted to a set of response spectrum compatible ground motions. Optimal layouts are presented for 4 different foundations and studied for the application to two different tanks, i.e. broad and slender fuel storage tanks. Due to the large system dimensions found in Chapter 4, Chapter 5 develops a negative stiffness mechanism that can be implemented in periodic foundations and significantly amplifies their functionality and metamaterial like properties. Simulations in the time and frequency domain show how the attenuation effect of a finite medium can be augmented for seismic applications, under the consideration of the full inevitable nonlinearity due to the local instability. Besides this, the resulting change in the band-gap is studied analytically, under the aid of the harmonic balance method, and later verified with numerical simulations to show the trend of the band-gap with increased nonlinearity. Moreover, in Chapter 6 wire ropes are investigated as resonator suspension mechanisms, in order to render the resonator motion more physical. Note that the non-linear behavior of the wire ropes is approximated with a Bouc Wen model and subsequently linearized by means of stochastic linearization to obtain an equivalent linear dynamic system. The linear system is then optimized with the previously developed optimization algorithm and used to choose appropriate wire rope setups for the foundation. Furthermore, multiple resonators are tuned to different frequencies and damping ratios, in order to further increase the system performance.

1.5.3 Structure of the thesis

The 5 main chapters of this thesis each contain one journal article, summarizing the main research output of the author. A brief statement of the contents follows herein:

- **Chapter 2** contains the publication: *V. La Salandra, M. Wenzel, G. Carta, O. S. Bursi and A. B. Movchan, "Conception of a 3D Metamaterial- Based Foundation for static and seismic Protection of Fuel storage Tanks", Frontiers in Materials, vol. 4, no. 30, 2017.* Here, the Metafoundation is introduced for the first time as a continuous concrete matrix with embedded resonators. A parametric study shows the importance of the horizontal stiffness for the functionality of the foundation and leads to a new design with columns as the primary load bearing system. Additionally, a study on small static cracks shows no significant impact on the band-gap properties.
- **Chapter 3** contains the publication: *M. Wenzel, F. Basone and O. S. Bursi, "Design of a Metamaterial-Based Foundation for Fuel Stor-*

age Tanks and Experimental Evaluation of Its Effect on a Connected Pipeline System", *Journal of Pressure Vessel Technology*, vol. 142, no. 021903, 2020. In this work, the foundation is further developed and an experimental study on a connected pipeline system conducted. The results suggest that the foundation could potentially reduce tank base shear, while at the same time limit pipeline stresses, which is a multi-functionality that traditional isolation system are not able to offer. Furthermore, an analysis on various liquid heights shows that the foundation reduces tank stresses even at reduced fluid levels.

- **Chapter 4** contains the publication: *Basone, M. Wenzel, O. S. Bursi and M. Fossetti, "Finite locally resonant Metafoundations for the seismic protection of fuel storage tanks", Earthquake Engineering and Structural Dynamics*, vol. 48, no. 2, pp. 1-21, 2019. This paper presents the first iteration of the optimization algorithm, based on linear computations in the frequency domain, which clearly highlighted the non-negligibility of the superstructure as well as the ground motion when designing metamaterial-based foundations. We further found that the foundation under study can be built according to common construction requirements, which on the flip side, imposes significant restrictions on the foundation size.
- **Chapter 5** contains the article under revision: *M. Wenzel, O. S. Bursi and I. Antoniadis, "Optimal finite locally resonant metafoundations enhanced with nonlinear negative stiffness elements for seismic protection", Journal of Sound and Vibration, under revision, 2020.* A negative stiffness element (NSE), for the implementation in the periodic foundation and subsequent amplification of its metamaterial properties, is conceived and studied in this work. Additionally, the previously established optimization algorithm is generalized, in order to cope with any linear system, including one with negative stiffness. From a seismic performance point of view the foundation improves substantially, with a height reduction from 3 m to 1 m with only 50% of the admissible NSE value. Furthermore, the wave propagation in the nonlinear material showed that the band gap range would reduce with an increase in nonlinearity.
- **Chapter 6** contains the article in preparation: *F. Basone, O. Bursi and M. Wenzel, "Optimal design of finite locally resonant metafoundations with linear and nonlinear devices for seismic isolation of fuel storage tanks".* The final paper treats the implementation of wire ropes in the foundation as resonator suspension. The wire ropes are approximated with the Bouc Wen model and subsequently linearized by means of stochastic linearization. The linear parameters are then optimized with the previously developed optimization procedure and used to find

functional wire rope setups. While the performance of the foundation did not improve, the wire ropes still add to the feasibility from a structural view point. Additionally, a study with multiple frequencies for various resonators shows that only a minimal advantage over a single frequency can be obtained in terms of base shear reduction. However, when using different frequencies the damping ratios of the individual resonators can be reduced, which may further improve the feasibility.

- **Chapter 7** closes the thesis with conclusions and future developments.

Chapter 2

Conception of the Metafoundation

Overview. Fluid-filled tanks in tank farms of industrial plants can experience severe damage and trigger cascading effects in neighboring tanks due to large vibrations induced by strong earthquakes. In order to reduce these tank vibrations, we have explored an innovative type of foundation based on metamaterial concepts. Metamaterials are generally regarded as manmade structures that exhibit unusual responses not readily observed in natural materials. If properly designed, they are able to stop or attenuate wave propagation. Recent studies have shown that if locally resonant structures are periodically placed in a matrix material, the resulting metamaterial forms a phononic lattice that creates a stop band able to forbid elastic wave propagation within a selected band gap frequency range. Conventional phononic lattice structures need huge unit cells for low-frequency vibration shielding, while locally-resonant metamaterials can rely on lattice constants much smaller than the longitudinal wavelengths of propagating waves. Along this line, we have investigated 3D structured foundations with effective attenuation zones conceived as vibration isolation systems for storage tanks. In particular, the three-component periodic foundation cell has been developed using two common construction materials, namely concrete and rubber. Relevant frequency band gaps, computed using the Floquet-Bloch theorem, have been found to be wide and in the low-frequency region. Based on the designed unit cell, a finite foundation has been conceived, checked under static loads and numerically tested on its wave attenuation properties. Then, by means of a parametric study we found a favorable correlation between the shear stiffness of foundation walls and wave attenuation. On this basis, to show the potential improvements of this foundation, we investigated an optimized design by means of analytical models and numerical analyses. In addition, we investigated the influence of cracks in the matrix

material on the elastic wave propagation, and by comparing the dispersion curves of the cracked and uncracked materials we found that small cracks have a negligible influence on dispersive properties. Finally, harmonic analysis results displayed that the conceived smart foundations can effectively isolate storage tanks.

2.1 Introduction

In 1999 the Izmit earthquake damaged the largest Turkish petrochemical plant and set it on fire. The fire took five and a half days to extinguish and almost spread to other industrial sites [37]. Such events can be described as natural technological events or NaTech events. It is of critical importance for the community and the environment to prevent such incidents from happening. Fuel storage tanks in petrochemical plants need to be regarded as high risk structures, due to their fragility to earthquakes and their potential for cascading effects [61]. Their low impulsive frequencies can fall within the excitation frequencies of earthquakes and significant effort is required to isolate them against seismic vibrations. A very innovative solution for isolating tanks at low frequencies is constructing a foundation based on phononic crystals. These crystals can create stop bands, which stop waves from propagating in certain frequency regions [7]. Various applications could benefit from these properties, for example, noise protection [6], seismic isolation [62] or coastal protection [63]. The present work is dedicated to the feasibility of such metamaterial-based structures for the seismic isolation of fuel storage tanks. Three- and two-component new foundations were conceived by [25]. A two-dimensional (2D) array of steel cylinders coated with rubber and embedded in a reinforced concrete matrix constituted the three-component foundation. Conversely, the two-component design was based on the same geometry, but replacing the steel cylinders inside the rubber with homogeneous rubber inclusions. By comparing these two designs, they showed that a three-component periodic foundation can generate useful band gaps for seismic vibration isolation. Furthermore, they concluded that the reinforcement of the concrete matrix has a negligible influence on the band gaps. However, it is important to underline the two-dimensional nature of their proposed designs, which would have to be improved for an omnidirectional wave. Another 2D approach was studied by [26], while a three-dimensional (3D) approach for a phononic crystal-based structure was proposed by [64]. The latter design showed the possibility for a 3D foundation to generate stop bands in the low frequency region. Furthermore, they carried out a parametric study on the structural components and their influence on the band gaps. The mass of the resonator core, the thickness of the rubber coating as well as the stiffness of the rubber have proven to be of special importance for the frequency range of the stop bands. In order to validate the

effects of stop bands in periodic structures, [65] conducted field experiments on scaled 2D periodic foundations. The comparison between experimental outcomes and numerical results showed that periodic foundations are able to mitigate seismic waves. Furthermore, they found good agreement between experimental tests and dispersion analysis. The work by [66] provides additional insight on filtering waves propagating through a foundation made of inertial resonators. The recent work by [67] has addressed the suppression of vibrations in fuel tanks via specially tuned systems of many multi-scale resonators attached to the tanks. In the present paper, we introduce a smart foundation based on metamaterial concepts that can both attenuate seismic waves and withstand static loads. More precisely, the foundation is capable of attenuating waves in targeted frequency ranges. In our analyses, we are particularly interested in the influence that both geometrical and mechanical properties of a foundation inspired by phononic crystals can have on its dynamic performance as well as its capabilities of bearing gravity loads. In fact, for its practical use, it is of outmost importance to design a foundation that can both attenuate seismic waves and withstand static loads relevant to the coupled structure. Therefore, a broad fuel storage tank, which poses a significant threat to the community and the environment, was considered as a case study for the present design. The materials employed in the foundation are concrete and construction grade silicon, which are commonly used in construction industry. With regard to the design process of the foundation, an iterative procedure was employed. Given the critical frequency region of seismic vibrations for the structure of interest, a unit cell is designed with the aid of a frequency dispersion analysis to cover critical frequencies by means of a stop band. Then, a finite lattice structure is extracted from the infinite lattice of unit cells and is checked on its static behavior at the ultimate limit state [68]. Furthermore, the coupled (foundation+structure) system is numerically tested on its wave attenuation properties. Since the proposed smart foundation was still excessive in size, we also investigated an optimized design endowed with improved performance and reduced dimensions. Therefore, an analytical study was performed to derive the wave propagation properties of the design, while numerical simulations assessed its performance. Although the proposed design is still in an early research stage, it already shows a great potential in optimizing such a foundation. As pointed out by [33] in the analysis of the dynamic behavior of strongly damaged beams, cracks due to static loading can exert marked effects on band gap formation. For this reason, the influence of cracks on the dynamic properties of the proposed foundation is also investigated. Finally, Section 2.4 discusses main results, draws conclusions and future perspectives.

2.2 Materials and methods

From a dynamic viewpoint, broad tanks like the one under study can be thought of being composed of an impulsive mass that vibrates in phase with the tank walls at a higher frequency (e.g. 3-5 Hz) and a sloshing mass that vibrates not in phase with the tank walls at a lower frequency (i.e. about 0.3 Hz), [69]. The relevant eigenvalue analysis was carried out with the FE software Comsol Multiphysics (version 5.2). The smart foundation under study is conceived for the higher frequency, since sloshing frequencies can be easily suppressed or mitigated with baffles [70]. Therefore, the design of the unit cell focused on the first impulsive frequency of the fully filled tank, i.e. 4.05 Hz. In fact, this is the eigenfrequency with the largest participant mass in the radial direction. A horizontal excitation at this frequency results in both the largest stresses and accelerations in the tank walls, and thus governs the requirements for the seismic resilience. After disregarding sloshing frequencies, it was possible to model the liquid as an acoustic medium, as shown by [67] and [71]. This approach significantly reduced the computational cost of the model. As a result, in all forthcoming analyses the liquid inside the tank is assumed to have the same properties as water. The tank itself has a cylindrical shape with a radius, height, liquid height and wall thickness of 24 m, 16 m, 15 m and 20 mm, respectively. A steel plate with a thickness of 50 mm was used as bottom plate. In order to simulate the traditional foundation system, the whole tank was set on a 1 m thick concrete slab, as depicted in Figure 2.1(A). Moreover, a damping ratio of 5 % was imposed at both 3 Hz and 5 Hz by means of proportional Rayleigh damping on all FE models to hand [72]. Furthermore, an additional modal analysis has been carried out to determine the modal frequencies of the coupled (tank + smart foundation) system. The geometry of the proposed smart foundation is presented in Section 2.3 Results and is shown in Figure 2.1(B). In order to further improve the foundation performance in terms of geometry and dynamic properties, we conceived and analysed a new unit cell. The optimized design was modelled by means of shell and beam elements and the assembly is depicted in Figure 2.1(C). The relevant cell dimensions are shown in Figure 2.3(A) in Subsection 2.3.5.2, respectively. Since the fluid level height is not a constant parameter in a storage tank, the impulsive frequency of the structure changes accordingly. Thus, the variable fluid level results in a frequency region, which is considered governing the foundation design. Clearly, we take into account that the varying fluid level height will change the eigenfrequencies of the coupled foundation-tank system.

2.2.1 Floquet-Bloch theorem and Brillouin zone

Periodic structures can be designed in order to suppress the propagation of seismic waves in a certain frequency regions. These regions are called band

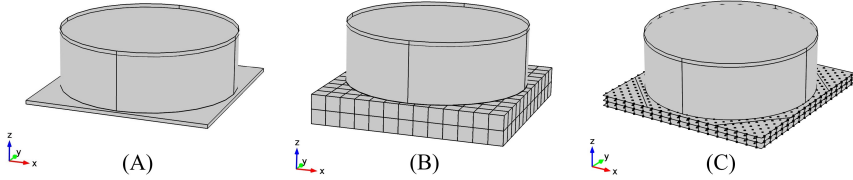


Figure 2.1: (A): Broad tank on a standard foundation; (B): Broad tank on a smart foundation; (C): Broad tank on a smart foundation with optimized unit cells.

gaps and can be determined with the Floquet-Bloch theorem [73]. This theorem reduces the study to an infinite lattice of unit cells to the analysis of a single unit cell with Floquet-Bloch quasi-periodicity conditions. After imposing these conditions, a frequency dispersion analysis can be carried out and the band gaps of the unit cell can be found as shown in Figure 2.5(B). In order to obtain the frequency dispersion diagram, we consider the equation of motion for an elastic medium in an Eulerian description,

$$\sum_{j=1}^3 \frac{\partial \sigma_{ij}}{\partial x_j} + F_i = \rho \frac{\partial^2 u_i}{\partial t^2} \quad (2.1)$$

where, the stress-strain relationship reads,

$$\sigma_{ij} = \mu(\mathbf{x}) \left(\frac{\partial u_i}{\partial x_j} + \frac{\partial u_j}{\partial x_i} \right) + \lambda(\mathbf{x}) \delta_{ij} \text{div}(\mathbf{u}(\mathbf{x})) \quad (2.2)$$

In particular, F_i ($i = 1, 2, 3$) are the components of the body force, ρ the mass density, $\mathbf{u}(\mathbf{x})$ displacement vector, $\mu(\mathbf{x})$ and $\lambda(\mathbf{x})$ Lamè constants, \mathbf{x} position vector and δ_{ij} the Kronecker delta function, respectively. Time t has been omitted for brevity. According to the Floquet-Bloch theorem the solution $\mathbf{u}(\mathbf{x}, t)$ for a periodic system can be expressed as,

$$u(\mathbf{x}, t) = \mathbf{u}_{\mathbf{k}} e^{i(\mathbf{q}\mathbf{x} - \omega t)} \quad (2.3)$$

where $q = [q_x, q_y, q_z]^T$ represents the wave vector in (2.3), while ω denotes the corresponding frequency in rad/s. As a consequence,

$$\mathbf{u}(\mathbf{x} + \mathbf{R}) = \mathbf{u}(\mathbf{x}) e^{i\mathbf{q}\mathbf{R}} \quad (2.4)$$

with R being the lattice vector. By imposing these boundary conditions on a system and solving the discrete eigenvalue problem of a typical cell, which takes on the following form,

$$(\mathbf{K} - \omega^2 \mathbf{M}) \mathbf{u} = 0 \quad (2.5)$$

it becomes possible to calculate the frequency dispersion curves. In Equation (2.5), \mathbf{K} and \mathbf{M} are the stiffness and mass matrix, respectively. The wave vector \mathbf{q} can be expressed in the reciprocal lattice. Due to the periodicity of the direct as well as the reciprocal lattice, it is possible to reduce the wave space to the first Brillouin zone [9]. Therefore, in order to find the desired band gaps of the frequency dispersion diagram, it is sufficient to calculate \mathbf{q} along the boundaries of this irreducible Brillouin zone [10]. For clarity, the Brillouin zone for the unit cell considered is depicted in the bottom left of Figure 2.5(A), where q_x , and q_y assume values between 0 and π , while remaining on the contour of the Brillouin zone.

2.2.2 Static analysis

For the unit cell to work properly as an element of the foundation, it is necessary to build a static system from the infinite lattice of unit cells. A two-layered grid of unit cells was chosen as a starting point for the foundation. Due to the cubical shape of the cells, it is easy to conceive a framework of walls and slabs suited for the derivation of the static loads. The dispersion analysis of the unit cell resulted in a 4 by 4 meters cube with an outer wall thickness of 10 cm, as shown in Subsection 2.3.2. When these cells are set adjacent to each other, the outer walls can be combined as a rectangular grid with a wall thickness of 20 cm and a spacing of 4 m. The same holds true for the slab between the two layers of unit cells, which results in a thickness of 20 cm for the intermediate slab, while the static analysis resulted in a slab thickness of 35 cm for the top slab. Figure 2.2 shows the conception of the static system and its dimensions. Details of the foundation are shown in the bottom right of Figure 2.2(A), where the increased top slab and the soil-structure interface are represented. For the present work, the soil was assumed to be bedrock, which allows the foundation to be sustained by line supports along the walls. Since the compression of the rubber, due to static loading, could influence the dynamic behavior of the system, the inner concrete cubes and the rubber coatings were considered as dead loads. A sketch of the FE model of the static system is shown in both Figure 2.2(B) and Figure 2.2(C). The calculation of both stresses and governing forces has been carried out with the FE software RFEM. All walls and slabs were modelled as shell elements with rigid connections to each other. The supports were modelled as simple line supports along the bottom edges of the walls. Once the static system was established, the loads of the tank, rubber and inner cubes were applied. The liquid was assumed to have the same density as water with a maximum liquid level of 15 m. The tank was modelled as a simple face load of 150 kN/m^2 and imposed on the foundation. A similar approach was chosen for the rubber and the inner concrete cubes. The weight of both the rubber and inner cubes corresponded to a total gravitational force of 1040 kN per cell. This force was then spread evenly across the slab

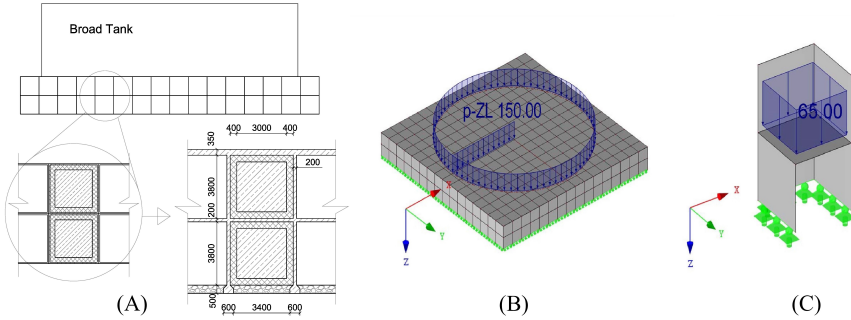


Figure 2.2: (A): Conception of a static system [Dimensions in mm]; (B): FE model of the foundation including the tank weight as a surface load [kN/m^2]; (C): two unit cells on line supports including the weights of the rubber and inner concrete cubes as surface loads [kN/m^2].

between the layers of unit cells, which resulted in a face load of $65 \text{ kN}/\text{m}^2$. In order to comply with Eurocode 0 [68] requirements for the ultimate limit state of the foundation, all dead loads (including gravitational forces of walls and slabs) were multiplied by the partial load safety coefficient $\gamma_G = 1.35$. Finally, all dimensions and steel reinforcements were checked according to the Eurocode 2 [74]. Shear walls were verified for their compressive strength, while the slabs were reinforced with steel rebars. With reference to the optimized unit cell design depicted in Figure 2.3(A), dimensions have been significantly reduced with respect to the original design. In particular, line moments decreased with the reduction of the span width by the power of two and the new slabs 200 mm thick suffice the Eurocode 2 [74] requirements. The columns of the optimized design need to be checked for their compressive strength. The relevant checks are presented in Subsection 2.3.3.

2.2.3 Materials

The first proposed model for the foundation consists of three components: the concrete resonator cubes, the rubber coatings and the reinforced concrete framework. For the concrete parts the strength grade was assumed to be C30/37 in agreement with Eurocode 2 [74], while the rubber was assumed to be construction grade silicon. Fuel storage tanks are commonly made of welded construction steel. For all FE models, the materials were considered homogeneous and linear elastic, and their main mechanical properties are collected in Table 2.1. The design of the optimized solution uses the same concrete as the original one, but replaces the rubber with steel springs as indicated in Figure 2.3(B). The spring stiffness k_2 has been tuned to provide a band gap with a lower bound at 2.4 Hz as discussed in Subsection 2.3.1.

Table 2.1: Mechanical properties of materials

Material [-]	Density [kg/m ³]	Elastic mod. [N/mm ²]	Bulk mod. [N/mm ²]	Possion [-]	Strength [N/mm ²]
Concrete	2500	30000	-	0.35	30
Rubber	1300	1.375	-	0.463	-
Steel	7860	210000	-	0.3	235
Liquid	1000	-	2200	-	-
Rebars	7860	195000	-	0.3	550

It was found that $k_2 = 3.7$ MN/m.

2.2.4 Functionality evaluation of the original design

Due to the finite dimensions of the original foundation and the necessary re-design for its static behaviour, the foundation can no longer be treated as an infinite lattice of perfectly equal unit cells. In order to determine the wave propagation properties, it is crucial to carry out additional computations, since the appearance of a stop-band in a finite structure is unrealistic. However, an attenuation zone is expected to appear in the frequency region of the predicted stop-band. In order to understand the behaviour of the finite structure, two models are investigated: i) the first model of the foundation does not include the tank; ii) the second one contains the complete system, including the tank and the fluid inside. The optimized design was carried out similarly and is described in Subsection 2.2.5. A horizontal harmonic acceleration was imposed at the bottom of the foundation. When comparing the response of the top of the foundation to the imposed wave, it becomes possible to show the effectiveness of the attenuation at a certain frequency. This results in a frequency response function of the type shown in Figure 2.8. The analysis was then carried out for a foundation with one, two and three layers. Furthermore, the foundation has also been analyzed with a thinner concrete wall thickness, in order to see whether the horizontal stiffness of the structure has an influence on the attenuation behavior. The FE model of the complete system, including foundation, tank and liquid as an acoustic medium, has 531684 DoFs. In order to minimize the computational effort due to the transient nature of seismic waves, all calculations were carried out in the frequency domain; accordingly, the steady-state response of the coupled system was checked for the frequencies of interest. In order to show the effectiveness of the attenuation, the steady state response of the broad tank on a traditional concrete slab foundation was compared to that of the tank sitting on the smart foundation. In particular, maximum accelerations of the uncoupled/coupled system were considered to be of special interest,

since they correlate with the highest stresses appearing in the system.

2.2.5 Optimization of the unit cell

In order to reduce the foundation’s size while maintaining its performance, the foundation was redesigned according to the results obtained in the Subsection 2.3.4 “Functionality evaluation”. We found that: i) the shear stiffness plays an important role for the effectiveness of the foundation, see Figure 2.8; ii) the rubber, due to its fixed Elastic Modulus, constrains our design in terms of variability of the band gap. The two main advantages of the redesign are the reduction in stiffness, by replacing the walls with columns, and attaching the resonators to the columns with steel springs instead of rubber as indicated in Figure 2.3(B). As evident from Figure 2.8, the reduction of stiffness leads to a more pronounced attenuation zone, while the steel springs provide the option of tuning the boundaries of the unit cell’s band gap. As a result, see Figure 2.3(A), the new dimensions of the unit cell are 3x3x1.5 m, 0.3x0.3 m column thickness, 0.2 m slab thickness and 2.5x2.5x1 m resonator size. Note that due to the reduction of the overall stiffness of the coupled system, the first impulsive frequency observed, decreased to 2.4 Hz, see Table 2.2, and, therefore, a band gap has to be tuned to this lower frequency. Furthermore, we assumed that the resonators move on a frictionless surface in the horizontal direction. This is a necessary assumption in order to keep the calculations linear for the frequency domain analysis. The functionality evaluation of the optimized design followed the same steps presented in Subsection 2.3.4. However, in contrast to the model of the original design, the optimized cell variant was discretized with beam and shell elements, which further reduced the computational effort.

2.2.5.1 Analytical model of the optimized design

In order to investigate the metamaterial-like properties of the new design, we conceived an analytical model of the foundation and calculated both the frequency response and the dispersion analysis of unit cells. The main dimensions of the unit cell, the horizontal shear model and the 1D MDoF system are depicted in Figure 2.3(A), (B), and (C), respectively. This model allows only shear type waves that act in the horizontal and propagate in the vertical direction. As can be seen in Figure 2.3(C), the j^{th} unit cell can be repeated in order to achieve as many layers as desired. The equations of motion read,

$$m_1^j \frac{d^2 u_1^j}{dt^2} - k_1 u_1^{j-1} + k_1 u_1^j + k_2 u_1^j + k_1 u_1^j - k_2 u_2^j - k_1 u_1^{j+1} = 0 \quad (2.6)$$

2. CONCEPTION OF THE METAFUNDATION

and,

$$m_2^j \frac{d^2 u_2^j}{dt^2} - k_2 u_1^j + k_2 u_2^j = 0 \quad (2.7)$$

where, m_1 denotes the mass of a slab between two layers of foundation including half the columns of the layer below and half the columns of the layer above; m_2 denotes the mass of the resonator; k_1 denotes the horizontal stiffness of two columns, which represents the equivalent stiffness of the columns pertaining to each resonator; k_2 represents the equivalent stiffness of the steel springs holding the resonator; and u describes the horizontal displacement. In order to relate the state variables across the system, the equations of motion must contain the displacement of the $j-1^{\text{th}}$ and $j+1^{\text{th}}$ unit cell. Therefore, u is endowed with a subscript (1, 2) that describes the corresponding mass, while the unit cell is determined by the superscript ($j-1, j, j+1$). For a finite system these equations can be written in matrix form. The generalized stiffness and mass matrix for a system with n unit cells reads,

$$\mathbf{K} = \left[\begin{array}{c|cccccccc} 1 & k_1 + k_2 + k_1 & -k_2 & -k_1 & \cdots & & & \\ 2 & -k_2 & k_2 & 0 & \cdots & & & \\ \vdots & \vdots & \vdots & \ddots & & & & \\ j^{th} & & -k_1 & 0 & k_1 + k_2 + k_1 & -k_2 & -k_1 & \cdots \\ j^{th} & & \vdots & \vdots & -k_2 & k_2 & 0 & \cdots \\ \vdots & & & & \vdots & \vdots & \ddots & \\ n^{th} & & & & & -k_1 & 0 & k_1 + k_2 & -k_2 \\ n^{th} & & & & & & -k_2 & k_2 \end{array} \right] \quad (2.8)$$

$$\mathbf{M} = \left[\begin{array}{c|cccccccc} 1 & m_1 & & \cdots & & & & \\ 2 & & m_2 & \cdots & & & & \\ \vdots & \vdots & \vdots & \ddots & & & & \\ j^{th} & & & & m_1 & & \cdots & \\ j^{th} & & & & & m_2 & \cdots & \\ \vdots & & & & \vdots & \vdots & \ddots & \\ n^{th} & & & & & & & m_1 \\ n^{th} & & & & & & & & m_2 \end{array} \right] \quad (2.9)$$

The relevant dispersion relation of the system can be found by imposing the Floquet-Bloch boundary conditions (2.3) on the equations (2.6) and (2.7), imposing a time-harmonic solution and looking for non-trivial solutions. The

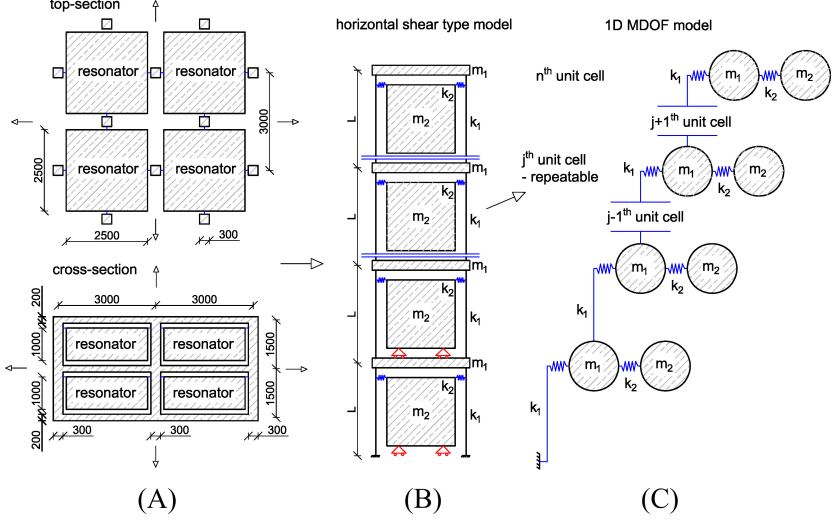


Figure 2.3: (A): Top-section and cross-section of the optimized foundation; (B): Simplified model for shear-wave propagation; (C): 1D mass-resonator chain model.

dispersion relation is given by,

$$m_1 m_2 \omega^4 - [(m_1 + m_2) k_2 + 2m_2 k_1 (1 - \cos(qL))] \omega^2 + 2k_1 k_2 (1 - \cos(qL)) = 0 \quad (2.10)$$

A similar solution has been found by [75], who analyzed the negative effective mass effect in an acoustic metamaterial. Here, ω denotes the circular frequency; L the length of the column or height of one layer; and q the wave number with dimension $1/m$. The values for m_1 , m_2 , k_1 , k_2 , and L are 5850 kg, 15625 kg, $12e7$ N/m, $3.6e6$ N/m, and 1.5 m, respectively. In order to compare the results provided by the numerical models, also quantitatively, damping ratios of 1, 3, and 5 % were imposed to 3 and 5 Hz by means of a Rayleigh model. Furthermore, a model with 1, 2, and 3 layers with damping of 5 % between 3 and 5 Hz was analysed too.

Table 2.2: First impulsive eigenfrequency of broad-tank-foundation systems with various liquid heights

Foundation type	Liquid level [m]	Imp. freq. of tank [Hz]
Traditional	15	4.15
	12	4.95
Smart	15	3.95
	12	4.80
Optimized	15	2.40
	12	3.70

2.3 Results

2.3.1 Modal analysis of a coupled broad-tank-foundation system

The analysed broad tank with the maximum fluid level of 15 m anchored to a standard foundation has its first impulsive frequency at 4.15 Hz. On the other hand, for the same tank on the proposed smart foundation, the first impulsive frequency appears at 3.95 Hz. The corresponding impulsive mode shapes for the two foundation typologies are shown in Figure 2.4(A) and (B), respectively. The coupled system obtained from the optimized design exhibits its first impulsive frequency at 2.4 Hz and is depicted in Figure 2.4(C). It is apparent that the impulsive frequency for a tank on the smart foundation is lower than for one on a standard foundation, and decreases even further for the optimized design. The impulsive frequency of the structure increases as the fluid level decreases. For this reason, the tank with a liquid level of 12 m was also studied. Relevant outcomes of the modal analysis for the two tank configurations are reported in Table 2.2. On the basis of these results, a frequency region that covers both frequencies for each tank would be desirable. Due to the fact that the fluid level can drop below 12 m, band gaps that stretch even beyond the increased impulsive frequency of the 12 m fluid level constellation were chosen for all the designs. For the standard tank this resulted in an aspired frequency region between 3.5 Hz and 6 Hz, while the optimized design was aimed at a frequency range between 2.40 Hz and 4.5 Hz.

2.3.2 Unit cell design of the original smart foundation

The unit cell was studied as a 2D problem in Comsol Multiphysics. When applying the Floquet Bloch boundary conditions introduced in Subsection 2.2.1, the dispersion relation can be obtained by calculating the eigenfrequencies of the system for different values of the wave vector q . Therefore,

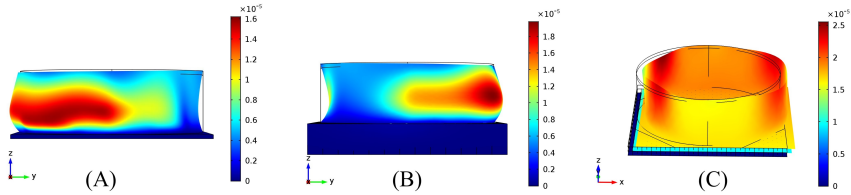


Figure 2.4: (A): first impulsive mode at 4.15 Hz for a broad tank on a traditional foundation; (B): first impulsive mode of a broad tank on the proposed smart foundation at 3.95 Hz; (C): first impulsive mode at 2.4 Hz for a broad tank on the optimized foundation.

it is sufficient to calculate the eigenfrequencies along the boundaries of the Brillouin zone, depicted for clarity, in the bottom left of Figure 2.5(A). Here, T, X, M mark the corners of the Brillouin zone, while bz denotes the edge length, which amounts to $\pi/a = 0.7854$ 1/m, where a defines the size of the unit cell. Our parametric study shows that a unit cell with side length, outer wall thickness, rubber coating and inner concrete cube size equal to 4 m, 0.1 m, 0.4 m and 3 m, respectively, see Figure 2.5 (A), creates a band gap with a lower bound of 3.5 Hz and an upper bound of 6.4 Hz as highlighted in Figure 2.5(B). By looking at the results in Table 2.2, this configuration represents the optimal design to reduce tank vibrations in the frequency range where waves can cause the greatest damage. Note that the shear wave velocity is very close to the pressure wave velocity for the diagonal path M to T of the Brillouin zone. Therefore, the shear wave branch is almost coincident with the pressure wave branch in both Figure 2.5(B) and 2.12(B). The effectiveness of the proposed solution in the low frequency range is in line with the results presented by Achaoui et al. [66], who proposed iron spherical resonators endowed with ligaments embedded in soil. However, the actual feasibility of their interesting design proposal has yet to be investigated.

2.3.3 Static analysis

Three essential components have to be verified under static loads for the original design: the top slab, the walls and the intermediate slab. When the system is subjected only to static loads, the walls need to resist only compressive stresses. According to Eurocode 2 [74], it is sufficient to verify that the compressive stress is lower than the design strength of concrete. As stated in Section 2.2.3 Materials, a strength grade of C30/37 was assumed. Since the maximum stress of 3.6 N/mm² shown in Figure 2.6(A) is below the design strength of 20 N/mm², the walls are checked for gravity loads. The slabs, on the other hand, need to sustain the flexural moments produced by static loads. This results in tension regions in the concrete matrix, see

2. CONCEPTION OF THE METAFUNDATION

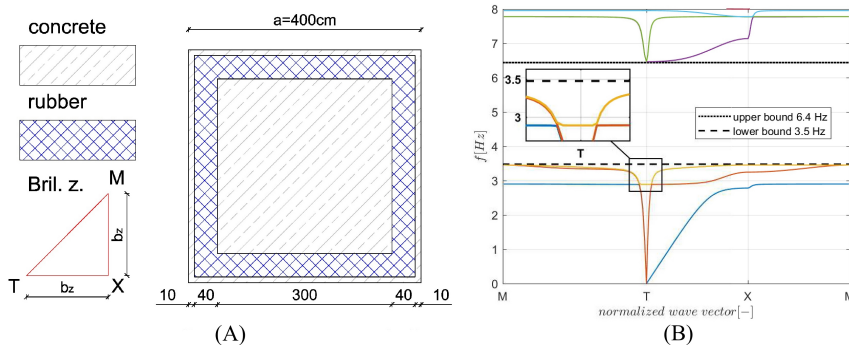


Figure 2.5: (A): The unit cell and its Brillouin zone (dimensions in cm); (B): Dispersion analysis of the unit cell.

Figure 2.6(B), which need to be reinforced in order to offer sufficient load-bearing capacity. Additionally, for corrosion protection a minimum concrete cover of the reinforcement bars is needed. Since the present work considers a general case, the concrete cover was chosen to be 5 cm, which satisfies most exposition classes mentioned in Eurocode 2 [74]. Given the negative line moment of -164.84 kNm/m at the ultimate limit state in the top slab above the walls, see Figure 2.6(B), the final chosen dimensions are 35 cm for the plate thickness and $12.12\text{ cm}^2/\text{m}$ for the reinforcements depicted in Figure 2.7(A) top left. A grid of 8 rebars with a diameter of 14 mm is sufficient for this part of design. Due to the symmetry of the system, the moments are the same in x and y direction. Therefore, the selected grid has to be set in both directions. The lower layer of reinforcements needs to cover a maximum moment of 75.22 kNm/m in the slab, which results in a minimum reinforcement area of $5.39\text{ cm}^2/\text{m}$ indicated in Figure 2.7(B) top right. A grid of 11 reinforcement bars per meter with a diameter of 8 mm fulfills the requirement.

The intermediate slab shows bending moments of -76.63 kNm/m above the walls and 31.97 kNm/m in the fields. When setting the slab thickness to 20 cm, the necessary reinforcement has to be $11.89\text{ cm}^2/\text{m}$ for the top layer, see Figure 2.7(C) bottom left, and $4.64\text{ cm}^2/\text{m}$ for the lower layer of reinforcements, look at Figure 2.7(D) bottom right. Thus, the same reinforcement grid chosen for the top slab was also sufficient for the intermediate slab.

The preliminary static evaluation of the optimized cell has been carried out as before. For the sake of brevity, only the design of columns is presented, while the remaining checks have been omitted. More precisely, the compressive concrete stresses in the columns of dimension $0.3\times 0.3\text{ m}$ amount to 18 N/mm^2 . This figure must be compared with a design strength of 20

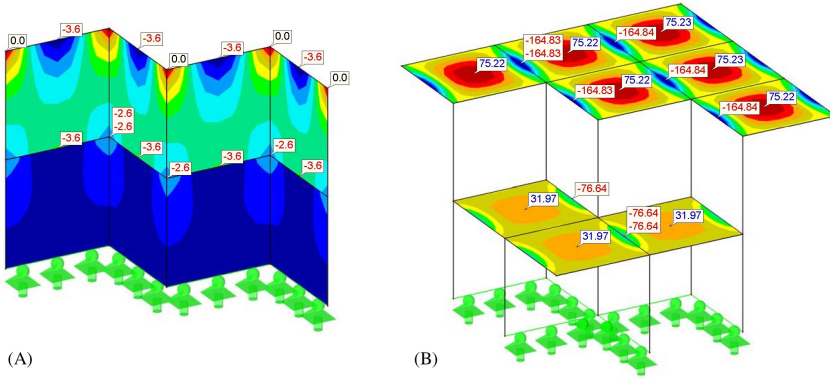


Figure 2.6: (A): compressive stresses in the walls at the ultimate limit state [N/mm²]; (B): line bending moments in slabs at the ultimate limit state [kNm/m].

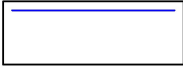
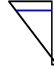
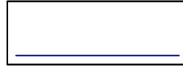
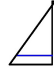
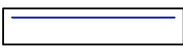
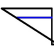
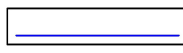
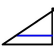
<p>Top Slab Wall</p> <p>As=12.12 cm²</p>  <p>(A)</p>	<p>Strain</p> <p>$\epsilon_s=2\%$</p>  <p>$\epsilon_c=-0.288\%$</p>	<p>Top Slab Field</p> <p>As=5.39 cm²</p>  <p>(B)</p>	<p>Strain</p> <p>$\epsilon_c=-0.159\%$</p>  <p>$\epsilon_s=2\%$</p>
<p>Interm. Slab Wall</p> <p>As=11.89 cm²</p>  <p>(C)</p>	<p>Strain</p> <p>$\epsilon_s=1.145\%$</p>  <p>$\epsilon_c=-0.35\%$</p>	<p>Interm. Slab Field</p> <p>As=4.64 cm²</p>  <p>(D)</p>	<p>Strain</p> <p>$\epsilon_c=-0.232\%$</p>  <p>$\epsilon_s=2\%$</p>

Figure 2.7: (A): compressive stresses in the walls at the ultimate limit state [N/mm²]; (B): line bending moments in slabs at the ultimate limit state [kNm/m].

N/mm² and, therefore, the optimized design is statically valid.

2.3.4 Functionality evaluation

The frequency response function at the top of the foundation for a sinusoidal excitation of amplitude 1 m/s², plotted in Figure 2.8, shows a clear attenuation zone in the frequency region from 3.5 Hz to 6.4 Hz. In this frequency region, a reader can observe that the acceleration output at the top of the foundation is smaller than the input at its bottom. An amplification area appears in the frequency region below 3.5 Hz, which is not relevant for the seismic protection of the tank. Furthermore, the influence of the number

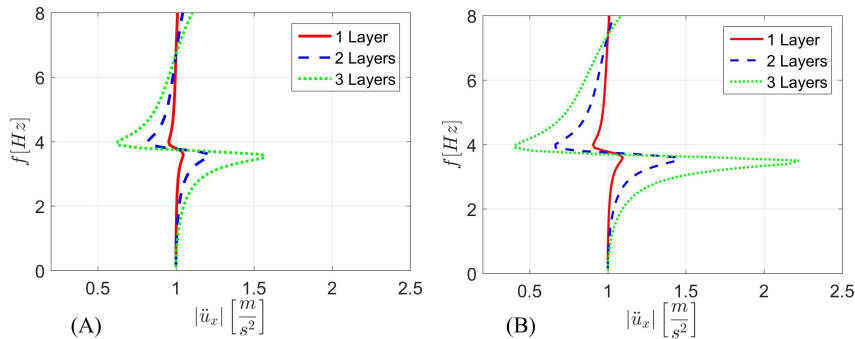


Figure 2.8: (A): acceleration response at the top of the foundation with a wall thickness of 20 cm; (B): acceleration response with a wall thickness of 10 cm.

of unit cell layers has been studied. The diagrams of Figure 2.8 show that the number of layers is clearly connected to the attenuation effectiveness. Moreover, the effectiveness of another model with a decreased concrete wall thickness from 20 cm to 10 cm has been evaluated. The comparison of Figure 2.8(A) with Figure 2.8(B) highlights that a smaller wall thickness enhances the attenuation behaviour and increases the intensity of the amplification area.

In order to compare foundation typologies, the response of the complete coupled (foundation+tank) system has been studied. The model is depicted in Figure 2.1(B) and was analyzed with a concrete wall thickness both of 20 cm and 10 cm. For the sake of brevity, only the results corresponding to the wall thickness of 10 cm are reported herein, due to its increased effectiveness. Since the maximum acceleration does not appear at the top of the tank, the maximum acceleration along the full height of the tank wall was plotted. The comparison in terms of maximum acceleration in the frequency domain between the smart and a traditional foundation is shown in Figure 2.9(A); the attenuation and advantages of using the smart foundation become clearly visible. Finally, the analysis of the tank with a fluid level of 12 m has been performed. Relevant outcomes in terms of accelerations are reported in Figure 2.9(B). A careful reader can note that the attenuation due to the smart foundation is still clear but less pronounced than in the case of a fully filled tank.

2.3.5 Results for the optimized unit cell

2.3.5.1 Numerical analysis of the optimized cell

Based on the results obtained for the original foundation design and in order to further reduce the horizontal stiffness, we investigated an optimized design

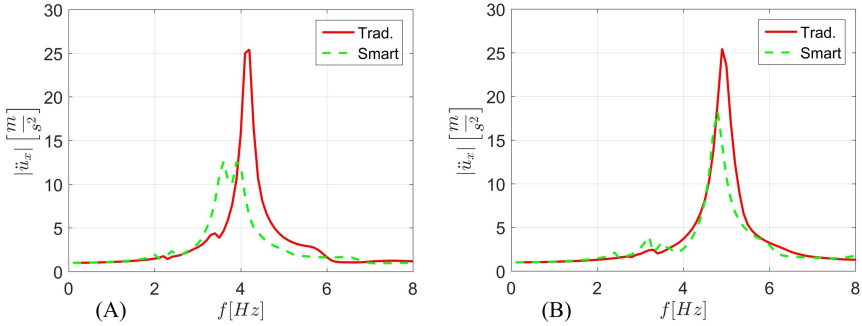


Figure 2.9: (A): maximum acceleration response function of the tank wall for traditional and smart foundation; (B): acceleration responses for a tank with a reduced liquid height of 12 m.

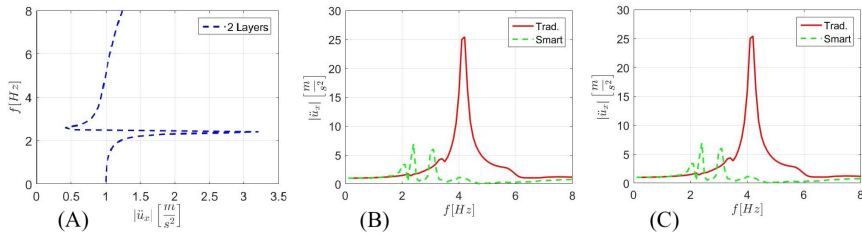


Figure 2.10: (A): Frequency response function of the optimized foundation alone subjected to a base acceleration of 1 m/s^2 ; (B): Tank response for a fully filled tank, on the optimized foundation, for a base acceleration of 1 m/s^2 ; (C): Tank response with a liquid level of 12 m, on the optimized foundation, for a base acceleration of 1 m/s^2 .

that employs columns instead of shear walls. When observing Figure 2.10(A) in contrast to both Figure 2.8(A) and Figure 2.8(B), it becomes evident that the performance of the foundation improves significantly due to the column design. The results shown in Figure 2.10(A) can also be compared to the analytical solution of Subsection 2.3.5 and the same conclusion holds. As done in Subsection 2.3.4, we also analyzed the coupled system in terms of frequency response function for a base-excitation of 1 m/s^2 . Figure 2.10(B) shows the results of the analysis of a full tank and Figure 2.10(C) depicts the results for a tank with a liquid level of 12 m. It is apparent that in both cases the proposed isolation system can reduce vibrations in the tank significantly, in particular when the tank is totally filled with fluid and, hence, when seismic loads can produce the most severe damage.

2.3.5.2 Analytical model of the optimized cell

In order to ascertain the results of our numerical study, we carried out various calculations on the analytical model introduced in Subsection 2.3.5.2. Firstly, we performed a frequency response analysis on the model with 1, 5, and 25 layers. Also in this case, a base excitation \ddot{u}_{in} of amplitude 1 m/s^2 was selected and compared to the output \ddot{u}_{out} at the top of the foundation. As shown in Figure 2.11(A), the foundation exhibits a distinctive attenuation zone that increases with the amount of layers. This calculation was carried out without damping and is depicted in decibel dB ($20 * \log(\ddot{u}_{out}/\ddot{u}_{in})$). Furthermore, we were interested whether a dispersion analysis of the system would yield a band gap in the predicted attenuation zone. Figure 2.11(B) shows the dispersion relation and the corresponding band gap of an infinite stack of unit cells, calculated with (2.10). In order to check how well the analytical model represents the numerical one and whether the analytical model can be used for further optimization investigations, we also conducted calculations on a damped system. Relevant results are shown in Figure 2.11(C) and 2.11(D) for Rayleigh damping of 1, 3, and 5 % imposed to both 3 Hz and 5 Hz. Moreover, an analytical study on the damped system (5 % of Rayleigh damping for both 3 Hz and 5 Hz) with a variation of the layers is reported in Figure 2.11(D). Relevant results are discussed in Section 2.4.

2.3.6 Influence of small cracks

In order to assess the influence of small cracks on elastic wave propagation, a cracked cell of the smart foundation was investigated. In fact, as shown in Figure 2.6(B) of Subsection 2.3.3, the maximum bending moment is located where the slabs join the walls. Due to the resulting tension in concrete, small cracks appear in the area close to the internal boundaries of the walls. Therefore, the cracks were modeled as 5 cm-deep and 1 cm-wide physical gaps with no stiffness as indicated Figure 2.12 (A). This was considered a conservative approach, since the presence of reinforcement bars was neglected in the cracks. In particular, two adjacent cubes along the vertical direction were endowed with small cracks and modeled in Comsol imposing Floquet-Bloch conditions. The relevant dispersion analysis, shown in Figure 2.12 (B), must be compared to the results depicted in Figure 2.5(B) that corresponds to the uncracked unit cell. The comparison shows that the presence of small cracks slightly modifies the group velocity of propagating elastic waves.

2.4 Discussion

In Subsection 2.3.2, we showed the dispersion relation of a unit cell that suits the needs for the isolation of a broad tank introduced in Subsection 2.3.1, with the first foundation design. Based on this unit cell, we designed a

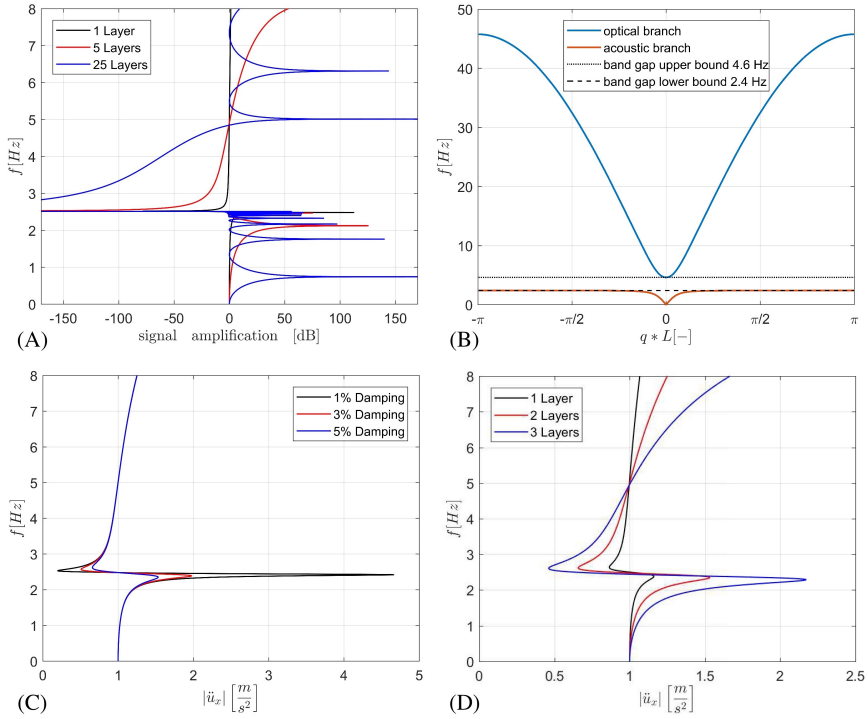


Figure 2.11: (A): Undamped frequency response function for 1, 5, and 25 layers of foundation for a base excitation of 1 m/s^2 ; (B): Dispersion relations for the optimized unit cell; (C): Frequency response function of the analytical model for two layers and Rayleigh damping of 1, 3, and 5 %; (D): Frequency response function of the analytical model with 5 % Rayleigh damping and 1, 2, and 3 layers.

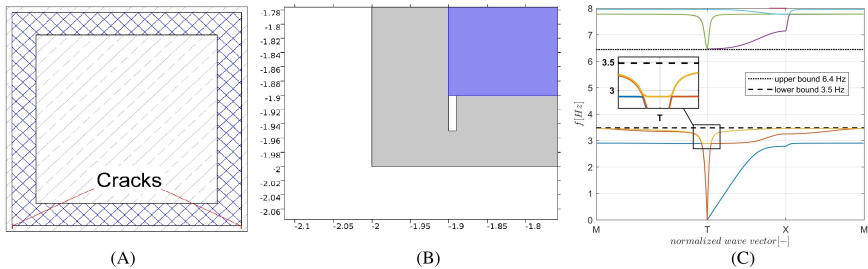


Figure 2.12: (A): Position of cracks in the unit cell; (B): Crack modeled as a physical gap in the slabs due to static loads (dimensions in m); (C): Dispersion analysis of the cracked foundation sector.

foundation and checked its static and dynamic properties in Subsection 2.3.3 and 2.3.4, respectively. The static analysis proved that the design is feasible, while the functionality evaluation showed that the metamaterial concept is applicable even for a finite foundation. The construction practice is assumed to be in situ for the present study. Furthermore, the first design of the foundation was rather excessive in size and needed to be reduced. Based on the functionality evaluation, where in Subsection 2.3.4 we found a correlation between the shear stiffness of foundation walls and the attenuation effectiveness, we introduced a new design that improves the isolation performance of the foundation and reduces its size. The optimized design includes columns instead of walls, in order to reduce its shear stiffness, and replaces the rubber with uniaxial steel springs, which make the structure more versatile. The new design discussed in Subsection 2.3.5 showed promising results by steady state analyses with a reduction of the foundation from 8 m to 3 m in height, while improving its performance. Besides this, we verified the results with an analytical model that returned very similar outcomes compared to numerical calculations and showed that the new design still exhibits band gaps. The small discrepancy between the results with the damped analytical model shown in Figure 2.11(C) and 2.11(D) and those of the numerical model presented in Figure 2.10(A) are mainly due to the difference between the two models, continuous and discrete, as well as the consequences of the imposed Rayleigh damping.

2.4.1 Conclusion

In order to check the feasibility of a metamaterial-based foundation for seismic application we conceived a smart foundation that was also designed and checked for gravity loads. As a result, we found that such a structure can be realized in accordance with the Eurocode standards while maintaining favorable band-gap like properties against seismic waves. In particular, we designed two versions of the smart foundation bearing a fuel storage tank with a varying fluid level and we showed that the proposed designs can attenuate the resulting frequency range. In addition, we found that the shear stiffness of the foundation due to lateral concrete walls has a significant impact on the attenuation efficiency, and, subsequently, we proposed an optimized design where the walls were replaced with less stiff concrete columns. Though the proposed smart foundation was able to attenuate the impulsive frequencies of the fuel storage tank under different liquid levels, it cannot yet be considered as a fully optimized solution. In particular, the dynamic behavior of the system with other liquid levels needs to be investigated, as well as the performance of the coupled system under several seismic waves. Finally, given the main drawback of standard isolators, i.e. the inherent high vertical stiffness, we expect that the use of the investigated foundation for large structures characterized by rocking motion can reveal great innovative

potential and undiscovered advantages.

Upcoming developments Since fuel storage tanks are typically connected to pipeline systems and can exert varying fluid levels, the next chapter treats the coupled tank foundation system in an experimental set-up. Furthermore, the efficiency of the foundation for varying fluid levels will be elaborated through various numerical studies in the frequency domain.

Chapter 3

Metafoundation development and Experimental Study on a coupled Pipeline

Overview. The recent advance of seismic metamaterials has led to various concepts for the attenuation of seismic waves, one of them being the locally resonant metamaterial. Based on this concept, the so-called metafoundation has been designed. It can effectively protect a fuel storage tank from ground motions at various fluid levels. In order to show the effectiveness of the proposed design, the response of the metafoundation is compared to the response of a tank on a traditional concrete foundation. The design process of conceiving the metafoundation, optimizing it for a specific tank, and its seismic response are described herein. Furthermore, the response of a tank during a seismic event can cause severe damages to pipelines connected to the tank. This phenomenon can be of critical importance for the design of a seismic tank protection system and must be treated with care. Since the coupled structure (tank + foundation + pipeline) exerts highly nonlinear behaviour, due to the complexity of the piping system, a laboratory experiment has been conducted. More precisely, a hybrid simulation (HS) that uses the metafoundation and a tank as a numerical substructure (NS) and a piping system as a physical substructure (PS) was employed. To make the results relatable to the current state of the art, additional experiments were performed with concave sliding bearings (CSBs) as an isolation system in the NS. The metafoundation offered a clear attenuation of tank stresses and, in some cases, also reduced the stresses in the piping system.

3.1 Introduction

Natural hazards such as earthquakes can cause significant damages to the environment and the community. Of special interest to many studies on natural hazards are NaTech events (natural technological events) [43, 44, 76], which can be caused by the interaction of a seismic incident with the failure of critical technical components. These events include loss of containment (LOC) of fuel storage tanks, pipelines, and other components of, e.g., petrochemical plants and nuclear power plants. LOC events of such critical infrastructures need to be avoided at the highest priority, as past NaTech disasters have displayed their potential in causing substantial damage to the community and the environment [37, 40]. In order to protect structures from seismic effects, various strategies have found application in the field of earthquake engineering. The standard form of seismic isolation uses lead-rubber bearings [50] or spherical bearing devices [77]. This type of seismic protection is able to isolate a structure of interest from the ground motion, and hence, reduce the stresses appearing in the structure induced by seismic waves at a wide range of frequencies. It has been shown by Jadhav and Jangid [78] that these types of isolation devices can effectively reduce the stresses in fuel storage tanks. In this work, we investigate a new type of seismic protection based on metamaterial concepts that may offer an alternative to classical isolators in the future. Many different types of metamaterials exist with interesting wave propagation properties for elastic as well as optical waves [1]. Only recently it has been discovered that a particular type of metamaterial, namely, phononic crystals, may be feasible to construct at a reasonable size for the isolation of structures against seismic waves. These phononic crystals exhibit so-called band gaps that prohibit waves from propagating through the material when their frequency falls within that gap [7]. Several studies tried to harvest this property for the design of a foundation for the seismic isolation of a superstructure, but none have taken the feedback coming from the structure into account [25–27, 63, 65]. In this work, a foundation is developed and optimized, based on the aforementioned concept, for the dynamic protection of a fuel storage tank, while considering realistic feedback from a superstructure. The developed system shows promising results for the reduction of the demand on the tank in the frequency and time domain and will be referred to as metafoundation. Furthermore, this work evaluates the effect that the proposed foundation may have on a connected piping system and compares the system to a system endowed with classical isolators. Due to the high nonlinearity of the studied piping system, the evaluation has been carried out under the aid of a hybrid simulation (HS), which can capture the interaction of the coupled system in a realistic manner [79, 80]. In particular, the piping system will be constructed in a laboratory as the physical substructure (PS) of the system, while the tank and the foundation are modeled as numerical substructures (NSs) that are coupled to the

Table 3.1: Material parameters

Material [-]	Density [kg/m ³]	Elastic mod. [N/mm ²]	Bulk mod. [N/mm ²]	Possion [-]	Strength [N/mm ²]
Concrete	2500	30000	-	0.35	30
Steel	7860	210000	-	0.3	235
Liquid	1000	-	2200	-	-
Steel	7860	210000	-	0.3	355

experimental setup. In summary, the metafoundation reduces stresses in a tank as a superstructure, while exhibiting a similar demand as a standard isolator on a connected piping system.

3.2 Design of the Foundation

3.2.1 Materials

The metafoundation consists of two components, namely, the structural matrix and the internal resonators. Both parts are made of concrete of strength grade C30/37 with material parameters given by Eurocode 2 [74] and are connected to each other with ideal steel springs. Furthermore, a fuel storage tank was chosen as a superstructure for the system and is considered to be made of common welded construction steel with a strength grade of S235. For the laboratory experiments, a welded piping system with a strength grade of S355 and a yield strain limit at 0.2% has been used. Table 3.1 shows the material parameters for density, elastic modulus, bulk modulus, Poisson ratio, and yield strength, for all components used in this work. Note that linear elasticity was assumed for all calculations.

3.2.2 Fuel storage tank modelling

Fuel storage tanks can be reduced to two fundamental modes, which are the impulsive and the convective mode. More precisely, the impulsive mode represents that part of the liquid that resonates in phase with the tank walls and appears to move mainly in the horizontal direction, while the convective mode embodies the sloshing motion of the liquid and moves mainly in the vertical direction. A simplified procedure for the modelling of storage tanks has been proposed by Malhotra et al. [69], where the tank is reduced to these two main modes under the aid of design coefficients dependent on the height to radius ratio. When applying the equations below to typical fuel storage tanks, it can be found that the impulsive frequency is commonly situated between 3 and 7 Hz, while the convective mode embodies a much

3. METAFUNDATION DEVELOPMENT AND EXPERIMENTAL STUDY ON A COUPLED PIPELINE

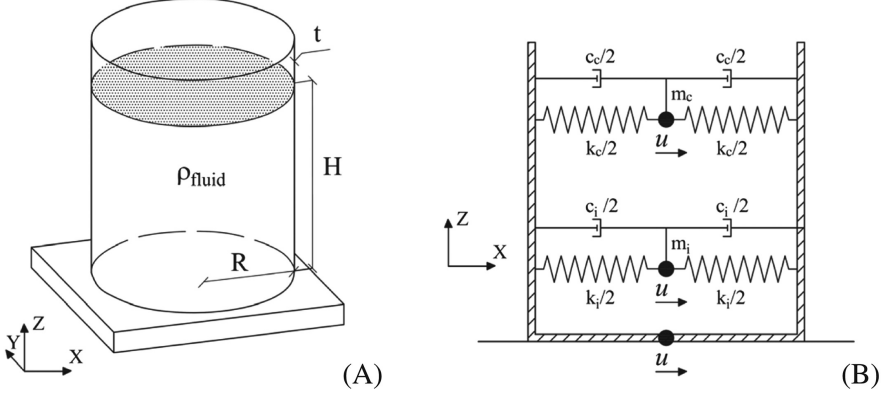


Figure 3.1: Modeling of a fuel storage tank: (A) drawing of a generic fuel storage tank; (B) representation of a fuel storage tank with two S-DOFs for the impulsive and convective modes (figure from [69])

lower frequency around 0.3 Hz. However, for the tank under investigation, the impulsive mode takes up a value of 6.84 Hz, while the sloshing mode resonates at 0.338 Hz. Figure 3.1(A) displays a sketch of storage tank with H and R denominating the height and radius of the tank, respectively. The two single degree of freedom point masses (S-DOFs) that simulate the impulsive and convective modes are denoted with the subscript i , and c , respectively, and can be seen in Figure 3.1 (B). Here, they are connected to a rigid frame that contains the remaining mass of the tank.

According to the procedure proposed by Malhotra et al. [69] the vibration periods of the impulsive and convective mode T_i and T_c , and modal masses m_i and m_c can be calculated with,

$$T_i = C_i H \sqrt{\frac{\rho R}{Et}}, \quad T_c = C_c \sqrt{R} \quad (3.1)$$

$$m_i = \gamma_i m_l, \quad m_c = \gamma_c m_l \quad (3.2)$$

here, i and c are describing the impulsive and convective mode, while E , ρ , and m_l denote the elastic modulus of the tank wall, the density of the liquid, and the total mass of the liquid, respectively. The parameters C_i , and C_c , are empirical parameters while γ_i and γ_c are the ratios between the impulsive and convective mass, m_i and m_c , with respect to the total liquid mass m_l . All of these parameters are given by Malhotra et al. [69] and are dependent on to the slenderness of the tank H/R . Note that t is the thickness of the tank wall. Based on these values the stiffness coefficients

can be evaluated as,

$$k_i = m_i \left(\frac{2\pi}{T_i} \right)^2, \quad k_c = m_c \left(\frac{2\pi}{T_c} \right)^2 \quad (3.3)$$

It has been shown by Belakroum et al. [70] and Maleki and Ziyaeifar [81] how baffles can increase the damping of the convective mode. Due to the possibility of using such baffles against resonance in the convective mode and the fact that the impulsive mode contains the highest participant mass, especially for slender tanks, the metafoundation has been designed for the attenuation of the impulsive mode solely. Furthermore, a storage tank can experience varying fluid levels, thus, increasing its impulsive frequency with a decrease in fluid height. In order to address this peculiarity, the band gap like properties of a locally resonant metamaterial are exploited. By tuning the lower bound of the band gap to the frequency of the full tank and the upper bound to a frequency a bit higher than the impulsive frequency of a $3/4$ filled tank, an attenuation of both frequencies can be achieved. From here onward, the tank with the full liquid height of 12 m shall be referred to as slender tank full (STF), while the tank with a liquid height of 9 m shall be referred to as slender tank not full (STnF). As mentioned in the Introduction section, it is necessary to take the feedback from the superstructure into account. One of the major impacts that this feedback has is the alteration of the modes of the tank. Due to the softening of the overall dynamic system for the coupled case, the new eigenfrequency, at which the impulsive mode gets excited most, appears to be smaller than for the tank alone. For all analyses in this work, a tank with height H , radius R , and tank wall thickness t of 12 m, 4 m, and 6 mm, respectively, has been used. Furthermore, Table 3.2 depicts the various impulsive frequencies caused by the STF and STnF setups in combination with and without the metafoundation. Here, the metafoundation, was considered without the resonators, as they will be tuned to the frequency resulting from this modal analysis. Note that the impulsive frequency is where the impulsive mode of the tank shows the strongest response, which depends on the liquid height and the coupled foundation system. Based on these results, a band gap with a lower bound of 1.1 Hz is desired, while the upper bound was found at 2.2 Hz for the proposed design.

3.2.3 Description of the structure and dynamic system

The foundation consists of slabs that differentiate the layers, while columns provide the vertical stability. Between the slabs, resonators will be attached to the columns via steel springs and are assumed to slide on a friction less surface, see Fig. 3.2. These layers are perfectly equivalent and can be regarded as the unit cells of the foundation, which can be repeated in the

3. METAFUNDATION DEVELOPMENT AND EXPERIMENTAL STUDY ON A COUPLED PIPELINE

Table 3.2: First impulsive eigenfrequencies of tank–foundation systems with various liquid levels

Foundation type	Tank type	Liquid lvl. (m)	Impulsive freq. (Hz)
Traditional	STF	12	6.84
	STnF	9	10.05
Metafoundation	STF	12	1.26
	STnF	9	1.48

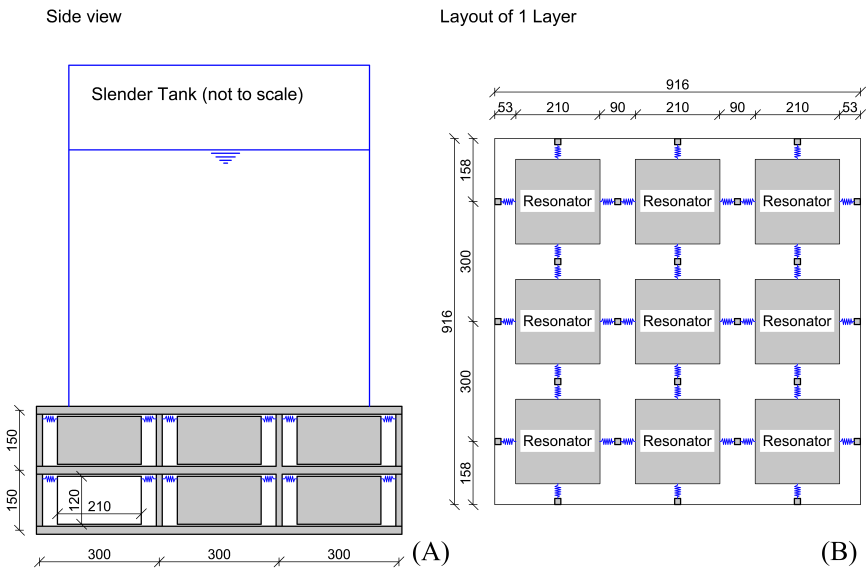


Figure 3.2: Drawings of the structure: (A) side view of tank and metafoundation; (B) layout of one layer (dimensions in cm).

vertical direction. Furthermore, a tank shall serve as a superstructure to evaluate the wave attenuation performance.

The dimensions of the components on the other hand, were chosen with common values for engineering practices. More precisely, a cross section of 15 by 15 cm was used for the columns, which are being spaced apart 3 m in a square grid. The slabs on the other hand were fixed to 20 cm thickness and 150 cm of vertical spacing, while the resonators consist of cuboids that are 210 by 210 cm wide and 120 cm high. For the exact geometry see Figure 3.3.

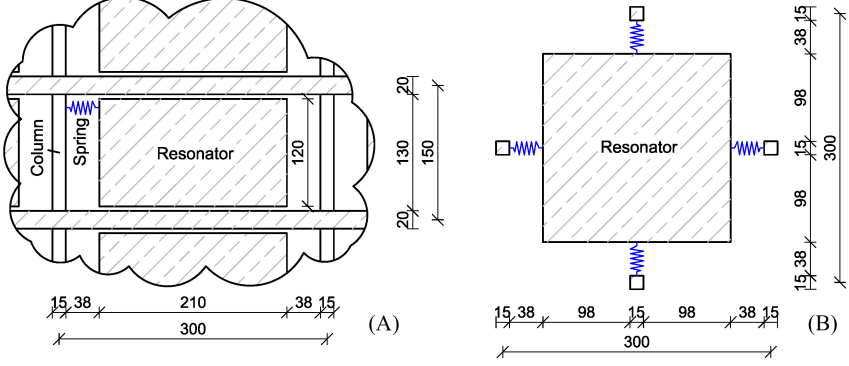


Figure 3.3: Geometry of the unit cell as part of the concrete matrix; (A) cross section of the foundation; (B) layout of one unit cell (dimensions in cm).

3.2.4 Analytical model and Floquet-Bloch theorem

When assuming that the horizontal displacement is governed by the flexibility of the columns, while the slabs move as rigid bodies, the system can be simplified to a one-dimensional (1D) model that propagates only shear type waves in the vertical direction (Fig. 3.4). This entails that the total shear stiffness of one layer can be calculated with the combined horizontal stiffness of all 24 columns. Furthermore, in this model, the layers can be regarded as the unit cells of the system and be repeated periodically in the vertical direction.

Band gaps can be found in periodic structures under the aid of the Floquet–Bloch theorem [73]. These gaps represent frequency regions where elastic waves cannot propagate through the material, and therefore, shall be used to attenuate the response of a superstructure that exerts a varying eigenfrequency. In order to estimate the behaviour of the system, the complete coupled structure will be analysed on its wave propagation behaviour. More precisely, frequency and time domain analyses will be carried out on the system, with and without tank, and compared with the dispersion relation of a single unit cell. For these analyses, it is necessary to formulate the equations of motion in a general form, so that the unit cell can be repeated in the vertical direction. This can be achieved by formulating the equations for the j th unit cell as,

$$m_1^j \frac{d^2 u_1^j}{dt^2} - k_1 u_1^{j-1} + 2k_1 u_1^j + k_2 u_1^j - k_2 u_2^j - k_1 u_1^{j+1} = 0 \quad (3.4)$$

$$m_2^j \frac{d^2 u_2^j}{dt^2} - k_2 u_1^j + k_2 u_2^j = 0 \quad (3.5)$$

3. METAFUNDATION DEVELOPMENT AND EXPERIMENTAL STUDY ON A COUPLED PIPELINE

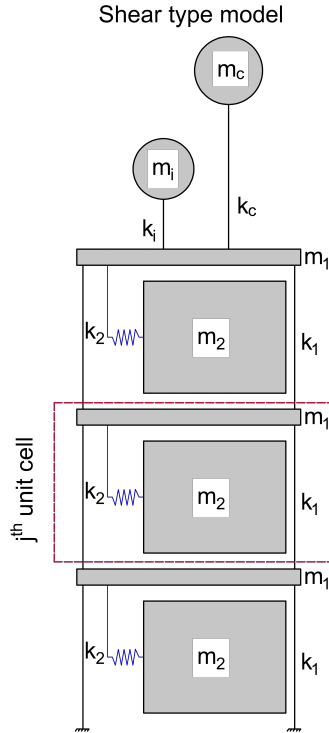


Figure 3.4: Dynamic system.

here, the mass of the columns is lumped to the slabs and the combined mass is denoted with m_1 ; the mass of the resonators (9 per layer) is described with m_2 ; 24 columns per layer provide the equivalent horizontal stiffness for one cell, which is denoted with k_1 ; the stiffness of the steel springs that provides the resonators with their resonance frequency is denoted with k_2 ; while the horizontal displacement is described with u . Since the j th unit cell is connected to the previous $(j-1)$ th and subsequent $(j+1)$ th unit cell, it is necessary to include the displacements of these cells in the equations. This is taken into account by the superscript $(j-1, j, j+1)$ for u , while the subscript $(1, 2)$ determines the corresponding mass. In principal, these equations are sufficient for analyzing the uncoupled mass. However, since the coupled response of the system is also of interest, the tank will be modeled with 2DoFs according to the Malhotra procedure and attached to the top layer of the foundation. In order to find the metamaterial like properties of the unit cell under study, it is necessary to extend the system to an infinite stack of unit cells. According to the Floquet-Bloch theorem, the study of an infinite

lattice of cells can be reduced to the study of a single cell with Floquet-Bloch quasi periodicity conditions. In line with this, $\mathbf{u}(\mathbf{x}, t)$ can be expressed as,

$$\mathbf{u}(\mathbf{x}, t) = \mathbf{u}_{\mathbf{k}} e^{i(\mathbf{q}\mathbf{x} - \omega t)} \quad (3.6)$$

where the frequency is represented by ω , while $q = [q_x, q_y, q_z]^T$ denotes the wave vector in (3.6). As a consequence,

$$\mathbf{u}(\mathbf{x} + \mathbf{R}) = \mathbf{u}(\mathbf{x}) e^{i\mathbf{q}\mathbf{R}} \quad (3.7)$$

with \mathbf{R} being the lattice vector. Furthermore, the eigenvalue problem for a dynamic system can be formulated as:

$$(\mathbf{K} - \omega^2 \mathbf{M}) \mathbf{u} = 0 \quad (3.8)$$

here, mass and stiffness matrix are denoted by \mathbf{K} and \mathbf{M} . In order to achieve the dispersion relation, it is necessary to apply the boundary condition (3.7) to equations (3.4) and (3.5), and successively solve the eigenvalue problem as described in (3.8). When searching for non-trivial solutions for this problem, the dispersion relation can be found as,

$$m_1 m_2 \omega^4 - [(m_1 + m_2) k_2 + 2m_2 k_1 (1 - \cos(q))] \omega^2 + 2k_1 k_2 (1 - \cos(q)) = 0 \quad (3.9)$$

3.2.5 Results for the uncoupled foundation

The configuration depicted in Figure 3.2 and Figure 3.3 resulted in values for m_1 , m_2 , and k_1 , of 4838 kg, 13230 kg, and 7.5e6 N/m, respectively. Note that these values are given by the geometric design of the foundation, thus leaving only k_2 , the stiffness of the steel springs, for tuning the system. When considering the foundation as a metamaterial, the layers of resonators and slabs become the unit cells. This arrangement has the capability of attenuating elastic waves, if its parameters are chosen correctly. To evaluate this effect, the transmission of an imposed signal will be measured in the frequency domain and the results will be compared to the dispersion relation of the unit cell. For a slender fuel storage tank, a band-gap with a lower bound of approximately 1.1 Hz was chosen resulting in k_2 equal to 6.22e6 N/m and an upper bound for the band gap of 2.2 Hz. After establishing the geometry and fixing the parameters of the system, the following analyses were carried out on the foundation and the unit cell: (i) A frequency response analysis of a foundation with 1, 5, and 25 layers without damping (Figure 3.5); (ii) The dispersion relation of the unit cell as part of an infinite lattice (Figure 3.6). Furthermore, the frequency response analysis was carried out by imposing a base excitation of $\ddot{u}_{in} = 1m/s^2$ at the bottom of the foundation and measuring the output acceleration \ddot{u}_{out} at the top of the foundation. For a linear

3. METAFUNDATION DEVELOPMENT AND EXPERIMENTAL STUDY ON A COUPLED PIPELINE

elastic undamped system, this can be achieved by writing the equations of motion,

$$\mathbf{M}\ddot{\mathbf{u}}(t) + \mathbf{K}\mathbf{u}(t) = \mathbf{F}(t) \quad (3.10)$$

and transforming them into the frequency domain with, $\mathbf{u}(t) = \mathbf{u}_f(\omega)e^{i\omega t}$, $\ddot{\mathbf{u}}(t) = -\omega^2\mathbf{u}_f(\omega)e^{i\omega t}$, and $\mathbf{F}(t) = \mathbf{M}\mathbf{I}u_{in}e^{i\omega t}$ (with \mathbf{I} being the identity vector). After dividing by $e^{i\omega t}$ and rearranging the terms we obtain,

$$\mathbf{u}_f(\omega) = (-\omega^2\mathbf{M} + \mathbf{K})^{-1} \mathbf{M}\mathbf{I}u_{in} \quad (3.11)$$

Where $\mathbf{u}_f(\omega)$ describes the vector containing the response amplitude functions in the frequency domain for the individual DOFs, while u_{in} is the ground acceleration, which was set to a constant amplitude of 1m/s^2 . Furthermore, ω is the circular frequency of the excitation and the response and is converted to Hz for Figure 3.5 and Figure 3.6. Figure 3.5 displays the signal amplification in dB, where the output acceleration is compared to the input acceleration with $(20 * \log(\ddot{u}_{out}/\ddot{u}_{in}))$. When observing Figure 3.5, a clear attenuation zone becomes apparent between 1.1 Hz and 2.2 Hz. Here the signal amplification drops to the negative dB regime, resulting in a decreased output at the top of the foundation. The dispersion relation depicted in Figure 3.6 yields a band gap between 1.1 Hz and 2.2 Hz, which is in line with the predicted attenuation zone of Figure 3.5. Note that the dispersion diagram maps the frequency of a wave traveling through a system to the resulting wavelength in that system. If no frequency-wavelength pair can be found, a wave at this frequency cannot propagate unhindered. Therefore, in the range from 1.1 Hz to 2.2 Hz, where there are no solutions for the dispersion equation, the system is expected to attenuate waves. For a more exhaustive explanation of this property see [22]. These results imply that, indeed, an attenuation zone is present in the foundation when regarded as an uncoupled system. However, in order to make a judgment on the viability of this concept, it is necessary to conduct analyses on the coupled system, as discussed in the following chapters.

3.2.6 Frequency response analysis of the coupled system

To evaluate the performance of the Metafoundation, two different types of analyses were carried out on the coupled system (tank clamped to the Metafoundation) as well as on the tank clamped to a concrete plate. In particular, a frequency response analysis showed the performance of the structure for a harmonic excitation, while a time history analysis gave insight in the performance for realistic seismic events. Note that for all analysis form here on forth a Rayleigh damping model of 5% between 1 Hz and 5 Hz has been used. The system, designed for a slender tank with a diameter of 8 m and 12 m height, comprises two layers with nine unit cells each. This system can have varying fluid levels, and therefore, was studied for the STF and the

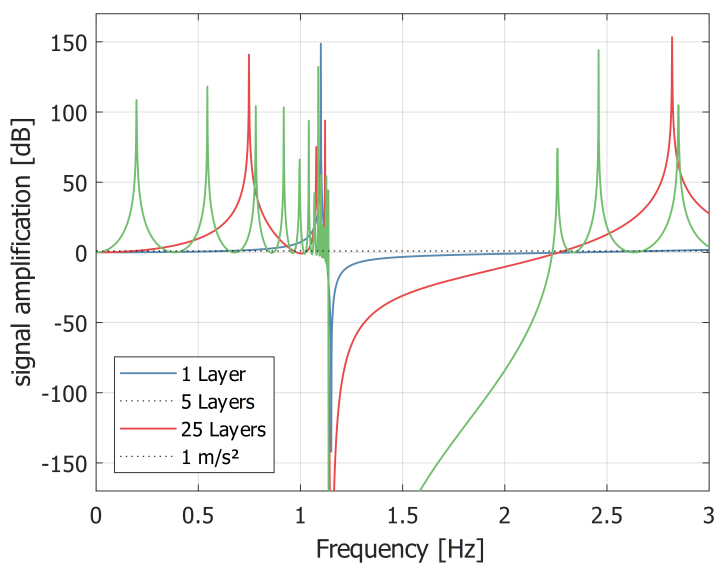


Figure 3.5: Frequency response function for a foundation with 1, 5, and 25 layers without damping.

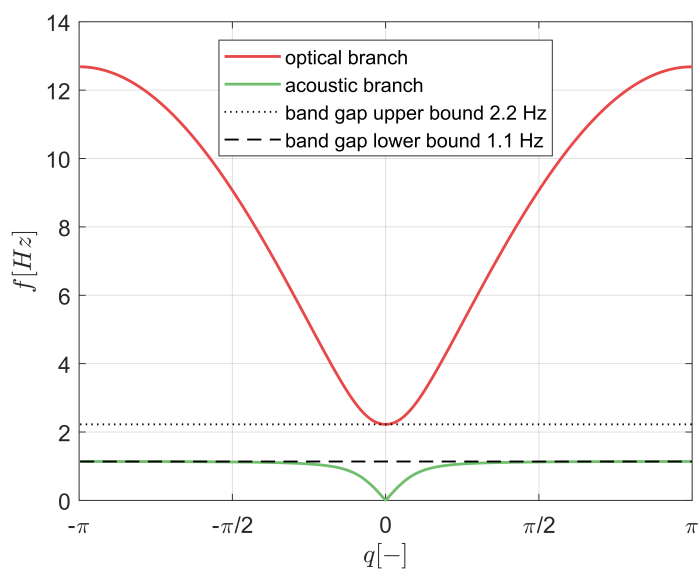


Figure 3.6: Dispersion relation of the unit cell.

3. METAFUNDATION DEVELOPMENT AND EXPERIMENTAL STUDY ON A COUPLED PIPELINE

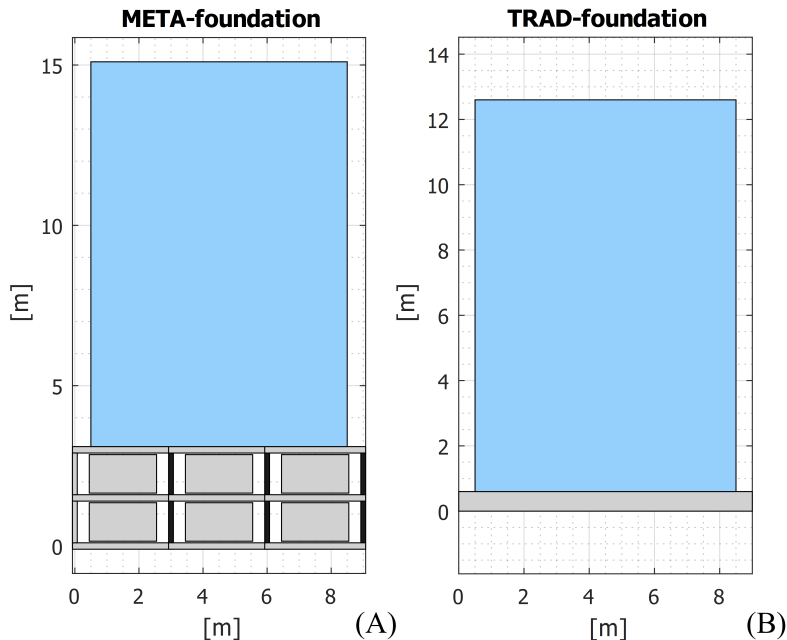


Figure 3.7: Geometrical characteristics: (A) slender tank including the Metafoundation META; (B) slender tank on a traditional foundation TRAD (dimensions in m).

STnF case. The relevant parameters, m_1 , m_2 , k_1 , and k_2 for the foundation and m_i , m_c , k_i , and k_c for the impulsive and convective modes of the tank, are represented in Table 3.3.

Figure 3.7 shows the configuration of the slender-tank–foundation system with the full liquid height (META) and the reference system of a tank with a solid concrete slab as a foundation (TRAD). Furthermore, Figs. 3.8 and 3.9 show the frequency response functions of the impulsive mode for the STF and STnF case, respectively.

The graphs depict the displacement response of the impulsive mode relative to its foundation and the absolute acceleration response of the impulsive mode. Clearly, the STF shows the most effective attenuation with respect to the traditional foundation, while the STnF performs a little less efficient. However, it is worth noting that in terms of magnitude of response the STnF still performs on a similar level as the STF does. Furthermore, the frequency of the resonator has been tuned to produce a lower bound of 1.1 Hz for the band gap, which also corresponds to the optimal tuning of the two spikes of the frequency response (see Figure 3.8 META curve). These results were

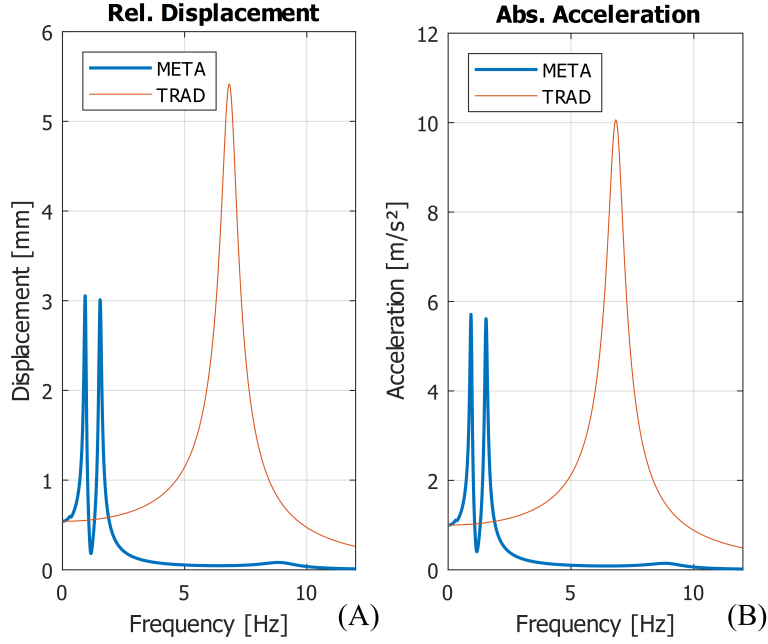


Figure 3.8: Frequency response function of the impulsive mode of a slender tank with full liquid height (STF); (A) displacement of impulsive mass compared to foundation; (B) absolute acceleration of the impulsive mass.

Table 3.3: Parameter values for the analysis of two tank–foundation systems with various fluid levels

System	m_1 (kg)	m_2 (kg)	k_1 (N/m)	k_2 (N/m)
Meta	4.35e4	1.19e5	6.75e7	6.22e6
System	m_i (kg)	m_c (kg)	k_i (N/m)	k_c (N/m)
STF	4.52e5	8.58e4	8.35e8	3.86e5
STnF	3.16e5	8.69e4	1.26e9	3.92e5

expected, since firstly, the attenuation zone for a finite foundation has different levels of effectiveness in its frequency range, and secondly, a tank with a reduced fluid level experiences less demand due to the reduced mass.

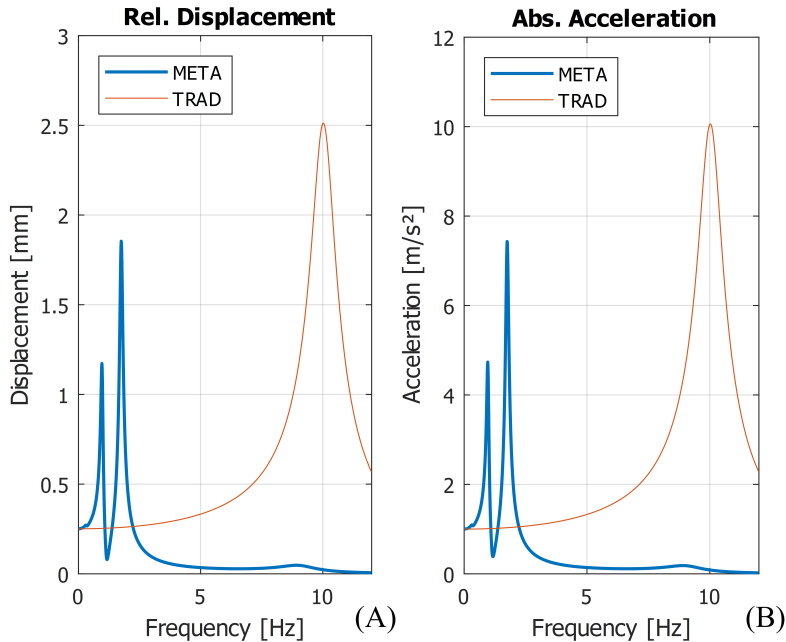


Figure 3.9: Frequency response of a slender-tank–foundation system for a reduced fluid level of $3/4$; fill (STnF); (A) displacement of impulsive mass compared to foundation; (B) absolute acceleration of the impulsive mass.

3.2.7 Seismic response analysis for the coupled system

For the assessment of the functionality of the structure, it is not sufficient to consider only calculations in the frequency domain. Therefore, additional analyses were carried out in the time domain for various earthquakes (Table 3.4) extracted from the European Strong-Motion Database (ESM). Here, R_{jb} is the epicentral distance with M_w being moment magnitude, while PGA represents the peak ground acceleration of that record.

Note that the set of seismic records is compatible for a site in Priolo Gargallo in Sicily, Italy with soil type B and a return period of 2475 years (according to Eurocode 8 [82]). For the time integration, we employed a classical Newmark-beta scheme with a time-step of 0.001 s and values for β and γ of 0.25 and 0.5, respectively. Figures 3.10 and 3.11 present the response of the system for an earthquake that occurred in South Iceland on the 21st of June 2000 with a magnitude of 6.4 and a PGA of 7.07 m/s. In order to judge the results of the time history simulations, the base shear and overturning moment of the tank were considered as governing for the limit state. More

Table 3.4: Set of EC 8 compatible ground motions for the site Priolo Gargallo (soil type B) with a return period of 2475 years

Event (component)	Event ID	M_w	R_{jb} (km)	PGA (m/s^2)
Erincan (X)	000535	6.6	13	3.81
South Iceland (X)	006263	6.5	7	6.23
South Iceland Aftersh. (Y)	006334	6.4	11	7.07
L'Aquila Mainshock (X)	IT0789	6.3	5	4.34
L'Aquila Mainshock (X)	IT0790	6.3	4	4.79
L'Aquila Mainshock (X)	IT0792	6.3	5	5.35

precisely, Fig. 3.10 depicts the absolute time evolution of the base shear and overturning moment for STF, while Fig. 3.11 shows the results for STnF. Clearly, the amplitudes of the base shear and the overturning moment are significantly smaller for the Metafoundation variant. For the sake of brevity, only the maximum values of the base shear and overturning moment are presented for the rest of the ground motions ordered by PGA (Figure 3.12). Note that the time history analysis was carried out for particularly strong ground motions, in order to estimate the performance of the foundation in extreme scenarios. When comparing the maximum values of base shear and overturning moment of the two tank setups, it becomes apparent that the Metafoundation greatly attenuates the forces in the tank with respect to a traditional concrete base plate.

3.2.8 Validation of the 1D model through FE-modelling

In order to numerically validate that our analytical model represents a real system, we studied an FE-model of the Metafoundation coupled with a slender tank in the frequency domain. The model was built in COMSOL Multiphysics 5.2 according to the geometry shown in Figures 3.2, 3.3, and 3.6 and contains the Metafoundation with resonators as lumped masses and a slender fuel storage tank. Note that in this section, the COMSOL specific names of the relevant FE-model elements is written in parenthesis. In particular, the columns were modelled with beam elements (Euler-Bernoulli beam), while the slabs and tank shells were modelled as shell elements (shell). The liquid inside the tank, on the other hand, was modeled as an acoustic medium with 3D elements (acpr) for the frequency domain, as this represents a good approximation when sloshing motions are neglected [67, 71]. The interaction between the tank shell and the acoustic medium was modeled with a boundary condition of the type sound hard boundary condition (asb). Furthermore, all beam and shell elements were considered to be linear elastic and endowed with 5% Rayleigh damping between 1 and 5 Hz, which is equiv-

3. METAFUNDATION DEVELOPMENT AND EXPERIMENTAL STUDY ON A COUPLED PIPELINE

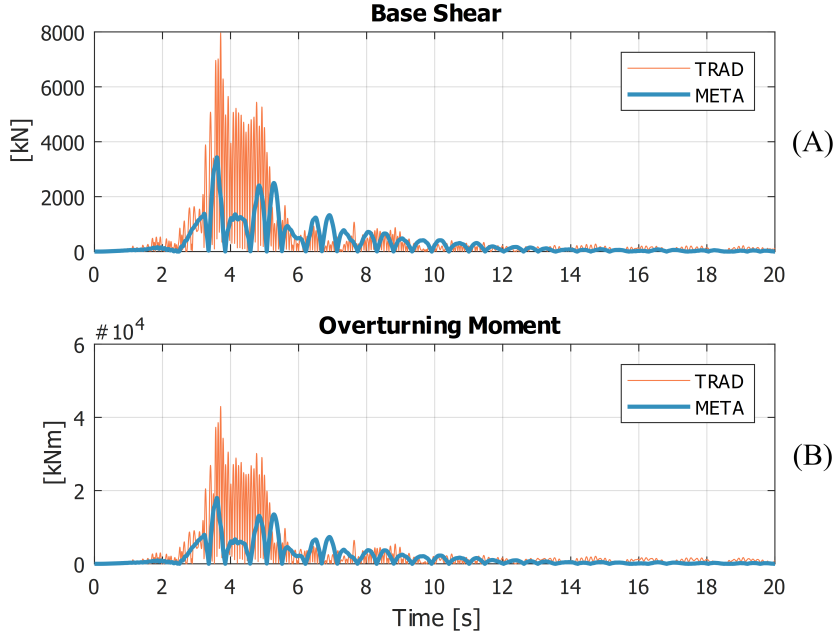


Figure 3.10: Absolute time evolution of the (A) base shear and the (B) overturning moment for STF.

alent to the damping used in the 1D model. The acoustic medium on the other hand was endowed with the properties of water and modelled with 3D tetrahedral elements. In sum 5313 tetrahedral elements, 2478 triangular elements, 672 edge elements, and 172 vertex elements were created with the finite element mesh. Figure 13 (A) shows the FE-model of the coupled system, while Figure 3.13 (B) gives an indication on the refinement of the mesh.

Analogous to the procedure for the analytical model, the coupled tank-foundation system has been studied in the frequency domain and compared to the response of a tank modeled with a traditional foundation. For this purpose, an harmonic excitation of constant acceleration was applied to the bottom of the foundation, while the maximum absolute acceleration of the tank shell was recorded. When comparing the results presented in Figure 3.14 to Figure 3.8, it becomes clear that the 1D model shows, qualitatively, a very similar response with respect to the finite element model. However, since the impulsive mode according to the Malhotra procedure is supposed to model the tank response in terms of base shear rather than displacement, the amplitude of the tank wall in the FE simulation is not equal to the

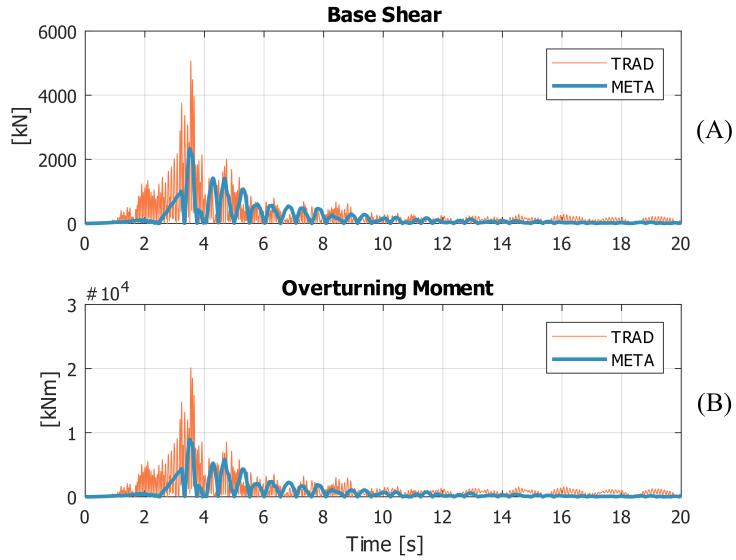


Figure 3.11: Absolute time evolution of the (A) base shear and the (B) overturning moment for STnF.

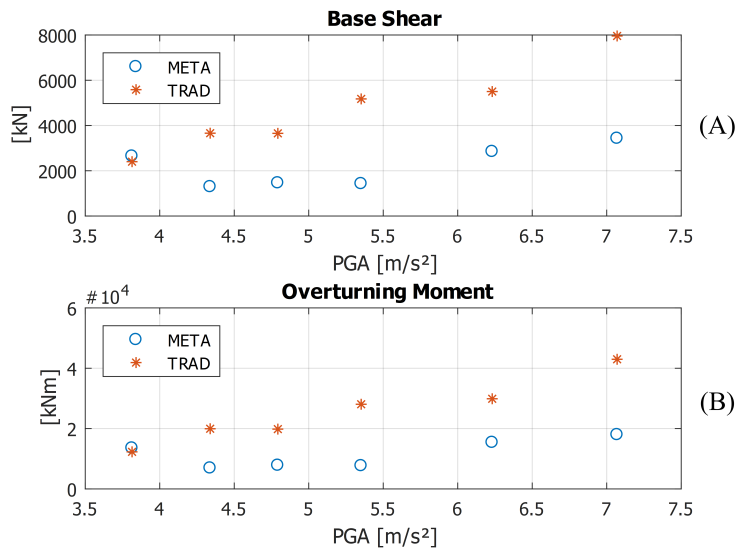


Figure 3.12: Maximum values of (A) base shear and (B) overturning moment in a full slender tank for all studied ground motions.

3. METAFUNDATION DEVELOPMENT AND EXPERIMENTAL STUDY ON A COUPLED PIPELINE

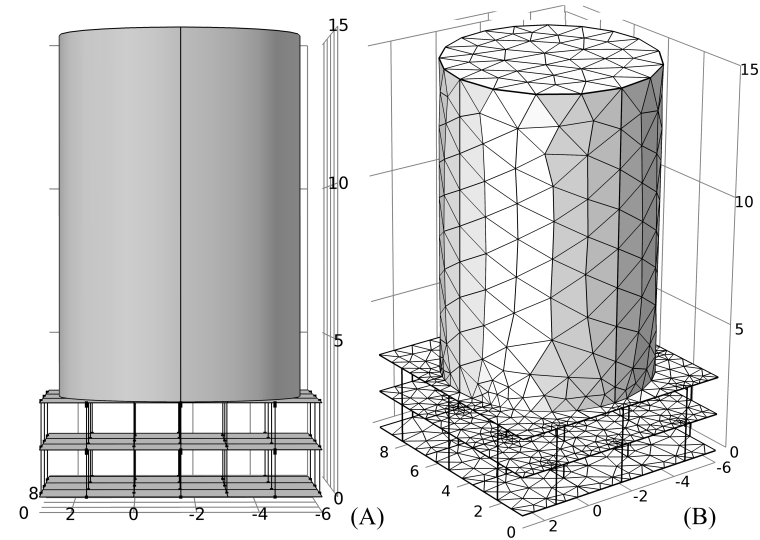


Figure 3.13: FE-model: (A) Side view of FE-model; (B) Isometric view of FE-model with finite element mesh.

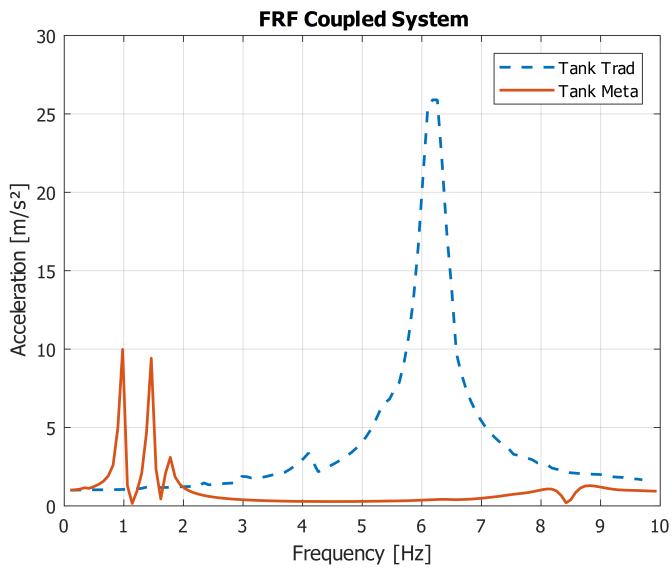


Figure 3.14: Frequency response function of the FE-Model of the coupled system.

simplified 1D model. Furthermore, due to the acoustic medium, the damping of the overall system becomes much more complicated than a simple Rayleigh model could do justice. In conclusion, the 1D system is considered to be a good approximation for the evaluation of the Metafoundation and may serve as a basis for an optimization procedure. Once a feasible system has been found, more detailed FE-simulations will need to be carried out in future studies.

3.3 Experimental Study

3.3.1 Experimental performance of the coupled tank-foundation-pipeline system

Pipelines are critical components of petrochemical plants and can be subjected to extreme loading conditions during earthquakes. Their potential to cause LOC events, and thus, trigger cascading effects must be treated with care. Furthermore, due to their slender nature, complicated geometry and complex boundary conditions, they are difficult to model in a realistic manner and often exert highly non-linear behaviour. As a consequence, it becomes reasonable to carry out experiments for the verification of their performance. In the present work, the interaction of a tank+foundation structure coupled with a realistic piping system is investigated. This type of coupling for laboratory experiments can be achieved with a hybrid simulation (HS), where the tank and the foundation are modeled as Numerical Substructures (NS), while a piping setup in a laboratory represents the Physical Substructure (PS). The setup for the studied experiment is based on the theoretical work of Abbiati et al. [60], where m substructures are coupled with localized Lagrange multipliers resulting in the following set of differential algebraic equations:

$$\mathbf{M}^{(l)}\ddot{\mathbf{u}}^{(l)} + \mathbf{C}^{(l)}\dot{\mathbf{u}}^{(l)} + \mathbf{K}^{(l)}\mathbf{u}^{(l)} = \mathbf{L}^{(l)\text{T}}\boldsymbol{\Lambda}^{(l)} - \mathbf{M}^{(l)}\mathbf{T}^{(l)}\mathbf{a}_{\mathbf{g}}(\mathbf{t}) \quad (3.12)$$

$$\forall l \in 1, \dots, m$$

$$\mathbf{L}^{(l)}\dot{\mathbf{u}}^{(l)} + \bar{\mathbf{L}}^{(l)}\dot{\mathbf{u}}_{\mathbf{g}}^{(l)} = \mathbf{0} \quad (3.13)$$

$$\sum_{l=1}^m \bar{\mathbf{L}}^{(l)\text{T}}\boldsymbol{\Lambda}^{(l)} = \mathbf{0} \quad (3.14)$$

Here, $\mathbf{M}^{(l)}$, $\mathbf{C}^{(l)}$, and $\mathbf{K}^{(l)}$ are the mass, damping and stiffness matrix of the l th substructure, respectively, while $\ddot{\mathbf{u}}^{(l)}$, $\dot{\mathbf{u}}^{(l)}$, and $\mathbf{u}^{(l)}$ denote acceleration, velocity and displacement of the l th substructure. Moreover, the interface DoFs are collocated by the signed Boolean matrices $\mathbf{L}^{(l)}$ and $\bar{\mathbf{L}}^{(l)}$ to the substructure DoFs $\dot{\mathbf{u}}^{(l)}$ and the generalized interface DoFs $\dot{\mathbf{u}}_{\mathbf{g}}^{(l)}$. In

order to enforce compatibility between multiple substructures, localized Lagrange multiplier vectors $\Lambda^{(l)}$ are used in (3.12) and (3.14) [83]. For more details on this procedure refer to [60]. Note that this technique can couple several numerical and/or physical substructures. Furthermore, in order to make the results relatable to the current state of the art, the Metafoundation will be compared to a system protected with concave sliding bearings (CSBs). Be aware that this system is different to the tank clamped to a traditional foundation. This change of reference system is necessary, since a tank subjected to very strong ground motions is unlikely to sustain its integrity when clamped to a concrete slab, while at the same time exhibiting very small deformations to a possible connected piping system. Therefore, a more realistic comparison was aspired by using a tank isolated with CSBs.

3.3.2 Physical substructure PS

The PS consists of a piping system with its main line having a diameter of 8 in (outer diameter: 219.08 mm, thickness: 8.18 mm) and its secondary line showing a diameter of 6 in (outer diameter: 168.28 mm, thickness: 7.11 mm). Furthermore, the system comprises two elbow elements, one t-joint, and one bolted flange joint, and is based on the U.S.NRC report from 2008 [84]. Here, a large-scale shaking table test was carried out on a piping system common for the nuclear industry. As discussed in the report, masses have to be added to the structure at specified positions, in order to take valves and other components into account. The exact geometry of our system is depicted in Figure 3.15, while the actual specimen is represented in Figure 3.16. When observing these figures, it becomes clear that the real boundary conditions of the system are rather complex and that the dynamic response may be difficult to predict with an FE model. Additionally, the piping system was filled with pressurized water (32 bar), in order to represent a realistic scenario. Of particular interest for the present study are the strains in the critical elbow element, since, as shown by Bursi et al. [85], elbow elements are highly vulnerable to seismic excitation and may lead to LOC events when damaged. Therefore, the strains in the critical elbow (Figure 3.15) are measured with strain gauges, and are considered governing for the following experimental verification. In Figure 3.17 the configuration of the strain gauges on the elbow is shown. Note that rose like strain gauges were applied on the inside and outside of the elbow, in order to capture the strain in radial and longitudinal direction of the pipe. The nomenclature of the strains shall be explained on the example of the REC strain gauge, where R stands for Rose, E for external gauge, and C for the vertical strain or in this case hoop strain (as indicated by the a-b-c coordinate system in the bottom right corner of Figure 3.17). Furthermore, the rose type strain gauges are type 3/120 RY31, while the simple gauges are type 3/350 LY41 by the company HBM Messtechnik.

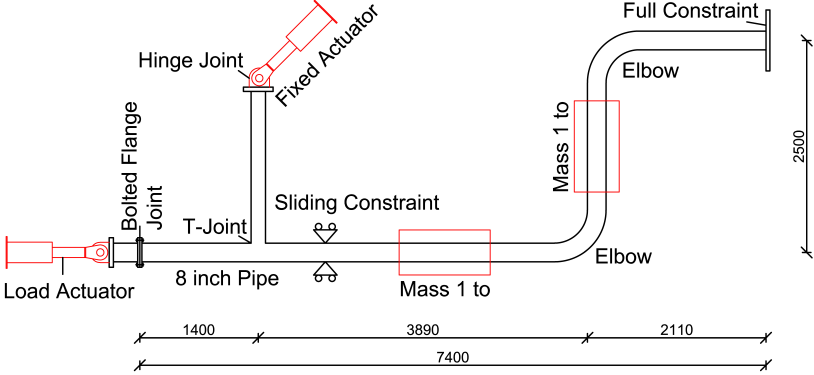


Figure 3.15: Schematic of the piping system (dimensions in cm).

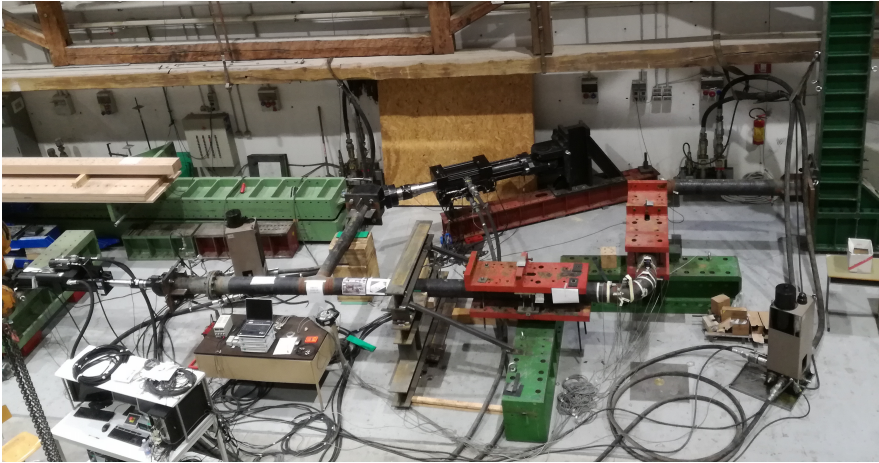


Figure 3.16: Experimental setup of the piping system.

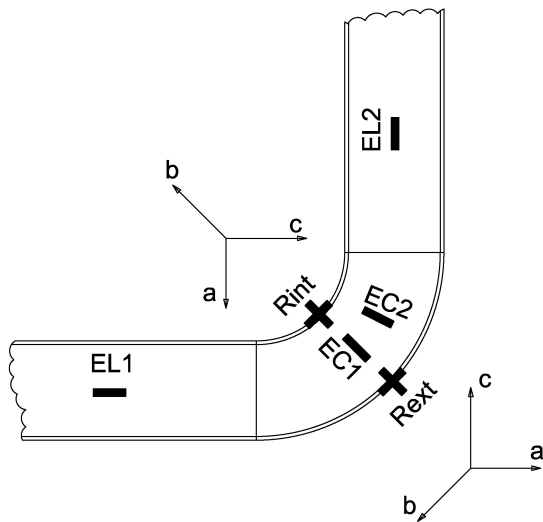


Figure 3.17: Configuration of strain gauges on the elbow element.

3.3.3 Numerical Substructure

The NS consists of the tank and Metafoundation equal to the configuration STF, where two layers of foundation were used. Pipes of petrochemical plants are often connected to tanks close to the tank base plate. When assuming that the relative tank deformation between ground and piping connection is very small, the pipe can be assumed to be connected to the bottom of the tank. This simplifies the numerical model, since the interface node can now be placed on the last layer of the foundation where tank, foundation and pipe coincide. Figure 3.18 shows a representation of the coupling of the NS with the PS. Furthermore, in order to draw a comparison to conventional isolation systems, an additional NS has been investigated. In particular, four CSBs (concave sliding bearings) were considered as an isolation variant for the slender tank and modeled as an alternative NS. The friction coefficient has been set to 8%, while the spherical radius amounts to 5000 mm. For a CSB, the isolation period can be calculated with $2\pi\sqrt{2R/g}$, where R is the spherical radius and g the gravitational constant. This amounts to an isolation period of 6.34 sec.

A common approach for modeling a CSB is to use the piece-wise linear Mostaghel model as it is represented in Figure 3.19. This model is well described in [86], with its governing parameters δ_{MST} , α_{MST} , and k_{MST}

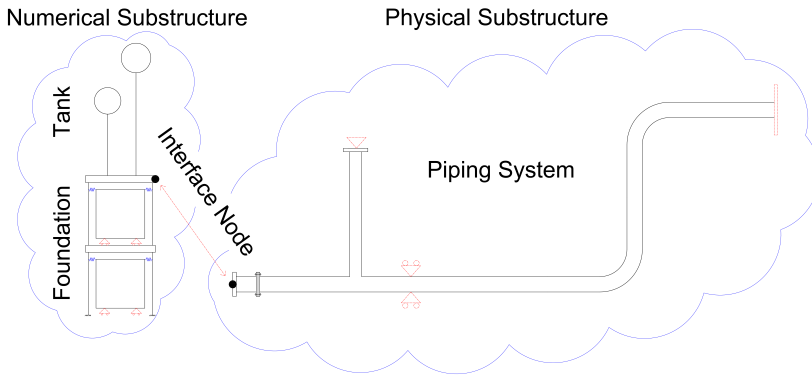


Figure 3.18: Coupling of the numerical and physical substructure.

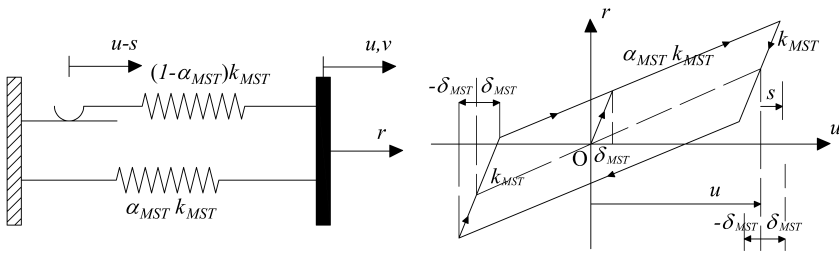


Figure 3.19: Generic Mostaghel model (Figure from [60]).

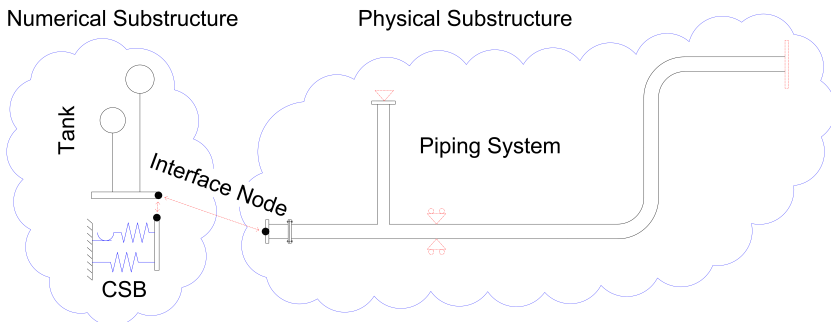


Figure 3.20: Numerical coupling of CSB, tank, and piping system.

being equal to $5\text{e-}4$ m, $1.3\text{e-}3$, and $2.18\text{e}8$ N/m, respectively. All four CSB devices work in parallel and therefore can be simulated by a single device with equivalent parameters. The resulting coupling of the PS and NS is represented in Figure 3.20.

3.3.4 Results of the experimental study

Table 3.5 lists the seismic records that have been used for the experiment. In particular, two sets of Eurocode 8 [82] compatible records have been used; (i) a set of three records compatible with a site situated in Priolo Gargallo with soil type B and a return period of 475 years; (ii) 2 records from the previous set as discussed in subsection analytical results for the coupled system (return period 2475 years). Note that in Table 3.5 T denotes the expected return period of the earthquake, which is used to divide them into medium and strong ground motions. Equivalent to the earthquakes for the time history analyses, these records were extracted from the European Strong-Motion Database (ESM).

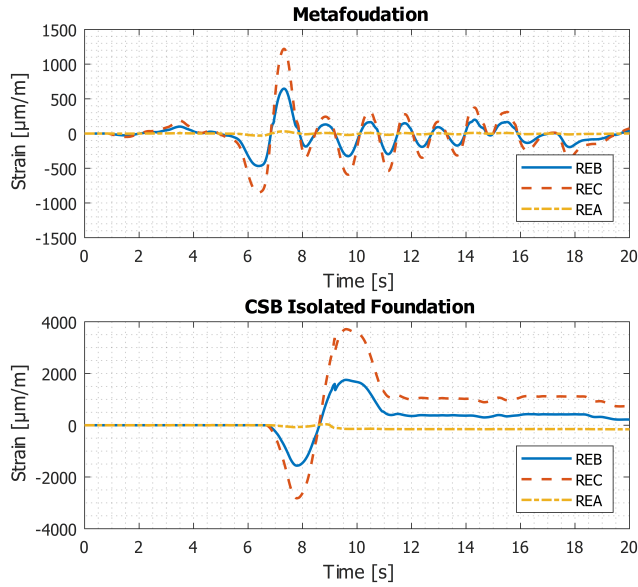
For the sake of clarity, only the results of the critical strain gauges for one of the seismic events, namely 000535, are depicted in Figure 3.21. Since the yield strain of the piping system amounts to $2000 \mu\text{m}/\text{m}$, the piping system remains in the elastic range when connected to the Metafoundation, while the setup comprising the CSB array exhibits yielding in the REC strain gauge (hoop strain). However, when comparing this result with the maximum appearing hoop strains recorded for all seismic events shown in Figure 3.22 (bottom), it becomes apparent that a reduction of hoop strain cannot be assumed for any given earthquake. On average, the Metafoundation reduces the hoop strain by 37%, while the maximal reduction, obtained for event 000535 amounts to 67%.

From the high dispersion of the results, it becomes clear that the average reduction is heavily influence by the extreme event. This excessive strain measured for the CSB, is due to the low post yielding stiffness of the non-linear system, which makes it difficult to predict what earthquakes may trigger yielding in the pipeline. However, since the Metafoundation is a linear system, also it's response scales linearly with the excitation and therefore, such extreme events are less likely. Moreover, the CSB setup shows a much better performance in terms of base shear, with an average decrease of 73% and a maximal reduction of 85% with respect to the Metafoundation. It is worth noting however, that a CSB is a highly specialized device that has been optimized over many years and requires regular maintenance and inspection.

From the obtained results, we deduce that the developed foundation is not a better solution than a CSB array, but that it clearly shows some positive wave attenuation behaviour and that with more research and optimization, it may provide a viable alternative. Additionally, for a more reliable performance of the system, it may be necessary to take the piping

Table 3.5: Seismic events for the experimental validation

T(yrs)	Event (comp.)	Event ID	M_w	R_{jb} (km)	PGA (m/s^2)
475	S. Iceland (Y)	004673	6.5	15	4.68
	L'Aquila M. (Y)	IT0791	6.3	9	3.24
	L'Aquila M. (Y)	IT0792	6.3	5	6.44
2475	Erincan (X)	000535	6.6	13	3.81
	L'Aquila M. (X)	IT0789	6.3	5	4.34

**Figure 3.21:** Strains in the critical elbow for the most severe seismic event.

system into account when tuning the foundation. This, on the other hand, is not within the scope of the present work.

3.4 Conclusion

The proposed Metafoundation represents a novel type of seismic shield and has been designed to protect fuel storage tanks from real ground motions. Through analyses in the frequency and time domain, we have demonstrated the effectiveness of the foundation at attenuating seismic effects. More precisely, a slender fuel storage tank may profit greatly from the proposed foundation in terms of attenuation of base shear and overturning moment with

3. METAFUNDATION DEVELOPMENT AND EXPERIMENTAL STUDY ON A COUPLED PIPELINE

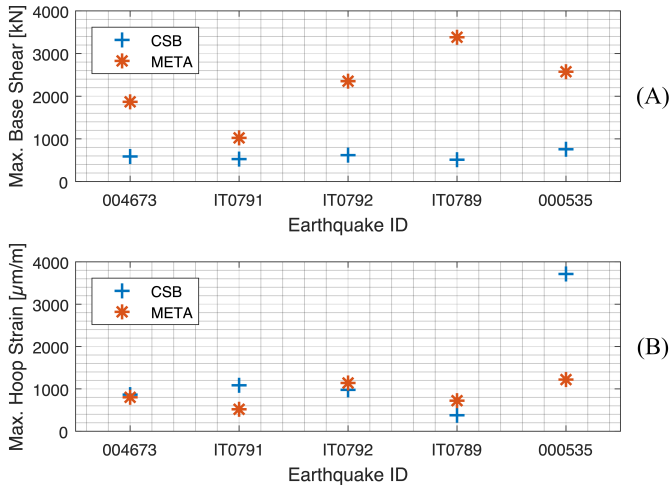


Figure 3.22: Experimental results: (A) Base shear of the tank; (B) maximal hoop strain in the elbow (REC).

respect to a traditional concrete foundation. Additionally, the conducted laboratory tests shed light on the interaction of the Metafoundation with the complete coupled structure (tank + foundation + pipeline) and made it comparable to standard isolation devices. The measured elbow strains show no plastification for the system coupled with the Metafoundation, while the configuration including the CSB array exceeds the critical yield strain for one of the investigated ground motions. However, since some seismic events showed a higher demand in the elbow when coupled to the Metafoundation, a clear advantage of the Metafoundation cannot be concluded yet. In future studies the tuning of the foundation could potentially be expanded to the complete coupled system and, consecutively, reduce stresses in a connected piping system more reliably. Besides the attenuation of horizontal excitation, the foundation may offer interesting properties regarding soil-structure interaction and vertical component damping.

Upcoming developments As demonstrated in this chapter, the foundation needs to be tuned to the superstructure of interest, which leads to the optimization algorithm developed in the next chapter. Furthermore, the complete system will to be designed according to common construction standards and subsequently validated with a set of site representative ground motions.

Chapter 4

Optimization of Locally Resonant Metafoundations

Overview. This paper introduces a novel seismic isolation system based on metamaterial concepts for the reduction of ground motion-induced vibrations in fuel storage tanks. In recent years, the advance of seismic metamaterials has led to various new concepts for the attenuation of seismic waves. Of particular interest for the present work is the concept of locally resonant materials, which are able to attenuate seismic waves at wavelengths much greater than the dimensions of their unit cells. Based on this concept, we propose a finite locally resonant Metafoundation, the so-called Metafoundation, which is able to shield fuel storage tanks from earthquakes. To crystallize the ideas, the Metafoundation is designed according to the Italian standards with conservatism and optimized under the consideration of its interaction with both superstructure and ground. To accomplish this, we developed two optimization procedures that are able to compute the response of the coupled foundation-tank system subjected to site-specific ground motion spectra. They are carried out in the frequency domain and both the optimal damping and frequency parameters of the Metafoundation embedded resonators are evaluated. As case studies for the superstructure, we consider one slender and one broad tank characterized by different geometries and eigenproperties. Furthermore, the expected site-specific ground motion is taken into account with filtered Gaussian white noise processes modeled with a modified Kanai-Tajimi filter. Both the effectiveness of the optimization procedures and the resulting systems are evaluated through time history analyses with two sets of natural accelerograms corresponding to operating basis and safe shutdown earthquakes, respectively.

4.1 Introduction

4.1.1 Background and motivations

Natural hazards such as earthquakes can interact with critical infrastructures and cause so-called NaTech [43] events (natural technological events). They can have serious consequences on both community and environment and, therefore, need to be treated with care. One example of such an event is the loss of containment (LoC) of fuel storage tanks, pipelines or other components of petrochemical plants and nuclear power plants. LoC events of such critical infrastructures need to be avoided at the highest priority, as past NaTech disasters have displayed their potential in causing substantial damage to the community and the environment [40]. Fuel storage tanks in petrochemical plants need to be regarded as high risk structures, due to their fragility to earthquakes and their potential for cascading effects [61]. Their low impulsive frequencies can fall within the excitation frequencies of earthquakes and significant effort is required to isolate them against seismic vibrations. In order to avoid LoC events from occurring during an earthquake, various strategies have been proposed in the field of seismic engineering. The most common solutions use lead-rubber bearings [50] or spherical bearing devices [77]. In this work, we investigate a new type of seismic isolation based on a metamaterial concept that may offer an alternative to classical seismic isolators. Although the performance of classical isolators on superstructures has been studied in depth [87, 88], they require two strong floors, exert a very high stiffness against the vertical component of an earthquake and seem to be ineffective for large structures subjected to rocking [89]. As a result, we propose an isolation system that does not require the use of additional strong floors or specialized devices. In recent years, periodic materials have received growing interest due to their ability to attenuate waves in certain frequency ranges [90]. In principle, there are two types of periodic materials currently investigated for seismic engineering use: phononic crystals (PCs) and locally resonant acoustic metamaterials (LRAMs). Although both are able to create a stop band to forbid elastic wave propagation within a selected frequency band, for the attenuation of low frequency vibrations, LRAMs are better suited than PCs. This is due to their capability to exhibit low frequency band gaps that can be endowed with unit cells much smaller than the wavelength of the desired frequency region. This particular property has opened an innovative direction to reduce earthquake-induced vibrations [29, 66, 91]. At the outset, two types of applications have been proposed based on this phenomenon: (i) foundations with embedded resonators [24, 27, 32, 92] capable of attenuating seismic waves effects, and: (ii) barriers that are able to redirect surface waves back into the ground [15, 19, 93, 94]. More precisely, Cheng and Shi [27] studied a periodic foundation composed of a reinforced concrete matrix and steel masses

that are connected to the matrix with rubber layers. They demonstrated the effectiveness of their isolation system for a large set of ground motions and applied it to a nuclear power plant. However, the feedback of the superstructure and the subsequent effects on the effectiveness of the foundation have been neglected. Another highly innovative approach has been proposed by Casablanca et al. [30] who studied a foundation composed of concrete plates with embedded cylindrical steel resonators. Although the efficiency of the foundation was proven with experimental tests for harmonic excitations, no considerations were made on the coupling foundation system-superstructure or the effects that expected seismic records could entail on system functionality. Furthermore, the foundation was not designed for gravity and/or seismic load combinations. In order to display the effects of the coupling between foundation and superstructure, La Salandra et al. [32] investigated a periodic foundation for the isolation of fuel storage tanks in the frequency domain. They found a significant shift in the desired frequency range for the band gap and, therefore, highlighted the importance of this feedback effect. On the other hand, they did not optimize their foundation to the coupled system or considered sets of seismic records for the evaluation of the foundation effectiveness in a realistic scenario. Following up on the most recent developments, a proper foundation must take into account both the feedback of the superstructure and the frequency content of the expected earthquake. Moreover, to ensure the feasibility of a realistic design, the structure needs to be conform to current seismic standards and be equipped with simple links, e.g. wire ropes, capable of achieving certain amount of hysteretic damping. In order to set a design that can comply with all the aforementioned constraints, we investigated two different types of optimization procedures. These procedures are carried out in the frequency domain and rely on the principal of tuned mass dampers (TMDs), which represent popular passive response control devices tuned to oscillate out of phase with the primary system [95–97]. It is generally recognized, indeed, that TMDs are not generally effective at reducing seismic responses, due to the fact that earthquakes include a wide frequency spectrum and often entails large vibrations for higher modes [52]. As a solution, multiple tuned mass dampers (MTMD) have been proposed. Thus, it has been shown that MTMDs, with multiple different eigenproperties, can reduce the effects that ground motions entail on buildings [98–101]. For these more complex systems, various optimization procedures have been established [102–105]. In contrast to classical MTMD systems, the resonators of the proposed design are located below the structure instead of in correspondence with the governing modes. This needs to be taken into account by the optimization procedures. More precisely, the procedures are characterized by two different optimization parameters that are studied and compared herein: i) the maximum absolute acceleration of the impulsive mode of a tank; ii) the dissipated energy of the resonators compared to the total amount of dissipated energy. The optimization of

non-conventional TMDs towards the dissipated energy is a procedure introduced by Reggio and De Angelis [106] and has been adapted to the proposed design. Finally, we validate the system with time history analyses (THAs) and highlight the advantage in terms of base shear reduction when compared to a traditional foundation.

4.1.2 Scope

Along those lines, the following issues are explored hereinafter: (i) a foundation design based on the concept of metamaterials compliant with common construction standards, i.e. the Italian structural code [107]; (ii) the effect of the foundation flexibility on its dynamic performance; (iii) an optimization procedure that takes the feedback of a superstructure and the relevant earthquake frequency content into account. More precisely, the elastic design of the foundation is carried out considering a response spectrum provided by the Italian code for an active seismic site located in Priolo Gargallo, Sicily, Italy. Once the principal dimensions are fixed, a set of ground motions that correspond to the uniform hazard spectrum (UHS) specified for the site, can be chosen. Then, an average power spectral density (PSD) of these accelerograms is evaluated and fitted with a modified Kanai-Tajimi filter. In detail, we use a Kanai-Tajimi filter modified by Clough and Penzien (KTCP-filter) and investigate three typical soil types and the above-mentioned fitted “soil type”. With the results of these initial calculations, the optimization procedures can be employed to set the optimal values for frequency and damping ratio of the metafoundation resonators. As a result, the structure is modelled as a whole and investigated on its effectiveness. This is done with THAs of the coupled optimized foundation-tank systems subjected to the previously chosen seismic records. The remainder of the paper is organized as follows. Firstly, the description of fuel storage tanks and the evaluation of the seismic activity of the construction site is presented in Section 4.2. Section 4.3 introduces considerations on the uncoupled metamaterial-based system and negativity concepts. Both modeling and design of the foundation-tank coupled system are presented in Section 4.4. Moreover, Section 4.5 provides optimization procedures for the evaluation of the optimal parameters of resonators. In addition, both evaluation and comparison of the coupled systems subjected to ground motions are given in Section 4.6. Finally, we draw conclusions and present future developments in Section 4.7.

4.2 Description of the foundation-tank coupled system

Steel columns with hollow steel sections and concrete slabs that define the unit cells compose the foundation. In each unit cell there is a concrete mass that is linked to the steel-concrete composite structure. In order to

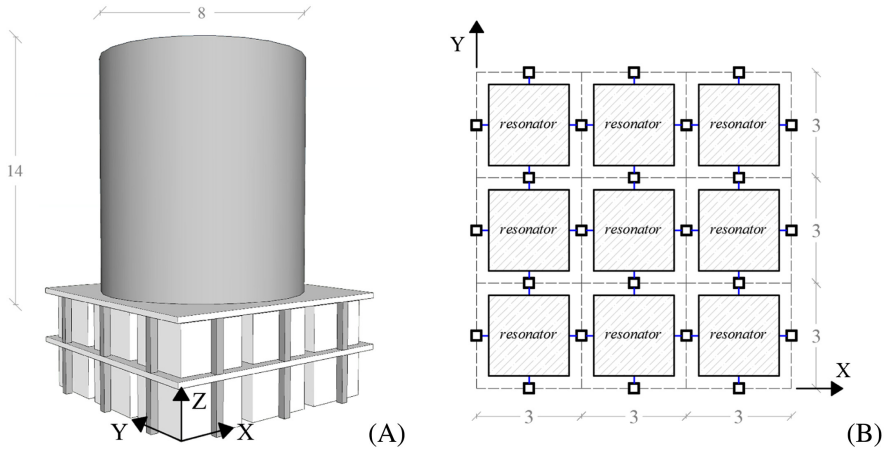


Figure 4.1: Foundation-slender tank coupled system: (A) isometric view with steel columns; (B) plan view. Dimensions in m.

provide high and controllable damping values as required by the optimization process, see Section 4.4, these links can be realized with wire ropes [108] as sketched in Figure 4.4 (A). If properly designed, wire ropes can achieve the required damping values collected in Tables 4.6 and 4.7, respectively, of Section 4.5. Moreover, to allow for the displacement of resonators, a gap of 200 mm between columns and concrete masses, i.e. resonators, was considered. Both the isometric and plan view of the coupled foundation-tank system are illustrated in Figure 4.1. In particular, the superstructure corresponds to a slender fuel storage steel tank.

4.2.1 Fuel storage tank modelling

The hydrodynamic response of a tank-liquid system is mainly characterised by two different contributions, called impulsive and convective component, respectively. If the tank walls are assumed to be rigid, the impulsive component represents the portion of liquid that moves synchronously with the tank walls. Conversely, the liquid that moves with a long-period sloshing motion in the upper portion of the tank is represented by the convective component. Since there are significant differences in their natural periods, they can be considered uncoupled [69]. A simplified procedure for modelling storage tanks with flexible walls has been proposed by Malhotra et al. [69], who reduced the tank response to the contribution of two main modes in a plane, through coefficients dependent on tank parameters. In this respect, Figure 4.2 shows the sketch of a fuel storage tank and its equivalent 2D lumped mass model. The two SDOFs that simulate both the impulsive and

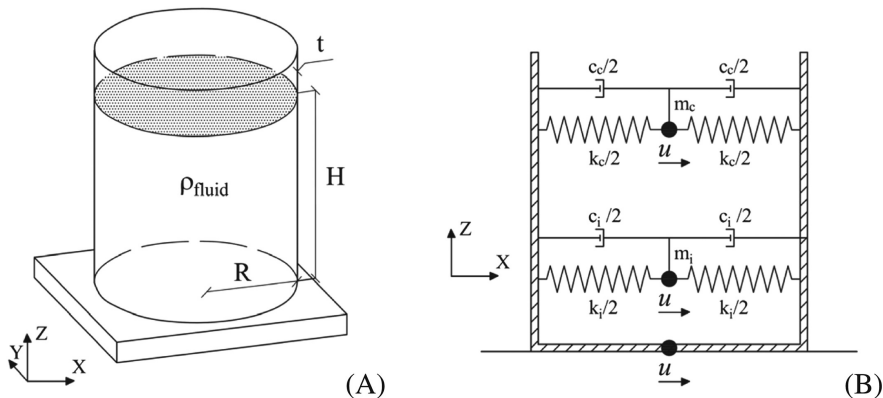


Figure 4.2: Fuel storage tank: (A) isometric view; (B) 2D modeling with two SDoFs for the impulsive and convective mode (Malhotra et al. [69]).

convective modes are connected to a rigid frame that includes the tank wall mass. Accordingly [69], the vibration periods T_i and T_c and the relevant modal masses m_i and m_c can be evaluated as,

$$T_1 = C_i H \sqrt{\frac{\rho R}{Et}}, \quad T_c = C_c \sqrt{R} \quad (4.1)$$

and,

$$m_i = \gamma_i m_l, \quad m_c = \gamma_c m_l \quad (4.2)$$

where, E , ρ and m_l denote the Young modulus of the tank wall, the material density and the total mass of the liquid, respectively; H and R define the liquid height and tank radius, respectively; t is the equivalent uniform thickness of the tank wall while C_i , C_c , γ_i and γ_c are the parameters that depend on the tank slenderness. This procedure considers also the remaining mass m_s lumped to the bottom plate of the tank.

Clearly, the impulsive mode is strongly dependent on the fluid level and the stiffness of the tank walls, while the convective mode is mainly influenced by the tank radius. The stiffness values of the equivalent linear springs k_i and k_c can be calibrated to match the tank properties as follows,

$$k_i = m_i \left(\frac{2\pi}{T_i} \right)^2, \quad k_c = m_c \left(\frac{2\pi}{T_c} \right)^2 \quad (4.3)$$

Since the impulsive mode contains the highest participant mass, especially for slender tanks, the Metafoundation has been designed for the attenuation of the impulsive mode. In this paper two types of tanks characterized by different height H , radius R and tank wall thickness t have been considered. Table 4.1 shows the main geometrical characteristics of the

Table 4.1: Main characteristics of broad and slender tank.

Parameter	Broad Tank	Slender Tank
Diameter [m]	48.0	8.0
Wall thickness [mm]	20.0	6.0
Tank height [m]	15.6	14.0
Maximum liquid height [m]	15.0	12.0
Convective frequency [Hz]	0.34	0.12
Impulsive frequency [Hz]	6.85	3.95

two considered tanks and the resulting frequencies for their impulsive and convective modes.

4.2.2 Modelling of the coupled foundation-tank system

The two SDoFs that simulate the tank-liquid system along the X-direction (see Figure 4.1) are defined in the previous sub-section and depicted in Figure 4.3. Moreover, the Metafoundation modelling is carried out condensing both masses and stiffnesses of the resonators of each layer to one stack of unit cells. This dynamic condensation in both X- and Y-direction is exact, since all the resonators are endowed with the same mass $m_{2,i}$ and stiffness $k_{2,i}$ and operate in parallel in each layer. The same condensation is also applied to masses $m_{1,i}$ and stiffnesses $k_{1,i}$ of the unit cells, which are assumed to behave as a shear-type system. Therefore, being interested in the motion along, let us say the X-direction, each layer consists of only two DoFs: one for the resonators and one for the cells, respectively. A sketch of the system and the corresponding lumped mass model is shown in Figure 4.3(A) for the single-layer foundation, and in Figure 4.3(B) for the two-layered foundation. From a model viewpoint, the resonators are attached to the upper layer via springs and are assumed to slide on a friction less surface. Hence, the system of the equations of motion (EOM) can be defined as follows:

$$\mathbf{M}\ddot{\mathbf{u}}(t) + \mathbf{C}\dot{\mathbf{u}}(t) + \mathbf{K}\mathbf{u}(t) = -\mathbf{M}\tau\ddot{u}_g(t) \quad (4.4)$$

where \mathbf{M} , \mathbf{C} , and \mathbf{K} are the mass, damping, and stiffness matrices, respectively, while $\ddot{\mathbf{u}}(t)$, $\dot{\mathbf{u}}(t)$, and $\mathbf{u}(t)$ denote the acceleration, velocity, and displacement vector. Furthermore, τ is the mass influence vector while $\ddot{u}_g(t)$ represents the ground acceleration. As a result, \mathbf{M} and \mathbf{K} read,

$$\mathbf{M} = \begin{pmatrix} m_1 + m_s & 0 & 0 & 0 \\ 0 & m_2 & 0 & 0 \\ 0 & 0 & m_c & 0 \\ 0 & 0 & 0 & m_i \end{pmatrix} \quad (4.5)$$

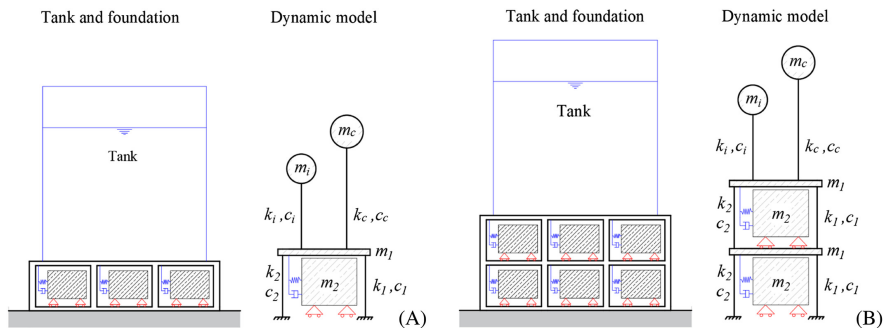


Figure 4.3: Tank-foundation coupled systems: (A) one-layer case and (B) two-layer case

$$\mathbf{K} = \begin{pmatrix} k_1 + k_2 + k_c + k_i & -k_2 & -k_c & -k_i \\ -k_2 & k_2 & 0 & 0 \\ -k_c & 0 & k_c & 0 \\ -k_i & 0 & 0 & k_i \end{pmatrix} \quad (4.6)$$

and,

$$\mathbf{M} = \begin{pmatrix} m_1 & 0 & 0 & 0 & 0 & 0 \\ 0 & m_2 & 0 & 0 & 0 & 0 \\ 0 & 0 & m_1 + m_s & 0 & 0 & 0 \\ 0 & 0 & 0 & m_2 & 0 & 0 \\ 0 & 0 & 0 & 0 & m_c & 0 \\ 0 & 0 & 0 & 0 & 0 & m_i \end{pmatrix} \quad (4.7)$$

$$\mathbf{K} = \begin{pmatrix} k_1 + k_2 + k_1 & -k_2 & -k_1 & 0 & 0 & 0 \\ -k_2 & k_2 & 0 & 0 & 0 & 0 \\ -k_1 & 0 & k_1 + k_2 + k_c + k_i & -k_2 & -k_c & -k_i \\ 0 & 0 & -k_2 & k_2 & 0 & 0 \\ 0 & 0 & -k_c & 0 & k_c & 0 \\ 0 & 0 & -k_i & 0 & 0 & k_i \end{pmatrix} \quad (4.8)$$

for the Metafoundation with one and two layers, respectively.

More precisely, m_1 , m_2 , k_1 , and k_2 denote the total mass of the cells, the mass of the resonators, the horizontal stiffness of all columns, and the stiffness of all springs attached to the resonators, respectively. Additionally, m_s is assigned to the top slab of the Metafoundation.

4.2.3 Seismic design of the Metafoundation

The construction site of the aforementioned foundation-tank system was chosen to be Priolo Gargallo (Italy), which is characterized by a peak ground acceleration PGA of 0.56 g for safe shutdown earthquake and soil type B.

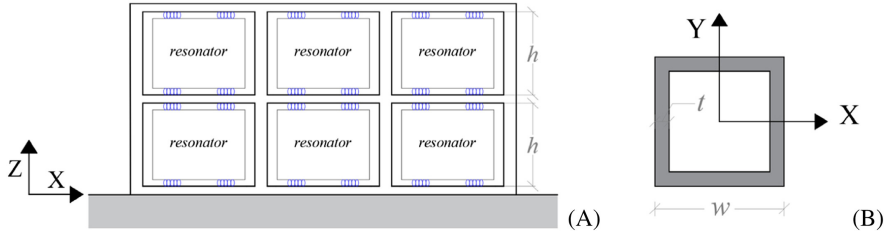


Figure 4.4: Two-layer metafoundation: (A) cross section of the foundation; (B) cross section of a steel column.

Table 4.2: Geometrical characteristics of each foundation layout.

Foundation layout	L2H3	L2H4	L1H3	L2H3
number of layers	2	2	1	1
h [m]	3.0	4.0	3.0	4.0
w [mm]	200	230	250	300
t [mm]	30	30	30	30

Since the foundation is supposed to remain undamaged even for SSE earthquakes, according to the conservative Italian code requirements for shallow foundations [107], the columns are designed to remain elastic for PGAs corresponding to a return period of 2475 years. The resulting stresses and modal displacements of the coupled system (see Figure 4.3) were combined with the complete quadratic combination and provided a lower bound for the cross-sectional dimensions of the steel columns shown in Figure 4.3(B). As a result, four Metafoundations characterized by different combinations of layers and column heights were designed. The relevant geometrical characteristics are collected in Table 4.2, and the nomenclature can be found in Figure 4.4.

4.2.4 Site-specific seismic hazard and accelerogram selection

In order to evaluate the seismic activity of the construction site, i.e. Priolo Gargallo, two sets of natural accelerograms were selected with 10% and 5% probability of exceedance in 50 years, i.e. the so-called operating basis earthquakes (OBE) and safe shutdown earthquakes (SSE), respectively [109]. These accelerograms are listed in Table 4.3 and 4.4. They are selected so that their mean spectrum fits in a least-square sense the uniform hazard spectrum (UHS), and are used in Section 4.6 for the validation of the metafoundation designs. Although more sophisticated techniques are

Table 4.3: List of natural accelerograms for OBE events.

Event	Country	M_w	R_{jb} [km]
Loma Prieta	USA	6.93	3.85
Kalamata	Greece	5.90	11.00
South Iceland	Island	6.50	15.00
L'Aquila Mainshock	Italy	6.30	4.87
Friuli Earthquake	Italy	5.60	26.21
Northridge-01	USA	6.69	20.11
Umbria Marche	Italy	6.00	11.00
Montenegro	Montenegro	6.90	16.00
Erzincan	Turkey	6.60	13.00
Friuli Italy-01	Italy	6.50	14.97
South Iceland	Island	6.40	12.00
Times New Roman	Greece	6.00	14.00
L'Aquila Mainshock	Italy	6.30	4.63
L'Aquila Mainshock	Italy	6.30	4.39
L'Aquila Mainshock	Italy	6.30	5.65
South Iceland	Island	6.50	7.00
Northridge-01	USA	6.69	35.03

present in the literature, see for instance, the conditional mean spectrum (CMS) [110], the aforementioned UHS procedure is considered herein [111]. More precisely, methods like the CMS can reduce the dispersion of the response spectra at different periods, which is very important for a probabilistic analysis based on fragility functions. Nonetheless, the present work focuses on the feasibility of an innovative metamaterial-based design, and therefore, the UHS-based procedure suffices. Both the response spectra of selected accelerograms and the UHS of Priolo Gargallo are shown in Figure 4.5; a careful reader can note that the seismic events exhibit a good mean fit of the UHS with a significant dispersion in frequency content.

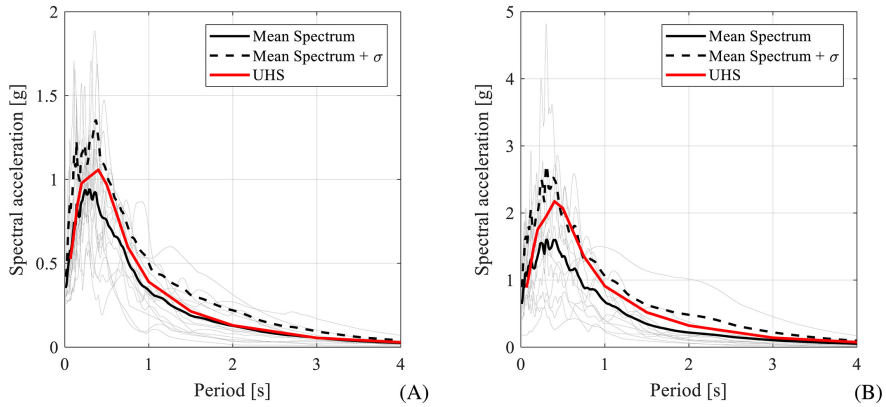
4.3 Uncoupled system properties and metamaterial concept

4.3.1 Properties of a periodic lattice

If the Metafoundation described in Subsection 4.2 can be designed as a periodic system, relevant unit cells can suppress the propagation of seismic waves in certain frequency regions [27, 92]. These regions are called band gaps and can be determined by means of a lattice dispersion analysis using the Floquet–Bloch theorem [73]. Under the aid of this theorem, it becomes possible

Table 4.4: List of natural accelerograms for SSE events.

Event	Country	M_w	R_{jb} [km]
Victoria Mexico	Mexico	6.33	13.8
Loma Prieta	USA	6.93	3.85
Northridge-01	USA	6.69	20.11
Montenegro	Montenegro	6.90	25.00
Erzincan	Turkey	6.60	13.00
South Iceland	Island	6.50	7.00
L'Aquila Mainshock	Italy	6.30	4.87
Loma Prieta	USA	6.93	11.03
Landers	USA	7.28	11.03
South Iceland	Island	6.40	11.00
L'Aquila Mainshock	Italy	6.30	4.63
L'Aquila Mainshock	Italy	6.30	4.39

**Figure 4.5:** Response spectra of the selected accelerograms: (A) UHS for OBE; (B) UHS for SSE.

to reduce the study of an infinite lattice to the analysis of a single unit cell with Floquet-Bloch quasi-periodic boundary conditions. After imposing these conditions, a frequency dispersion analysis can be carried out and the band gaps of the system can be found. According to the Floquet-Bloch theorem, the solution $u(x, t)$ for a periodic system reads,

$$u(\mathbf{x}, t) = \mathbf{u}_{\mathbf{k}} e^{i(\mathbf{q}\mathbf{x} - \omega t)} \quad (4.9)$$

where $q = [q_x, q_y, q_z]^T$ is the wave vector which becomes a scalar $q = q_x = 2\pi/\lambda$ in the uniaxial case, where λ defines the wavelength, while ω represents the circular frequency. In the uniaxial case, the solution $u(x + R)$ of the periodic lattice becomes,

$$u(x + R) = u e^{iqR} \quad (4.10)$$

where R is the lattice constant. Furthermore, in order to apply these conditions, the EOMs of a typical cell need to be considered,

$$m_1^j \ddot{u}_1^j - k_1 u_1^{j-1} + k_1 u_1^j + k_2 u_1^j + k_1 u_1^j - k_2 u_2^j - k_1 u_1^{j+1} = 0 \quad (4.11)$$

and,

$$m_2^j \ddot{u}_2^j - k_2 u_1^j + k_2 u_2^j = 0 \quad (4.12)$$

where m_i , k_i , and u_i denote masses, stiffnesses and displacements of both cells and resonators indicated in Figure 4.6(A), while the superscript j determines the position of the unit cell, i.e. j , unit cell under study, $j - 1$, unit cell below and $j + 1$: unit cell above. After the imposition of the boundary condition (4.10) onto the terms u_i^{j+1} and u_i^{j-1} in (4.11) and (4.12), respectively, the discrete eigenvalue problem can be formulated as,

$$(\mathbf{K} - \omega^2 \mathbf{M}) \mathbf{u} = 0 \quad (4.13)$$

The non-trivial solutions of (4.13), with applied boundary conditions and under consideration of the trigonometric relationship $e^{iqR} = \cos(qR) + i \sin(qR)$, yields the following dispersion relationship,

$$m_1 m_2 \omega^4 - [(m_1 + m_2)k_2 + 2m_2 k_1 (1 - \cos(qR))] \omega^2 + 2k_1 k_2 (1 - \cos(qR)) = 0 \quad (4.14)$$

Thus, Figure 4.6 illustrates the dispersion relation and corresponding band gap of an infinite periodic stack of unit cells for the configuration L2H4 presented in Subsection 4.2.3. Clearly, a band gap forms in the frequency range of 1-1.7 Hz, which according to the Floquet-Bloch theorem does not allow the propagation of elastic waves. However, this result is only valid for an infinite lattice. Therefore, additional analyses are presented hereinafter for the case of a finite foundation.

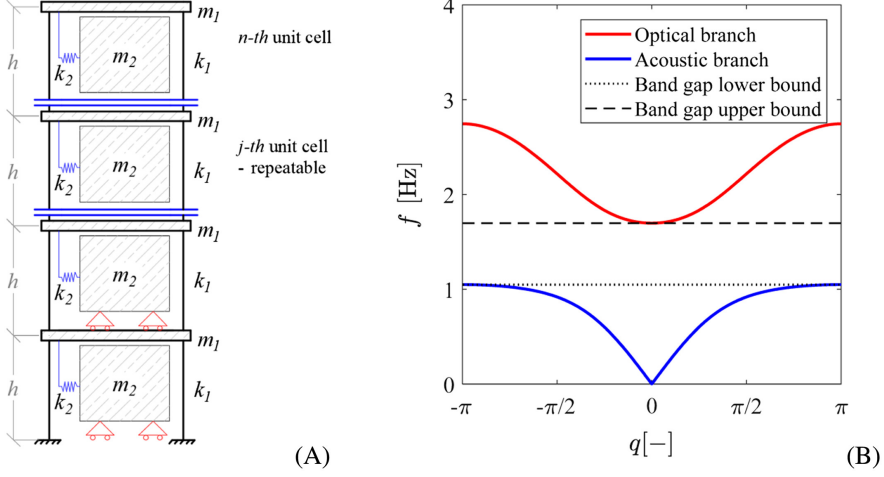


Figure 4.6: (A) 1D mass-resonator chain model. (B) dispersion relation for an infinite stack of unit cells with the geometric properties of L2H4.

4.3.2 Concept of seismic isolation and negative apparent mass

Another well-known concept for the protection of critical infrastructures is seismic isolation [50]. In this regard, the linear theory of seismic isolation [50] entails that the dynamic response of a base-isolated structure is governed by the parameter $\epsilon = \omega_b^2/\omega_s^2$, where ω_b is the frequency of the base-isolated structure and ω_s is the fundamental frequency of the fixed-base structure. If ϵ is of the order of 10^{-2} or less, the design of the seismic isolation can be considered effective. For the case at hand, the impulsive mode of the tank, described in Subsection 4.2.1 is the one of interest. Therefore, ω_s becomes the impulsive frequency of the uncoupled system, i.e. $\omega_s = \omega_i$ and ω_b defines the frequency of the impulsive mass m_i of the tank. With regard to the coupled system, see Figure 4.3, it becomes evident that the stiffness of the columns has a direct influence on ϵ . In fact, note that a weakening of the columns entails a reduction of ϵ , which in turn improves the isolation behaviour of the coupled system. Hence, the elastic design of the Metafoundation discussed in Subsection 4.2.3, provides a minimum value for the columns cross-section, and therefore, governs the horizontal stiffness value. Furthermore, to exploit the negative apparent mass concept [75], we consider resonators endowed with masses larger than the one of the unit cell, as shown in Figure 4.7(A). The apparent mass of the system $M_{app}(\omega)$

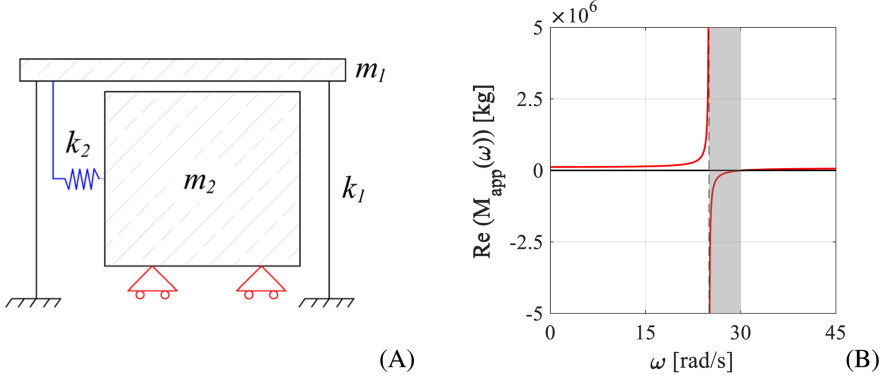


Figure 4.7: (A) Schematization of a unit cell; (B) Apparent mass as a function of forcing frequency.

depicted in Figure 4.7(B) reads,

$$M_{app}(\omega) = m_1 - \frac{k_1}{\omega^2} + \frac{k_2}{\omega_2^2 - \omega^2} \quad (4.15)$$

where ω_2 is the frequency of the resonator and ω represents the forcing frequency. It is clear from Figure 4.7(B), that the effective mass becomes negative when the forcing frequency is near to the resonance one. Since the acceleration response is opposing to the applied force, the response amplitude is reduced. This effect is greatly magnified as the input frequency ω approaches the local resonance frequency ω_2 .

4.4 Optimization procedure of the Metafoundation

Metamaterials are typically designed for their band gap properties. However, for a finite lattice the interaction of the metamaterial with the superstructure can have a significant impact on its dynamic behavior [99]. Furthermore, it is established that the frequency content of an earthquake is highly site specific and may change significantly for different sites. Therefore, to take these issues into account, we propose two optimization procedures herein, that are able to optimize the coupled system, for a specific frequency content and a chosen superstructure. In particular, these procedures evaluate the optimal parameters of the resonators, namely k_2 and ζ_2 . With regard to m_2 , based on both the considerations of Subsection 4.3.2 on the apparent mass, and the main limitation of TMDs, being the low mass of the damper [106, 112], we design the resonators to exert the largest mass compatible with the unit cell dimensions. As a result, the remaining free parameters in

the optimization procedure are: i) the stiffness k_2 of each resonator; ii) the damping ratio ζ_2 of each resonator.

4.4.1 Ground motion modelling

In a first step, the earthquake ground motions are modelled as a stationary Gaussian filtered white noise random process with zero mean and spectral intensity S_0 . In this respect, Kanai and Tajimi [113] proposed an analytical formulation able to simulate a site specific PSD, which has later been modified by Clough and Penzien [114]. This formulation is based on the Kanai-Tajimi filter modified by Clough and Penzien and, for brevity, is referred to as KTCP. The KTCP filter is evaluated as,

$$H_{KTCP}^2(i\omega) = H_{CP}^2(i\omega)H_{KT}^2(i\omega) \quad (4.16)$$

where $H_{CP}(i\omega)$ attenuates the very low-frequency component introduced by Clough and Penzien, and $H_{KT}(i\omega)$ denotes the soil filter suggested by Kanai and Tajimi. The filters read,

$$H_{CP}(i\omega) = \frac{\frac{\omega^2}{\omega_1}}{\left(1 - \frac{\omega^2}{\omega_1^2}\right) + 2i\zeta_g \frac{\omega}{\omega_g}} \quad (4.17)$$

$$H_{KT}(i\omega) = \frac{1 + 2i\zeta_g \frac{\omega}{\omega_g}}{\left(1 - \frac{\omega^2}{\omega_g^2}\right) + 2i\zeta_g \frac{\omega}{\omega_g}} \quad (4.18)$$

where ω_g and ζ_g are the frequency and damping ratio that describe the characteristics of the soil, while ω_1 and ζ_1 denote the parameters of the low pass filter introduced by Clough and Penzien.

4.4.2 Optimization procedures in the frequency domain

The evaluation of the response of the coupled system is evaluated in the frequency domain herein. Hence, the system of EOMs of the coupled foundation-tank system can be written as,

$$\mathbf{M}\ddot{\mathbf{u}}(t) + \mathbf{C}\dot{\mathbf{u}}(t) + \mathbf{K}\mathbf{u}(t) - \mathbf{Y}(t) = -\mathbf{M}\tau\ddot{u}_g(t) \quad (4.19)$$

$$m_{jl}\ddot{y}_{jl}(t) + m_{jl}2\zeta_{rl}\omega_{rl}\dot{y}_{jl}(t) + m_{jl}\omega_{rl}^2 y_{jl}(t) = -m_{jl}[\ddot{u}_g(t) + \ddot{u}_j(t)] \quad (4.20)$$

where $\mathbf{Y}(t)$ is the force vector applied to the Metafoundation by the resonators; $\ddot{y}_{jl}(t)$, $\dot{y}_{jl}(t)$ and $y_{jl}(t)$ define the acceleration, velocity and displacement of the l -th resonator on the j -th layer, while, m_{jl} , ζ_{rl} and ω_{rl} represent the mass, damping ratio and frequency of the resonators, respectively. We condense the masses of the resonators of each layer as shown in

the Subsection 4.2.2. Therefore, the j -th component of the vector $\mathbf{Y}(t)$ can be evaluated as,

$$\sum_{l=1}^{N_r} m_{jl} [2\zeta_{rl}\omega_{rl}\dot{y}_{jl}(t) + \omega_{rl}^2 y_{jl}(t)] \quad (4.21)$$

where N_r is the number of resonators in each layer. Through modal transformation, the displacement vector $u(t)$ can be defined as,

$$\mathbf{u}(t) = \mathbf{\Phi}\mathbf{q}(t) \quad (4.22)$$

where $\mathbf{q}(t)$ is the vector that represents the generalized coordinates of the coupled system, while $\mathbf{\Phi}$ denotes the eigenvector matrix. Substituting (4.22) in (4.19) and premultiplying by $\mathbf{\Phi}^T$, the j -th equation of motion becomes,

$$\begin{aligned} \ddot{q}_k(t) + 2\zeta_k\omega_k\dot{q}_k(t) + \omega_k^2 q_k(t) \\ - \sum_{j=1}^N \psi_k(j) \sum_{l=1}^{N_r} m_{jl} [2\zeta_{rl}\omega_{rl}\dot{y}_{jl}(t) + \omega_{rl}^2 y_{jl}(t)] \\ = -\Gamma_k \ddot{u}_g(t) \end{aligned} \quad (4.23)$$

where $q_k(t)$, ζ_k , ω_k , Γ_k , and $\psi_k(t)$ are the generalized coordinate, damping ratio, eigenfrequency, mass participation factor, and mode value, of the k -th mode at the j -th layer, respectively. In order to obtain the transfer functions of the system, we define ground acceleration, modal displacement, displacement and forcing term as $\ddot{u}_g(t) = 1e^{\omega t}$, $q_k(t) = T_{qk}(\omega)e^{\omega t}$, $u_j(t) = T_{u_j}(\omega)e^{\omega t}$ and $y_{jl}(t) = T_{y_{jl}}(\omega)e^{\omega t}$, respectively, assuming a unit amplitude for $\ddot{u}_g(t)$. Substituting these relationships into (4.20) and (4.23), we obtain,

$$\frac{T_{qk}(\omega)}{H_k(\omega)} - \sum_{j=1}^N \psi_k(j) \sum_{l=1}^{N_r} m_{jl} [i2\zeta_{rl}\omega_{rl}\omega + \omega_{rl}^2] T_{y_{jl}}(i\omega) = -\Gamma_k \quad (4.24)$$

$$\frac{T_{y_{jl}}(\omega)}{H_{rl}(\omega)} = -1 + \omega^2 T_{u_j}(\omega) \quad (4.25)$$

where $H_k(\omega)$ and $H_{rl}(\omega)$ define the transfer functions of an SDoF system,

$$H_k(\omega) = \frac{1}{\omega_k^2 - \omega^2 + i2\zeta_k\omega_k\omega} \quad (4.26)$$

$$H_{rl}(\omega) = \frac{1}{\omega_{rl}^2 - \omega^2 + i2\zeta_{rl}\omega_{rl}\omega} \quad (4.27)$$

The modal transformation (4.22) combined with (4.24) and (4.25) entail the displacement transfer function of (4.25). Subsequently, the transfer functions of the interstorey drift $D_j(\omega)$, relative velocity $V_j(\omega)$ and absolute

acceleration $A_j(\omega)$ can be evaluated as,

$$D_j(\omega) = T_{u_j}(\omega) - T_{u_{j-1}}(\omega) \quad (4.28)$$

$$V_j(\omega) = i\omega T_{u_j}(\omega) \quad (4.29)$$

$$A_j(\omega) = 1 - \omega^2 T_{u_j}(\omega) \quad (4.30)$$

Hence, the power spectral density (PSD) of $u(t)$ can be evaluated as,

$$S_{uu}(\omega) = |H_{uu}(\omega)|^2 S_{KTCP}(\omega) \quad (4.31)$$

where $S_{uu}(\omega)$ denotes the PSD of $u(t)$, while $H_{uu}(\omega)$ represents a generic transfer function of the coupled system. Furthermore, based on the Wiener-Khintchine transformations, the autocorrelation function $R_{uu}(\tau)$ the variance σ^2 of a generic response can be calculated as,

$$\sigma_{uu}^2 = R_{uu}(0) = \int_{-\infty}^{+\infty} S_{uu}(\omega) d\omega \quad (4.32)$$

Hence, the variance of drift $\sigma_{D_j}^2$, velocity $\sigma_{V_j}^2$ and absolute acceleration $\sigma_{A_j}^2$ at the j -th layer can be computed by means of (4.31) and (4.32) as,

$$\sigma_{D_j}^2 = \int_0^{+\infty} |D_j(\omega)|^2 H_{KTCP}^2(\omega) d\omega \quad (4.33)$$

$$\sigma_{V_j}^2 = \int_0^{+\infty} |V_j(\omega)|^2 H_{KTCP}^2(\omega) d\omega \quad (4.34)$$

$$\sigma_{A_j}^2 = \int_0^{+\infty} |A_j(\omega)|^2 H_{KTCP}^2(\omega) d\omega \quad (4.35)$$

4.4.3 Optimization parameters

In order to compute the optimal parameters of the resonators, we can use the variances of the responses of the coupled system defined in (4.32). More precisely, to evaluate the effectiveness of the Metafoundation and the optimal stiffness and damping ratio of the system, two parameters, the Performance Index PI and the Energy Dissipation Index EDI are defined based on: i) the reduction of the absolute acceleration of the impulsive mass m_i ; ii) the energy dissipated by the resonators. The performance index PI can be defined as,

$$PI(\zeta_2, \omega_2) = \frac{\sigma_{A_i}^2(\zeta_2, \omega_2)}{\sigma_{A_i fix}^2} \quad (4.36)$$

where $\sigma_{A_i}^2$ is the variance of the absolute acceleration of the impulsive mass of the coupled system as a function of the damping ratio and the frequency of

the resonators, while $\sigma_{A_{ifix}}^2$ defines the same quantity for a coupled system with a fixed base. As a result, the optimal values of the unknown parameters are obtained reducing the absolute acceleration of the impulsive mass of the superstructure as follows,

$$\zeta_2^{opt}, \omega_2^{opt} = \min[PI(\zeta_2, \omega_2)] \quad (4.37)$$

As far as the energy dissipation index EDI is concerned, it is based on the dissipated energy by the resonators with respect to the input energy [106]. In this case, the j -th equation of motion can be written in terms of relative energy balance by multiplying each term by the velocity of the j -th degree of freedom and then integrating over time, yielding,

$$E_{k_j}(t) + E_{d_j}(t) + E_{e_j}(t) = E_{i_j} + E_{f_j}(t) \quad (4.38)$$

where $E_{k_j}(t)$ is the relative kinetic energy, $E_{d_j}(t)$ defines the energy dissipated by viscous damping, $E_{i_j}(t)$ is the elastic strain energy, $E_{f_j}(t)$ represents the relative input energy and is the energy flowing between the degrees of freedom. Since the seismic input is a stochastic process, (4.38) has to be formulated in terms of expected values as,

$$E[E_{k_j}] + E[E_{d_j}] + E[E_{e_j}] = E[E_{i_j}] + E[E_{f_j}] \quad (4.39)$$

In particular, if we consider the conservation of mechanical energy in a finite time increment Δt , (4.39) becomes,

$$E[\Delta E_{d_j}] - E[\Delta E_{f_j}] = E[\Delta E_{i_j}] \quad (4.40)$$

Reggio and De Angelis [106] proved that the relative input energy of the system is equal to the dissipated one, thus resulting in,

$$\sum_{j=1}^N E[E_{f_j}] = 0 \quad (4.41)$$

where N defines the degree of freedom of the system. Thus, the EDI can be expressed as,

$$EDI(\zeta_2, \omega_2) = \frac{\sum_{r=1}^{N_r} E[\Delta E d_r(\zeta_2, \omega_2)]}{\sum_{j=1}^N E[\Delta E d_j(\zeta_2, \omega_2)]} \quad (4.42)$$

where N_r indicates the number of resonators. More details about the evaluation of these terms can be found in [106]. Finally, the optimal damping ratio ζ_2^{opt} and frequency parameter ω_2^{opt} are obtained by maximizing the energy dissipated by the resonators with respect to the one dissipated by the whole coupled system,

$$\zeta_2^{opt}, \omega_2^{opt} = \max[EDI(\zeta_2, \omega_2)] \quad (4.43)$$

4.5. Results of Metafoundation optimizations

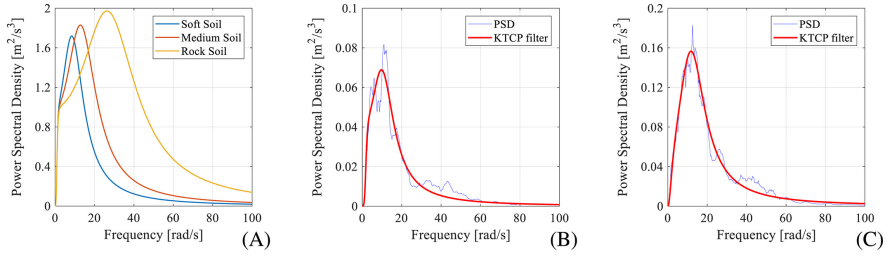


Figure 4.8: PSD functions of filtered white noises: (A) KT TCP filter for three types of soil; (B) average PSD and KT TCP fit for OBE events; (C) average PSD and KT TCP fit for SSE events

Table 4.5: Parameters of the KT TCP filter.

Soil type	S_0 [m^2/s^3]	ω_g [rad/s]	ζ_g	ω_1 [rad/s]	ζ_1
Soft	1.0	10.5	0.65	1.0	0.7
Medium	1.0	15.6	0.60	1.0	0.7
Rock	1.0	31.4	0.55	1.0	0.7
Priolo G. OBE	0.037	12.0	0.60	2.0	0.62
Priolo G. SSE	0.090	14.0	0.60	0.75	1.90

4.5 Results of Metafoundation optimizations

In order to apply the optimization procedures described in the previous Section, three different types of soils - soft, medium and rock soil [115] - modeled with the KT TCP filter are considered, as shown in Figure 4.8(A). Furthermore, to evaluate the PSD of the ground motions representative for the construction site, the procedure described in Section 4.8 is applied to the seismic records selected in Subsection 4.2.4. Thus, in order to fit the PSD functions that characterize the OBE and SSE events, the parameters of the KT TCP filter ($S_0, \omega_g, \zeta_g, \omega_1, \zeta_1$) were evaluated. The resulting PSD functions and the fitted KT TCP filtered estimates are shown in Figure 4.8(B) and Figure 4.8(C), respectively, while Table 4.5 displays the relevant parameters.

The optimization procedure is carried out for each Metafoundation described in Table 4.2. Thus, with reference to the L1H4 foundation with a slender tank, typical results are depicted in Figure 4.9, that shows both the surface and the contour line of PI, respectively, corresponding to the SSE case for the Priolo Gargallo site. The same information is illustrated in Figure 4.10 for EDI. In order to select the optimal combination of coupled Metafoundation-tank systems, taking into account different soil properties, 4 different foundations with 2 distinct tanks, as described in Subsection 4.2.1 and 4.2.3, are subjected to 5 different PSDs and evaluated by means of PI

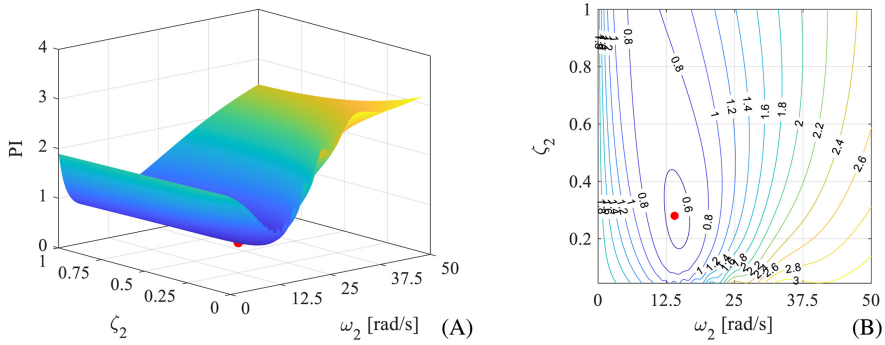


Figure 4.9: PI optimization of a slender tank on an L1H4 foundation with SSE records: (A) optimization surface vs. resonator parameters; (B) contour lines of the optimization surface

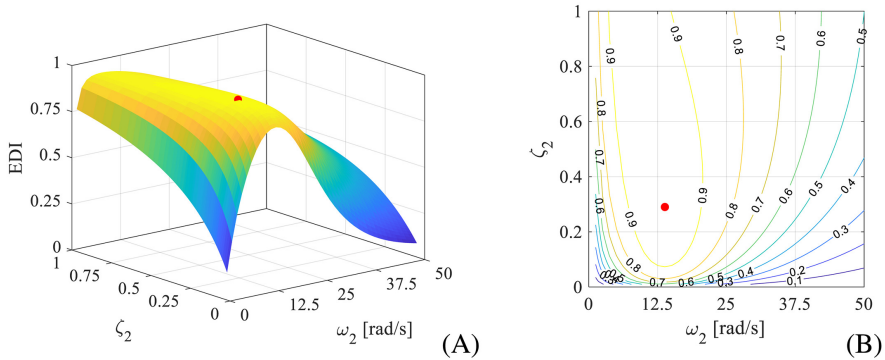


Figure 4.10: EDI optimization of a slender tank on an L1H4 foundation with SSE records: (A) optimization surface vs. resonator parameters; (B) contour lines of the optimization surface

and EDI parameters. Thus, Tables 4.6 and 4.7 summarize the optimal parameter values ζ_2^{opt} and ω_2^{opt} of the resonators for slender and broad tanks, respectively. The results show that PI and EDI yield very similar optimal frequencies for the resonators, while the optimal damping ratio is found to be higher for the EDI approach. Clearly, this is related to the fact that the EDI parameter focuses on the amount of energy that is being dissipated by the resonators. A better comparison between the results provided by the two indices can be done after time history analyses carried out in Section 4.6.

The results of the optimization also confirm the effectiveness of the isolation effect provided by the unit cells. With regard to the PI and EDI values of the system for different foundations, while also observing the isola-

tion parameter ϵ , it becomes clear that the Metafoundation reduces stresses not only due to its metamaterial like or TMD like properties, but also because of its capability to exert a limited amount of seismic isolation. As a result, the L1H4 foundation performs better in terms of both PI and EDI due to its small epsilon value. With regard to the ground-metafoundation coupling, more flexible foundations perform better in firm soils due to the maximum decoupling between soil and foundation frequency content. The best performance is obtained for the L1H4 foundation with rock soil for both PI and EDI values. When comparing the parameters of the KTCP fitted PSD obtained for the Priolo Gargallo soil to the standard KTCP soil filters, see Table 4.5, it becomes apparent that the Priolo Gargallo site is in between medium and soft soil. Moreover, Table 4.6 shows that similar optimal resonator parameters are obtained for both Priolo Gargallo soils.

The optimization procedure for the broad tank provides lower values for ζ_2^{opt} and ω_2^{opt} compared to the slender tank, since it has a different geometry and, therefore, exerts lower eigenfrequencies. However, analogously to the slender tank, also the broad tank shows better results for a more flexible foundation in firm soils. Note that more favorable results are obtained for the broad tank, with respect to the slender one, despite the increased ϵ value. This is due to the decoupling of the eigenfrequency of the coupled system and the frequency content of the soil filter. In addition, the results show that the fitted KTCP filtered soils are located between medium and soft soil types.

4.6 Time history analysis

In order to evaluate the performance of the proposed Metafoundation under realistic ground motions, THAs were carried out for the OBE and SSE events. The base shear of the tank was assumed to be the governing factor for the performance of the system and can be calculated as follows,

$$V = k_i(u_i - u_{tl}) + k_c(u_c - u_{tl}) \quad (4.44)$$

where u_i , u_c and u_{tl} denote the displacement of the impulsive mass, the displacement of the convective mass, and the displacement of the top layer of the foundation, which coincides with the bottom of the tank, respectively. As a result, the reduction of the tank base shear due to the presence of a Metafoundation can be evaluated as,

$$\alpha^{(i)} = \frac{V_{RMS}^{(i)}}{V_{RMS,fix}^{(i)}} \quad (4.45)$$

where V_{RMS} and $V_{RMS,fix}$ are the root mean square (RMS) values of the base shear of a tank on a Metafoundation and a tank on a fixed-base foundation, while i denotes the seismic event under study. This index displays the

Table 4.6: Optimal parameters based on both PI and EDI for the slender tank.

Type of soil	Parameters	L2H3 $\epsilon = 0.48$		L2H4 $\epsilon = 0.38$		L1H3 $\epsilon = 0.33$		L1H4 $\epsilon = 0.27$	
		PI	EDI	PI	EDI	PI	EDI	PI	EDI
SOFT	ζ_2^{opt}	0.17	0.20	0.22	0.28	0.25	0.29	0.29	0.33
	ω_2^{opt}	24.40	22.62	19.60	16.34	17.20	15.08	14.00	11.31
	Performance	0.80	0.85	0.76	0.92	0.70	0.92	0.65	0.94
MEDIUM	ζ_2^{opt}	0.17	0.18	0.21	0.23	0.24	0.27	0.26	0.30
	ω_2^{opt}	24.30	23.88	19.70	18.85	17.60	16.34	15.10	13.82
	Performance	0.78	0.88	0.70	0.93	0.61	0.93	0.52	0.94
ROCK	ζ_2^{opt}	0.15	0.17	0.20	0.24	0.25	0.28	0.31	0.33
	ω_2^{opt}	26.00	26.39	22.10	21.36	20.10	18.85	17.00	15.08
	Performance	0.44	0.87	0.31	0.91	0.23	0.90	0.17	0.95
Priolo G. OBE	ζ_2^{opt}	0.17	0.20	0.22	0.25	0.25	0.28	0.28	0.30
	ω_2^{opt}	24.30	22.62	19.40	17.59	17.00	15.08	14.00	12.57
	Performance	0.82	0.87	0.79	0.93	0.72	0.93	0.66	0.95
Priolo G. SSE	ζ_2^{opt}	0.17	0.18	0.21	0.24	0.24	0.27	0.27	0.29
	ω_2^{opt}	24.30	23.88	19.50	18.85	17.40	16.34	14.60	13.82
	Performance	0.79	0.89	0.73	0.94	0.65	0.94	0.56	0.95

Table 4.7: Optimal parameters based on both PI and EDI for the broad tank.

Type of soil	Parameters	L2H3 $\epsilon = 0.77$		L2H4 $\epsilon = 0.69$		L1H3 $\epsilon = 0.63$		L1H4 $\epsilon = 0.57$	
		PI	EDI	PI	EDI	PI	EDI	PI	EDI
SOFT	ζ_2^{opt}	0.08	0.10	0.14	0.16	0.18	0.21	0.23	0.27
	ω_2^{opt}	18.70	18.85	16.90	16.34	15.30	15.08	13.20	12.57
	Performance	0.79	0.80	0.71	0.88	0.64	0.89	0.56	0.91
MEDIUM	ζ_2^{opt}	0.08	0.10	0.13	0.14	0.18	0.20	0.23	0.27
	ω_2^{opt}	18.80	18.85	17.00	17.59	15.80	16.34	14.10	13.82
	Performance	0.72	0.80	0.60	0.88	0.52	0.88	0.42	0.92
ROCK	ζ_2^{opt}	0.09	0.09	0.14	0.14	0.17	0.20	0.22	0.28
	ω_2^{opt}	20.10	20.11	17.90	18.85	17.70	17.59	15.90	15.08
	Performance	0.49	0.75	0.36	0.84	0.28	0.84	0.21	0.94
Priolo G. OBE	ζ_2^{opt}	0.10	0.10	0.15	0.15	0.19	0.21	0.23	0.27
	ω_2^{opt}	18.90	18.85	16.70	16.34	15.50	15.08	13.40	12.57
	Performance	0.78	0.81	0.70	0.89	0.62	0.90	0.53	0.93
Priolo G. SSE	ζ_2^{opt}	0.09	0.10	0.14	0.14	0.18	0.20	0.23	0.26
	ω_2^{opt}	19.00	18.85	16.90	17.59	15.90	16.34	13.90	13.82
	Performance	0.73	0.81	0.63	0.89	0.54	0.89	0.44	0.92

stress reduction of the Metafoundation with respect to a traditional foundation.

4.6.1 Results for the coupled foundation-slender tank system

Herein, Figure 4.11 shows the RMS of the base shear of the coupled system subjected to SSE events. More precisely, it compares the results of the Metafoundation optimized with PI and EDI with the response of a fixed-base tank. It is worth noting that the results of the THAs show a high dispersion for the base shear when correlated with the PGA. This is due to the wide variety of frequency and amplitude content of the accelerograms depicted in Figure 4.5. Therefore, the PGA may not represent the most significant intensity measure for the structure under consideration. However, since the interest is not on a fragility analysis of the system, the PGA has been considered as a sufficient parameter for result interpretation. A linear regression of the base shear against the PGA, presented in Figure 4.11, shows that the Metafoundation reduces the base shear with respect to a traditional foundation, and that the optimization procedure based on PI seems to deliver slightly better results than the EDI procedure. Furthermore, the general trend shows that the performance of the Metafoundation increases with the foundation flexibility, as predicted by the optimization results discussed in Section 4.5.

It is possible to observe that the L2H3 foundation increases the base shear although the corresponding linear regression shows a slight reduction, as depicted in Figure 4.11(A). This is because the regression defines a law between the base shear and PGA of accelerograms, whereas the mean value of parameter α doesn't take this relationship into account. Note that the reduction of base shear of Figure 4.12 exhibits a certain dispersion due to the variability of accelerograms. This can be quantified by the coefficient of variation (COV) value computed for each type of foundation. More precisely, COV varies from 0.292 to 0.359 for the PI optimized coupled structure, and from 0.290 to 0.357 for the EDI optimized coupled structure. Furthermore, in order to display the effect of their isolation capability, the foundation typologies are ordered by their ϵ value. An average reduction of the base shear between 10% and 15% can be achieved with the optimized foundations L1H3 and L1H4. Conversely, poor results are obtained for the two-layered cases due to the increased stiffness of the foundation. These graphs also support the conclusion that the PI procedure provides a slightly better optimized foundation than the EDI procedure. The fundamental difference between these procedures is that the PI evaluates the minimal absolute acceleration of the impulsive mode while the EDI takes into account the energy dissipated by the resonators. THAs of the coupled foundation-slender tank systems for the Priolo Gargallo soil corresponding to the OBE events are not presented

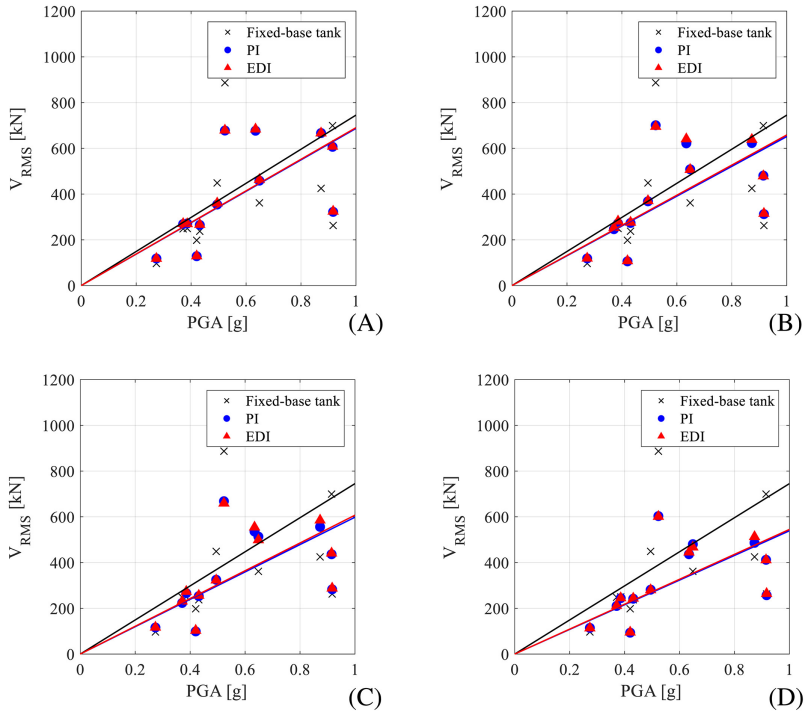


Figure 4.11: RMS of the base shear of a slender tank vs. PGA of the SSE records: (A) L2H3; (B) L2H4; (C) L1H3; (D) L1H4.

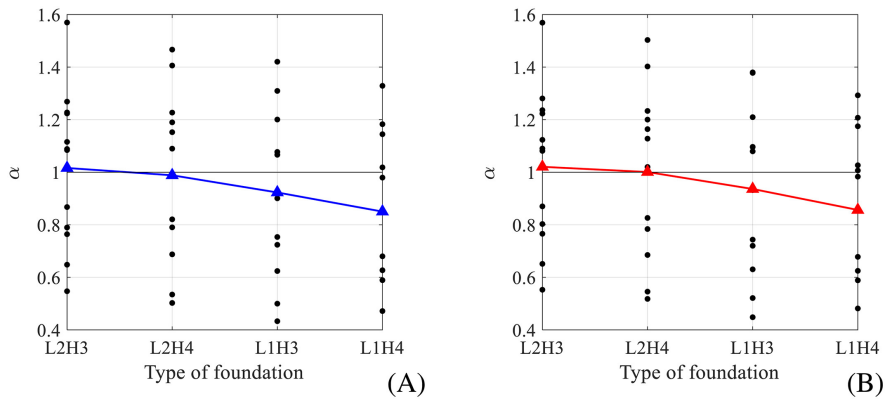


Figure 4.12: Base shear reduction for a slender tank subjected to SSE events: (A) PI optimization; (B) EDI optimization.

for brevity. It shall be mentioned that they show very similar results as for the SSE events and further underline the functionality of the system.

4.6.2 Results for the coupled foundation-broad tank system

Figure 4.13 shows the RMS of the base shear of the coupled system foundation-broad tank with the optimal parameters obtained for the Priolo Gargallo soil corresponding to the SSE events. Also in this case, each Metafoundation reduces the base shear with respect to a traditional foundation. The general trend, shown in Figure 4.14, highlights the impact of the flexibility on the effectiveness of the Metafoundation systems. Here it can be seen that the best performance, for SSE events, was obtained for the L1H4 foundation system achieving a base shear reduction of up to 30%. When comparing these results to the slender tank analyses, it becomes evident that the Metafoundation has a much greater effect on the broad tank system. Even for the two layered setups the broad tank may experience a demand reduction of about 10%-15%. This is caused by the decoupling of the frequencies of the tank from the expected ground motion and further underlines the importance of the superstructure to the performance of the overall system. Furthermore, COVs of α vary from 0.133 to 0.210 for the PI optimized coupled structure and from 0.127 to 0.217 for the EDI optimized coupled structure. The COVs appear to be smaller than those of the slender tank. As a result, the Metafoundations entail a superior performance for the coupled foundation-broad tank.

4.7 Conclusion

In this article, we presented a foundation based on a finite locally resonant metamaterial concept, i.e. the Metafoundation, that has been both designed and optimized. In particular, it exploits the properties of metamaterials and combines them with classical seismic isolation concepts. In order to show that this class of structures can be built under realistic circumstances, the proposed Metafoundation system has been designed according to the Italian standards with conservatism. Note that the construction details are not fully developed; however, in order to address the durability of the system at this early stage, we only use common construction materials and devices such as steel, concrete and wire ropes. Furthermore, the system was designed for a highly vulnerable superstructure, namely fuel storage tanks, and for a very active seismic-prone site. The tuning of this coupled system has been achieved via two optimization algorithms operating in the frequency domain, which are able to account for the superstructure as well as the ground motion spectrum. These algorithms are newly established in the field of mechanical

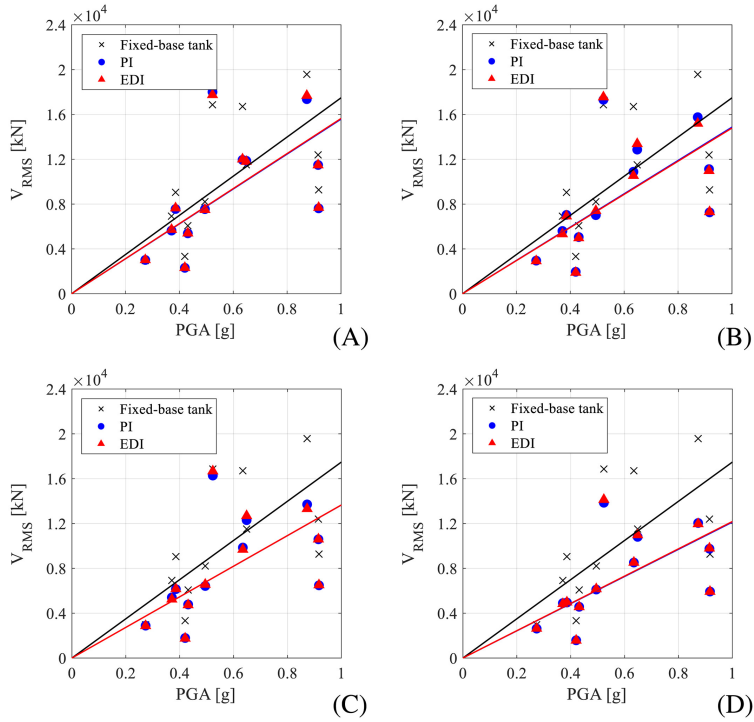


Figure 4.13: RMS of the base shear of a broad tank vs. PGA of the SSE records: (A) L2H3; (B) L2H4; (C) L1H3; (D) L1H4.

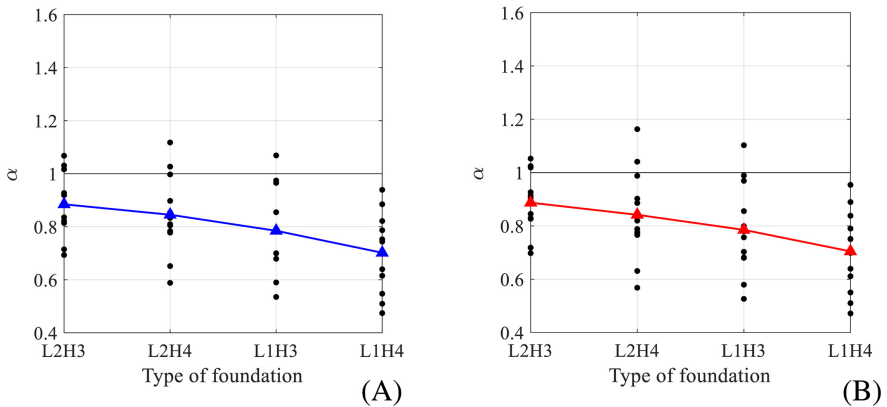


Figure 4.14: Base shear reduction for a broad tank subjected to SSE events: (A) PI optimization; (B) EDI optimization.

metamaterials, and show that the superstructure has a significant influence on the functionality of the Metafoundation. Additionally, they clearly display the influence of the shear stiffness, and therefore, the isolator-like properties. After optimizing the parameters of the Metafoundation, time history analyses were carried out. Favourable results were obtained for the isolation of a broad fuel storage tank with a base shear reduction of about 30%, while for the slender tank the proposed system seems to be a bit less effective with maximum reduction capabilities of about 15%. These results lay down the basis for future studies and developments of the Metafoundation such as, tuning several resonators to different frequencies, employing more advanced optimization procedures, adding another metamaterial-like concept like negative stiffness elements, or designing the foundation for the attenuation of the vertical component of an earthquake. Overall, the proposed standards-compliant metamaterial-based foundation, if properly optimized, can effectively reduce stresses in broad/slender fuel storage tanks for site-specific seismic hazards.

Upcoming developments The building code conform and optimized foundation developed in this chapter shows that this type of structure can be built, but that the required dimensions are clearly beyond what can be considered common for standard civil engineering applications. Therefore, the next chapter develops a mechanism that can be implemented in the foundation, in order to make it more efficient at smaller scales.

4.8 Appendix: Non-stationary power spectral density

This appendix explains how to estimate the time modulating function of the power spectral density (PSD) for time modulated zero-mean Gaussian processes that represent the seismic records introduced in Subsection 4.2.4. At the outset, the PSD function can be written as,

$$S(\omega, t) = \phi^2(t)S_{st}(\omega) \quad (4.46)$$

in which $\phi(t) \leq 1$, is the time modulating function and $S_{st}(\omega)$ is the stationary PSD function. With a set of N seismic records denoted with $\tilde{u}_g^{(i)}(t)$ where $i = 1, 2, \dots, N$ we can define an estimate $\tilde{\phi}(t)$ of $\phi(t)$ as,

$$\tilde{\phi}(t) = \frac{\tilde{\sigma}(t)}{\max(\tilde{\sigma}(t)|t \in [0, T])} \quad (4.47)$$

where $\tilde{\sigma}(t)$ is the estimate of the standard deviation of the recorded signals and T is the duration of the process. By means this time modulating function $\tilde{\phi}(t)$, to a set of non-stationary signals $\tilde{u}_{g,st}^{(i)}(t)$, a set of pseudo stationary

signals $\tilde{u}_{g,st}^{(i)}(t)$ can be evaluated as,

$$\tilde{u}_{g,st}^{(i)}(t) = \frac{\tilde{u}_g^{(i)}(t)}{\tilde{\phi}(t)} \quad (4.48)$$

with the Fourier transform of $\tilde{u}_{g,st}^{(i)}(t)$, we can discretize a finite set of normal random variables realized as stationary Gaussian processes as,

$$\tilde{u}_{g,st}^{(i)}(t) \cong \sum_{p=1}^{M/2} [A_p \cos(\omega_p t) + B_p \sin(\omega_p t)] \quad (4.49)$$

where ω_p is the sampled frequency with frequency increment $\Delta\omega = 2\pi/T$, and M being the total amount of time steps of each signal. A_p and B_p are zero mean Gaussian random variables, the so called Fourier coefficients, and can be evaluated as,

$$A_p^{(i)} = \frac{2}{M} \sum_{k=1}^{\bar{M}} [\tilde{u}_{g,st}^{(i)}(t_k) \cos(\omega_p t_k)] \quad (4.50)$$

$$B_p^{(i)} = \frac{2}{M} \sum_{k=1}^{\bar{M}} [\tilde{u}_{g,st}^{(i)}(t_k) \sin(\omega_p t_k)] \quad (4.51)$$

Since the Fourier coefficients are uncorrelated for different frequencies, more precisely, $E[A_p A_q] = E[B_p B_q] = E[A_p B_q]$, for $p \neq q$, we can find,

$$E[A_p A_p] = E[B_p B_p] = 2S_{st}(\omega_p) \Delta\omega \quad (4.52)$$

$$E[A_p B_p] = 0 \quad (4.53)$$

Finally, using (4.50), (4.51), (4.52) and (4.51), an estimate of the stationary PSD function $\tilde{S}_{st}(\omega_p)$ of the records $\tilde{u}_{g,st}^{(i)}(t)$ can be estimate as,

$$\tilde{S}_{st}(\omega_p) = \frac{1}{N\bar{M}^2 \delta\omega} \sum_{i=1}^N \left| \sum_{k=1}^{\bar{M}} [\tilde{u}_{g,st}^{(i)}(t_k) e^{i\omega_p t_k}] \right|^2 \quad (4.54)$$

Chapter 5

Negative Stiffness Element for Periodic Foundations

Overview. Metamaterials represent a new trend in the field of seismic engineering. Their capacity to attenuate waves at the superstructure level is highly desirable and sought after in recent years. One of their main drawbacks to date, is the excessive size of the necessary resonators and, consequently, the uneconomic design they require. In order to tackle this problem, we apply the concept of negative stiffness to a metamaterial-based foundation system and analyse the potential improvements such a mechanism may have on the metamaterial as well as the coupled structural behaviour. Since negative stiffness is a property that cannot be achieved through conventional measures, a novel mechanism, designed for the implementation in periodic metamaterial-based structures, is proposed herein. The inevitable nonlinearity of the mechanism will be discussed and taken into account, while the advantages of the negative stiffness element (NSE) will be treated analytically and verified numerically. Additionally, through an optimization in the frequency domain and nonlinear time history analyses (THAs), the performance of the system coupled with a fuel storage tank is elaborated. With only 50% of the theoretically allowable NSE value, the foundation system could be reduced to 1/3 of its size. Furthermore, the nonlinear effect of the device has proven to diminish the band-gap of the periodic system, which led us to introduce nonlinearity parameters that can help avoid the strongly nonlinear range. In sum, this article tackles three problems that are intertwined: (i) reducing the size of metamaterial-based structures; (ii) the design of a mechanism that exerts a negative stiffness in a periodic structure; and (iii) the study of the inevitable nonlinearity of NSEs and the subsequent effect on the metamaterial behaviour.

5.1 Introduction

Metamaterials are entering the field of seismic engineering and other research areas with a variety of interesting structures. The two most prevalent concepts in the field of seismic protection are phononic crystals [116] and locally resonant metamaterials [117], where both are able to create the so called band gap phenomenon. Band-gaps signify frequency regions where waves cannot propagate through the material and are therefore able to provide new solutions to existing vibration problems. For the present work we focus on locally resonant materials, due to their ability to attenuate waves at wave lengths much greater than their unit cell size, which is a particularly important property for seismic metamaterials. To date, locally resonant materials have been used to conceive foundation systems [24, 27, 30, 32, 92] and wave barriers [15, 19, 93, 94]. While metabarriers have the advantage of being placed besides the structure, and can therefore be installed after the completion of the building, they can only attenuate surface waves. Metamaterial-based foundations on the other hand, can in principle attenuate any type of incoming wave, but have to be placed below the structure of interest, hence limiting their application to new buildings. The present work is concerned with foundation systems, which show a variety of different designs and applications in the current literature. A particularly interesting foundation was proposed by Cheng and Shi [27] who conceived a system tuned to the ground motion for the protection of nuclear power plants. Their foundation showed different band-gaps for the vertical and horizontal direction, thereby addressing the vertical component of earthquakes. This is especially relevant for high consequence structures like nuclear power plants, since classical isolation systems, like concave sliding bearings, are not able to address the vertical motion [89]. Besides this, also Casablanca et al. [30] developed an interesting foundation based on concrete plates separated by Teflon sliding surfaces and verified its behaviour with laboratory experiments. Their experiments clearly depicted that these types of structures are feasible with common construction materials and can exert the band-gap phenomenon. However, neither Cheng and Shi nor Casablanca et al. took the feedback from the structure into account. La Salandra et al. [32] on the other hand designed a foundation system and conducted a study on the most influencing factors on the attenuation behaviour. Two important findings shall be mentioned, namely, the influence of the stiffness and the non-negligibility of the feedback of the superstructure. Subsequently, Basone et al. [31] developed a foundation system based on their results and conceived an optimization procedure that can take a structure as well as an ensemble of expected ground motions into account. However, their design shows significant restrictions in terms of effectiveness due to the constraints given by the governing building codes (i.e. Eurocode 3 and 8, [82, 118, 119]). Besides this, an experimental study on the coupling effects between a tank isolated with a metamaterial-based foundation and a

pipeline suggested that this type of foundation may provide a compromise between base shear attenuation and horizontal displacement [120], which is a property that cannot be obtained with classical isolation systems. Further worth mentioning is the work of Witarto et al. [121] who studied the application of metamaterial-based systems to small scale nuclear reactors; and the work done by Ungureanu et al. [122] who used auxetic like materials to protect high-rise buildings. Finally, a comprehensive review of seismic metamaterials including metabarriers as well as foundation systems was given recently by Mu et al. [123]. From their review one can clearly conclude that one of the most pressing problems of metamaterial-based foundations is the excessive size necessary to obtain a functional foundation. However, two advantages may become attainable through such foundations in future, namely: (i) attenuation of the vertical component [27]; and (ii) a compromise between base shear reduction and horizontal displacement [120]. One idea to improve the performance of a metamaterial-based system was proposed by Antoniadis et al. [124] who showed that a negative stiffness element (NSE) inserted in the resonator mechanism could potentially improve the system behaviour significantly. Note that this is not an effective negative stiffness as discussed in e.g. [125], but a composite spring system where the resulting force assists motion and does not oppose it. Note that Antoniadis et al. [124] included only a conceptual negative stiffness element that would exert the desirable amplification force, while a design for an actual mechanism that could be applied to a periodic structure was still missing. To date, most proposals including negative stiffness and metamaterials aim at the continuum level [126, 127], while Morris et al. [128] conducted an experimental study on such a continuous metamaterial with buckling type instabilities and showed the energy dissipation capabilities of the structured medium. These proposals are interested mainly in the material level, and therefore, do not investigate the application to a structure or the inevitable nonlinear effect of an NSE on the band-gap.

It is worth noting that research work on nonlinear metamaterials is still limited and primarily concerned with weakly nonlinear resonant chains. A perturbation approach for the dispersion analysis of weakly nonlinear chains has been proposed by Chakraborty and Mallik [129], which clearly depicts that: (i) solutions to nonlinear wave equations are amplitude dependent; (ii) wave amplitudes influence their own propagation characteristics, the so-called self-action; and (iii) analysis methods in the presence of self-action often do not trace all solutions when more than one dominant component is involved. Another neat approach to calculating the band-gaps for such materials relies on the harmonic balance method (HBM) as has been demonstrated by Lazarov and Jensen [130]. Banerjee et al. [131] on the other hand provide a comprehensive review of 1D metamaterials including materials with nonlinear oscillators. Both showed classical bi-atomic lattices with nonlinear oscillators, e.g. Duffing oscillator, pendulum, impacting res-

onators, and concluded that an increase in elastic nonlinearity, entails a shift and an elongation of the band-gap. Based on the current state of the art, the present work conceives a new mechanism applicable to periodic structures, which is able to reduce the size of metamaterial-based foundations. In order to present a realistic application, a fuel storage tank was chosen as a superstructure and its feedback taken into account when designing and optimizing the foundation. Note that fuel storage tanks represent the most vulnerable and consequence intensive components of industrial plants during earthquakes, and that their seismic protection is still an ongoing issue [37, 40, 43, 44, 76]. The coupled Metafoundation tank system is analysed on its performance for various foundation heights and different levels of applied negative stiffness herein. Note that the practical application includes only a one layered foundation, while further analyses, carried out on the system considered as a periodic structure, shed light on the wave propagation in nonlinear negative stiffness enhanced materials.

5.1.1 Scope

The present work tackles three main research issues, namely: (i) Size reduction of metamaterial-based structures for seismic applications; (ii) Development of an NSE that can be implemented in a metamaterial; and (iii) investigation of the inevitable nonlinear behaviour. The manuscript discusses these issues in the following order: Section 5.2 elaborates the structure, the foundation, and the mechanism and shows the simplified dynamic system used in the subsequent analyses; Section 5.3 shows the metamaterial-like behaviour of a periodic system with and without considering the nonlinear effect; Section 5.4 demonstrates an optimization algorithm for the optimal design of the foundation; Section 5.5 investigates the behaviour of the complete coupled and optimized structure under real seismic action; and Section 5.6 closes the paper with conclusions.

5.2 Description of the structure

The Metafoundation was initially conceived in [32] and later developed and designed according to common construction standards by [31]. The proposed foundation is based on steel columns that support concrete slabs, with resonators placed in between the columns, in order to provide the system with its locally resonant properties, see Figure 5.1(a). Additionally, for an improved performance of the system, a new type of NSE is designed and implemented in the structure by mounting it to the columns and resonators as displayed in Figure 5.1(b) and 5.2. It is further worth noting that the columns govern the horizontal stiffness of the system, which has a significant impact on the functionality of the foundation during earthquakes as shown

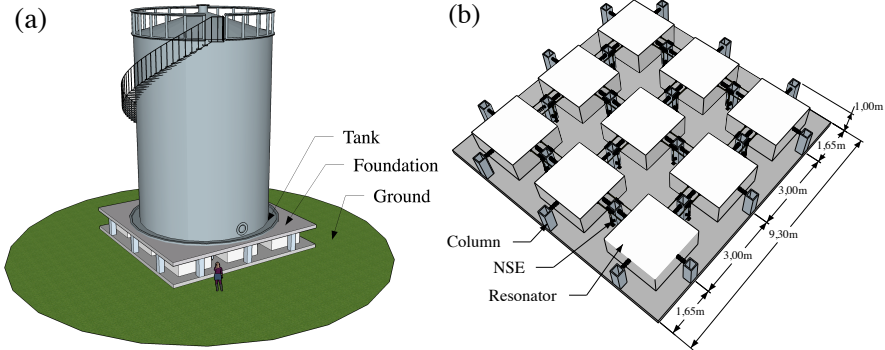


Figure 5.1: Layout of the Metafoundation for the MINIMAL system: (a) Isometric view; (b) Internal view of the foundation components.

Table 5.1: Geometric properties of the various foundation setups.

	FULL	REDUCED	MINIMAL
Foundation height	3 m	2 m	1 m
Resonator height	2.7 m	1.7 m	0.75 m
Column width	0.3 m	0.24 m	0.17 m
Comp. mem. length l	2.7 m	1.7 m	0.7 m

by [31, 32]. They also investigated multiple foundation set-ups, where the one layered design turned out to be the most material efficient version, due to construction standard requirements on the steel columns. Therefore, the present work treats a one layered foundation for feasibility investigations, while a multi-layered foundation system will be discussed only on its wave propagation behaviour. Along these lines, 3 different foundations, namely the FULL, REDUCED and MINIMAL systems, are studied herein, which are distinguished by their heights and column cross sections, as listed in Table 5.1. Note that Figure 5.1 shows the MINIMAL foundation layout where the foundation height amounts to 1 m, while the column width is 0.17 m. Moreover, the columns consist of steel hollow sections with a plate thickness of 0.03 m for all foundation set-ups. It is worth mentioning that each system has been designed to remain elastic for a return period of 2475 years at the site Priolo Gargallo, Italy, according to Eurocode 3 and 8 [82, 118]. Finally, due to the double symmetry of the structure, the system is condensed to a 1D representation that propagates only shear type waves to the superstructure, which is elaborated in Sections 5.2.1 and 5.2.2.

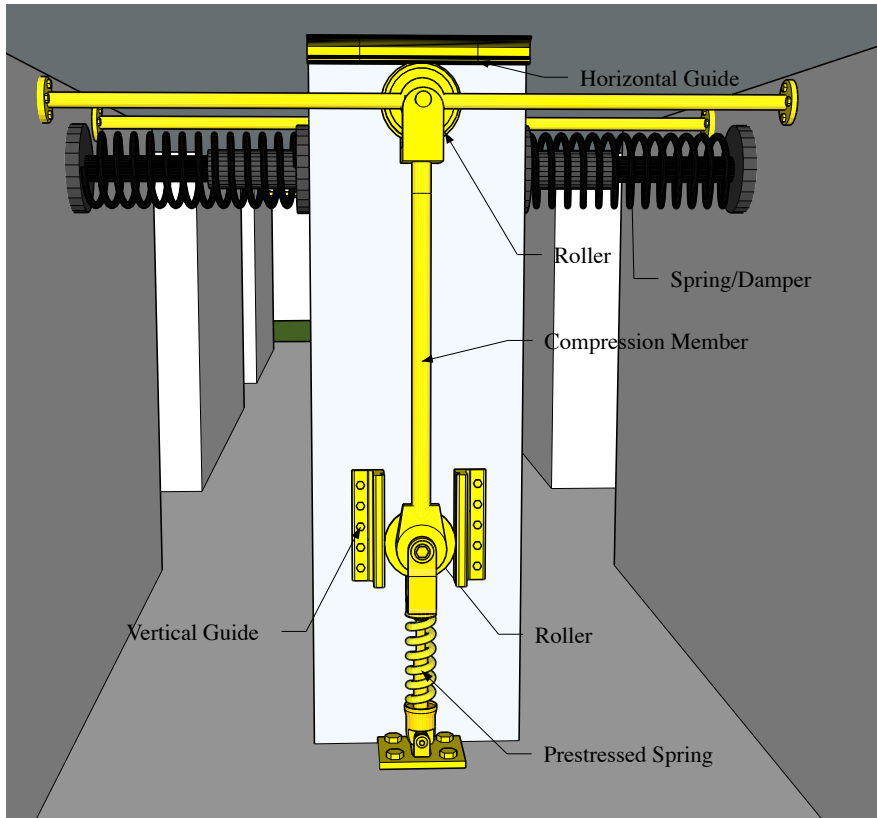


Figure 5.2: Negative stiffness mechanism.

5.2.1 Negative stiffness element NSE

Since a simple spring with a negative effective stiffness does not exist, it is necessary to design a suitable mechanism that can exert the desired forces. For the mechanism at hand we employ a compression member and subject it to a prestress force, as depicted in Figure 5.2. Note that the compression member is guided vertically along the column and horizontally along the slab above, in order to allow for an inclination in the displaced state. Due to this inclination, the compression member releases the stored potential energy from the prestressed spring as a horizontal force pair on the resonators and the columns, see Figure 5.3. Furthermore, as can be seen from Figure 5.1, the mechanism is placed between resonators on both sides of the relevant columns, which amounts to a total of 12 mechanisms per horizontal axis of the foundation. The 9 resonators on the other hand are assumed to slide on frictionless surfaces and have identical properties.

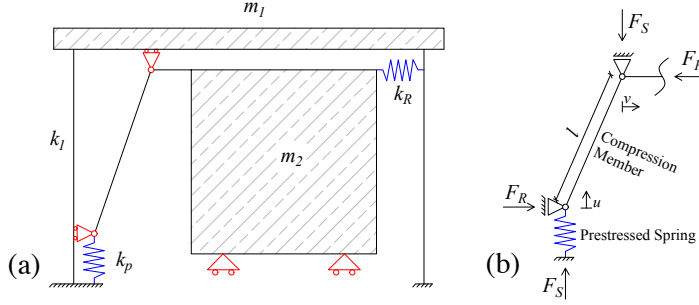


Figure 5.3: Kinematic system in the displaced state: (a) Resonator and mechanism in displaced state; (b) Force equilibrium on the displaced system.

5.2.1.1 NSE analytical model

All resonators, columns and installed mechanisms are identical, and are therefore condensed to one resonator, one column and one mechanism for one layer of foundation. The kinematics of the system can subsequently be simplified as depicted in Figure 5.3(a), where k_1 denotes the condensed stiffness of all columns in one layer, m_2 is the mass of all resonators, m_1 represents the mass of the concrete slab, k_R denotes the condensed spring stiffness of all springs that support the resonators (see also Figure 5.2), and k_p is the stiffness of all prestressed springs. In order to substitute the mechanism with an equivalent nonlinear spring, the force equilibrium needs to be formulated on the displaced system, as shown in Figure 5.3(b). Here, F_R denotes the horizontal force applied to the resonator and the bottom slab; F_S describes the vertical force applied by the pre-stressed spring; l is the length of the compression member; u is the vertical displacement of the member; and v is the horizontal displacement of the resonator and the compression member at its top. When establishing the force equilibrium around the member as depicted in Figure 5.3 (b), the following geometrical relationships can be drawn,

$$F_S = uk_p - P \quad (5.1)$$

$$F_R = \frac{F_S}{(l-u)/l} \frac{v}{l} \quad (5.2)$$

$$(l-u)^2 = l^2 - v^2 \quad (5.3)$$

Here, P is the prestress force applied to the spring when the member is in its vertical position. After some algebra the horizontal force F_R can be put in relation to the displacement of the resonator v with,

$$F_R(v) = \frac{v(-P + k_p(l - \sqrt{l^2 - v^2}))}{\sqrt{l^2 - v^2}} \quad (5.4)$$

Eq. (5.4) clearly is a nonlinear relation for the force displacement path of the resonator, due to the relationship between the displacements u and v . It is important to note that the denominator of this function becomes 0 for $v \rightarrow l$, which has the effect of an infinite stiffness at $v = l$. The length of the mechanism, therefore, plays a significant role in the behaviour of the nonlinearity. Furthermore, a Taylor series approximation of (5.4) at the origin is also desired, in order to allow simplified nonlinear calculations in the frequency domain with the HBM. With the classical formulation of the Taylor series,

$$T(x) = \sum_{n=0}^{\infty} \frac{f^n(a)}{n!} (x-a)^n \quad (5.5)$$

the force-displacement relationship (5.4) can be rewritten for a 3rd order approximation at the origin, with $a = 0$, and $n \in \{0, 1, 2, 3\}$, as,

$$F_R(v) = -\frac{P}{l}v + \frac{k_p l - P}{2 l^3}v^3 + HO(v^5) \quad (5.6)$$

The behaviour of the mechanism can now be dissected into a negative linear and positive nonlinear part,

$$F_R(v) = a_{NSE}v + b_{NSE}v^3 \quad (5.7)$$

with,

$$a_{NSE} = -\frac{P}{l} = k_N \quad (5.8)$$

$$b_{NSE} = \frac{k_p l - P}{2 l^3} = \frac{k_p}{2 l^2} \left(1 - \frac{P}{k_p l}\right) \quad (5.9)$$

From these expressions the maximal stiffness of the mechanism appears at the initial configuration and amounts to $k_N = a_{NSE} = -P/l$, which will be used as an approximation of the NSE for linear analyses. Furthermore, since k_p appears exclusively in the nonlinear part of the polynomial approximation, it can be used to tune the nonlinear shape of the mechanisms force displacement path. Note that when $k_p l$ results in a value smaller than P , the system is subjected to softening instead of hardening, which is physically not meaningful for the system under study. The limits of the mechanism can therefore be set to $\frac{P}{l} \leq k_p \leq \infty$ and a dimensionless nonlinearity parameter established with,

$$\epsilon = 1 - \frac{P}{k_p l}, \quad 0 \leq \epsilon \leq 1 \quad (5.10)$$

When $\epsilon \rightarrow 0$ the system behaves linear, while when $\epsilon \rightarrow 1$ the nonlinear component becomes infinite and the system enters it's nonlinear state immediately. The following values were chosen for the sake of demonstration for Figure 5.4(a), $l = 2.7$ m, $P = 10\,000$ kN and ϵ as 0, 0.5, 0.75, and 0.9.

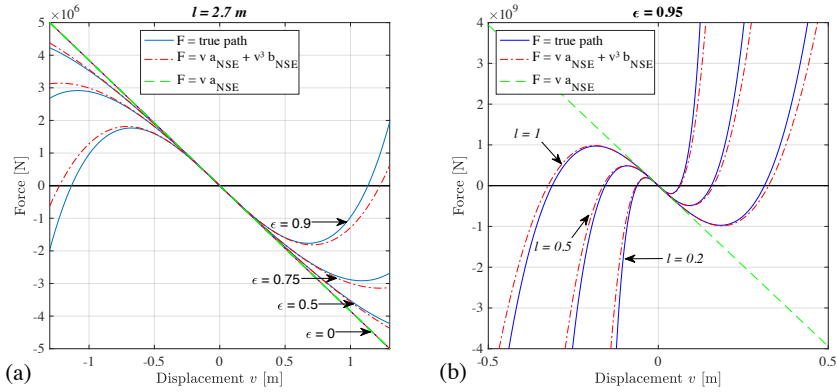


Figure 5.4: Force displacement path: (a) Variation of parameter ϵ ; (b) Variation of member length l .

Besides this, a value of $\epsilon = 0.95$ was regarded as a realistic value for all set-ups, as it resulted in prestress distances of the prestressed spring equal to 13.5 cm, 8.5 cm, and 3.5 cm for the FULL, REDUCED, and MINIMAL system, respectively. Since the length of the compression member plays a vital role in the nonlinear behaviour, a second force-displacement diagram was investigated with length l of 1, 0.5 and 0.2 m for $\epsilon = 0.95$, and displayed in Figure 5.4(b). Clearly, the linear approximation is very close to the exact path for small displacements, which is desirable not only for the sake of simplicity, but also for the later proposed optimization algorithm, based on computations in the frequency domain.

5.2.2 Dynamic system

Once the mechanism can be substituted with a simple nonlinear spring endowed with the force-displacement relationship of Eq. (5.4) or (5.7), the dynamic system can be established for the condensed structure as depicted in Figure 5.5(a). Here, a fuel storage tank with a diameter of 8 m, a height of 12 m and a steel wall thickness of 6 mm is used as a superstructure and modelled as a 2 degree of freedom (DOF) system. The two DOFs represent the impulsive and convective mode according to the procedure proposed by Malhotra et al. [69] and are characterized by their stiffness k_i , k_c and masses m_i , m_c , respectively. In the interest of brevity, the procedure is not elaborated here, while only the stiffness, mass and damping coefficients are listed in Table 5.2. The reader may note that in Figure 5.5 the stiffness of the resonators k_R is a compound stiffness comprised of $k_F - k_N$. Here, k_N represents the linearized stiffness of the NSE, which also corresponds to

Table 5.2: Parameters for the discretized system.

Parameter	FULL	REDUCED	MINIMAL
m_1 [kg]	5.88358e+04	5.00074e+04	4.36692e+04
m_2 [kg]	2.67907e+05	1.78605e+05	7.93800e+04
k_1 [N/m]	8.50176e+08	1.36080e+09	3.30624e+09
k_F [N/m]	to be evaluated	to be evaluated	to be evaluated
k_N [N/m]	to be evaluated	to be evaluated	to be evaluated
c_R [Ns/m]	to be evaluated	to be evaluated	to be evaluated
m_i [kg]	4.51666e+05	4.51666e+05	4.51666e+05
m_c [kg]	8.57730e+04	8.57730e+04	8.57730e+04
k_i [N/m]	8.35184e+08	8.35184e+08	8.35184e+08
k_c [N/m]	3.86480e+05	3.86479e+05	3.86479e+05
c_i [Ns/m]	1.94223e+06	1.94222e+06	1.94222e+06
c_c [Ns/m]	1.82070e+03	1.82070e+03	1.82070e+03

the maximal negative stiffness value, while k_F denotes that part of k_R that determines the resonant frequency of the resonator. Modelling the springs in this way has the following advantages: (i) when k_N is small, k_F becomes the dominant stiffness and can be used to evaluate the eigenfrequency of the resonator with $\omega_R = \sqrt{k_F/m_2}$; and (ii) if k_F becomes small, the local stability of the resonator is still fulfilled by the opposing positive stiffness $-k_N$. Furthermore, in Figure 5.5 the displacement of the foundations top slab and resonator are denoted with u_1 and u_2 , respectively, while the relative ground displacement is represented with u_g .

For the damping of the structure, we chose a Rayleigh model with 5% damping at 0.5 and 7 Hz applied to the structure without resonators and tank. The resonators on the other hand are assigned with a linear viscoelastic damper, denoted with c_R , which works in parallel with k_R , and is also subjected to the optimization procedure described later in this work. Furthermore, the two DOFs of the tank have been endowed with damping values of 5% and 0.5% for the impulsive and convective mode, respectively, and are denoted with c_i and c_c . All relevant values of the condensed dynamic system for all subsequent analyses are shown in Table 5.2.

Besides this, the proposed foundation will be analysed not only as a one layered system for the protection of fuel storage tanks, but also on its wave propagation properties when arranged as a periodic stack. For this purpose, a multi-layered foundation can be imagined as depicted in Figure 5.5(b), where one layer represents the unit cell of the system.

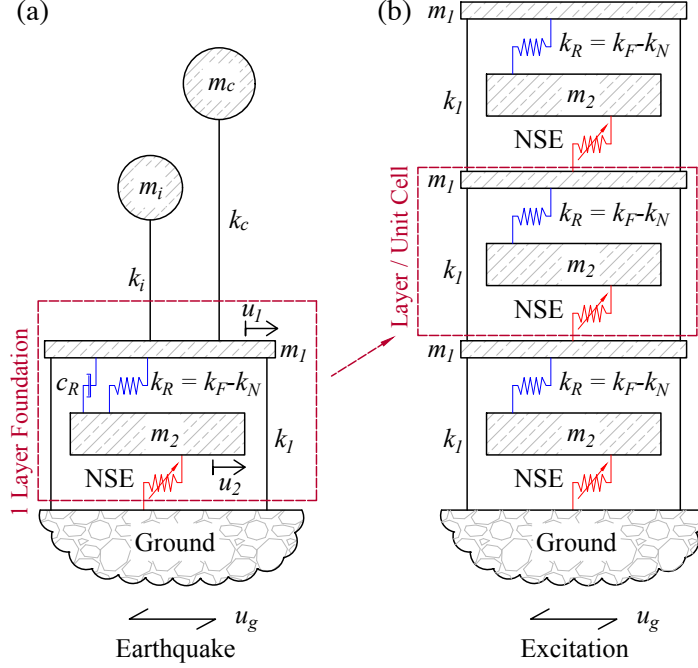


Figure 5.5: Dynamic systems: (a) Coupled foundation tank system; (b) Foundation modelled as a periodic structure.

5.2.3 Stability condition of the system

Due to the use of a local instability, it is necessary to determine the maximal allowable parameters, where the local instability does not impose a global instability on the system. The failure mode interesting for this analysis is the collapse of the unit cell due to an excessive negative force in the NSE, which leads to the analysis of a single layer without tank, see also Figure 5.5(a). The system of equations of motion (EOMs) can be written as,

$$m_1 \ddot{u}_1(t) + k_1 u_1(t) + (k_F - k_N) u_1(t) - (k_F - k_N) u_2(t) = m_1 \ddot{u}_g(t) \quad (5.11)$$

$$m_2 \ddot{u}_2(t) - (k_F - k_N) u_1(t) + (k_F - k_N) u_2(t) + k_N u_2(t) = m_2 \ddot{u}_g(t) \quad (5.12)$$

Here, u_1 denotes the displacement of the slab, u_2 describes the motion of the resonator, and \ddot{u}_g is the relative ground acceleration. Under harmonic excitation $\ddot{u}_g(t) = u_{g0} e^{i\omega t}$ the displacement responses can be assumed harmonic with $u_1(t) = u_{10} e^{i\omega t}$, and $u_2(t) = u_{20} e^{i\omega t}$, and the system expressed

in the frequency domain (after dividing by $e^{i\omega t}$ on both sides) with,

$$(-\omega^2 + k_1 + k_F - k_N)u_{10} - (k_F - k_N)u_{20} = m_1 u_{g0} \quad (5.13)$$

$$(-\omega^2 m_2 + k_F - k_N + k_N)u_{20} - (k_F - k_N)u_{10} = m_2 u_{g0} \quad (5.14)$$

When substituting (5.14) into (5.13) and rearranging the terms, the frequency response function FRF for u_{10} can be written as,

$$u_{10} = \frac{k_N m_2 - k_F m_1 - k_F m_2 + m_1 m_2 \omega^2}{k_N^2 - k_1 k_F - k_F k_N + (k_F m_1 + k_1 m_2 + k_F m_2 - k_N m_2) \omega^2 - m_1 m_2 \omega^4} u_{g0} \quad (5.15)$$

The denominator of the FRF, being the characteristic equation of the system, takes up the form,

$$y = \omega^4 \alpha_1 + \omega^2 \alpha_2 + \alpha_3 \quad (5.16)$$

with,

$$\begin{aligned} \alpha_1 &= -m_1 m_2 \\ \alpha_2 &= k_F m_1 + k_1 m_2 + k_F m_2 - k_N m_2 \\ \alpha_3 &= k_N^2 - k_1 k_F - k_F k_N \end{aligned} \quad (5.17)$$

This represents a fourth order polynomial without odd terms, which therefore is symmetric. Due to its symmetry, the equation has two positive real roots that are mirrored around the y-axis, and can be expressed in its factored form as,

$$y = -m_1 m_2 (\omega - \omega_1)(\omega - \omega_2)(\omega + \omega_1)(\omega + \omega_2) \quad (5.18)$$

After expansion this equation yields,

$$y = \omega^4 \beta_1 + \omega^2 \beta_2 + \beta_3 \quad (5.19)$$

with,

$$\begin{aligned} \beta_1 &= -m_1 m_2 \\ \beta_2 &= m_1 m_2 (\omega_1^2 + \omega_2^2) \\ \beta_3 &= -m_1 m_2 \omega_1^2 \omega_2^2 \end{aligned} \quad (5.20)$$

A comparison of the coefficients of (5.17) and (5.20) yields the following equations,

$$k_2 m_1 + k_N m_1 + k_1 m_2 + k_2 m_2 = m_1 m_2 (\omega_1^2 + \omega_2^2) \quad (5.21)$$

$$k_1 k_2 + k_1 k_N + k_2 k_N = m_1 m_2 \omega_1^2 \omega_2^2 \quad (5.22)$$

In order to be dynamically stable, the systems eigenfrequencies have to be real and positive,

$$\omega_1 > 0; \quad \omega_2 > 0 \quad (5.23)$$

This necessitates the right-hand sides of (5.21) and (5.22) to be greater than 0, and therefore, two conditions for k_N can be elaborated,

$$k_N > -\frac{k_F m_1 + k_1 m_2 + k_F m_2}{m_1} \quad (5.24)$$

and,

$$k_N > \frac{k_F}{2} - \sqrt{\frac{k_F^2}{4} + k_1 k_F} \quad (5.25)$$

A parametric study, which is omitted in the interest of brevity here, has shown that the latter condition is stricter than the former one, and therefore, is governing for the design. For the remainder of this work, the maximum negative stiffness of the NSE will be determined relative to the maximal value of eq. (5.25) in percent %.

5.3 Band-gaps and wave propagation

On the one hand the effect of the NSE on the band-gap behaviour is expected to be advantageous due to the amplification force, while on the other hand the effect of its inevitable nonlinearity is yet unknown. In this section the potential band gaps of the system will be investigated for the linearized as well as the elastic non-linear structure with parameters corresponding to the FULL system.

5.3.1 Band gaps of the linear system

Based on the multi-layered foundation depicted in Figure 5.5(b), a chain of unit cells endowed with NSEs can be established as shown in Figure 5.6, where u denotes the displacement of the discretized mass with the subscript (1,2) determining the mass and the superscript $(j-1, j, j+1)$ defining the relative location of the unit cell. Note that for the linear case the NSE is represented by a linear negative spring with value k_N from Eq. (5.8). Under the aid of the Floquet-Bloch theorem [73] it becomes possible to relate the movement of the previous and subsequent unit cells, to the unit cell under study with,

$$\mathbf{u}(x, t) = \mathbf{u}_0 e^{i(\mathbf{q}\mathbf{x} - \omega t)} \quad (5.26)$$

Here, $\mathbf{u}(x, t)$ denotes the displacement vector at position \mathbf{x} at time t , \mathbf{u}_0 the amplitude of the displacement at the reference position ($\mathbf{x} = 0$), ω the frequency of the propagating wave, and \mathbf{q} the wave vector. For a 1D system the wave vector becomes a scalar and is defined as the inverse of the wavelength ($q = 1/\lambda$). Furthermore, the distance between the cells will be set to unity, therefore reducing the position vector \mathbf{x} to a scalar of ± 1 and the range of

q to $-\pi \leq q \leq \pi$. It is now possible to write the boundary conditions in the frequency domain for a discretized chain with,

$$u_{1,2}^{j\pm 1} = u_{1,2}^j e^{\pm iq} \quad (5.27)$$

This condition can be applied to the EOMs of a typical periodic unit cell which read,

$$m_1 \ddot{u}_1^j + (2k_1 + k_F)u_1^j - k_1 u_1^{j+1} - k_1 u_1^{j-1} - (k_F - k_N)u_2^j = 0 \quad (5.28)$$

$$m_2 \ddot{u}_2^j - (k_F - k_N)u_1^j + k_F u_2^j - k_N u_1^{j-1} = 0 \quad (5.29)$$

After the application of the boundary condition (5.28) to (5.29), the discrete eigenvalue problem can be formulated with,

$$(\mathbf{K} - \omega^2 \mathbf{M}) \mathbf{u} = 0 \quad (5.30)$$

The non-trivial solution for this problem yields the dispersion relation,

$$\begin{aligned} \text{Cos}(q) = & \\ & \frac{2k_1 k_F + 2k_F k_N - 2k_N^2 + (-k_F m_1 - 2k_1 m_2 - k_F m_2)\omega^2 + m_1 m_2 \omega^4}{2(-k_1 k_F - k_F k_N + k_N^2) + 2k_1 m_2 \omega^2} \end{aligned} \quad (5.31)$$

which sheds light on the wave propagation behaviour. For the sake of demonstration, the frequency of the resonator shall be set to 3 Hz, while all other structural values match the FULL system from Table 5.2. The dispersion is depicted in Figure 5.7(a) for varying NSE values, with the percentage indicating the relationship of the applied NSE to the maximal allowable negative stiffness value from (5.25). Here the maximum values of the acoustic branches are highlighted with dotted lines, while also the minimum value of the optical branch is marked with a dotted line, in order to highlight the band-gap. When observing the dispersion branches, it becomes clear that an increase in negative stiffness entails a downwards shift of the band gaps lower bound, i.e. the acoustic branch, while the upper bound, i.e. optical branch, remains unchanged. Clearly, this is related to the shift of Eigenfrequencies in the system, which can be attributed to the softening effect of the NSE. Furthermore, Figure 5.7(b) depicts the frequency response function FRF of the system with 75% of the maximal allowable NSE for 1, 10, and 100 Layers. The reader may note that for the constellations of 1, and 10 Layers, the attenuation zone stretches further than the band gap predicts, which is a property that cannot be found in classical metamaterials and is most likely due to the assembly of the springs. More precisely, the resonators are connected not only to the slab they are intended to act upon, but also, by means of the NSE, to the previous slab.

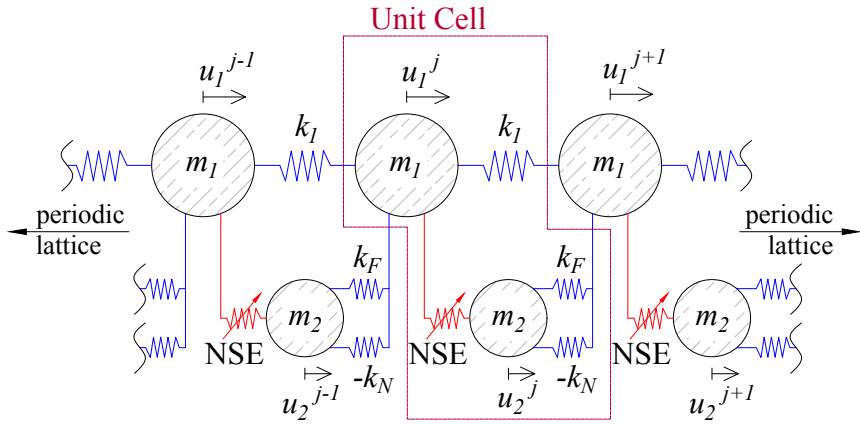


Figure 5.6: Infinite lattice and unit cell depiction.

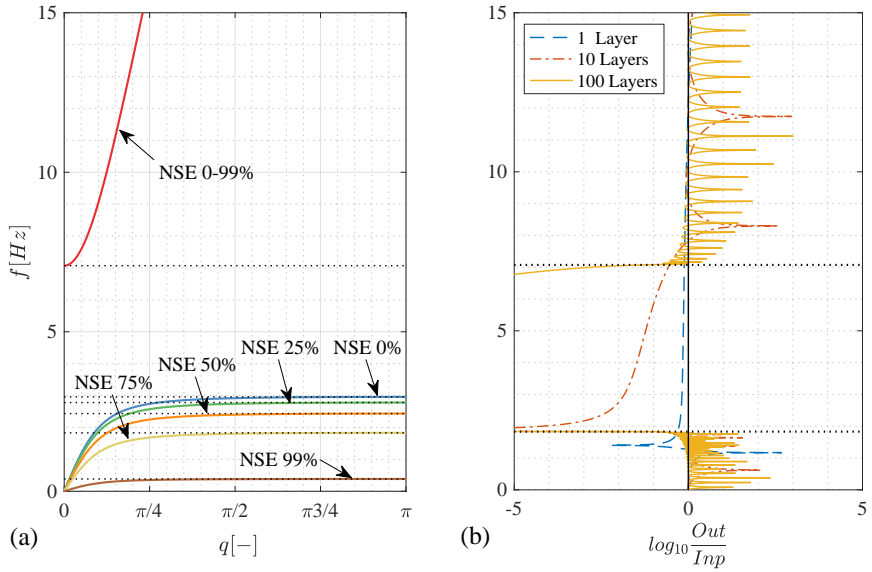


Figure 5.7: Wave propagation behaviour of the linear system: (a) Dispersion relation of the unit cell for varying NSE values (acoustic branch = AB); (b) FRF of the linear system for 1, 10, and 100 Layers with an NSE value of 75%.

5.3.2 Band gaps in the nonlinear system

In this subsection, the effect of nonlinearity on the band gap behaviour is discussed. More precisely, the HBM will be applied to the unit cell formulation of the system of EOMs and a dispersion relation, dependent on the nonlinearity of the system, established. Note that this procedure will provide an approximate but analytical solution for the nonlinear band-gap problem, where the Floquet-Bloch theorem is not strictly applicable. However, some studies have shown that periodic structures with weak nonlinearities can propagate Bloch-like waves with one dominant component and can, therefore, be analysed by means of standard techniques [132]. As a result, the HBM can be applied to find Bloch wave compatible solutions when coupled with the Floquet 1D boundary conditions [130, 133]. Additionally, THAs will be run for different excitation frequencies and amplitudes, in order to obtain an amplitude dependent FRF, which subsequently can be compared to the results of the band-gap analysis.

5.3.2.1 Analytical evaluation of nonlinear band gaps

In order to apply the HBM, we first need to define the EOMs of the nonlinear system. For the sake of simplicity, the displacement of the resonator is defined as relative to the main mass and is denoted with v^x , where $x \in \{j-1, j, j+1\}$ denotes the relative unit cell. The EOMs read,

$$m_1 \ddot{u}_1^j + (2k_1 + k_F)u_1^j - k_1 u_1^{j-1} - (k_F - k_N)(u_1^{j-1} + v^{j-1}) - k_1 u_1^{j+1} - f = 0 \quad (5.32)$$

$$m_2(\ddot{u}_1^j + \ddot{v}^j) + (k_F - k_N)(u_1^j + v^j) + u_1^{j+1}(k_F - k_N) + f = 0 \quad (5.33)$$

Here, f describes the nonlinear force, which will be simplified with (5.4) (5.7) and (5.9) to read,

$$f(t) = a_{NSE}v(t) + b_{NSE}v(t)^3 \quad (5.34)$$

This system is reminiscent of a duffing oscillator. Note however, that the resonators are connected to the unit cells above and below them, therefore, representing a new type of resonator chain. The general formulation of the harmonic balance method with complex exponentials can be written as,

$$y(t) = \sum_{n=1}^{\infty} Y_n e^{in\omega t} + \bar{Y}_n e^{-in\omega t} \quad (5.35)$$

with $y(t)$ being the motion of a generic degree of freedom in time, n denotes the harmonic, while Y_n and \bar{Y}_n are the complex and complex conjugate

amplitudes of the complex exponential series. Conveniently, the Floquet-Bloch boundary condition can be applied to this formula as follows,

$$y^{j\pm 1}(t) = \sum_{n=1}^{\infty} (Y_n e^{in\omega t} + \bar{Y}_n e^{-in\omega t}) e^{\pm iq_n} \quad (5.36)$$

with q_n being the wave number for harmonic n . Note that this formulation is equivalent to the formulation for the linear system and assumes a resonator mass chain with unitary distance between unit cells. This method can now be truncated for the first harmonic ($n = 1$) yielding,

$$u^{j\pm 1}(t) = (U_1 e^{i\omega t} + \bar{U}_1 e^{-i\omega t}) e^{\pm iq_1} \quad (5.37)$$

$$v^{j\pm 1}(t) = (V_1 e^{i\omega t} + \bar{V}_1 e^{-i\omega t}) e^{\pm iq_1} \quad (5.38)$$

Here U_1 , \bar{U}_1 , V_1 and \bar{V}_1 , denote the complex and complex conjugate amplitudes of the harmonic motion of $u(t)$ and $v(t)$, respectively. Subsequently these expressions must be applied to the EOMs (5.32) and (5.33) and their harmonics balanced, by equating the coefficients in front of $e^{i\omega t}$ with 0, which yields the following set of equations,

$$\begin{aligned} & - (U_1 + U_1 (k_F - k_N) + V_1 (k_F - k_N)) e^{-iq_1} - U_1 k_1 e^{iq_1} - a_{NSE} V_1 \\ & - 3b_{NSE} V_1^2 \bar{V}_1 + 2U_1 k_1 + U_1 (k_F - k_N) - U_1 m_1 \omega^2 = 0 \end{aligned} \quad (5.39)$$

$$\begin{aligned} & - U_1 (k_F - k_N) e^{iq_1} + a_{NSE} V_1 + 3b_{NSE} V_1^2 \bar{V}_1 + U_1 (k_F - k_N) \\ & + V_1 (k_F - k_N) - (U_1 m_2 + U_1 m_2) \omega^2 = 0 \end{aligned} \quad (5.40)$$

After the substitution of (5.40) in (5.39), U_1 can be eliminated and the following dispersion relation can be obtained,

$$\cos(q_1) = \frac{N}{D} \quad (5.41)$$

with the numerator N and the denominator D being equal to,

$$\begin{aligned} N &= 3b_{NSE} V_1 \bar{V}_1 [2k_1 + 2(k_F - k_N) - (m_1 + m_2) \omega^2] \\ &+ a_{NSE} [2k_1 + 2(k_F - k_N) - (m_1 + m_2) \omega^2] \\ &- \omega^2 [(k_F - k_N) (m_1 + m_2) + 2k_1 m_2] \\ &+ 2k_1 (k_F - k_N) + \omega^4 m_1 m_2 \end{aligned} \quad (5.42)$$

and,

$$\begin{aligned} D &= 6b_{NSE} V_1 \bar{V}_1 [k_1 + k_F - k_N] \\ &+ 2a_{NSE} [k_1 + k_F - k_N] \\ &+ k_1 [k_F - k_N - m_2 \omega^2] \end{aligned} \quad (5.43)$$

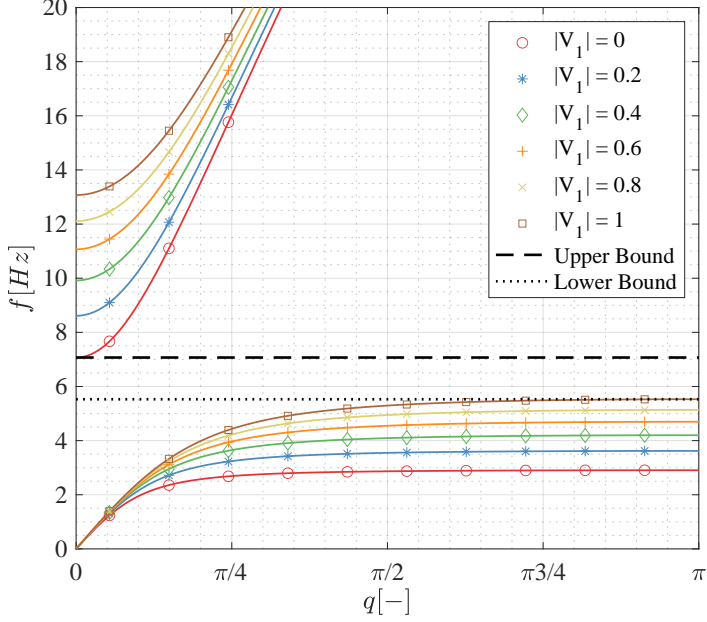


Figure 5.8: Dispersion diagram of the non-linear FULL system with varying amplitudes and 75% of the maximum NSE value.

The new dispersion relation is dependent on $b_{NSE}V_1\bar{V}_1$, which represents the nonlinearity of the system, and is plotted dependent on the amplitude $|V_1| = \sqrt{V_1\bar{V}_1}$, but for a constant b_{NSE} in Figure 5.8. Here, the dispersion branches move to a higher frequency spectrum since an increase of nonlinearity entails a higher participation of b_{NSE} , which in turn causes a stiffening of the system. The upwards shift of the dispersion branches may seem to indicate that the band-gap shifts towards higher frequencies and that the band-gap widens, as has been found for classical duffing oscillator type metamaterials [130, 131]. However, when waves that fall within the band-gap of a specific level of nonlinearity are attenuated, their change in intensity subsequently changes the level activated nonlinearity and therefore also the resulting band gap of the system. Based on this we conclude that only the common band-gap of the linear and nonlinear system can be retained, which entails that the frequency range narrows towards the upper bound with an increase in nonlinearity. This is highlighted with the dotted line for the lower bound and the dashed line for the upper bound in Figure 5.8 and will be illustrated more clearly with the simulations in the time domain conducted in the next section.

The reader may note that Figure 5.8 shows amplitudes of up to 1 m

relative displacement, which is not possible for the geometry shown earlier. However, the motion range of the resonators is restricted only by the spacing of the columns, which in turn can easily be changed in order to achieve the highly nonlinear range. Furthermore, the trend of the dispersion branches may be interesting for other application at different scales, where the highly nonlinear regime plays a more pronounced role.

5.3.2.2 FRF of the nonlinear system

In order to evaluate the FRF of the nonlinear system, an iterative time integration procedure was implemented based on a Newton-Raphson solver inserted into an implicit Newmark beta scheme. The equations of motion for the system read,

$$\mathbf{M}\ddot{\mathbf{u}}(t) + \mathbf{C}\dot{\mathbf{u}}(t) + \mathbf{K}\mathbf{u}(t) + \mathbf{R}(\mathbf{u}, t) = \mathbf{F}(t) \quad (5.44)$$

where \mathbf{M} , \mathbf{C} , and \mathbf{K} are the linear mass, damping and stiffness matrices, which can be written for the system displayed in Figure 5.5(b) with an arbitrary number of layers. Note that the damping matrix \mathbf{C} contains Rayleigh damping of 3% between 2 and 8 Hz for the system without resonators, in order to attenuate the vibration of the eigenmodes induced by the transient nature of the simulation. This further provides the band gap range with low damping values of less than 3%, while the resonators remain undamped, which minimizes the effect that the overall damping has on the band-gap phenomenon. Moreover, $\mathbf{R}(\mathbf{u}, t)$ denotes the vector containing the nonlinear restoring forces, deriving from the NSE i.e. eqs. (5.4) or (5.7), while the forcing term $\mathbf{F}(t)$ can be rewritten as $\mathbf{M}\mathbf{I}\ddot{u}_g(t)$, since the EOMs were formulated in terms of relative ground displacement. A harmonic ground acceleration for every frequency can be obtained with,

$$\ddot{u}_g(t) = Ae^{i\omega_g t} \quad (5.45)$$

with A being the amplitude of the wave and ω_g being the radial frequency of the excitation. Integrate twice over time and a harmonic ground displacement can be obtained with,

$$u_g = -\omega_g^2 Ae^{i\omega_g t} \quad (5.46)$$

In order to obtain an FRF, a finite chain of masses and resonators is subjected to this harmonic excitation on one side (the ground) and its absolute displacement response, once the steady state is reached, recorded on the other side. For these simulations the true nonlinearity and the polynomial approximation were considered for 1, 10 and 20 layers, without the presence of a superstructure and an NSE level of 25% of the maximum. In Figures 5.9(a), (b), (c), (d), (e) and (f) the FRFs are displayed with the

frequency on the x-axis, the amplitude of excitation in meters on the y-axis, and the absolute displacement response of the top layer relative to the excitation frequency on the z-axis. Furthermore, a gray horizontal plane is drawn at unity, where the response at the top is equal to the input at the bottom, which highlights the attenuation of the excitation. If the response is smaller than unity, the signal is being attenuated and a band gap can be expected. Note that the first mode of the complete 20 layered system (including the resonators) was located at $\omega_1 = 3.68\text{rad/s}$ at a modal damping value of $\zeta_1 = 1.4\%$, which resulted in a settling time of $t_S = 4/(\zeta_1\omega_1) = 80\text{s}$. Therefore a simulation length of 100 seconds was chosen.

For low excitations the structure remains in the linear range, which entails that the numerical FRF resembles the linear FRF for the lowest amplitude. When observing the FRFs for the true nonlinear system, an area without convergence can be seen in the high frequency, high excitation, region, due to the infinite stiffness at $v \rightarrow l$. Furthermore, when comparing the true nonlinear system to the polynomial approximation, it becomes clear that the approximation yields very similar results, even in the highly nonlinear range, where higher harmonics start to appear. This becomes particularly evident for the one layered system where a clear upwards shift of the eigenfrequency can be observed and a second spike representing a higher harmonic appears at 3 times the value of the systems first eigenfrequency. Furthermore, as discussed in the previous section, the upper bound of the band-gap, or in the finite case the attenuation zone, does not shift upwards with an increase in excitation amplitude (activation of nonlinearity). Instead, Figure 5.9 depicts clearly that the upper bound shows only a slight upwards shift, due to the finiteness of the system, while the lower bound approaches the upper bound with increased nonlinearity. Moreover, with more layers the system tends to show a better attenuation within the band-gap, which is due the added layers, but also due to the necessary damping present in the systems. From these results and the nonlinear dispersion analysis from the previous section, we conclude that with an increase of excitation amplitude the band-gap will gradually disappear towards the upper bound.

However, for the system to introduce resonance in the higher harmonics, some of the wave energy must be shifted away from the primary modes, which will be discussed with further THAs in Section 5.5. With respect to the band-gap behaviour on the other hand, the effects of the nonlinearity are clearly detrimental.

5.4 Optimization of the coupled system

As shown in previous publications [32] and [31], once the Metafoundation is coupled to a superstructure, the complete coupled system needs to be optimized. For this reason, we propose an optimization algorithm herein, based

5.4. Optimization of the coupled system

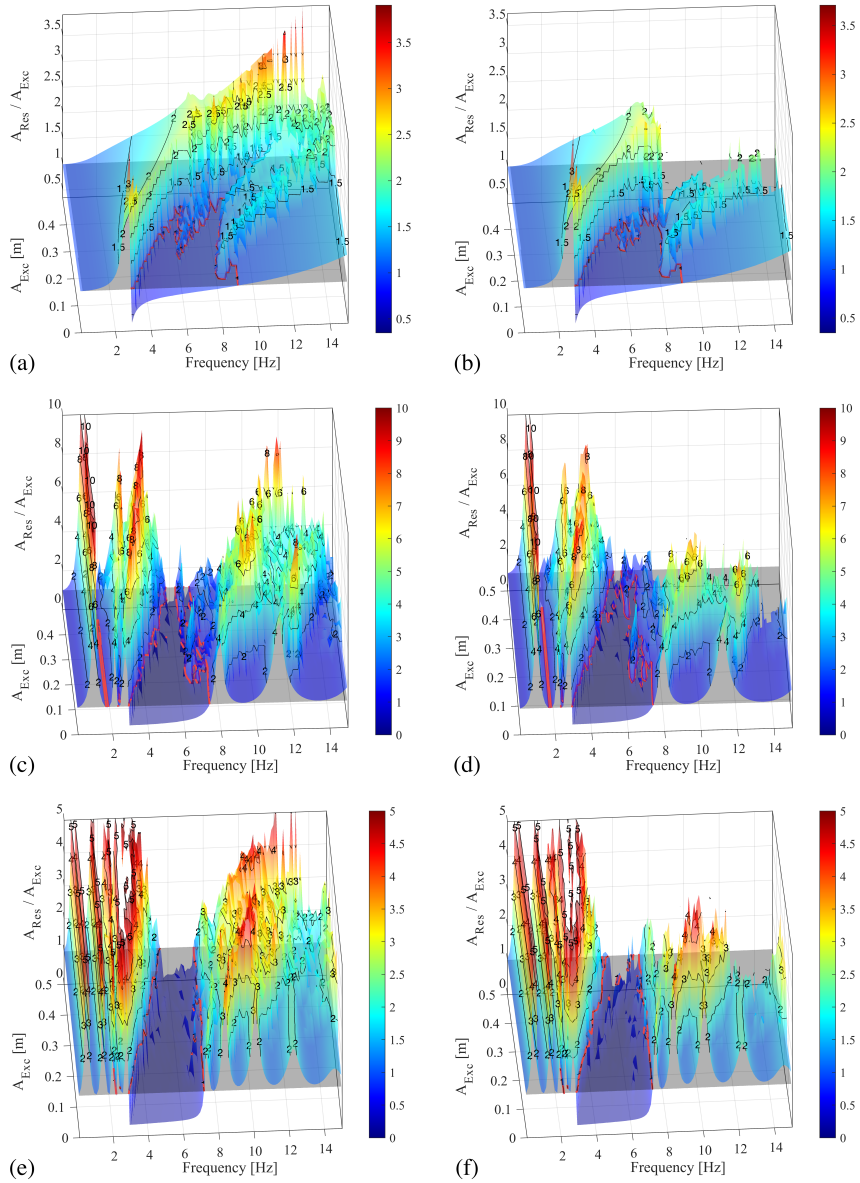


Figure 5.9: Numerical FRF for the FULL system with 25% NSE: (a) 1 layer and polynomial nonlinearity; (b) 1 layer and true nonlinearity; (c) 10 layers and polynomial nonlinearity; (d) 10 layers and true nonlinearity; (e) 20 layers and polynomial nonlinearity; (f) 20 layers and true nonlinearity.

Table 5.3: List of ground motion records.

Event	ID	M	RJb [km]	PGA [m/s^2]
Loma Prieta	BRN090	6.93	3.85	0.4067
Kalamata	000414ya	5.9	11	0.3738
South Iceland	004673ya	6.5	15	0.4224
L'Aquila Mainshock	IT0792ya	6.3	4.8698	0.6287
Friuli 2nd Shock	IT0078ya	5.6	26.2079	0.4023
Northridge-01	ORR360	6.69	20.11	0.3749
Umbria Marche	000594ya	6	11	0.4224
Montenegro	000199ya	6.9	16	0.3071
Erzincan	000535ya	6.6	13	0.4224
Friuli Italy-01	A-TMZ270	6.5	14.97	0.2585
South I. (aftershock)	006328ya	6.4	12	0.3914
Ano Liosia	001715ya	6	14	0.3103
L'Aquila Mainshock	IT0789ya	6.3	4.6338	0.4024
L'Aquila Mainshock	IT0790ya	6.3	4.3919	0.4459
L'Aquila Mainshock	IT0791ya	6.3	5.6501	0.3300

on calculation in the frequency domain, which represents a simplification of the algorithm established in [31] and depends on the structure and the ground motion.

5.4.1 Ground motion models

To narrow down the expected vibrations for the structure at hand, we chose to place it at a seismic prone site in Italy, namely Priolo Gargallo, and characterized it with a uniform hazard spectrum (UHS). The red solid line in Figure 5.10 shows the UHS of Priolo Gargallo for a return period of 475 years, which can be fitted with real records of ground motions (Figure 5.10(a) dashed grey lines). Here, the average response spectrum of the seismic events, see Figure 5.10(a) black dashed-dotted line, was fitted to the UHS in a least square sense. These records will later also be used to validate the functionality of the system and are listed in Table 5.3.

In order to obtain the power spectral density (PSD) of the selected records, which can be used in the optimization algorithm, Welch's method was applied with the following parameters: 8000 data points per seismic record, 1000 data points per finite section of the signal, 500 data points overlap, and a standard Hamming window. The resulting average PSD for each individual record (dashed grey lines) and the total average over all records (solid red line) are displayed in Figure 5.10(b).

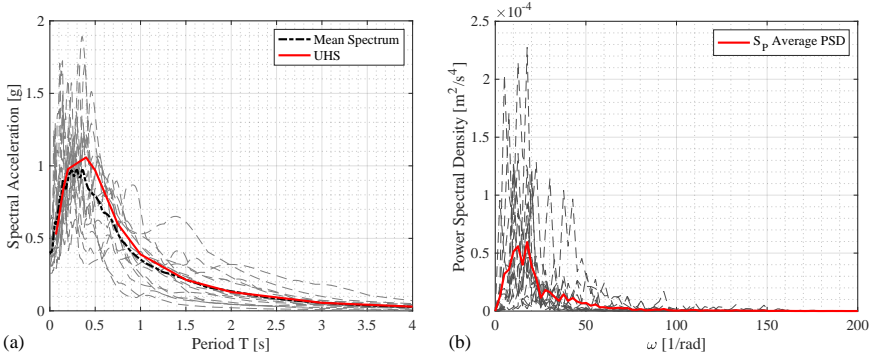


Figure 5.10: Ground motion spectra: (a) Response spectra including the UHS and the mean response spectrum; (b) PSDs of all ground motion records and their average estimated with Welch's method.

5.4.2 Optimization algorithm

In order to design the Metafoundation, it is necessary to take the feedback from the superstructure and the expected excitation into account. The herein proposed optimization algorithm can do both by imposing the power spectrum of the ground motion on the complete coupled system. The general form of the Equations Of Motion (EOMs) reads,

$$\mathbf{M}\ddot{\mathbf{u}}(t) + \mathbf{C}\dot{\mathbf{u}}(t) + \mathbf{K}\mathbf{u}(t) = \mathbf{M}\mathbf{I}\ddot{u}_g(t) \quad (5.47)$$

The mass, stiffness and damping matrices, \mathbf{M} , \mathbf{K} and \mathbf{C} can be constructed for the dynamic system displayed in Figure 5.5 (a) with the values of Table 5.2 and the indication about the damping given in the text, while \mathbf{I} represents the identity vector. Note that for the optimization procedure, the negative stiffness enters as a linear spring, since the computations in the frequency domain demand linearity. Firstly, we multiply the EOMs with $e^{-i\omega t}$ and integrate over time to obtain,

$$\int_{-\infty}^{+\infty} [\mathbf{M}\ddot{\mathbf{u}}(t) + \mathbf{C}\dot{\mathbf{u}}(t) + \mathbf{K}\mathbf{u}(t)] e^{-i\omega t} dt = \int_{-\infty}^{+\infty} \mathbf{M}\mathbf{I}\ddot{u}_g(t) e^{-i\omega t} dt \quad (5.48)$$

Subsequently, the response and excitation are transformed into the frequency domain via a Fourier transform with,

$$\mathcal{U}(\omega) = \int_{-\infty}^{+\infty} \mathbf{u}(t) e^{-i\omega t} dt \quad (5.49)$$

$$\mathcal{F}(\omega) = \int_{-\infty}^{+\infty} \mathbf{M}\mathbf{I}\ddot{u}_g(t) e^{-i\omega t} dt \quad (5.50)$$

where the derivatives of the response can be obtained with,

$$\int_{-\infty}^{+\infty} \dot{\mathbf{u}}(t)e^{-i\omega t} dt = i\omega \int_{-\infty}^{+\infty} \mathbf{u}(t)e^{-i\omega t} dt = i\omega \mathcal{U}(\omega) \quad (5.51)$$

$$\int_{-\infty}^{+\infty} \ddot{\mathbf{u}}(t)e^{-i\omega t} dt = -\omega^2 \int_{-\infty}^{+\infty} \mathbf{u}(t)e^{-i\omega t} dt = -\omega^2 \mathcal{U}(\omega) \quad (5.52)$$

With expressions 5.49 - 5.52 the system can be reformulated in the frequency domain as,

$$(-\omega^2 \mathbf{M} + i\omega \mathbf{C} + \mathbf{K}) \mathcal{U}(\omega) = \mathcal{F}(\omega) \quad (5.53)$$

Here, the transmission matrix can be defined and parametrized as,

$$\mathcal{H}(\omega, k_F, c_R) = [-\omega^2 \mathbf{M} + i\omega \mathbf{C}(c_R) + \mathbf{K}(k_F)]^{-1} \quad (5.54)$$

where k_F is a variable in the stiffness matrix \mathbf{K} , and c_R represents a viscous damper, which works in parallel with $(k_F - k_N)$, in the damping matrix \mathbf{C} . Note that the frequency of the resonator can be approximated with $\omega_R = \sqrt{k_F/m_2}$, while its damping can be represented with the critical damping ratio $\zeta_R = c_R/2\sqrt{(k_F - k_N)m_2}$. With these expressions and the definition of the approximate Power Spectral Density (PSD) of the response given by [114] we can rewrite the system response in terms of PSD as,

$$\mathbf{S}_U(\omega, \omega_R, \zeta_R) = |\mathcal{H}(\omega, \omega_R, \zeta_R)|^2 \mathbf{S}_g(\omega) \quad (5.55)$$

where $\mathcal{H}(\omega, \omega_R, \zeta_R)$ denotes the transmission matrix as defined in eq. (5.54) and $\mathbf{S}_g(\omega)$ describes the PSD of the excitation $\mathcal{F}(\omega)$, which is comprised of the average PSD obtained in Section 5.4.1, multiplied with $\mathbf{M}\mathbf{I}$. Furthermore, with the transformation by Wiener-Khintchine [114], the variance of a signal can be calculated based on the relationship of the autocorrelation function with the PSD as,

$$\sigma^2 = R(0) = \int_{-\infty}^{+\infty} S(\omega) d\omega \quad (5.56)$$

here, $R(0)$, $S(\omega)$, and σ_u^2 denote the autocorrelation function, the PSD, and the variance of the response, respectively. In line with this, the relative displacement of the impulsive mode and the top slab can be estimated with,

$$\sigma_{rel}^2 = \int_{-\infty}^{+\infty} S_j(\omega, \omega_R, \zeta_R) - S_k(\omega, \omega_R, \zeta_R) d\omega \quad (5.57)$$

where, $S_j(\omega, \omega_R, \zeta_R)$ and $S_k(\omega, \omega_R, \zeta_R)$ are the PSDs of the relative ground displacements of the j th and k th degree of freedom (DOF), while σ_{rel}^2 represents the variance of the relative displacement between those DOFs. Hence, we formulate the Performance Index $PI(\omega_R, \zeta_R)$ as,

$$PI(\omega_R, \zeta_R) = \frac{\sigma_{META}^2(\omega_R, \zeta_R)}{\sigma_{TRAD}^2} \quad (5.58)$$

where, σ_{META}^2 and σ_{TRAD}^2 denote the variance of the relative drift of the impulsive mode for a system with and without Metafoundation, respectively.

5.5 Behaviour of the coupled system

5.5.1 Behaviour of the system in the frequency domain

When running the optimization procedure on the coupled system subjected to the average PSD of the earthquakes, the PI can be computed and plotted for various frequency and damping ratios for the resonators, as displayed in Figures 5.11(a), (b), (c), and (d). Here, f_R corresponds to the optimal frequency of the resonators, while ζ_R is the optimal damping ratio of the resonators, which are computed for the Metafoundation with 0%, 25%, 50%, and 99% of the maximal admissible NSE value (obtained from eq. (5.25)). Note that a change in frequency allows for a recalculation of the maximal value of k_N , which would entail an iteration of the optimization scheme for every increase in frequency. This would multiply the computational effort by the amount of iterations necessary to find the final value, and has therefore been omitted in the interest of efficiency. Note further that the actual applicable NSE value is most likely determined by construction requirements, hence smaller than the theoretically possible one. Instead, the initial guess of k_F was chosen to produce a frequency of 3 Hz and used to determine the maximal admissible NSE value.

As shown in Figure 5.11 the value of the PI decreases with an increase in NSE value, while the optimal tuning frequency and damping ratio of the resonator have a clear effect on the PI. Table 5.4 summarizes the optimal parameters for all investigated systems and displays that the optimal value of the stiffness tends to increase for high NSE values in the REDUCED and MINIMAL systems, while for the FULL system it decreases first and then increases again. This is most likely due to the NSE changing the frequency of the resonators, as can be observed in Figure 5.7; and the NSE reducing the overall stiffness, thereby shifting the critical excitation frequency of the tank. From this tendency we conclude that an optimization, as carried out herein, is necessary for the design of a negative stiffness endowed system and that the superstructure should not be neglected. Furthermore, it is worth noting that the surface becomes flatter with an increase in NSE value, which entails that for higher NSE values the system becomes less dependent on the optimal tuning of the resonators. This effect is particularly interesting for the frequency of the resonator, as a precise tuning can be challenging in a real-life application. A similar trend can be observed for the damping ratio, where the optimal values are located at very high damping ratios of 19% to 30%, while only small improvements in terms of PI can be obtained above a value of 10%.

5. NEGATIVE STIFFNESS ELEMENT FOR PERIODIC FOUNDATIONS

Table 5.4: Results from the optimization for the relevant Metafoundation setups.

NSE	FULL			REDUCED			MINIMAL		
k_{Nmax}	f_R	ζ_R	PI	f_R	ζ_R	PI	f_R	ζ_R	PI
0	4.00	0.19	0.502	4.75	0.11	0.62	5.85	0.03	0.882
25	3.70	0.23	0.388	4.85	0.14	0.496	5.95	0.04	0.726
50	3.55	0.24	0.286	4.90	0.17	0.407	6.10	0.06	0.617
75	3.95	0.27	0.211	4.80	0.19	0.332	6.25	0.07	0.530
99	4.50	0.30	0.161	5.00	0.20	0.265	6.45	0.08	0.462

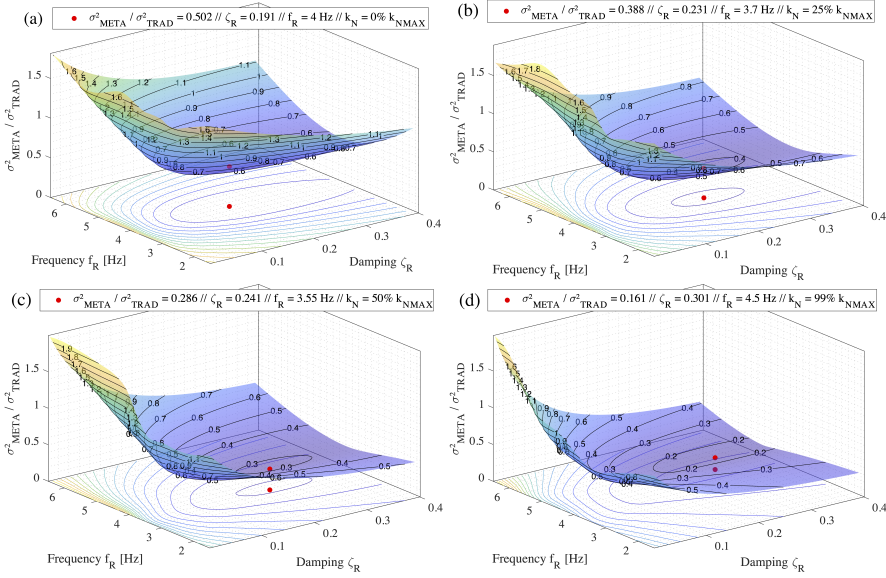


Figure 5.11: Optimization surface plots for: (a) PI for the FULL system with 0% k_{Nmax} ; (b) PI for the FULL system with 25% k_{Nmax} ; (c) PI for the FULL system with 50% k_{Nmax} ; (d) PI for the FULL system with 99% k_{Nmax} .

5.5.2 System response in the time domain

From the optimal values determined in the previous section, the stiffness of spring k_F and the damping value of c_R can be evaluated from the expressions $k_F = \omega_R^2 m_2$ and $c_R = \zeta_R 2\sqrt{(k_F - k_N)m_2}$. Furthermore, the length of the compression member was chosen beforehand and is shown in Table 5.1, while the Prestress force in the compression member can be obtained from the relationship $a_{NSE} = -P/l$ where $a_{NSE} = k_N$ with,

$$P = -k_N l \quad (5.59)$$

Besides this, the nonlinearity parameter ϵ yields realistic values for k_P when set to 0.95, where k_P can be evaluated from (5.10) as,

$$k_p = \frac{P}{(1 - \epsilon)l} \quad (5.60)$$

With these parameters and the optimal values found from the optimization, summarized in Table 5.4, the complete nonlinear system can be constructed and subjected to the ground motions from Table 5.3. For the sake of comparison, various Metafoundation layouts were considered and the resulting base shear developments of the respective tank evaluated with,

$$V(t) = [u_i(t) - u_1(t)]k_i + [u_c(t) - u_1(t)]k_c \quad (5.61)$$

where, $V(t)$, $u_i(t)$, k_i , $u_c(t)$, k_c , and $u_1(t)$ are the base shear development, the displacement of the impulsive mode, the stiffness of the impulsive mode, the displacement of the convective mode, the stiffness of the convective mode and the displacement of the top slab of the foundation, respectively. For calculating the response of the traditional system, the two SDOFs representing the tank were subjected to the ground motions without Metafoundation, which is equivalent to the tank being clamped to a traditional foundation, such as a concrete slab. The maximum base shear during each earthquake was considered as the governing performance measure and recorded for the Metafoundation and traditional foundation layouts with,

$$\eta = \frac{\sum_{n=1}^{15} \max(V(t)_n^{meta})}{\sum_{n=1}^{15} \max(V(t)_n^{trad})} \quad (5.62)$$

Here, n identifies the earthquake, while the sums simply cumulate the maximum base shear values of each seismic event. Figure 5.12(a), (b), and (c) shows the results for the FULL, REDUCED, and MINIMAL systems endowed with varying levels of NSE, thereby displaying how the performance measure η improves with an increase in NSE value. Moreover, when comparing the various setups without NSE (0% NSE), it becomes clear that the η value is significantly lower for the larger systems FULL $\eta = 0.79$ and REDUCED $\eta = 0.82$ compared to $\eta = 0.93$ for the MINIMAL system. This is due to the stiffness of the structure, which is determined by the structural design of the columns, limiting the minimal size of the Metafoundation without NSEs. However, when considering the positive impact that the NSE has on the system performance, it becomes possible to achieve a similar performance with the MINIMAL system with 50% of the maximal allowable NSE value. Furthermore, it is interesting to observe that the maximal recorded base shear for each earthquake tends to show less variation for higher NSE values. This suggests that with greater NSE, the performance of the system becomes more reliable across various seismic records, which is a very desirable property, due to the extreme variability of frequency and amplitude content of earthquakes.

5. NEGATIVE STIFFNESS ELEMENT FOR PERIODIC FOUNDATIONS

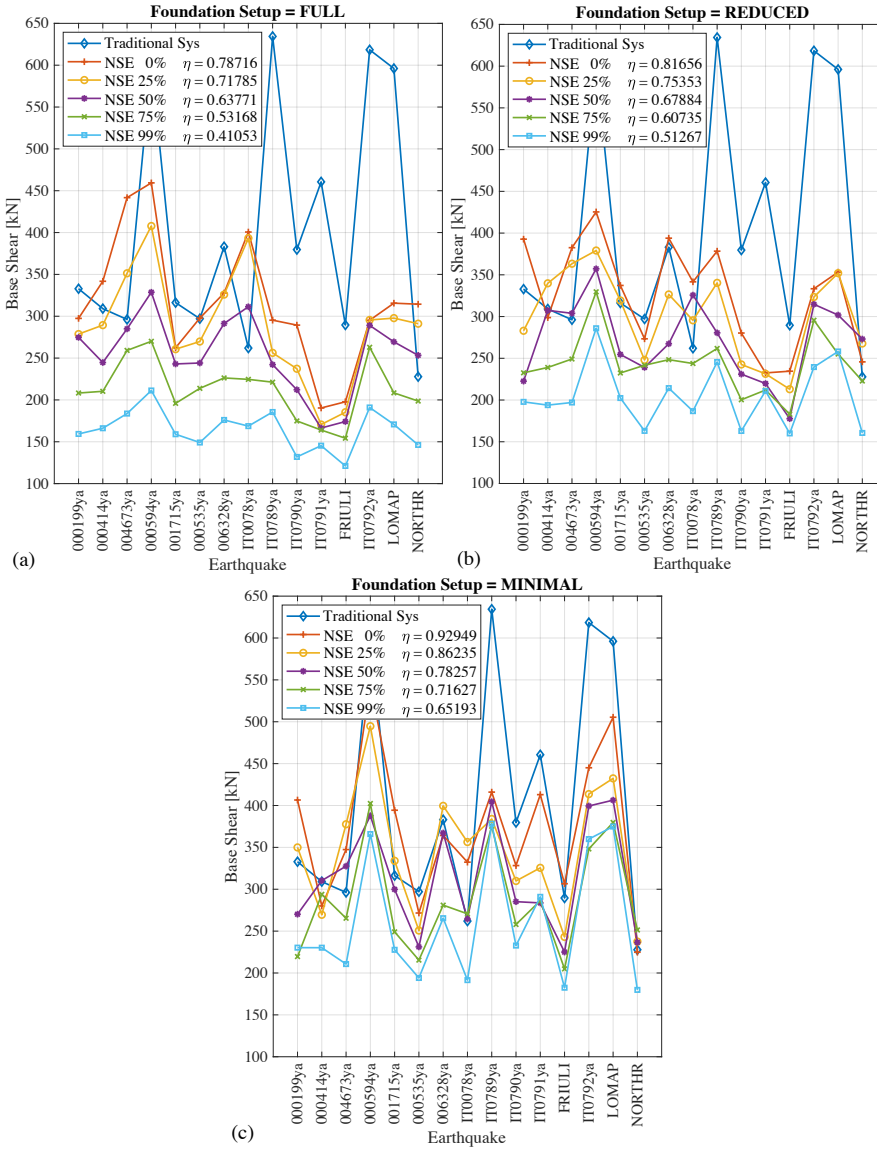


Figure 5.12: Time history analyses with $\epsilon = 0.95$ and various levels of NSE: (a) FULL system; (b) REDUCED system; (c) MINIMAL system.

In Subsection 5.3.2.2 we mentioned that the introduction of the 3rd harmonic may transfer some energy from the first mode to this higher harmonic, and therefore, has the potential to improve the systems performance. However, the investigated systems FULL, REDUCED and MINIMAL do not enter the strongly nonlinear range, and therefore, further calculations are carried out herein. A study of the two established nonlinear parameters l and ϵ is conducted for l being equal to 1, 0.1, 0.09, 0.05, 0.02, and 0.01 m, and ϵ being equal to 0.5, 0.9, and 0.99. These values are applied to the FULL system with 75% NSE, while the results are reported in Figure 5.13(a), (b), and (c). Although these values are geometrically very unrealistic for the system under study, other applications with a different scale may reach the nonlinear range, and therefore, may profit from the nonlinear effects. However, Figure 5.13(a), (b), and (c) depicts the trend of the system when entering the nonlinear regime and shows clearly that an increase in nonlinearity acts detrimental on the performance of the system. More precisely, there is an obvious degradation of the performance value from $\eta = 0.532$ for the system with a compression member length of 1 m, to $\eta = 0.90$ for a compression member length of 0.01 m. Curiously, the setups with $l = 0.05$ m and $l = 0.09$ m show a very small improvement over the quasi linear system for the earthquakes 004673ya and 000594ya. For most other events however, the systems perform significantly worse and an advantage cannot be concluded. On the other hand, the trend of the system with a decrease in ϵ value shows that the system is less likely to go in the nonlinear range even for very small l values, which may be useful for the design of the mechanism.

5.6 Conclusion

In this work, a new type of NSE, based on a compression member in a stable snap through position, has been developed for the application to seismic metamaterials. The composite system showed enhanced wave attenuation characteristics and was studied on its fully nonlinear behavior via time and frequency domain analyses. Due to the implemented NSE as well as the new type of established resonator chain, the system displayed a widening of the band-gap and an amplification of the attenuation capabilities with an increase in NSE. It is further worth noting that a finite system exerted an attenuation zone that stretched into an even lower frequency range than the band-gap of the periodic system predicted. The nonlinearity on the other hand, proved to have a detrimental effect on the band-gap range, since an increase in activated nonlinearity narrowed the band-gap towards its upper bound. Besides the study of the NSE enhanced foundation as a periodic structure, also its application to fuel storage tanks as a seismic protection system was discussed herein. Due to the feedback from the superstructure and the shift of eigenfrequencies caused by the NSE, the tuning of the finite

5. NEGATIVE STIFFNESS ELEMENT FOR PERIODIC FOUNDATIONS

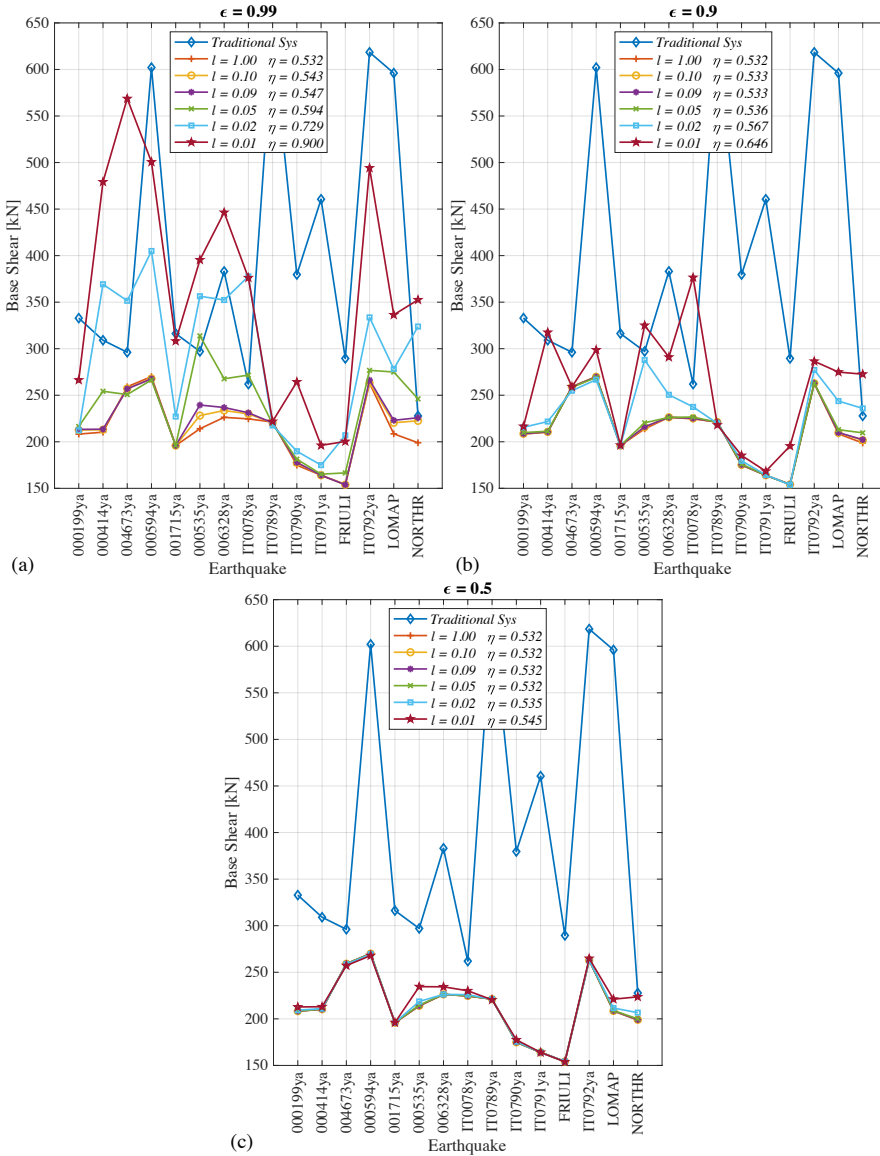


Figure 5.13: Time history analyses with various ϵ and l values for a system with 75% NSE: (a) $\epsilon = 0.99$; (b) $\epsilon = 0.90$; (c) $\epsilon = 0.50$.

systems necessitated an optimization algorithm. Note that the algorithm proposed herein considered the superstructure as well as the ground motion spectrum and could in principle optimize any number of system parameters. After optimizing the system a set of spectrum compatible ground motions was used to evaluate its performance, which demonstrated that a size reduction to 1/3 of the original size was achievable with 50% of the physically allowable negative stiffness. Additionally, the NSE enhanced systems showed a more reliable performance across various earthquakes, which is a highly desirable property, due to the strong variability in frequency and amplitude content of seismic records. It is further worth mentioning that soil structure interaction has not been taken into account directly, i.e. by modelling the soil underneath the foundation, but indirectly by selecting a ground motion spectrum that corresponds to a specific site with a specific soil type. Therefore, the full coupling effects of soil structure interaction need to be investigated in future studies, since they may provide further interesting resonant behavior, especially for vertical component damping. Lastly, it should be acknowledged that the mechanism was designed in a general way and may be applied to other vibration problems, where shear type waves need to be attenuated.

Upcoming developments With the proposed mechanism the system can be significantly reduced in terms of size. However, the actual motion of the resonators is still assumed to be on frictionless sliding surfaces, which leads to the investigation of wire ropes as resonator suspension in the next chapter.

Chapter 6

Wire Ropes for Resonator Suspension

Abstract. Periodic metafoundations have proven to inherit valuable properties from wave propagation in phononic periodic structures in the very low-frequency regime. In this context, the impact that massive resonators with varying frequencies or devices with hysteretic behaviour can entail on the system performance is still unknown. For this purpose, we develop and optimize two finite locally resonant metafoundation systems in this paper: (i) a foundation endowed with resonators, linear springs and linear viscous dampers (linear devices) tuned to multiple frequencies; and (ii) a foundation equipped with nonlinear hysteretic dampers (nonlinear devices). Both are optimized considering the stochastic nature of the ground motion, modelled with a modified Kanai-Tajimi filter in the stationary frequency domain, and a massive superstructure, chosen to be a fuel storage tank. In order to take all of the above-mentioned effects into account, we establish a procedure that is able to optimize any number of parameters. More precisely, to optimize the nonlinear behaviour of damper devices we employ a Bouc-Wen hysteretic model and subsequently approximate it with stochastically equivalent linear differential equations. The optimal values for the Bouc-Wen coefficients can then be found with iteration of the stochastic linearisation technique and the previously established optimization procedure. Finally, we test the optimized systems against natural seismic records both with linear and nonlinear time history analyses.

6.1 Introduction

Applied research in phononic (periodic) materials and structures has been abundant in recent years especially in the mid-frequency regime. See among others, the dense state of art of Hussein et al [134], the investigation in acous-

tic metamaterials [135], the review of waves behaviour in structured mediums [131] and the relevant problems of optimization [136, 137]. Investigations in the field of solid-state physics have shown that certain crystal arrangements may be used to manipulate the energy or patterns of acoustic (mechanical) wave energy [5, 6, 138]. These elastic materials, termed phononic crystals, can be designed to produce specific gaps in the frequency response of the structure. More precisely, when the frequency contents of a wave fall within the range of the frequency band gap of a periodic structure, the wave, and its energy, cannot propagate and become evanescent. While acoustic/elastic metamaterials have provided a root to subwavelength applications, it is still challenging to control and attenuate waves in the ultralow-frequency domain. Moreover, the analysis of nonlinear metamaterials is still challenging. For instance, from a perturbation approach specifically designed for weakly nonlinear periodic chains [129] clearly appears that: (i) nonlinear wave equations change with amplitude; (ii) the so called self action changes wave propagation characteristics; and (iii) analysis methods in the presence of self-action often do not trace all solutions when more than one dominant component is involved. Within linear metamaterials, a new category of applications of phononic – or periodic - structures as alternative to classical seismic isolators to earthquake mitigation has received growing interest [27, 30, 32, 92]. Their increasing popularity resides in the possibility of exploiting the advantages of periodic structures that are able to attenuate waves in certain frequency ranges. In particular, the authors exploit the advantages of locally resonant acoustic metamaterials (LRAMs), due to their capability of attenuating low-frequency waves by means of unit cells much smaller than the wavelength of the desired frequency region. In fact, the most common solutions of isolation use lead-rubber bearings [50] or spherical bearing devices [77]. Although they are quite effective for the horizontal components of earthquakes, they require two strong floors, exert a very high stiffness against the vertical component of an earthquake [139], and seem to be ineffective for large structures subjected to rocking [89]. In order to reduce the seismic response of a superstructure, Casablanca et al and Cheng and Shi studied periodic and finite locally resonant foundations [27, 30]. Although good results were obtained in terms of response reduction, neither of the proposed periodic systems were designed for gravity and/or seismic load combinations. Furthermore, the authors did not take into account the feedback forces from superstructures to metafoundations. In order to overcome these drawbacks, other researchers [31, 32] proposed a finite lattice LRAM, the so-called Metafoundation, for the seismic protection of storage tanks. The foundation consists of standard steel columns and concrete slabs that define the primary load bearing structure, while massive concrete masses are considered as resonators. Moreover, the foundation was designed to remain undamaged for safe shutdown earthquakes (SSEs). In order to evaluate the optimal parameters of the resonators and to account for the stochastic

nature of seismic waves, the authors proposed an optimization procedure based on computations in the frequency domain. As a result, they showed that the one-layered Metafoundation is the most efficient solution for attenuating seismic waves. Eventually, LRAMs can be profitably used for seismic mitigation of new plant components [77]. For existing plant components other arrangements of resonators were proposed [139]. Nonetheless, two basic issues remain unresolved: first, the optimization of multiple resonators acting in the Metafoundation associated with different parameters; and second, the optimization of some structural devices, i.e. springs and/or dampers, operating in the nonlinear regime. With regard to the first issue, i.e. the optimization of multiple resonators, Ma and Sheng [135] highlighted the potential benefits of designing multiple resonators exhibiting both mass and bulk modulus dispersion between resonances. More precisely, a meta-material endowed with local resonators can exert an apparent negative mass as well as an apparent negative bulk modulus. These properties can be exploited for the attenuation of acoustic waves, and therefore, can be suitably adopted for the design of optimal multiple tuned resonators. As far as the second issue is concerned, i.e. the selection of proper hysteretic dampers, Basone et al [31] suggested to use wire ropes; they represent simple devices able to both effectively suspend concrete resonators inside the foundation and allow motion in all three main directions. Their behaviour is quite complex and some researchers [108, 140, 141], among others, characterized their main nonlinear properties. Nonetheless, while the mechanical flexibility of wire ropes provides good isolation properties, the sliding friction between the intertwined cables results in high dissipative capabilities. As a result, these devices can achieve equivalent damping ratios of 15-20 percent while showing low production and maintenance costs. In view of optimization, the cyclic behaviour of wire ropes can be reproduced with the well-known hysteretic Bouc-Wen model [108, 141–143]. This model is quite popular because it describes the behaviour of a nonlinear hysteretic system with a compact first-order differential equation [144]. Due to its versatility and mathematical tractability, the Bouc-Wen model has gained popularity and has been applied extensively to a wide variety of seismic engineering problems [145–147]. In order to estimate the peak inelastic response of yielding structures modelled as nonlinear MDoF systems, Spanos, Giaralis and co-workers [148–150] profitably used bilinear and hysteretic models within a frequency domain-based stochastic framework.

6.1.1 Scope

In order to achieve the best performance of a finite locally resonant Metafoundation, the following objectives are pursued hereinafter: (i) the optimal tuning of multiple resonators to different frequencies and damping within different configurations of metafoundations; and (ii) the optimization of the non-

linear behaviour of wire ropes reproduced with hysteretic Bouc-Wen models. The superstructure is represented by a fuel storage tank and its equivalent 1D lumped mass model [69]. Therefore, the objective function for both (i) and (ii) is represented by the interstory drift or the absolute acceleration of the impulsive mode of the tank. In particular, the metafoundation is designed to remain undamaged for an active seismic site located in Priolo Gargallo, Sicily, Italy. The slender tank (superstructure) instead, was part of an existing plant, i.e. tank nr. 23 or nr. 24 of Case Study nr. 1, analyzed in a European research project [151]. In view of a consistent seismic input for linear/nonlinear time history analyses, a set of natural earthquakes that correspond to safe shutdown earthquakes (SSE) events are selected from Italian and European databases and fitted in average to the uniform hazard spectrum (UHS) of Priolo Gargallo. In order to take into account the stochastic nature of the seismic input, the computations are carried out in the frequency domain; and because the analysis of nonlinear periodic systems entails the aforementioned difficulties [129], a linearization technique is assumed for the Bouc-Wen model considered in objective (ii). More precisely, a stochastic equivalent linearization technique (SLT) is employed [152]; in fact, an SLT can, in a relatively straightforward manner, be extended to MDoF systems [150]. Therefore, an average power spectral density (PSD) function of those accelerograms is evaluated. The resulting PSD function is fitted with a Kanai-Tajimi filter [113] modified by Clough and Penzien [114] and, subsequently, adopted in the optimization procedure. The resulting optimized Metafoundations were then verified through nonlinear time history analyses (THAs) of the coupled systems subjected to the aforementioned ground motions. The rest of the paper is organized as follows. Firstly, details about the modelling of the various components of the coupled foundation-tank system are provided in Section 6.2. Section 6.3 provides the optimization procedure in the frequency domain for purely linear elements, while the performance of the linear optimized system is verified by means of THAs. Section 6.5 on the other hand deals with the coupled system endowed with nonlinear components, where the SLT and its implementation in the optimization procedure is discussed. The choice of the optimal parameters of BW models that describe the hysteretic behaviour of the damper devices are discussed in Section 6.6, where the results from the optimization are commented. Furthermore, each optimized nonlinear system is evaluated by means of nonlinear THAs for all considered earthquakes. Finally, conclusions and future developments are presented in Section 6.7.

6.2 Metamaterial concept and dynamic system

The Metafoundation is composed of a finite number of unit cells realized with standard steel columns endowed with hollow sections and concrete

slabs, sketched in Figure 6.1(A). In each unit cell there are moving concrete masses, i.e. the resonators, that are linked via springs to the foundation as shown in Figures 6.1(B) and (C). The construction site was chosen to be Priolo Gargallo (Italy), which is characterized by a peak ground acceleration (PGA) of 0.56g at a return period of 2475 years. In agreement with the paper objectives, the metafoundation was designed to remain undamaged even for safe shutdown events (SSE), according to the Italian seismic code NTC [107]. Two foundations were designed with one and two layers of resonators, respectively. Both systems have a height of 4 m, and are comprised of columns, which represent the vertical load bearing system, and slabs that support the resonators. The columns are made of steel hollow sections and govern the horizontal stiffness of the structure. Their dimensions are 300x300 mm and 230x230 mm for the one and two layered case, respectively, while the wall thickness of the hollow section is 30 mm for both. These dimensions are the results of the linear elastic design according to the NTC 201839, and determine the minimal allowable column stiffness. The hydrodynamic response of liquid containers, can be profitably simulated by means of Housner's models [153, 154]. The models can approximate internal actions for regular containers assuming that the water can be split into impulsive and convective masses. More recently, Malhotra [69] developed a simplified procedure for seismic analysis of cylindrical liquid-storage tanks. The relevant model reduces the tank response to the contribution of two main impulsive and convective modes, in which also the tank wall thickness is taken into account. Furthermore, in view of effectiveness, the concrete resonators are assumed to be suspended by wire ropes, as depicted in Figure 6.1(B) and (C), that allow each resonator to move in X, Y and Z directions. Details on the distribution of steel wire ropes in the single unit cell are provided in Figure 6.2.

6.2.1 Metamaterial concept and negative apparent mass

In seismic engineering, two types of periodic materials are currently investigated: phononic crystals (PCs) and LRAMs. The main advantage of both consist in designing a periodic structure that exhibits stop bands capable of forbidding elastic wave propagation within a desired frequency region. In particular, LRAMs are more suitable than PCs at ultralow frequencies due to their capability to exhibit very low frequency band gaps, endowed with unit cells much smaller than the wavelength of the desired frequency region [29, 30, 66, 91]. In this regard, the Metafoundation depicted in Figure 6.1 can be designed as a finite periodic system that can suppress seismic waves in certain frequency regions [27, 92]; these regions, the so-called band gaps, are analytically defined through a lattice dispersion analysis using the Floquet–Bloch theorem [73]. More precisely, it is possible to reduce the study of an infinite lattice to the analysis of a single unit cell with Floquet-Bloch

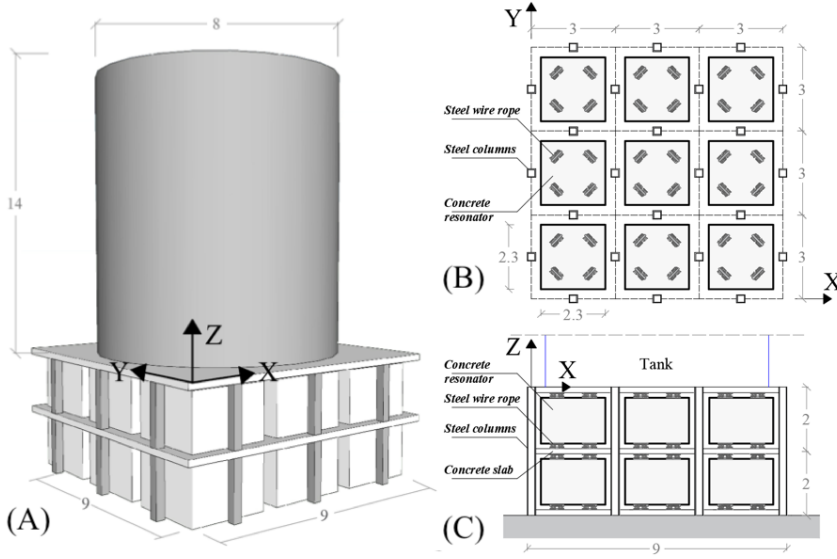


Figure 6.1: Coupled foundation-tank system with two layers: (A) isometric view, (B) layout and (C) cross section.

quasi-periodic boundary conditions. As a result, a frequency dispersion analysis can be carried out and the band gaps of the system can be found [32]. More precisely, Figure 6.3 shows the dispersion relation of an infinite periodic stack of the unit cells described in Figure 6.1. It demonstrates that a band gap forms in a predefined low-frequency range where elastic waves become evanescent. It should be emphasized that these considerations are obtained considering the foundation system depicted in Figure 6.1 as an infinite lattice. However, since the Metafoundation is finite, further analyses are needed. As shown by [32] the horizontal stiffness of the foundation is one of the governing factors for its effectiveness. It follows that the elastic design of the foundation required by NTC 201839 provides a minimum value for the columns cross-section depicted in Figure 6.2(A). Conversely, in order to achieve the largest antiresonance effects or the maximum attenuation effects, resonator masses are massive and compatible with cell geometry to exploit the negative apparent mass concept [135]. In this respect and based on Figure 6.4, the apparent masses experienced by the exterior cells read,

$$M_{app}^1(\omega) = m_1 - \frac{k_1}{\omega^2} + \frac{k_2}{\omega_2^2 - \omega^2} \quad (6.1)$$

$$M_{app}^2(\omega) = m_1 - \frac{k_1}{\omega^2} + \frac{k_2}{\omega_2^2 - \omega^2} + \frac{k_3}{\omega_3^2 - \omega^2} \quad (6.2)$$

where m_1 and k_1 are the mass and stiffness of the exterior unit cell, m_2

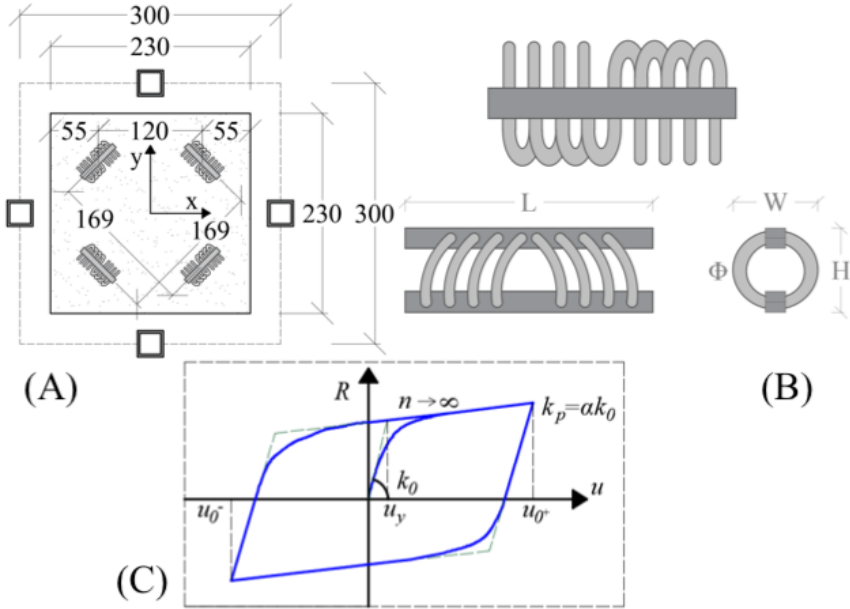


Figure 6.2: (A) Configuration of a single unit cell equipped with steel wire ropes (measures in cm); (B) details of a single wire rope and (C) hysteretic loop of Bouc-Wen model.

and m_3 are masses, k_2 and k_3 are stiffnesses of resonators, ω_2 and ω_3 are relevant frequencies of resonators while ω represents the forcing frequency. It is clear that the effective mass $M_{app}^1(\omega)$ becomes negative, in Figure 6.4(A), when the forcing frequency is close to resonance. Since the acceleration response is opposing to the applied force, the response amplitude is reduced and attenuation zones appear. This effect is greatly magnified as the input frequency ω approaches the local resonance frequency. Further enhancements can be obtained adding resonators with different resonant frequencies, as shown in Figure 6.4(B). Indeed, a double negativity can be observed close to the second resonant frequency of the system. As a result, further benefits can be obtained when multiple resonators are differently tuned. These benefits will be achieved with different optimal configurations of Metafoundations presented in the next subsection.

6.2.2 System modelling and reduction

For simplicity and without loss of generality, we consider only a seismic input along the X direction. As a result, through dynamic condensation of

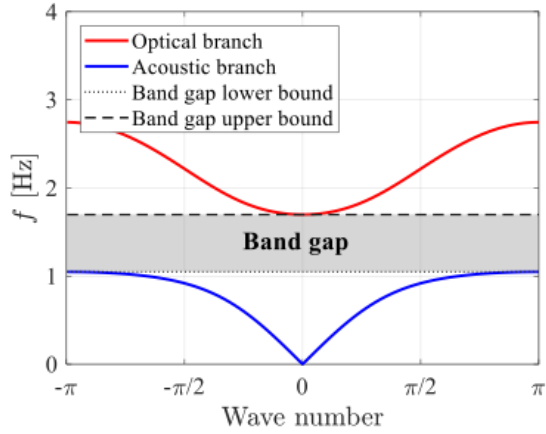


Figure 6.3: Dispersion relation for an infinite stack of unit cells with the geometric properties of the two-layered foundation case. Figure from [31]

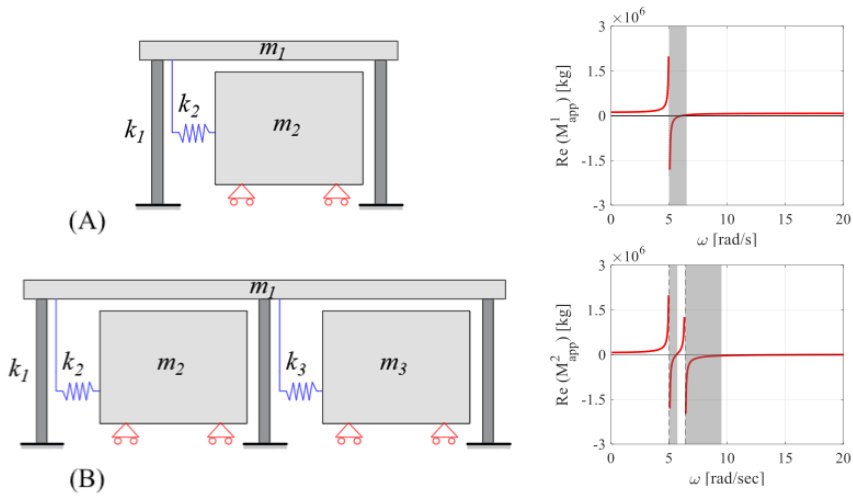


Figure 6.4: Apparent mass as a function of forcing frequency: (A) single and (B) double unit cell case.

both mass and stiffness, the foundation-tank coupled system sketched in Figure 6.1 can be modelled as a full mass system (FMS) in the X-Z plane, as shown in Figure 6.5(A). The result of the dynamic condensation is exact since all resonators in the Y direction are assumed to be endowed with the same mass and stiffness in each layer. In order to deal with simpler coupled systems and to take benefit in the optimization from different stiffness and damping values, both condensed mass (CMSs) and reduced mass systems (RMSs) have been also considered, as indicated in Figure 6.5(B) and (C), respectively. More precisely, to considerably reduce the computational effort during the optimization procedure, the CMS is obtained condensing all resonators in the X direction. However, the CMS cannot benefit from different modal contributions in each layer. As a result, the RMS can consider different resonator parameters during the optimization, entailing a slight increase in computational effort. Along these lines, Figure 6.5 shows the principal configuration of the three analysed systems, for the two-layered case. Here, m_i , c_i and k_i represent mass, stiffness and damping coefficients of the impulsive mass of the tank, respectively, while m_c , c_c and k_c represent mass, stiffness and damping coefficients of the relevant convective mass. We underline that resonators considered equal are endowed with the same mass and the same stiffness. This represents an ideal condition, since statistically some variations of mass and stiffness exist. However, their variations were neglected for this study. The system of equations of motions (EOMs) of the systems depicted in Figure 6.5 reads,

$$\mathbf{M}\ddot{\mathbf{u}}(t) + \mathbf{C}\dot{\mathbf{u}}(t) + \mathbf{K}\mathbf{u}(t) = \mathbf{F}(t) \quad (6.3)$$

where \mathbf{M} , \mathbf{C} , and \mathbf{K} are the mass, damping, and stiffness matrices, respectively, while $\ddot{\mathbf{u}}(t)$, $\dot{\mathbf{u}}(t)$ and $\mathbf{u}(t)$ denote acceleration, velocity, and displacement vectors. Furthermore, $\mathbf{F}(t) = -\mathbf{M}\tau\ddot{u}_g(t)$ is the forcing vector, where τ is the mass influence vector and $\ddot{u}_g(t)$ represents the ground acceleration. In order to evaluate the dynamic properties of the RMS depicted in Figure 6.5(C), we employ the system equivalent reduction expansion procedure (SEREP) proposed by O'Callahan [155]. This procedure allows for the reduction of some modal vectors of the FMS systems. More precisely, the convective mode and the relevant DoF of the tank can be eliminated from the full set of 'n' DoFs, while the effects on the lower 'a' modes can be retained. Hence, the SEREP technique is based on the following transformation,

$$\mathbf{u}_n = \mathbf{T}\mathbf{u}_a \quad (6.4)$$

where $\mathbf{T} = \Phi_n\Phi_a^g$ is the transformation matrix, with Φ_n being the modal matrix of the original system, while Φ_a^g represents the generalized inverse of the modal matrix of the active/reduced system. More precisely, Φ_a^g can be evaluated as,

$$\Phi_a^g = (\Phi_a^T\Phi_a)^{-1}\Phi_a^T \quad (6.5)$$

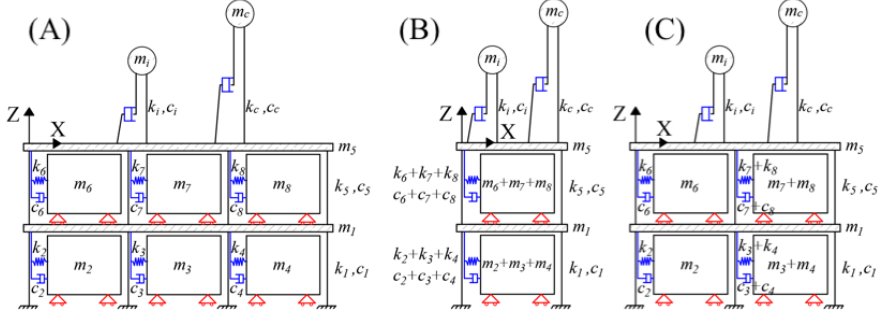


Figure 6.5: Models of the Metafoundation for the two-layered case: (A) FMS; (B) CMS and (C) RMS.

As a result, the system matrices of the reduced system read $\tilde{\mathbf{M}} = \mathbf{T}^T \mathbf{M} \mathbf{T}$, $\tilde{\mathbf{K}} = \mathbf{T}^T \mathbf{K} \mathbf{T}$ and $\tilde{\mathbf{C}} = \mathbf{T}^T \mathbf{C} \mathbf{T}$, while the forcing term becomes $\tilde{\mathbf{F}} = -\mathbf{T}^T \mathbf{M} \mathbf{T} \ddot{\mathbf{u}}_g$. Since the optimization procedure requires an inversion of the transmission matrix \mathbf{T} for each frequency interval, as illustrated in Section 6.3, SEREP contributes to the reduction of the run time of the optimization algorithm.

6.2.3 Modelling of wire ropes

In order to model the nonlinear behaviour of wire ropes, we employ the Bouc-Wen model, which has been extensively used in the literature to capture the hysteretic behaviour of many seismic devices [108, 140, 141, 146]. In accordance with this model, for a SDoF system we get

$$m\ddot{u}(t) + c\dot{u}(t) + R(t) = F(t) \quad (6.6)$$

where $R(t)$ defines the nonlinear restoring force,

$$R(t) = \alpha k u(t) + (1 - \alpha) k u_y z(t) \quad (6.7)$$

In particular, k and u_y represent the yielding stiffness and displacement, respectively, whereas the dimensionless hysteretic component z is given by the solution of the nonlinear differential equation,

$$\dot{z}(t) = u_y^{-1} [A\dot{u}(t) - \gamma|\dot{u}(t)||z(t)|^{n-1}z(t) - \beta\dot{u}(t)|z(t)|^n] \quad (6.8)$$

Here A , β , γ , and the exponent n are parameters that control the shape and smoothness of the force-displacement loop. Moreover in (6.7), $\alpha = kp/k_0$ defines the post-yielding to pre-yielding stiffness ratio, with

$$k_0 = \left(\frac{\delta R(u, \dot{u}, z)}{\delta u} \right)_{z=0} = \alpha k + (1 - \alpha) k A \quad (6.9)$$

$$k_p = \left(\frac{\delta R(u, \dot{u}, z)}{\delta u} \right)_{z=z_{max}} = \alpha k_0 \quad (6.10)$$

where $z_{max} = [A/(\beta + \gamma)]^{1/n}$. For suitable values of the parameters A , β , γ and n , the Bouc-Wen model can yield hardening or softening nonlinearities. A hardening behaviour is simulated when $|\gamma| > |\beta|$ and $\gamma < 0$; otherwise, a softening behaviour is obtained. Furthermore, n modulates the sharpness of yield, with $n \rightarrow \inf$ representing the bi-linear elasto-plastic hysteresis case. By choosing $n = 1$, (6.8) can be analytically solved with simple exponential functions [146]. Explicit expressions for $n = 1$ and $n = 2$ are also available in Demetriades et al. [145]. Other parameter values used for the optimization process are discussed in Subsection 6.6.1.

6.2.4 Accelerogram selection and seismic input model

In order to evaluate the seismic activity of the construction site, i.e. Priolo Gargallo, a set of 12 natural accelerograms were selected from Italian and European databases with 2% probability of exceedance in 50 years. These accelerograms are selected so that their mean spectrum fits in a least-square sense the uniform hazard spectrum (UHS) of Priolo Gargallo. It is well known that the UHS is often overly conservative because it combines the hazard from different sources and does not reflect a realistic spectrum that can be expected to occur during a single earthquake. However, the use of a conditional mean spectrum (CMS) that matches the UHS level at the fundamental period of the system is overly complex and limiting for the problem at hand. The optimization procedures performed in the frequency domain, see Section 6.3 and 6.5, assume that the seismic input is a weakly stationary Gaussian filtered white noise random process with zero mean and spectral intensity S_0 . In order to approximately take soil into account, we use the Kanai-Tajimi filter [113]; and to avoid unrealistic high values in the low-frequency range, a second filter in series proposed by Clough and Penzien [114] was adopted. For brevity, it is referred to as KTCP filter. The relevant power spectral density (PSD) function can be expressed as,

$$S_{\ddot{u}_g} = S_0 \frac{4\zeta_g^2 \omega_g^2 \omega^2 + \omega_g^4}{4\zeta_g^2 \omega_g^2 \omega + (\omega_g^2 - \omega^2)^2} \frac{\omega^4}{4\zeta_f^2 \omega_f^2 \omega^2 + (\omega_f^2 - \omega^2)^2} \quad (6.11)$$

where ω_g and ζ_g are the frequency and damping ratio that describe the soil characteristics, while ω_f and ζ_f denote the parameters of the low pass-filter [114], respectively. In the time domain, the KTCP model is governed by the following differential equation,

$$\ddot{u}_g = \omega_g^2 u_g + 2\zeta_g \omega_g \dot{u}_g - \omega_f^2 u_f - 2\zeta_f \omega_f \dot{u}_f \quad (6.12)$$

which can be completed in a state-space variable form as follows,

$$\ddot{u}_g = \mathbf{a}_f^T \mathbf{u}_f \quad (6.13)$$

$$\dot{\mathbf{u}}_f = \mathbf{A}_f \mathbf{u}_f + \mathbf{V}_f f(t) \quad (6.14)$$

with,

$$\mathbf{A}_f = \begin{bmatrix} 0 & 1 & 0 & 0 \\ -\omega_f^2 & -2\zeta_f\omega_f & \omega_g^2 & 2\zeta_g\omega_g \\ 0 & 0 & 0 & 1 \\ 0 & 0 & -\omega_g^2 & -2\zeta_g\omega_g \end{bmatrix} \quad (6.15)$$

and,

$$\mathbf{u}_f = \begin{bmatrix} u_f \\ \dot{u}_f \\ u_g \\ \dot{u}_g \end{bmatrix} \quad \mathbf{a}_f = \begin{bmatrix} \omega_f^2 \\ -2\zeta_f\omega_f \\ \omega_g^2 \\ -2\zeta_g\omega_g \end{bmatrix} \quad \mathbf{V}_f = \begin{bmatrix} 0 \\ 0 \\ 0 \\ 1 \end{bmatrix} \quad (6.16)$$

where $f(t)$ is the bedrock Gaussian zero-mean white-noise process. The filter parameters are chosen to match the ground motion characteristics of Priolo Gargallo, at a return period of 2475 years. More precisely, the parameters of the KTCP filter fit in a least square sense the stationary PSD function of the aforementioned 12 accelerograms. Their values amount to $S_0 = 0.09$ (m^2/s^3), $\omega_g = 14$ (rad/s), $\zeta_g = 0.6$, $\omega_f = 0.75$ (rad/s) and $\zeta_f = 1.9$.

6.3 Optimization of the Metafoundation endowed with linear devices

The proposed Metafoundation is characterized by two sets of parameters: (i) parameters that derive from construction or feasibility constraints, e.g. column size, slab thickness, etc.; and (ii) parameters that can be chosen more freely, i.e. stiffness and damping parameters of the resonators. In this regard, to maximize antiresonance or negativity effects, resonator masses are set as the largest mass compatible with the unit cell dimensions. Owing to the seismic input defined in (6.11), the herein proposed optimization procedure is based on computations in the frequency domain, can, in principle, optimize any number of parameters. The application of the Fourier transform to (6.3) and elimination of $e^{i\omega t}$, entails,

$$\omega^2 \mathbf{M}\mathbf{u}(\omega) + i\omega \mathbf{C}\mathbf{u}(\omega) + \mathbf{K}\mathbf{u}(\omega) = \mathbf{F}(\omega) \quad (6.17)$$

where ω represents the circular frequency. From (6.17) we can define the transmission matrix $H(\omega)$ as follows,

$$\mathbf{H}(\omega) = [-\omega^2 \mathbf{M} + i\omega \mathbf{C} + \mathbf{K}]^{-1} \quad (6.18)$$

Therefore, the PSD of the j -th DoF can be approximated with,

$$S_{Q_j}(\omega) = |H_j(\omega)|^2 S_{\ddot{u}_g}(\omega) \quad (6.19)$$

where $H_j(\omega)$ and $S_{\ddot{u}_g}(\omega)$ are the j -th transfer function component and the PSD of the force acting on the system, respectively. Furthermore, we assume

the validity of the Wiener–Khinchin theorem for a weakly stationary random process, which results in $R(\tau)$ and the PSD being a Fourier-transform pair. Subsequently, the Variance of a signal can be calculated with,

$$\sigma_j^2 = \int_0^{+\infty} S_{Q_j}(\omega) d\omega \quad (6.20)$$

The optimization criterion is chosen to be the minimization of the interstory drift or the absolute acceleration of the impulsive mode of the tank. Note, that for slender tanks, this mode has proven to dominate the base shear response of the whole system. Moreover, from (6.6), for the linear case, one obtains,

$$|m\ddot{u}_{tot}| = |-c\dot{u} - ku| \quad (6.21)$$

where the relationship between interstory drift and absolute acceleration depend on damping forces. Therefore, the variance of the interstory drift and the absolute acceleration read,

$$\sigma_{dr}^2 = \int_0^{+\infty} |H_{imp}(\omega) - H_{tl}(\omega)|^2 S_{\ddot{u}_g}(\omega) d\omega \quad (6.22)$$

$$\sigma_{acc}^2 = \int_0^{+\infty} |1 - \omega^2 H_{imp}(\omega)|^2 S_{\ddot{u}_g}(\omega) d\omega \quad (6.23)$$

where $H_{imp}(\omega)$ and $H_{tl}(\omega)$ are the transfer functions of the impulsive mass and top layer, respectively. Furthermore, the dimensionless performance indices can be defined as follows,

$$PI_{dr} = \frac{\sigma_{dr}^2}{\sigma_{dr,fix}^2} \quad (6.24)$$

$$PI_{acc} = \frac{\sigma_{acc}^2}{\sigma_{acc,fix}^2} \quad (6.25)$$

where $\sigma_{dr,fix}^2$ and $\sigma_{acc,fix}^2$ represent the variances of interstory drift and absolute acceleration of the impulsive mass for a tank without Metafoundation, respectively. These indices provide an estimation of the response reduction, and therefore, need to take up their minimal value for an optimal coupled system.

6.3.1 Definition of optimization problem

The design variables $\zeta_{k,n}$ and $f_{k,n}$ define damping ratio and frequency of the n -th resonator in the k -th layer, respectively. They are collected in the parameter vector,

$$\mathbf{X} = [\zeta_{1,1}, \zeta_{k,n}, f_{1,1}, f_{k,n}]^T \quad (6.26)$$

Therefore, the optimization problem can be stated as,

$$\min(PI_{dr}(\mathbf{X})) \quad \text{or} \quad \min(PI_{acc}(\mathbf{X})) \quad (6.27)$$

for CMS, RMS and FMS cases, respectively. Furthermore, the following bounds hold,

$$0.05 \leq \zeta_{k,n} \leq 0.20 \quad \text{and} \quad 1Hz \leq f_{k,n} \leq 4Hz \quad (6.28)$$

Details on the chosen bounds in (6.28) are provided in the following Subsection. The optimization procedure is carried out with the aid of a numerical search algorithm, i.e. the built-in MATLAB 'fmincon' function. It implements a nonlinear programming solver, based on the interior-point algorithm [156], with embedded constraint functions for the sought tuning variables collected in the parameter vector X .

6.3.2 Results of optimization

The optimization procedure described in Subsection 6.3.1 is carried out for CMS, RMS and FMS, for both one and two-layered foundation cases. In this respect, Table 6.1 summarizes the values for CMS, while Tables 6.2 and 6.3 show the results for RMS, and FMS, respectively. When comparing the different systems to each other, the PI value slightly decreases from CMS to RMS. The RMS allows multiple frequencies for different resonators, thereby increasing its performance. This consideration is consistent with the concept of double negativity described in Subsection 6.2.1. However, the advantage obtained with multiple resonator frequencies is very small, partly due to the large resonator masses. In sum, the mass of the resonators provides a great contribution to the seismic isolation of the system; tuning the resonators to different frequencies and damping ratios, on the other hand, does not provide a significant advantage. The optimization of the PI via the interstory drift or the absolute acceleration of the superstructure yield almost the same values for resonator frequencies and damping ratios. In fact, interstory drift and absolute acceleration of the impulsive mode of the tank differ only through damping forces as implied by (6.21). Damping ratios, on the other hand, seem to decrease when multiple resonators are tuned to different frequencies. This could potentially be useful when it may be difficult to achieve high damping ratios. With regard to the bounds of (6.28), Figure 6.6(A) shows the optimization plane of the one-layered CMS with its corresponding contour lines. This surface is obtained by removing the upper bound of the damping ratio, in order to show the trend of the optimization surface. It is evident that when the damping ratio exceeds a certain threshold, the advantage gained on PI_{dr} is minimal. Moreover, Figure 6.6(B) depicts the optimization plane of the one-layered RMS case, where the x and y-axis denote the frequencies of the two independent resonators.

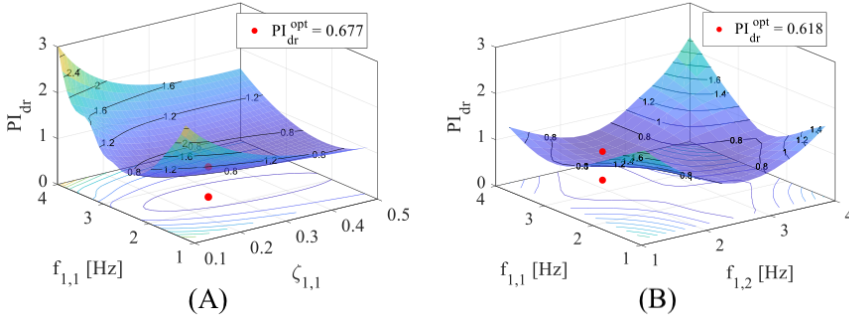


Figure 6.6: Optimization surfaces of one-layered (A) CMS case and (B) RMS case.

Table 6.1: Optimal parameters of the CMS for both one and two-layered cases.

One-layered case ($k=1$)					
Performance index	f_1 [Hz]	ζ_1			
PI_{dr}	0.677	2.5	0.20		
PI_{acc}	0.845	2.5	0.20		
Two-layered case ($k=1,2$)					
Performance index	f_1 [Hz]	ζ_1	f_2 [Hz]	ζ_2	
PI_{dr}	0.807	2.6	0.10	3.6	0.18
PI_{acc}	0.877	2.6	0.10	3.6	0.18

The contour lines of this plot show a wide area for the optimal values of the two resonators, where the value of the PI does not change significantly. Clearly, the resonators can be tuned to any set of two frequencies in this area, without inhibiting the functionality of the Metafoundation. Similar to the aforementioned damping ratio trend, this could have positive effects for practical applications, where the tuning of the resonators may not be very precise. In sum, the optimization of multiple resonators with different frequencies and damping ratios offer a slight advantage in terms of demand reduction from CMS to RMS, while no advantages are obtained with FMS. However, a system with optimal multiple resonators may be employed due to technological constraints.

6.4 Results of time history analyses

In order to verify the results of the previous Subsection and to take into account the actual amplitude and phase variation of seismic waves, the performance of the optimized Metafoundation is evaluated with time history

Table 6.2: Optimal parameters of the RMS for both one and two-layered cases (frequency in Hz).

		One-layered case ($k=1$)											
Performance index	$f_{1,1}$	$\zeta_{1,1}$	$f_{1,2}$	$\zeta_{1,2}$	$f_{1,3}$	$\zeta_{1,3}$							
<i>PIdr</i>	0.618	3.4	0.16	2.2	0.17	2.2	0.17						
<i>PIacc</i>	0.783	3.4	0.16	2.2	0.17	2.2	0.17						
		Two-layered case ($k=1,2$)											
Performance index	$f_{1,1}$	$\zeta_{1,1}$	$f_{1,2}$	$\zeta_{1,2}$	$f_{1,3}$	$\zeta_{1,3}$	$f_{2,1}$	$\zeta_{2,1}$	$f_{2,2}$	$\zeta_{2,2}$	$f_{2,3}$	$\zeta_{2,3}$	
<i>PIdr</i>	0.802	2.6	0.15	2.6	0.15	2.6	0.15	3.0	0.15	3.8	0.16	3.8	0.16
<i>PIacc</i>	0.873	2.6	0.15	2.6	0.15	2.6	0.15	3.0	0.15	3.8	0.16	3.8	0.16

Table 6.3: Optimal parameters of the FMS for both one and two-layered cases (frequency in Hz).

		One-layered case ($k=1$)											
Performance index	$f_{1,1}$	$\zeta_{1,1}$	$f_{1,2}$	$\zeta_{1,2}$	$f_{1,3}$	$\zeta_{1,3}$							
<i>PIdr</i>	0.617	2.2	0.15	3.4	0.16	2.2	0.18						
<i>PIacc</i>	0.776	2.0	0.12	3.4	0.16	2.4	0.14						
		Two-layered case ($k=1,2$)											
Performance index	$f_{1,1}$	$\zeta_{1,1}$	$f_{1,2}$	$\zeta_{1,2}$	$f_{1,3}$	$\zeta_{1,3}$	$f_{2,1}$	$\zeta_{2,1}$	$f_{2,2}$	$\zeta_{2,2}$	$f_{2,3}$	$\zeta_{2,3}$	
<i>PIdr</i>	0.802	3.6	0.16	3.6	0.18	2.6	0.16	3.6	0.16	3.6	0.18	2.6	0.16
<i>PIacc</i>	0.870	3.6	0.20	2.6	0.20	3.4	0.16	3.6	0.20	2.6	0.20	3.4	0.16

6.5. Optimization of the Metafoundation endowed with nonlinear devices

analyses (THAs). Therefore, the Metafoundation is subjected to the 12 natural seismic waves corresponding to a safe shutdown event (SSE) at the Priolo Gargallo site. As a reference indicator, we use the root-mean square of the tank base shear V_{rms} ,

$$V_{rms} = \sqrt{\frac{1}{n} \sum_{j=1}^n [k_i(u_j^{imp} - u_j^{tl}) + k_c(u_j^{conv} - u_j^{tl})]} \quad (6.29)$$

where, u_j^{imp} , u_j^{conv} and u_j^{tl} denote the displacement of the impulsive mass, the convective mass, and the top layer of the foundation, while n defines the number of time steps. The same quantities a_{rms} and d_{rms} have been evaluated for both absolute acceleration and interstory drift of the impulsive mass. Figures. 6.7(A), (B) and (C) show the aforementioned quantities as a function of PGA. More precisely, they compare the results of THAs obtained for the optimized one-layered CMS on both PI_{dr} and PI_{acc} with the results of the fixed-base tank. It is worth noting that the results of the THAs show a high dispersion for rms values. Therefore, PGA may not represent the most significant intensity measure for the engineering demand parameters under consideration. Nonetheless, since we are not interested in a fragility analysis of the system, the PGA has been considered as a sufficient parameter for result interpretation. On average, the V_{rms} values corresponding to the Metafoundation are below the values corresponding to the fixed-based tank. Moreover, similar results can be obtained with a_{rms} and d_{rms} for both PI_{dr} and PI_{acc} . Along those lines, both Figure 6.8(A) and (B) depict V_{rms} values for the one and two layered RMS systems, respectively. Similarly, Figure 6.8(C) and (D) show results for the FMS case. It becomes apparent that all systems perform on a comparable level, independently of the number of individual resonators in the system or the chosen optimization parameter. The only major difference that can be noticed is that the systems with only one layer outperforms the systems with two layers. This can be attributed to the lower horizontal stiffness of the one layered system.

6.5 Optimization of the Metafoundation endowed with nonlinear devices

Motivated by the use of simple hysteretic devices, i.e. wire ropes able to both effectively suspend concrete resonators inside the Metafoundation, allow motion in all three main directions, and provide significant damping; we propose an optimization procedure based on the stochastic linearisation technique from [148–150]. In addition, the treatment of a linearised system allows to bypass several difficulties related to the definition of the dispersion properties of a nonlinear periodic system [129]. Similar to the linear

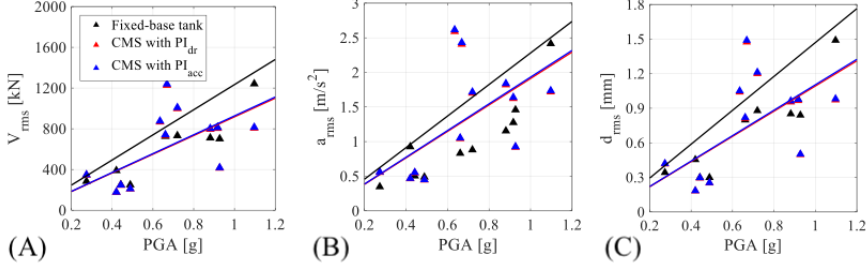


Figure 6.7: Root mean square values of the (A) base shear, (B) interstory drift and (C) absolute acceleration of one-layered CMS for both PI_{dr} and PI_{acc} .

case, we need to define a set of parameters to be optimized. These parameters, are chosen among the parameters of the Bouc-Wen model introduced in Subsection 6.2.3. Along these lines, we start with the following system of EOMs,

$$\mathbf{M}\ddot{\mathbf{u}}(t) + \mathbf{C}\dot{\mathbf{u}}(t) + \mathbf{K}\mathbf{u}(t) + u_y \mathbf{K}^{NL} \mathbf{z}(t) = \mathbf{F}(t) \quad (6.30)$$

where K^{NL} defines the nonlinear component of the stiffness matrix that contains the terms $(1 - \alpha n)k_n$ introduced in (6.7). In this model, n denotes the n -th resonator of the system, while $z(t)$ is the vector that contains the components $z_n(t)$ of the n -th resonator. Since (6.30) defines a nonlinear system, it is not amenable to the classical linear random vibration theory introduced in Section 6.3. Therefore, a stochastic linearisation technique (SLT) is employed to replace the nonlinear vector $u_y \mathbf{K}^{NL} \mathbf{z}(t)$.

6.5.1 Stochastic linearisation technique

The SLT is a relatively straightforward tool to define an equivalent linear system, equating its stochastic response to the response of the nonlinear system. More precisely, for a SDoF system with $N = 1$, the nonlinear differential equation (6.8) becomes,

$$\dot{z} + c_{eq} \dot{u} + k_{eq} u = 0 \quad (6.31)$$

where c_{eq} and k_{eq} are linearisation coefficients that are “equivalent” in a statistical sense [157–159]. At this stage, it is useful to introduce a state-space formulation of (6.30) and (6.31),

$$\frac{d}{dt} \mathbf{Y} = \mathbf{G} \mathbf{Y} + \mathbf{V} f(t) \quad (6.32)$$

with,

$$\mathbf{G} = \begin{bmatrix} \mathbf{0}_{N \times N} & \mathbf{I}_{N \times N} & \mathbf{0}_{N \times N} & \mathbf{0}_{N \times r} \\ -\mathbf{M}^{-1} \mathbf{K}^L & -\mathbf{M}^{-1} \mathbf{C} & -\mathbf{M}^{-1} \mathbf{K}^{NL} & -\mathbf{1} \mathbf{a}_f^T \\ \mathbf{0}_{N \times N} & -c_{eq} & -k_{eq} & \mathbf{0}_{N \times r} \\ \mathbf{0}_{r \times N} & \mathbf{0}_{r \times N} & \mathbf{0}_{r \times N} & \mathbf{A}_F \end{bmatrix} \quad (6.33)$$

6.5. Optimization of the Metafoundation endowed with nonlinear devices

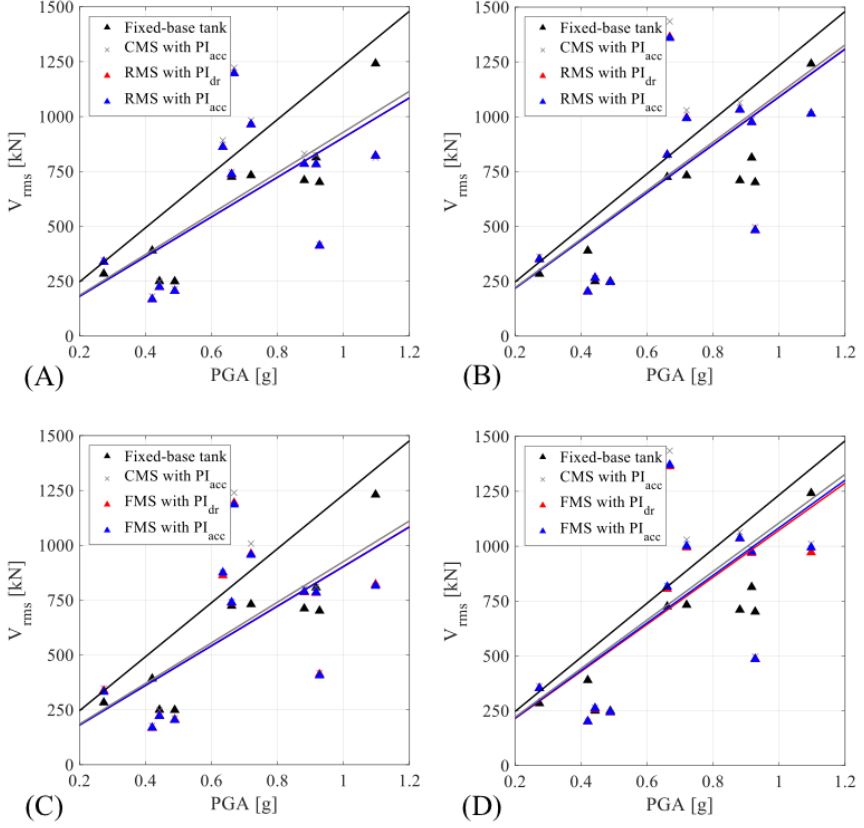


Figure 6.8: Root mean square values of the tanks base shear for: (A) one-layered RMS; (B) two-layered RMS; (C) one-layered FMS; (D) and two-layered FMS.

and,

$$\mathbf{Y} = \begin{bmatrix} \mathbf{u} \\ \dot{\mathbf{u}} \\ \mathbf{z} \\ \mathbf{u}_f \end{bmatrix}, \quad \mathbf{V} = \begin{bmatrix} \mathbf{0}_{N \times 1} \\ \mathbf{0}_{N \times 1} \\ \mathbf{0}_{N \times 1} \\ \mathbf{V}_f \end{bmatrix} \quad (6.34)$$

where \mathbf{Y} is the state-space vector, K^L and K^{NL} define the linear and non-linear components of the stiffness matrix, respectively, while k_{eq} and c_{eq} represent the matrices including the equivalent linear coefficients. Moreover, N defines the number of DoFs of the system and $r = 4$ defines the number of equations of the KTCP filter introduced in Subsection 6.2.4. Let the covariance matrix of \mathbf{Y} be \mathbf{S} with $S_{ij} = E[y_i y_j]$. Then, we assume that the seismic input is stationary. The solution of (6.33) can be derived from

the following Lyapunov system of equations,

$$\mathbf{GS} + \mathbf{SG}^T + \mathbf{B} = \mathbf{0} \quad (6.35)$$

where \mathbf{B} is a zero matrix except for the generic diagonal element corresponding to the nonzero row of the forcing function vector, i.e. $B_{ij} = 2\pi S_0$. The Lyapunov equation (6.35) was solved with the algorithm proposed by Bartels and Steward [160]. Because k_{eq} and c_{eq} are not known a priori, an iterative solution procedure is required. In this regard, Maldonado et al. [157] suggested to set as initial values $c_{eq} = 1$ and $k_{eq} = 0.05$ for a faster convergence. Further details about the procedure are available in [157–159].

6.5.2 Optimization of linearised devices

In order to define the transfer function $H(\omega)$ of the coupled systems depicted in Figure 6.5 we start from (6.6). In fact, (6.33) includes the KTCP filter and the derivation is more burdensome. Therefore, the relevant $H(\omega)$ for a SDoF reads,

$$H(\omega) = \left[\omega^2 m + i\omega c + \alpha k - \frac{i\omega}{i\omega + k_{eq}} c_{eq} (1 - \alpha) k u_y \right]^{-1} \quad (6.36)$$

where the derivation details can be found in Appendix A. Its generalization reads,

$$\mathbf{H}(\omega) = [-\omega^2 \mathbf{M} + i\omega \mathbf{C} + \mathbf{K} + \mathbf{K}^{eq}]^{-1} \quad (6.37)$$

where \mathbf{K}^{eq} contains zero terms except those in which the n -th resonator is physically connected to the k -th layer of the Metafoundation as depicted in Figure 6.5. More precisely, the nonzero terms k_{ij}^{eq} of matrix \mathbf{K}^{eq} read,

$$k_{ij}^{eq} = -\frac{i\omega}{i\omega + k_{eq}} c_{eq} (1 - \alpha_n) u_y k_n \quad (6.38)$$

in which α_n and k_n are referred to the n -th resonator of the Metafoundation. Note that (6.37) degenerates into (6.18) when $\alpha = 1$.

6.5.3 Definition of optimization problem

The optimization procedure for the nonlinear devices relies on the design variables $k_{k,n}$ and $\beta_{k,n}$ gathered in the parameter vector X_{NL} ,

$$X_{NL} = [k_{1,1}, k_{k,n}, A_{1,1}, A_{k,n}, \beta_{1,1}, \beta_{k,n}, \gamma_{1,1}, \gamma_{k,n}]^T \quad (6.39)$$

Therefore, the optimization problem can be stated as,

$$\min(PI_{dr}(X^{NL})) \quad \text{or} \quad \min(PI_{acc}(X^{NL})) \quad (6.40)$$

where $k = 1, \dots, n_k$ and $n = 1, \dots, n_r$. Finally, bounds on the design variable β_k, n are,

$$0 < \beta_{k,n} < 1 \quad (6.41)$$

Further details about the bound in (6.41) are provided in Subsection 6.6.1.

6.6 Hysteretic dampers, Bouc-Wen parameters and optimization results

6.6.1 Hysteretic dampers and Bouc-Wen parameters

The optimization procedure presented in Section 6.5 allows the evaluation of the main parameters of a Bouc-Wen model employed to reproduce a hysteretic damper. With regard to hysteretic devices, steel wire ropes schematically depicted in Figure 6.2(B), represent a commonly used solution in seismic engineering due to their capability to dissipate a relatively large amount of energy. Moreover, they are fairly cheap both in terms of production and maintenance costs, and allow motion along X, Y and Z direction as indicated in Figure 6.1. Many authors investigated the effectiveness of wire ropes subjected to shear forces; see, among others, [108, 140–143]. In this respect, Paolacci and Giannini [140] fitted the parameters of a Bouc-Wen model to sets of experimental data. Based on their work, we selected the wire rope WR36-400-08, with its geometric dimensions being collected in Table 6.4 and the relevant nomenclature shown in Figure 6.9(B). In particular, k_p and R_v represent the horizontal stiffness and the vertical load-bearing capacity, respectively. The authors have found $\alpha = 0.254$ and $u_y = 2.2$ mm; in addition, the quality of the fitting can be appreciated in Figure 6.9(A). Once the geometric and mechanical characteristics of a typical wire rope is established, some considerations on the Bouc-Wen parameters need to be made. In fact, some parameters of the Bouc-Wen model presented in Subsection 6.2.3 are functionally redundant and can be appropriately set. More precisely, Constantinou and Adnane [161] showed that by setting $A = 1$ and $\beta + \gamma = 1$, the model collapses to a rate-dependent Maxwell model with a nonlinear dashpot, i.e. an Ozdemir model. As a result, with $A = 1$ in (6.9), the value of the initial stiffness $k = R_y/u_y = k_0$ is retrieved. Furthermore, we define $z_{max} = [A/(\beta + \gamma)]^{1/n} = 1$ and $z \in [-1, 1]$ for (6.8).

6.6.2 Optimization results and time history analyses

The results of Subsection 6.4 underscore that only small differences in base shear values of the superstructures are achieved with CMS, RMS and FMS in the linear case. Therefore, only optimizations of one and two-layered CMSs are carried out herein. In Subsections 6.6.1 we set n, α and u_y based on the

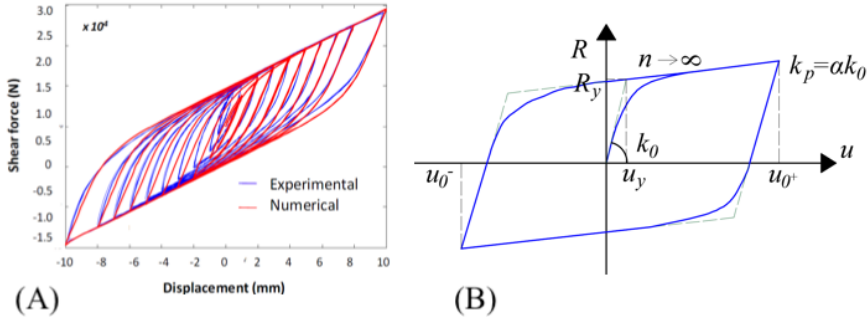


Figure 6.9: (A) Hysteretic behaviour under cyclic shear loading (after Paolacci and Giannini [140]) and (B) typical hysteretic loop of a Bouc-Wen model.

Table 6.4: Geometric and mechanical properties of wire ropes.

Type	Parameter	Value
Geometric	H [mm]	178
	W [mm]	216
	L [mm]	520.7
	Φ [mm]	26.6
	k_0 [kN/mm]	1.35
Bouc-Wen	R_y [kN]	2.97
	u_y [mm]	2.2
	n	1.0
	A	1.0
	α	0.254

Table 6.5: Bouc-Wen Setups.

Parameter Configurations
$\beta = 0.9$ and $\gamma = 0.1$
$\beta = 0.5$ and $\gamma = 0.5$
$\beta = 0.1$ and $\gamma = 0.9$

properties collected in Table 6.4. As a result, we search for optimal values of k , β and γ with the constraints $A = 1$ and $\beta + \gamma = 1$, respectively.

The results of the optimization for PI_{dr} are depicted in both Figure 6.10(A) and (B), for the one-layered and two-layered CMS. Notably, k_2 represents the horizontal stiffness of a single resonator of the Metafoundation. Figure 6.10(A) highlights a smooth surface in the range 50-60 kN/mm for the one-layered case; conversely, a narrow valley of possible optimal stiffness values characterizes the two-layered case. Furthermore, the two-layered

CMS shows poor results in terms of PI_{dr} due to the increased horizontal stiffness of the system. The parameters β and γ quantify the dissipation characteristics of wire ropes. One can observe that an increase of β , i.e. a decrease of γ , does not entail a significant reduction of PI_{dr} . In fact, the constraint $\beta + \gamma = 1$ strongly sets the shape of the backbone loops and the relevant dissipated energy, as shown by the loops -in blue- depicted in Figure 6.11.

In order to confirm the performance of the foundation-tank coupled system with the properties provided by Figure 6.10, THAs in the nonlinear regime are carried out. More precisely, k_2 values of 56.8 and 40.5 kN/mm are employed for one and two-layered foundation cases, respectively. These values entail a number of wire ropes per resonator equal to 42 and 30 for one and two-layered cases, respectively, which is greater than those needed to bear each resonator's weight, i.e. 16 and 8.

In particular, Figure 6.11 shows hysteretic loops of one wire rope -blue lines- for a one-layered CMS subjected to one of the 12 natural seismic waves. In all figures, u_{res} and u_{tl} represent the displacements of a generic resonator and the top-layer, respectively. More precisely, Figure 6.11(A) refers to the optimized system in which each resonator is equipped with 42 wire ropes while Figure 6.11(B) refers to the one in which each resonator is equipped with the minimum number of wire ropes necessary to bear a resonator. In both cases, β and γ read 0.9 and 0.1, respectively. One can observe that the hysteretic dampers exert a positive displacement demand of about 60 mm versus an actual experimental maximum displacement of about 10 mm shown in Figure 6.9(A). Therefore, an effective Metafoundation requires a significant amount of ductility and dissipated energy for quite strong earthquakes. Hence, given the size of the Metafoundation, we locate 12 and 6 dampers per resonator, for the one and two-layered case. Their relevant horizontal dissipation capability is equal to the one provided by the aforementioned optimization procedure. THA results are shown herein only for the one-layered Metafoundation case, based on Bouc-Wen parameter values collected in Table 6.5. In fact, as argued from Figure 6.10(B), the two-layered Metafoundation achieves a limited performance when hysteretic dampers are used. This can also be understood from Figure 6.11, where the limited performance of hysteretic dampers versus linear dampers is evident.

Figure 6.12 shows root-mean square values of the tanks base shear for each considered optimal configuration. Note that the benefits with respect to the case of a tank with a fixed foundation are evident. In agreement with the optimization outcomes, partly explained through Figure 6.10(A), there are no significant differences among the Metafoundations equipped with wire ropes endowed with the parameters of Table 6.5. An additional comparison between the non-linear foundation tank coupled system and the fixed-base solution is made in terms of maximum and median response. Figure 6.13 depicts: (A) the maximum values of base shear; (B) absolute acceleration of

6. WIRE ROPES FOR RESONATOR SUSPENSION

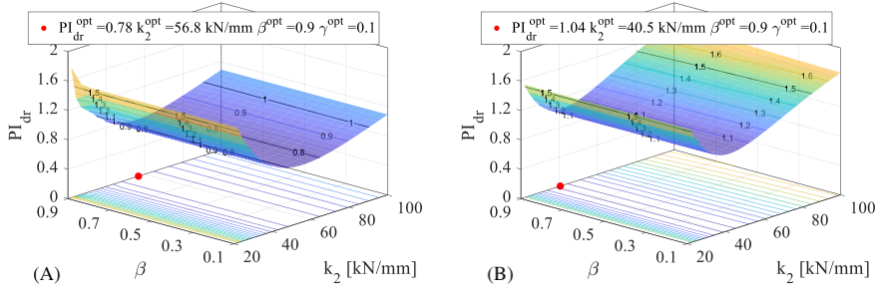


Figure 6.10: Optimal surfaces in the nonlinear case: (A) one layered CMS and (B) two-layered CMS.

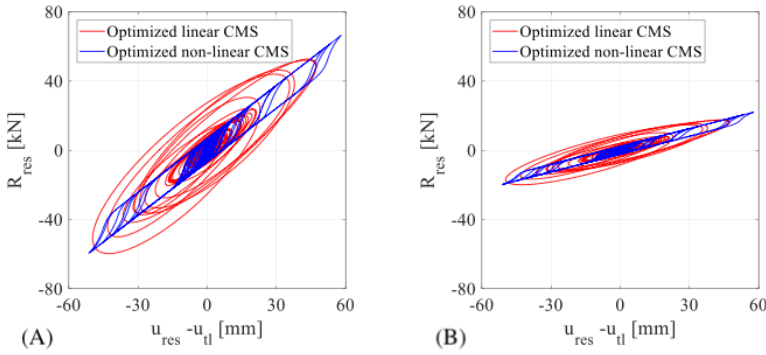


Figure 6.11: Hysteretic loops of one-layered CMS hysteretic damper -blue lines, $A = 1$, $\beta = 0.9$ and $\gamma = 0.1$ - and linear viscous damper -red lines, $\zeta_{1,1} = 0.2$ - resonators equipped with (A) optimal and (B) minimum number of wire ropes.

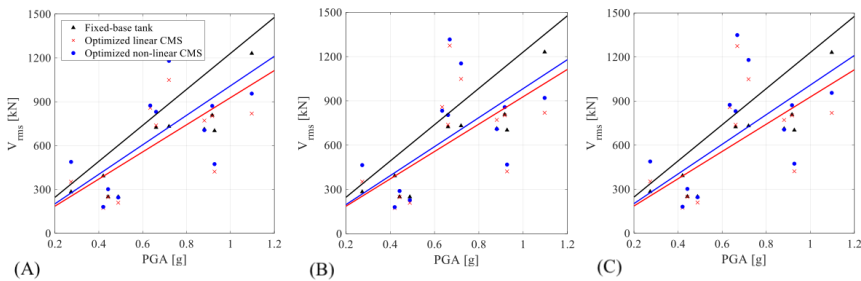


Figure 6.12: Root-mean square values of the tank base shear for one-layered CMS: (A) $\beta = 0.9$ and $\gamma = 0.1$, (B) $\beta = 0.5$ and $\gamma = 0.5$ and (C) $\beta = 0.1$ and $\gamma = 0.9$.

6.6. Hysteretic dampers, Bouc-Wen parameters and optimization results

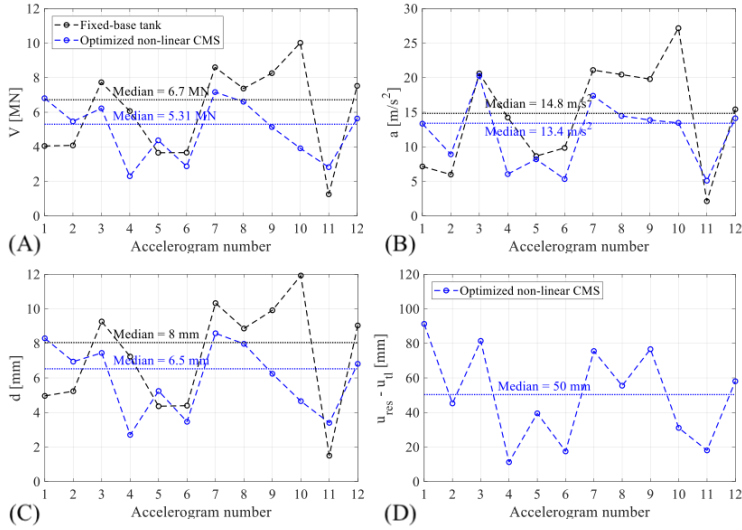


Figure 6.13: Time history results for a fixed base tank and CMS: (A) Maximum base shear; (B) Absolute acceleration of the impulsive mode; (C) Maximum displacement of wire ropes; (D) Maximum interstorey drift.

the impulsive mode; (C) maximum wire rope displacement; and (D) interstorey drift of the impulsive mass, obtained for the 12 accelerograms at hand. Maximum and median values are again referred to the optimized one-layered CMS equipped with nonlinear devices in which β and γ are equal to 0.9 and 0.1, respectively. Figure 6.13 clearly shows that the nonlinear Metafoundation generally reduces seismic demand. Furthermore, median values achieve reductions of about 21%, 10% and 19% for base shear, absolute acceleration and interstorey drift, with respect to the fixed tank. Similar conclusions apply for the linear metafoundations analysed in Subsection 6.4.

With regard to nonlinear devices, Figure 6.13(C) shows both maximum and median values of wire rope displacements for the optimized nonlinear CMS relevant to each accelerogram. Maximum displacements reach approximately 12 mm with a median equal to 8 mm. These figures are feasible for standard wire ropes. An additional comparison between linear and nonlinear devices entails that damping devices with a linear behaviour provide more favourable results than those characterized by a hysteretic behaviour. This trend is also justified by the amount of dissipated viscous and hysteretic energy. In this regard, Figure 6.14 depicts the $E_d^{non-lin}/E_d^{lin}$ ratio for the one-layered CMS for each considered accelerogram. The limited performance of hysteretic dampers becomes evident, since none of the parameter setups reaches close to unity. Needless to say, that for the Metafoundations to

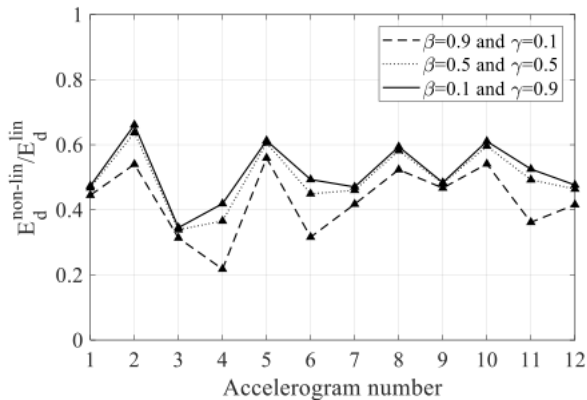


Figure 6.14: $E_d^{\text{non-lin}}/E_d^{\text{lin}}$ ratio of dissipated energy by nonlinear hysteretic dampers and linear viscous dampers for the optimal cases of one-layered CMS.

hand endowed with resonators that move in X and Y directions, wire ropes represent a technological solution that is both much cheaper and feasible than fluid viscous dampers coupled to linear springs. Moreover, they can potentially be competitive against the vertical component of an earthquake.

6.7 Conclusion and future developments

In this paper, we proposed two Metafoundations designed to inherit favourable properties from seismic wave propagation in phononic periodic structures in the ultralow-frequency regime: (i) a foundation endowed with resonators and linear dampers tuned to multiple frequencies; and (ii) a foundation equipped with resonators and nonlinear hysteretic devices. They are composed by steel-concrete composite and steel components that define exterior unit cells containing resonant concrete masses. The tuning of these coupled tank-foundation systems was achieved through an optimization algorithm in the frequency domain, which is able to optimize any number of parameters, to account for the superstructure as well as the stochastic nature of the seismic input. In particular, to optimize the nonlinear behaviour of hysteretic damper devices we employed a Bouc-Wen hysteretic model; which was subsequently reduced via a system of stochastically linearised equations. Then, we tested the optimized systems against natural seismic records both with linear and nonlinear time history analyses. In particular, optimization results showed that a Metafoundation with multiple resonant frequencies provides limited benefits to the structural response during earthquake events. This is mainly due to the massive resonator masses. However, a system with multiple resonators can attain an optimal response with reduced damping values,

which entails that simple linear devices can be used. With regard to the use of nonlinear hysteretic devices, the optimization showed that favourable results can be achieved with dampers endowed with relatively high dissipative characteristics, like wire ropes. Nonetheless, the limited performance of wire ropes with respect to linear dampers in terms of dissipated energy reduces the utility of a two-layered finite-lattice Metafoundation. These results lay down the basis for future developments of Metafoundations, where a proper use of nonlinear hysteretic devices arranged for instance at 45° , see Fig. 6.2(A), requires a physical characterization of the whole wire rope set. Finally, a Metafoundation equipped with wire ropes that move in all 3 spatial directions may provide a seismic isolation system that can take care of both the horizontal as well as the vertical component in the future.

6.8 Appendix: Obtaining the transmission matrix after SLT

In order to obtain the transmission matrix $H(\omega)$, we can solve (6.31) as a Cauchy problem,

$$z(t) = -c_{eq}e^{-k_{eq}t} \int e^{k_{eq}t} \dot{u}(t) dt \quad (6.42)$$

The initial conditions $z(t = 0) = 0$ and $\dot{u}(t = 0) = 0$ entails that also the resulting integration constant equates to 0. Subsequently, we substitute (6.42) in (6.6) and (6.7) and obtain,

$$m\ddot{u}(t) + c\dot{u}(t) + \alpha ku(t) + (1 - \alpha)ku_y \left[-c_{eq}e^{-k_{eq}t} \int e^{k_{eq}t} \dot{u}(t) dt \right] \quad (6.43)$$

The solutions $u(t) = u_0e^{i\omega t}$ and $F(t) = e^{i\omega t}$ entail,

$$-\omega^2 u_0 e^{i\omega t} m + i\omega u_0 e^{i\omega t} k + (1 + \alpha)ku_y \left[-c_{eq}e^{-k_{eq}t} \int i\omega e^{k_{eq}t} u_0 dt \right] = F_0 e^{i\omega t} \quad (6.44)$$

More precisely, the integral in (6.44) has the following solution,

$$\int i\omega u_0 e^{(i\omega + k_{eq})t} dt = \frac{i\omega}{i\omega + k_{eq}} u_0 e^{(i\omega + k_{eq})t} \quad (6.45)$$

thus, (6.44) becomes,

$$-\omega^2 u_0 e^{i\omega t} m + i\omega u_0 e^{i\omega t} k + (1 + \alpha)ku_y \frac{i\omega}{i\omega + k_{eq}} u_0 e^{(i\omega + k_{eq})t} = F_0 e^{i\omega t} \quad (6.46)$$

Eventually the transfer function $H(\omega)$ reads,

$$H(\omega) = \left[-\omega m + i\omega c + \alpha k - \frac{i\omega}{i\omega + k_{eq}} c_{eq} (1 - \alpha) u_y k \right]^{-1} \quad (6.47)$$

Chapter 7

Summary, conclusion and future developments

7.1 Summary

The recent advance of seismic metamaterials introduced novel ideas to the field of earthquake engineering. Inspired by these developments, this thesis explored the possibility of using locally resonant metamaterials for the conception of a new type of foundation, namely the Metafoundation. Of particular interest was the band-gap property of locally resonant materials, since this property denies elastic waves from propagating within a specific frequency region, and therefore may be advantageous for earthquake mitigation measures. Based on this phenomenon a foundation was conceptualized as a continuous metamaterial and later redesigned as a discrete column based structure for the seismic protection of fuel storage tanks. The developed foundation could potentially prevent NaTech events, related to the petrochemical industry, from occurring, since storage tanks and connected pipeline systems have proven to be extraordinarily vulnerable to seismic action.

The foundation proposed herein, offered the desired band-gap properties, if considered as an infinite periodic material, while when arranged as a finite system, this property was reduced to an attenuation zone. Additionally, the feedback from the superstructure and the frequency content of the expected ground motion influence the behaviour of the overall system, which led to the development of an optimization algorithm. The algorithm was based on computations in the frequency domain, allowed for an efficient tuning of multiple foundation parameters and was made available as an open source software on GitHub. It is worth noting that soil structure interaction was not taken into account directly, by modelling the soil underneath the foundation, but considered indirectly through the ground motion spectrum used

for the optimization. Here, the site and soil type of the chosen location have an influence on the frequency content of the seismic spectrum, thereby acknowledging the filtering effects of the soil. However, proper soil structure interaction should be investigated in future studies, since its effects may yield additional benefits, especially for vertical component damping. Besides the foundation tank interaction, which was treated with the optimization algorithm, also the effect that the Metafoundation has on connected pipelines was investigated in an experimental study. It is worth noting that pipeline systems connected to base isolated storage tanks can be damaged due to the large displacements that occur when traditional isolators get activated. This issue was touched upon with a hybrid simulation, where a tank with classical isolation was compared to a tank protected via the Metafoundation. The study was conducted experimentally, because of the highly nonlinear response of liquid filled pipelines, which can be difficult to model numerically in a realistic manner. Besides this, the strict construction requirements of Eurocodes [68, 74, 82, 118, 119] and NTC 2018 [107] have proven to be a limiting factor for the functionality of the foundation and resulted in a foundation height of 4 m for a reliable attenuation of seismic effects. In order to reduce this excessive height, a negative stiffness element, based on a local instability, was implemented in the foundation and reduced its height to 1 m at a similar performance level. Furthermore, also the effects of the negative stiffness as well as its nonlinear behaviour on the wave propagation properties of the periodic medium were investigated. The analyses showed that the mechanism amplified the band-gap property in terms of range as well as efficiency, while the nonlinearity of the device had the effect of reducing the band-gap width. Last but not least, the implementation of wire ropes as resonator suspension rendered the overall design more realistic with respect to the previously assumed ideal sliding surfaces and may allow for vertical component damping, due to their flexibility in all 3 spatial directions. The main conclusions drawn from the development and analysis of the Metafoundation are elaborated in individual paragraphs below.

7.2 Conclusions

The importance of the horizontal stiffness. The first draft of the herein discussed Metafoundation was proposed in Chapter 2, where a continuous concrete matrix with embedded resonators was studied. Through varying the wall thickness of a finite stack of unit cells, it was demonstrated, in the frequency domain, that the horizontal stiffness of the foundation plays a vital role in its wave attenuation effectiveness. Based on this, a new design with columns as primary load bearing system was conceived and tested on its steady state response when coupled to a tank. Overall, the foundation was reduced from an 8 m continuous system to a 3 m column based structure

with a far better wave attenuation efficiency in Chapter 2.

Effects of small cracks on the band-gap behaviour. As discussed in Chapter 2, small cracks can appear in the foundation due to static loading, which may change the wave propagation properties of the periodic medium. However, since the investigated cracks were relatively small compared to the unit cell dimensions and located in the slabs, which have only a small impact on the shear wave propagation, no significant alteration of the band-gap was detected.

The superstructure is non-negligible. In Chapter 2 the band gap was designed to include the resonant frequency of the coupled foundation-tank system, in order to provide the most effective seismic protection. Furthermore, Chapter 3 built on this development and tuned the foundation according to the frequency response of the system when subjected to an harmonic input. However, since seismic events are not harmonic, but behave more like a random Gaussian process, an optimization algorithm was proposed in Chapter 4. This algorithm can take both, the superstructure as well as the expected frequency content into account and demonstrated, after a study of 4 different foundation layouts coupled with 2 different tanks subjected to various ground motion spectra, that the resonators are dependent on the superstructure and the foundation layout. The variance in optimal design with respect to the ground motion was less pronounced, yet still significant enough to be considered in all further studies.

Optimization of the Metafoundation unavoidable. As mentioned above, an optimization algorithm that is able to consider the superstructure as well as the ground motion was conceptualized in Chapter 4. It was later generalized in Chapter 5, where direct parametrization of the transmission matrix allowed for the optimization of any number of different linear parameters. In particular, the methodology was used in Chapter 5 for a foundation endowed with negative stiffness elements and in Chapter 6 to optimize multiple frequencies for different resonators and to fine tune the linearized parameters deriving from a stochastic linearization. In sum, the optimization algorithm yields reliable results, could be used also for other vibration isolation problems and has been made available as a Python module on GitHub at: <https://github.com/moritz343/Optimization>.

Design of the foundation under common construction practice possible. The first static design check was conducted on the continuous system in Chapter 2, where the concrete matrix was evaluated on static resistance and potential cracks. Subsequently in Chapter 4, the design checks were expanded to an elastic response spectrum analysis, in order to comply with

common construction practices, such as the Eurocode or the Italian standard NTC 2018. The restrictive nature of these requirements becomes particularly apparent, when observing the average base shear reduction of various foundation layouts, where a foundation height of 4 m diminishes the average base shear of a broad tank by 30%. On the one hand, this clearly displays that the foundation can be designed under realistic circumstances, while on the other hand, a 4 m tall foundation cannot be regarded as economical. It was therefore concluded that the foundation is possible, yet more work needs to be done before it can become a viable option in a real life application.

Effects on a coupled pipeline. Since not only fuel storage tanks but also connected pipeline systems can be damaged by seismic events, and subsequently cause NaTech disasters, an experiment on the coupled structure has been carried out and presented in Chapter 3. The Metafoundation setup was compared to a concave sliding bearing (CSB), where the results showed that the CSB performed more efficient in terms of base shear, while the Metafoundation was able to reduce the pipeline stresses with respect to the CSB. It is worth mentioning that the response of the complete coupled system may further be improved by considering the tank as well as the pipeline when designing the foundation, since their dynamic interaction has been disregarded when designing the foundation for the numerical substructure of the experiment.

Comparison with standard isolation devices. As demonstrated with the experiment carried out in Chapter 3, traditional base isolation systems such as CSBs outperform the Metafoundation in terms of base shear reduction for storage tanks. However, the function of traditional base isolation systems is to reduce the eigenfrequency of the superstructure by decoupling it from the ground, which necessarily entails large horizontal displacements that may impose significant stresses on connected pipelines. Besides this, traditional isolators are generally not able to address the vertical component of seismic events due to their high vertical stiffness. Therefore, two advantages may be obtained by the Metafoundation over traditional solutions after further developments, namely: (i) reduction of pipeline stresses induced by horizontal tank displacements; and (ii) vertical component damping.

Performance at various liquid levels. Additional to the experimental study, Chapter 3 also contains a numerical evaluation of the foundations performance when the tank is not full. The results showed that the demand reduction of the 3/4 filled tanks diminished with respect to the full tanks, while the absolute demand for the tanks with reduced liquid height still fell below the full tank setups.

Wire ropes as resonator suspension. In Chapter 4 it was mentioned that wire ropes could potentially serve as devices to suspend the concrete resonators, which was later elaborated in more detail in Chapter 6. Here, a stochastic linearization technique was applied to the Bouc-Wen model, in order to find an equivalent linear system that could approximate the wire rope setup and subsequently be optimized with the method proposed in Chapter 5. With the optimal parameters for the linearized system, a realistic wire rope setup was chosen and analysed on its performance via time history analyses. While the hysteretic behavior of the wire ropes did not improve the system response, it is clear that from an engineering point of view, a wire rope construction is more realistic than endowing the resonators with ideal friction less sliding surfaces and visco-elastic dampers. Furthermore, wire ropes allow the resonators to move also in the vertical direction and may provide vertical component damping in the future.

Negative stiffness elements for reduced foundation height and improved performance. Since the resulting foundation height, due to the restrictions from engineering requirements, was considered excessive for a tank foundation, a device that can exert an amplification effect on the resonators was studied in Chapter 5. The device is based on a snap through mechanism, held in a stable position, that for all practical purposes behaves like a spring with negative stiffness. On the one hand the mechanism amplifies the motion of the resonators, while on the other hand it softens the overall stiffness of the foundation; thus improving the system performance significantly. It was found that for 50% of the maximum physically admissible negative stiffness, the foundation could be reduced from a 3 m high layout to only 1 m, while maintaining its performance. Furthermore, the analysis in the time and frequency domain showed that the NSE endowed foundation was less sensitive to resonant frequency changes and seismic record variability.

Effect of the nonlinear NSE on the wave propagation. In Chapter 5 the application of the NSE to the foundation resulted in a new type of periodic chain, where not only the main masses, but also the resonators were connected to the next and previous unit cell via nonlinear springs. Recent works on nonlinear elastic metamaterials treated the dispersion analysis of classical diatomic lattices, endowed with duffing type oscillators, with the harmonic balance method (HBM) and found an elongation and shift of the band-gap. However, when applying the HBM to the new resonator chain with a polynomial nonlinearity, a closing of the band-gap was found for increased levels of nonlinearity. Therefore, it can be concluded that for this type of nonlinear metamaterial an activation of the nonlinearity should be avoided.

Effects of the nonlinear NSE on seismic analyses in the time domain. Since the introduction of a nonlinearity introduces higher harmonics to the system, a further study on the energy transfer from the first to the third harmonic was conducted in Chapter 5. Through a variation of the nonlinear parameters, the behavior of the structure was forced to go into the highly nonlinear range, which, unfortunately, did not yield any additional improvements in terms of base shear reduction. However, with the proposed nonlinear parameters, the structure can effectively be designed to enter or stay outside of the nonlinear regime.

7.3 Future developments

The work done on the Metafoundation can be regarded as a first step towards introducing metamaterial-based foundations into the realm of civil engineering. While more work is needed before foundations of this type can be realized, some advantages may be obtained in the future. Possible advantages include the attenuation of vertical earthquake motions, most common at near fault locations with a shallow focal depth; the reduction of rocking motions; and the attenuation of base shear with limited horizontal displacements. Structures that could profit from this constitute mainly large buildings with a high consequence intensity, such as nuclear power plants and fuel storage tanks. In particular, the safety of tanks and their connected pipelines needs to be improved, since these structures are still particularly vulnerable to seismic events. To date, only classical isolation has been applied to fuel storage tanks, which can result in large horizontal displacements during earthquakes, thereby damaging connected pipeline systems. The herein proposed foundation on the other hand may provide a suitable protection system that limits tank as well as pipeline stresses in the future. Additionally, the high vertical stiffness of isolators makes them generally inefficient at attenuating the vertical component of an earthquake, which can have damaging effects on nuclear power plants. With resonators that can oscillate in all 3 spatial directions, by suspending them with wire ropes for example, these vertical excitations may be addressed by the Metafoundation after further iterations.

Besides this, an NSE comprised of a local instability, can in theory drastically reduce the system size of a periodic foundation, and therefore, make the overall system more economical. This is particularly important for seismic metamaterials, since the typical system dimensions found in the literature are still relatively large. Moreover, its applicability to a periodic structure targeted at the attenuation of shear type waves makes it a versatile device that could, in principle, also find implementation in other vibration isolation issues or metamaterial-based structures. Finally, it is worth mentioning that the field of seismic metamaterials is a rapidly expanding one, where new ad-

vances emerge frequently. Hopefully other researchers can profit from the ideas and concepts discussed in this thesis and bring further developments to this fascinating field of research.

Bibliography

- [1] Solymar L., Shamoniina E. (2009). *Waves in metamaterials*. Oxford University Press.
- [2] Smith D.R., Padilla W.J., Vier D.C., Nemat-Nasser S.C., Schultz S. (2000). Composite medium with simultaneously negative permeability and permittivity. *Physical Review Letters*, 84(18): 4184–4187.
- [3] Zouhdi S., Sihvola A., Arsalane M. (2002). *Advances in Electromagnetics of Complex Media and Metamaterials*. Springer Netherlands.
- [4] Grimberg R. (2013). Electromagnetic metamaterials. *Materials Science and Engineering B: Solid-State Materials for Advanced Technology*, 178(19): 1285–1295.
- [5] Maldovan M. (2013). Sound and heat revolutions in phononics. *Nature*, 503(7475): 209–217.
- [6] Liu Z., Xixiang Z., Mao Y., Zhu Y.Y., Yang Z., Chan C.T., Sheng P. (2000). Locally Resonant Sonic Materials. *Science*, 289(5485): 1734–1736.
- [7] Sigalas M., Kushwaha M.S., Economou E.N., Kafesaki M., Psarobas I.E., Steurer W. (2005). Classical vibrational modes in phononic lattices: Theory and experiment. *Zeitschrift fur Kristallographie*, 220(9-10): 765–809.
- [8] Deymier P.A. (2013). *Introduction to Phononic Crystals and Acoustic Metamaterials*. Springer Series in Solid-State Sciences.
- [9] Brillouin L. (1953). *Wave propagation in periodic structures; electric filters and crystal lattices*. Dover Publications.
- [10] Kittel C. (1962). *Elementary solid state physics : a short course*. Wiley, New York.
- [11] Floquet G. (1883). Sur les equations differentielles lineaires a coefficients preiodiques. *Annales scientifiques de l'E.N.S. 2e serie*, 12: 47–88.

- [12] Bloch F. (1929). Über die Quantenmechanik der Elektronen in Kristallgittern. *Zeitschrift für Physik*, 52(7-8): 555–600.
- [13] Brillouin L. (1930). Les electrons dans les metaux et le classement des ondes de de Broglie correspondantes. *Comptes Rendus Hebdomadaires des Séances de l'Académie des Sciences*, 191(292).
- [14] Brûlé S., Javelaud E.H., Enoch S., Guenneau S. (2013). Experiments on seismic metamaterials: Molding surface waves. *Physical Review Letters*, 112(13).
- [15] Huang J., Shi Z. (2013). Attenuation zones of periodic pile barriers and its application in vibration reduction for plane waves. *Journal of Sound and Vibration*, 332(19): 4423–4439.
- [16] Achaoui Y., Antonakakis T., Brûlé S., Craster R.V., Enoch S., Guenneau S. (2017). Clamped seismic metamaterials: Ultra-low frequency stop bands. *New Journal of Physics*, 19(6).
- [17] Krödel S., Thomé N., Daraio C. (2015). Wide band-gap seismic metastructures. *Extreme Mechanics Letters*, 4: 111–117.
- [18] Miniaci M., Krushynska A., Bosia F., Pugno N.M. (2016). Large scale mechanical metamaterials as seismic shields. *New Journal of Physics*, 18(8).
- [19] Palermo A., Krödel S., Marzani A., Daraio C. (2016). Engineered metabarrier as shield from seismic surface waves. *Scientific Reports*, 6.
- [20] Colombi A., Roux P., Guenneau S., Gueguen P., Craster R.V. (2016). Forests as a natural seismic metamaterial: Rayleigh wave bandgaps induced by local resonances. *Scientific Reports*, 6.
- [21] Roux P., Bindi D., Boxberger T., Colombi A., Cotton F., Douste-Bacque I., Garambois S., Gueguen P., Hillers G., Hollis D., Lecocq T., Pondaven I. (2018). Toward seismic metamaterials: The METAFORET project. *Seismological Research Letters*, 89(2A): 582–593.
- [22] Colombi A., Colquitt D., Roux P., Guenneau S., Craster R.V. (2016). A seismic metamaterial: The resonant metawedge. *Scientific Reports*, 6.
- [23] Xiang H.J., Shi Z.F., Wang S.J., Mo Y.L. (2012). Periodic materials-based vibration attenuation in layered foundations: Experimental validation. *Smart Materials and Structures*, 21(11).

-
- [24] Bao J., Shi Z., Xiang H. (2012). Dynamic responses of a structure with periodic foundations. *Journal of Engineering Mechanics*, 138(7): 761–769.
- [25] Cheng Z., Shi Z. (2013). Novel composite periodic structures with attenuation zones. *Engineering Structures*, 56: 1271–1282.
- [26] Jia G., Shi Z. (2010). A new seismic isolation system and its feasibility study. *Earthquake Engineering and Engineering Vibration*, 9(1): 75–82.
- [27] Cheng Z., Shi Z. (2018). Composite periodic foundation and its application for seismic isolation. *Earthquake Engineering & Structural Dynamics*, 47(4): 925–944.
- [28] Yan Y., Cheng Z., Meng F., Mo Y.L., Tang Y., Shi Z. (2015). Three dimensional periodic foundations for base seismic isolation. *Smart Materials and Structures*, 24(7).
- [29] Finocchio G., Casablanca O., Ricciardi G., Alibrandi U., Garescì F., Chiappini M., Azzerboni B. (2014). Seismic metamaterials based on isochronous mechanical oscillators. *Applied Physics Letters*, 104(19).
- [30] Casablanca O., Ventura G., Garescì F., Azzerboni B., Chiaia B., Chiappini M., Finocchio G. (2018). Seismic isolation of buildings using composite foundations based on metamaterials. *Journal of Applied Physics*, 123(17).
- [31] Basone F., Wenzel M., Bursi O., Fossetti M. (2019). Finite locally resonant Metafoundations for the seismic protection of fuel storage tanks. *Earthquake Engineering and Structural Dynamics*, 48(2).
- [32] La Salandra V., Wenzel M., Bursi O., Carta G., Movchan A. (2017). Conception of a 3D metamaterial-based foundation for static and seismic protection of fuel storage tanks. *Frontiers in Materials*, 4.
- [33] Carta G., Brun M., Movchan A.B. (2014). Dynamic response and localization in strongly damaged waveguides. *Proceedings of the Royal Society A: Mathematical, Physical and Engineering Sciences*, 470(2167).
- [34] Mishuris G.S., Movchan A.B., Slepyan L.I. (2007). Waves and fracture in an inhomogeneous lattice structure. *Waves in Random and Complex Media*, 17(4): 409–428.
- [35] Mishuris G.S., Movchan A.B., Slepyan L.I. (2008). Dynamics of a bridged crack in a discrete lattice. *Quarterly Journal of Mechanics and Applied Mathematics*, 61(2): 151–160.

- [36] Slepian L.I., Movchan A.B., Mishuris G.S. (2010). Crack in a lattice waveguide. *International Journal of Fracture*, 162(1-2): 91–106.
- [37] Barka A. (1999). The 17 August 1999 Izmit earthquake. *Science*, 285(5435): 1858–1859.
- [38] Yang J.E. (2014). Fukushima dai-ichi accident: Lessons learned and future actions from the risk perspectives. *Nuclear Engineering and Technology*, 46(1): 27–38.
- [39] Anzai K., Ban N., Ozawa T., Tokonami S. (2012). Fukushima Daiichi Nuclear Power Plant accident: Facts, environmental contamination, possible biological effects, and countermeasures. *Journal of Clinical Biochemistry and Nutrition*, 50(1): 2–8.
- [40] Nakashima M., Lavan O., Kurata M., Luo Y. (2014). Earthquake engineering research needs in light of lessons learned from the 2011 Tohoku earthquake. *Earthquake Engineering and Engineering Vibration*, 13(1): 141–149.
- [41] Krausmann E., Cruz A.M. (2012). Impact of the 11 March, 2011, Tohoku earthquake and tsunami on the chemical industry. In *European Geoscience Union*, volume 14, pages 2012–6041.
- [42] Kazama M., Noda T. (2012). Damage statistics (Summary of the 2011 off the Pacific Coast of Tohoku Earthquake damage). *Soils and Foundations*, 52(5): 780–792.
- [43] Cruz A.M., Steinberg L.J., Vetere-Arellano A.L. (2006). Emerging issues for natech disaster risk management in Europe. *Journal of Risk Research*, 9(5): 483–501.
- [44] Steinberg L.J., Sengul H., Cruz A.M. (2008). Natech risk and management: An assessment of the state of the art. *Natural Hazards*, 46(2): 143–152.
- [45] Krausmann E., Renni E., Campedel M., Cozzani V. (2011). Industrial accidents triggered by earthquakes, floods and lightning: Lessons learned from a database analysis. *Natural Hazards*, 59(1): 285–300.
- [46] Haroun M.A. (1983). Vibration studies and tests of liquid storage tanks. *Earthquake Engineering & Structural Dynamics*, 11(2): 179–206.
- [47] Jaiswal O.R., Kulkarni S., Pathak P. (2008). A STUDY ON SLOSHING FREQUENCIES OF FLUID-TANK SYSTEM. In *The 14 th World Conference on Earthquake Engineering*.

-
- [48] Soong T.T., Constantinou M.C. (1994). *Passive and Active Structural Vibration Control in Civil Engineering*. Springer-Verlag.
- [49] Kasai K., Fu Y., Watanabe A. (1998). Passive Control Systems for Seismic Damage Mitigation. *Journal of Structural Engineering*, 124(5): 501–512.
- [50] Kelly J.M., Konstantinidis D.A. (2011). *Mechanics of Rubber Bearings for Seismic and Vibration Isolation*. John Wiley and Sons.
- [51] Zayas V.A., Low S.S., Mahin S.A. (1990). A Simple Pendulum Technique for Achieving Seismic Isolation. *Earthquake Spectra*, 6(2): 317–333.
- [52] Chowdhury A.H., Iwuchukwu M.D., Garske J.J. (1987). The Past and Future of Seismic Effectiveness of Tuned Mass Dampers. In *Structural Control*, pages 105–127. Springer Netherlands. doi:10.1007/978-94-009-3525-9-7.
- [53] Papazoglou A.J., Elnashai A.S. (1996). ANALYTICAL AND FIELD EVIDENCE OF THE DAMAGING EFFECT OF VERTICAL EARTHQUAKE GROUND MOTION. *Earthquake Engineering & Structural Dynamics*, 25(10): 1109–1137.
- [54] Newmark N., Hall W. (1978). Development of criteria for seismic review of selected nuclear power plants. Technical report, Other U.S. Government Agency. doi:10.2172/6704054.
- [55] Martí J., Crespo M., Martínez F. (2010). Seismic isolation of liquefied natural gas tanks: A comparative assessment. *Seismic Isolation and Protective Systems*, 1(1): 125–140.
- [56] Fischer F.D., Seeber R. (1988). Dynamic response of vertically excited liquid storage tanks considering liquid-soil interaction. *Earthquake Engineering & Structural Dynamics*, 16(3): 329–342.
- [57] Fukasawa T., Okamura S., Somaki T., Miyagawa T., Uchita M., Yamamoto T., Watakabe T., Fujita S. (2019). Research and development of three-dimensional isolation system for sodium-cooled fast reactor: Part 4 - Proposal of optimal combination method for disc spring units and newly friction model for sliding elements. In *American Society of Mechanical Engineers, Pressure Vessels and Piping Division (Publication) PVP*, volume 8. American Society of Mechanical Engineers (ASME).
- [58] Shing P.B., Nakashima M., Bursi O.S. (1996). Application of pseudodynamic test method to structural research. *Earthquake Spectra*, 12(1): 29–56.

- [59] Bursi O.S., Gonzalez-Buelga A., Vulcan L., Neild S.A., Wagg D.J. (2008). Novel coupling Rosenbrock-based algorithms for real-time dynamic substructure testing. *Earthquake Engineering and Structural Dynamics*, 37(3): 339–360.
- [60] Abbiati G., La Salandra V., Bursi O.S., Caracoglia L. (2018). A composite experimental dynamic substructuring method based on partitioned algorithms and localized Lagrange multipliers. *Mechanical Systems and Signal Processing*, 100: 85–112.
- [61] Fabbrocino G., Iervolino I., Orlando F., Salzano E. (2005). Quantitative risk analysis of oil storage facilities in seismic areas. *Journal of Hazardous Materials*, 123(1-3): 61–69.
- [62] Shi Z., Huang J. (2013). Feasibility of reducing three-dimensional wave energy by introducing periodic foundations. *Soil Dynamics and Earthquake Engineering*, 50: 204–212.
- [63] Ha Y.K., Kim J.E., Park H.Y., Lee I.W. (2002). Propagation of water waves through finite periodic arrays of vertical cylinders. *Applied Physics Letters*, 81(7): 1341–1343.
- [64] Cheng Z.B., Yan Y.Q., Menq F.M., Mo Y.L., Xiang H.J., Shi Z.F., Stokoe K.H. (2013). 3D periodic foundation-based structural vibration isolation. In *Proceedings of the World Congress on Engineering*, pages 1797–1802.
- [65] Yan Y., Laskar A., Cheng Z., Menq F., Tang Y., Mo Y.L., Shi Z. (2014). Seismic isolation of two dimensional periodic foundations. *Journal of Applied Physics*, 116(4).
- [66] Achaoui Y., Ungureanu B., Enoch S., Brûlé S., Guenneau S. (2016). Seismic waves damping with arrays of inertial resonators. *Extreme Mechanics Letters*, 8: 30–37.
- [67] Carta G., Movchan A.B., Argani L.P., Bursi O.S. (2016). Quasi-periodicity and multi-scale resonators for the reduction of seismic vibrations in fluid-solid systems. *International Journal of Engineering Science*, 109: 216–239.
- [68] European Standard (2004). Eurocode 0 - Basis of structural design.
- [69] Malhotra P.K., Wenk T., Wieland M. (2000). Simple procedure for seismic analysis of liquid-storage tanks. *Structural Engineering International: Journal of the International Association for Bridge and Structural Engineering (IABSE)*, 10(3): 197–201.

-
- [70] Belakroum R., Kadja M., Mai T.H., Maalouf C. (2010). An efficient passive technique for reducing sloshing in rectangular tanks partially filled with liquid. *Mechanics Research Communications*, 37(3): 341–346.
- [71] Ding W.P., Chen H.L. (2001). A symmetrical finite element model for structure-acoustic coupling analysis of an elastic, thin-walled cavity. *Journal of Sound and Vibration*, 243(3): 547–559.
- [72] Liu M., Gorman D.G. (1995). Formulation of Rayleigh damping and its extensions. *Computers and Structures*, 57(2): 277–285.
- [73] Phani A.S., Woodhouse J., Fleck N.A. (2006). Wave propagation in two-dimensional periodic lattices. *The Journal of the Acoustical Society of America*, 119(4): 1995–2005.
- [74] European Standard (2003). Eurocode 2 - Design of concrete structures – Part 1-1: General rules and rules for buildings.
- [75] Huang H.H., Sun C.T., Huang G.L. (2009). On the negative effective mass density in acoustic metamaterials. *International Journal of Engineering Science*, 47(4): 610–617.
- [76] Cozzani V., Antonioni G., Landucci G., Tugnoli A., Bonvicini S., Spadoni G. (2014). Quantitative assessment of domino and NaTech scenarios in complex industrial areas. *Journal of Loss Prevention in the Process Industries*, 28: 10–22.
- [77] Mokha A., Constantinou M.C., Reinhorn A.M., Zayas V.A. (1991). Experimental Study of Friction-Pendulum Isolation System. *Journal of Structural Engineering*, 117(4): 1201–1217.
- [78] Uckan E., Umut Ö., Sisman F.N., Karimzadeh S., Askan A. (2018). Seismic response of base isolated liquid storage tanks to real and simulated near fault pulse type ground motions. *Soil Dynamics and Earthquake Engineering*, 112: 58–68.
- [79] Bursi O.S., Abbiati G., Reza M.S. (2014). A novel hybrid testing approach for piping systems of industrial plants. *Smart Structures and Systems*, 14(6): 1005–1030.
- [80] Bursi O.S., Reza M.S., Abbiati G., Paolacci F. (2015). Performance-based earthquake evaluation of a full-scale petrochemical piping system. *Journal of Loss Prevention in the Process Industries*, 33: 10–22.
- [81] Maleki A., Ziyaeifar M. (2008). Sloshing damping in cylindrical liquid storage tanks with baffles. *Journal of Sound and Vibration*, 311(1-2): 372–385.

- [82] European Standard (2005). Eurocode 8: Design of Structures for Earthquake Resistance—Part 1: General Rules, Seismic Actions and Rules for Buildings.
- [83] Park K.C., Felippa C.A., Gumaste U.A. (2000). Localized version of the method of Lagrange multipliers and its applications. *Computational Mechanics*, 24(6): 476–490.
- [84] U.S. Nuclear Regular Commission (2008). Seismic Analysis of Large-Scale Piping Systems for the JNES-NU-PEC Ultimate Strength Piping Test Program.
- [85] Bursi O.S., di Filippo R., La Salandra V., Pedot M., Reza M.S. (2018). Probabilistic seismic analysis of an LNG subplant. *Journal of Loss Prevention in the Process Industries*, 53: 45–60.
- [86] Mostaghel N. (1999). Analytical Description of Pinching, Degrading Hysteretic Systems. *Journal of Engineering Mechanics*, 125(2): 216–224.
- [87] Karimzadeh Naghshineh A., Akyüz U., Caner A. (2014). Comparison of fundamental properties of new types of fiber-mesh-reinforced seismic isolators with conventional isolators. *Earthquake Engineering & Structural Dynamics*, 43(2): 301–316.
- [88] Van Ngo T., Dutta A., Deb S.K. (2017). Evaluation of horizontal stiffness of fibre-reinforced elastomeric isolators. *Earthquake Engineering & Structural Dynamics*, 46(11): 1747–1767.
- [89] Schellenberg A.H., Sarebanha A., Schoettler M.J., Mosqueda G., Benzoni G., Stephen A.M. (2015). PEER Report: "Hybrid Simulation of Seismic Isolation Systems Applied to an APR-1400 Nuclear Power Plant". Technical report, Pacific Earthquake Engineering Research Center.
- [90] Wang P., Casadei F., Shan S., Weaver J.C., Bertoldi K. (2014). Harnessing buckling to design tunable locally resonant acoustic metamaterials. *Physical Review Letters*, 113(1).
- [91] Aravantinos-Zafiris N., Sigalas M.M. (2015). Large scale phononic metamaterials for seismic isolation. *Journal of Applied Physics*, 118(6).
- [92] Shi Z., Cheng Z., Xiang H. (2014). Seismic isolation foundations with effective attenuation zones. *Soil Dynamics and Earthquake Engineering*, 57: 143–151.
- [93] Kim S.H., Das M.P. (2012). Seismic waveguide of metamaterials. *Modern Physics Letters B*, 26(17).

-
- [94] Dertimanis V.K., Antoniadis I.A., Chatzi E.N. (2016). Feasibility Analysis on the Attenuation of Strong Ground Motions Using Finite Periodic Lattices of Mass-in-Mass Barriers. *Journal of Engineering Mechanics*, 142(9): 04016060.
- [95] Ghosh A., Basu B. (2004). Effect of soil interaction on the performance of tuned mass dampers for seismic applications. *Journal of Sound and Vibration*, 274(3-5): 1079–1090.
- [96] Wang A.P., Fung R.F., Huang S.C. (2001). Dynamic analysis of a tall building with a tuned-mass-damper device subjected to earthquake excitations. *Journal of Sound and Vibration*, 244(1): 123–136.
- [97] Poh'sie G.H., Chisari C., Rinaldin G., Amadio C., Fragiacomio M. (2016). Optimal design of tuned mass dampers for a multi-storey cross laminated timber building against seismic loads. *Earthquake Engineering and Structural Dynamics*, 45(12): 1977–1995.
- [98] Yamaguchi H., Harnpornchai N. (1993). Fundamental characteristics of Multiple Tuned Mass Dampers for suppressing harmonically forced oscillations. *Earthquake Engineering & Structural Dynamics*, 22(1): 51–62.
- [99] Abé M., Fujino Y. (1994). Dynamic characterization of multiple tuned mass dampers and some design formulas. *Earthquake Engineering & Structural Dynamics*, 23(8): 813–835.
- [100] Igusa T., Xu K. (1994). Vibration control using multiple tuned mass dampers. *Journal of Sound and Vibration*, 175(4): 491–503.
- [101] Li C. (2000). Performance of multiple tuned mass dampers for attenuating undesirable oscillations of structures under the ground acceleration. *Earthquake Engineering & Structural Dynamics*, 29(9): 1405–1421.
- [102] Li H.N., Ni X.L. (2007). Optimization of non-uniformly distributed multiple tuned mass damper. *Journal of Sound and Vibration*, 308(1-2): 80–97.
- [103] Bakre S.V., Jangid R.S. (2004). Optimum multiple tuned mass dampers for base-excited damped main system. *International Journal of Structural Stability and Dynamics*, 4(4): 527–542.
- [104] Fadel Miguel L.F., Lopez R.H., Miguel L.F.F., Torii A.J. (2016). A novel approach to the optimum design of MTMDs under seismic excitations. *Structural Control and Health Monitoring*, 23(11): 1290–1313.

- [105] Hoang N., Warnitchai P. (2005). Design of multiple tuned mass dampers by using a numerical optimizer. *Earthquake Engineering & Structural Dynamics*, 34(2): 125–144.
- [106] Reggio A., De Angelis M. (2015). Optimal energy-based seismic design of non-conventional Tuned Mass Damper (TMD) implemented via inter-story isolation. *Earthquake Engineering & Structural Dynamics*, 44(10): 1623–1642.
- [107] Italian Standard (2008). NTC - Norme tecniche per le costruzioni.
- [108] Alessandri S., Giannini R., Paolacci F., Malena M. (2015). Seismic retrofitting of an HV circuit breaker using base isolation with wire ropes. Part 1: Preliminary tests and analyses. *Engineering Structures*, 98: 251–262.
- [109] NEA/CSNI/R(2007)17 (2008). Differences in approach between nuclear and conventional seismic standards with regard to hazard definition, In: CSNI Integrity and Ageing Working Group, Nuclear Energy Agency Committee on the Safety of Nuclear Installations.
- [110] Baker J.W., Allin Cornell C. (2005). A vector-valued ground motion intensity measure consisting of spectral acceleration and epsilon. *Earthquake Engineering & Structural Dynamics*, 34(10): 1193–1217.
- [111] Caputo A.C., Paolacci F., Bursi O.S., Giannini R. (2019). Problems and Perspectives in Seismic Quantitative Risk Analysis of Chemical Process Plants. *Journal of Pressure Vessel Technology, Transactions of the ASME*, 141(1).
- [112] Feng M.Q., Mita A. (1995). Vibration Control of Tall Buildings Using Mega SubConfiguration. *Journal of Engineering Mechanics*, 121(10): 1082–1088.
- [113] Kanai K. (1957). Semi-empirical Formula for the Seismic Characteristics of the Ground.
- [114] Clough R.W., Penzien J. (1975). *Dynamics of structures*. McGraw-Hill.
- [115] Palazzo B., Petti L. (1997). Stochastic response comparison between base isolated and fixed-base structures. *Earthquake Spectra*, 13(1): 77–96.
- [116] Lu M.H., Feng L., Chen Y.F. (2009). Phononic crystals and acoustic metamaterials. *Materials Today*, 12(12): 34–42.

-
- [117] Zhou X., Liu X., Hu G. (2012). Elastic metamaterials with local resonances: an overview. *Theoretical and Applied Mechanics Letters*, 2(4): 041001.
- [118] European Standard (2005). Eurocode 3: Design of steel structures.
- [119] European Standard (2006). Eurocode 8: Design of Structures for Earthquake Resistance—Part 4: Silos, tanks and pipelines.
- [120] Wenzel M., Basone F., Bursi O. (2020). Design of a Metamaterial-Based Foundation for Fuel Storage Tanks and Experimental Evaluation of Its Effect on a Connected Pipeline System. *Journal of Pressure Vessel Technology*, 142(021903-1).
- [121] Witarto W., Wang S.J., Yang C.Y., Nie X., Mo Y.L., Chang K.C., Tang Y., Kassawara R. (2018). Seismic isolation of small modular reactors using metamaterials. *AIP Advances*, 8(4): 045307.
- [122] Ungureanu B.S., Achaoui Y., Enoch S., Brûlé S., Guenneau S., Christos A., Alessio M. (2015). Auxetic-like metamaterials as novel earthquake protections. *EPJ Applied Metamaterials*.
- [123] Mu D., Shu H., Zhao L., An S. (2020). A Review of Research on Seismic Metamaterials.
- [124] Antoniadis I., Chronopoulos D., Spitas V., Koulocheris D. (2015). Hyper-damping properties of a stiff and stable linear oscillator with a negative stiffness element. *Journal of Sound and Vibration*, 346(1): 37–52.
- [125] Oh J.H., Kwon Y.E., Lee H.J., Kim Y.Y. (2016). Elastic metamaterials for independent realization of negativity in density and stiffness. *Scientific Reports*, 6.
- [126] Ren C., Yang D., Qin H. (2018). Mechanical performance of multidirectional Buckling-based Negative Stiffness metamaterials: An analytical and numerical study. *Materials*, 11(7).
- [127] Yoon G.H., Mo J.S. (2017). Tailoring a bidirectional negative stiffness (BNS) structure with mechanical diodes for mechanical metamaterial structures. *Smart Materials and Structures*, 26(5).
- [128] Morris C., Bekker L., Spadaccini C., Haberman M., Seepersad C. (2019). Tunable Mechanical Metamaterial with Constrained Negative Stiffness for Improved Quasi-Static and Dynamic Energy Dissipation. *Advanced Engineering Materials*, 21(7): 1900163.

- [129] Chakraborty G., Mallik A.K. (2001). Dynamics of a weakly non-linear periodic chain. *International Journal of Non-Linear Mechanics*, 36(2): 375–389.
- [130] Lazarov B.S., Jensen J.S. (2007). Low-frequency band gaps in chains with attached non-linear oscillators. *International Journal of Non-Linear Mechanics*, 42(10): 1186–1193.
- [131] Banerjee A., Das R., Calius E.P. (2018). Waves in Structured Mediums or Metamaterials: A Review. *Archives of Computational Methods in Engineering*, pages 1–30.
- [132] Sen Gupta G. (1970). Natural flexural waves and the normal modes of periodically-supported beams and plates. *Journal of Sound and Vibration*, 13(1): 89–101.
- [133] Sorokin V.S., Thomsen J.J. (2016). Effects of weak nonlinearity on the dispersion relation and frequency band-gaps of a periodic Bernoulli-Euler beam. *Proceedings of the Royal Society A: Mathematical, Physical and Engineering Sciences*, 472(2186).
- [134] Hussein M.I., Leamy M.J., Ruzzene M. (2014). Dynamics of phononic materials and structures: Historical origins, recent progress, and future outlook. *Applied Mechanics Reviews*, 66(4).
- [135] Ma G., Sheng P. (2016). Acoustic metamaterials: From local resonances to broad horizons. *Science Advances*, 2(2).
- [136] Diaz A.R., Haddow A.G., Ma L. (2005). Design of band-gap grid structures. *Structural and Multidisciplinary Optimization*, 29(6): 418–431.
- [137] Rupp C.J., Evgrafov A., Maute K., Dunn M.L. (2007). Design of phononic materials/structures for surface wave devices using topology optimization. *Structural and Multidisciplinary Optimization*, 34(2): 111–121.
- [138] Xiao W., Zeng G.W., Cheng Y.S. (2008). Flexural vibration band gaps in a thin plate containing a periodic array of hemmed discs. *Applied Acoustics*, 69(3): 255–261.
- [139] Fukasawa T., Okamura S., Somaki T., Miyagawa T., Uchita M., Yamamoto T., Watakabe T., Fujita S. (2019). Research and Development of Three-Dimensional Isolation System for Sodium-Cooled Fast Reactor: Part 4 — Proposal of Optimal Combination Method for Disc Spring Units and Newly Friction Model for Sliding Elements. In *Volume 8: Seismic Engineering*. American Society of Mechanical Engineers.

-
- [140] Paolacci F., Giannini R. (2008). Study of the Effectiveness of Steel Cable Dampers for the Seismic Protections of Electrical Equipment. In *World Conference in Earthquake Engineering*.
- [141] Alessandri S., Giannini R., Paolacci F., Amoretti M., Freddo A. (2015). Seismic retrofitting of an HV circuit breaker using base isolation with wire ropes. Part 2: Shaking-table test validation. *Engineering Structures*, 98: 263–274.
- [142] Balaji P.S., Moussa L., Rahman M.E., Vuia L.T. (2015). Experimental investigation on the hysteresis behavior of the wire rope isolators. *Journal of Mechanical Science and Technology*, 29(4): 1527–1536.
- [143] Balaji P.S., Moussa L., Rahman M.E., Ho L.H. (2016). An analytical study on the static vertical stiffness of wire rope isolators. *Journal of Mechanical Science and Technology*, 30(1): 287–295.
- [144] Wen Y.K. (1976). Method for random vibration of hysteretic systems. *Journal of the Engineering Mechanics Division*, 102(2): 249–263.
- [145] Demetriades G.F., Constantinou M.C., Reinhorn A.M. (1993). Study of wire rope systems for seismic protection of equipment in buildings. *Engineering Structures*, 15(5): 321–334.
- [146] Bonelli A., Bursi O.S. (2004). Generalized- α methods for seismic structural testing. *Earthquake Engineering & Structural Dynamics*, 33(10): 1067–1102.
- [147] Yuen K.V., Shi Y., Beck J.L., Lam H.F. (2007). Structural protection using MR dampers with clipped robust reliability-based control. *Structural and Multidisciplinary Optimization*, 34(5): 431–443.
- [148] Giaralis A., Spanos P.D. (2010). Effective linear damping and stiffness coefficients of nonlinear systems for design spectrum based analysis. *Soil Dynamics and Earthquake Engineering*, 30(9): 798–810.
- [149] Giaralis A., Spanos P.D. (2013). Derivation of equivalent linear properties of Bouc-Wen hysteretic systems for seismic response spectrum analysis via statistical linearization. In *10th HSTAM International Congress on Mechanics*, pages 25–27.
- [150] Mitseas I.P., Kougioumtzoglou I.A., Giaralis A., Beer M. (2018). A novel stochastic linearization framework for seismic demand estimation of hysteretic MDOF systems subject to linear response spectra. *Structural Safety*, 72: 84–98.

- [151] Bursi O.S., al. E. (2012). Component fragility evaluation, seismic safety assessment and design of petrochemical plants under design-basis accident conditions (INDUSE-2-SAFETY). Technical report. doi:10.2777/5667.
- [152] Caughey T.K. (1963). Equivalent Linearization Techniques. *Journal of the Acoustical Society of America*, 35(11): 1706–1711.
- [153] Housner G.W. (1955). Dynamic pressures on accelerated fluid containers. *Bulletin of the Seismological Society of America*, 47(1): 15–35.
- [154] Housner G.W. (1963). The dynamic behavior of water tanks. *Bulletin of the Seismological Society of America*, 53(2): 381–387.
- [155] O’Callahan J., Avitabile P., Riemer R. (1989). System Equivalent Reduction Expansion Process (SEREP). In *7th International Modal Analysis Conference*, pages 29–37.
- [156] Forsgren A., Gill P.E., Wright M.H. (2002). Interior methods for non-linear optimization. *SIAM Review*, 44(4): 525–597.
- [157] Maldonado O., Singh M.P., Casciati F., Faravelli L. (1987). Stochastic response of single degree of freedom hysteretic oscillators.
- [158] Baber T.T., Hen Y.K. (1980). Stochastic Equivalent Linearization for Hysteretic, Degrading, Multistroy Structures. Technical report, University of Illinois Engineering Experiment Station. College of Engineering. University of Illinois at Urbana-Champaign.
- [159] Roberts J.B., Spanos P.D. (2003). *Random vibration and statistical linearization*. Chichester, England : Wiley, 1990.
- [160] Bartels R.H., Stewart G.W. (1972). Solution of the Matrix Equation $AX + XB = C$ [F4]. *Communications of the ACM*, 15(9): 820–826.
- [161] Constantinou M. (1987). *Dynamics of soil-base-isolated-structure systems evaluation of two models for yielding systems*. [Dept. of Civil Engineering] Drexel University, Philadelphia Pa.

List of Figures

1.1	Frequency spectra of phononic waves.	2
1.2	Monoatomic lattice.	3
1.3	Oscillation of neighbouring unit cells in the imaginary plane.	4
1.4	Dispersion relation of the Monoatomic lattice.	5
1.5	Three different substructures coupled via localized Lagrange multipliers (figure from [60]).	10
1.6	View of the Metafoundation placed under a tank.	12
2.1	(A): Broad tank on a standard foundation; (B): Broad tank on a smart foundation; (C): Broad tank on a smart foundation with optimized unit cells.	21
2.2	(A): Conception of a static system [Dimensions in mm]; (B): FE model of the foundation including the tank weight as a surface load [kN/m ²]; (C): two unit cells on line supports including the weights of the rubber and inner concrete cubes as surface loads [kN/m ²].	23
2.3	(A): Top-section and cross-section of the optimized foundation; (B): Simplified model for shear-wave propagation; (C): 1D mass-resonator chain model.	27
2.4	(A): first impulsive mode at 4.15 Hz for a broad tank on a traditional foundation; (B): first impulsive mode of a broad tank on the proposed smart foundation at 3.95 Hz; (C): first impulsive mode at 2.4 Hz for a broad tank on the optimized foundation.	29
2.5	(A): The unit cell and its Brillouin zone (dimensions in cm); (B): Dispersion analysis of the unit cell.	30
2.6	(A): compressive stresses in the walls at the ultimate limit state [N/mm ²]; (B): line bending moments in slabs at the ultimate limit state [kNm/m].	31
2.7	(A): compressive stresses in the walls at the ultimate limit state [N/mm ²]; (B): line bending moments in slabs at the ultimate limit state [kNm/m].	31

LIST OF FIGURES

2.8	(A): acceleration response at the top of the foundation with a wall thickness of 20 cm; (B): acceleration response with a wall thickness of 10 cm.	32
2.9	(A): maximum acceleration response function of the tank wall for traditional and smart foundation; (B): acceleration responses for a tank with a reduced liquid height of 12 m.	33
2.10	(A): Frequency response function of the optimized foundation alone subjected to a base acceleration of 1 m/s^2 ; (B): Tank response for a fully filled tank, on the optimized foundation, for a base acceleration of 1 m/s^2 ; (C): Tank response with a liquid level of 12 m, on the optimized foundation, for a base acceleration of 1 m/s^2	33
2.11	(A): Undamped frequency response function for 1, 5, and 25 layers of foundation for a base excitation of 1 m/s^2 ; (B): Dispersion relations for the optimized unit cell; (C): Frequency response function of the analytical model for two layers and Rayleigh damping of 1, 3, and 5 %; (D): Frequency response function of the analytical model with 5 % Rayleigh damping and 1, 2, and 3 layers.	35
2.12	(A): Position of cracks in the unit cell; (B): Crack modeled as a physical gap in the slabs due to static loads (dimensions in m); (C): Dispersion analysis of the cracked foundation sector.	35
3.1	Modeling of a fuel storage tank: (A) drawing of a generic fuel storage tank; (B) representation of a fuel storage tank with two S-DOFs for the impulsive and convective modes (figure from [69])	42
3.2	Drawings of the structure: (A) side view of tank and metafoundation; (B) layout of one layer (dimensions in cm).	44
3.3	Geometry of the unit cell as part of the concrete matrix; (A) cross section of the foundation; (B) layout of one unit cell (dimensions in cm).	45
3.4	Dynamic system.	46
3.5	Frequency response function for a foundation with 1, 5, and 25 layers without damping.	49
3.6	Dispersion relation of the unit cell.	49
3.7	Geometrical characteristics: (A) slender tank including the Metafoundation META; (B) slender tank on a traditional foundation TRAD (dimensions in m).	50
3.8	Frequency response function of the impulsive mode of a slender tank with full liquid height (STF); (A) displacement of impulsive mass compared to foundation; (B) absolute acceleration of the impulsive mass.	51

3.9	Frequency response of a slender-tank–foundation system for a reduced fluid level of $3/4$; fill (STnF); (A) displacement of impulsive mass compared to foundation; (B) absolute acceleration of the impulsive mass.	52
3.10	Absolute time evolution of the (A) base shear and the (B) overturning moment for STF.	54
3.11	Absolute time evolution of the (A) base shear and the (B) overturning moment for STnF.	55
3.12	Maximum values of (A) base shear and (B) overturning moment in a full slender tank for all studied ground motions.	55
3.13	FE-model: (A) Side view of FE-model; (B) Isometric view of FE-model with finite element mesh.	56
3.14	Frequency response function of the FE-Model of the coupled system.	56
3.15	Schematic of the piping system (dimensions in cm).	59
3.16	Experimental setup of the piping system.	59
3.17	Configuration of strain gauges on the elbow element.	60
3.18	Coupling of the numerical and physical substructure.	61
3.19	Generic Mostaghel model (Figure from [60]).	61
3.20	Numerical coupling of CSB, tank, and piping system.	61
3.21	Strains in the critical elbow for the most sever seismic event.	63
3.22	Experimental results: (A) Base shear of the tank; (B) maximal hoop strain in the elbow (REC).	64
4.1	Foundation-slender tank coupled system: (A) isometric view with steel columns; (B) plan view. Dimensions in m.	69
4.2	Fuel storage tank: (A) isometric view; (B) 2D modeling with two SDoFs for the impulsive and convective mode (Malhotra et al. [69]).	70
4.3	Tank–foundation coupled systems: (A) one-layer case and (B) two-layer case	72
4.4	Two-layer metafoundation: (A) cross section of the foundation; (B) cross section of a steel column.	73
4.5	Response spectra of the selected accelerograms: (A) UHS for OBE; (B) UHS for SSE.	75
4.6	(A) 1D mass-resonator chain model. (B) dispersion relation for an infinite stack of unit cells with the geometric properties of L2H4.	77
4.7	(A) Schematization of a unit cell; (B) Apparent mass as a function of forcing frequency.	78
4.8	PSD functions of filtered white noises: (A) KTCP filter for three types of soil; (B) average PSD and KTCP fit for OBE events; (C) average PSD and KTCP fit for SSE events	83
4.9	PI optimization of a slender tank on an L1H4 foundation with SSE records: (A) optimization surface vs. resonator parameters; (B) contour lines of the optimization surface	84

LIST OF FIGURES

4.10	EDI optimization of a slender tank on an L1H4 foundation with SSE records: (A) optimization surface vs. resonator parameters; (B) contour lines of the optimization surface	84
4.11	RMS of the base shear of a slender tank vs. PGA of the SSE records: (A) L2H3; (B) L2H4; (C) L1H3; (D) L1H4.	89
4.12	Base shear reduction for a slender tank subjected to SSE events: (A) PI optimization; (B) EDI optimization.	89
4.13	RMS of the base shear of a broad tank vs. PGA of the SSE records: (A) L2H3; (B) L2H4; (C) L1H3; (D) L1H4.	91
4.14	Base shear reduction for a broad tank subjected to SSE events: (A) PI optimization; (B) EDI optimization.	91
5.1	Layout of the Metafoundation for the MINIMAL system: (a) Isometric view; (b) Internal view of the foundation components.	99
5.2	Negative stiffness mechanism.	100
5.3	Kinematic system in the displaced state: (a) Resonator and mechanism in displaced state; (b) Force equilibrium on the displaced system.	101
5.4	Force displacement path: (a) Variation of parameter ϵ ; (b) Variation of member length l	103
5.5	Dynamic systems: (a) Coupled foundation tank system; (b) Foundation modelled as a periodic structure.	105
5.6	Infinite lattice and unit cell depiction.	109
5.7	Wave propagation behaviour of the linear system: (a) Dispersion relation of the unit cell for varying NSE values (acoustic branch = AB); (b) FRF of the linear system for 1, 10, and 100 Layers with an NSE value of 75%.	109
5.8	Dispersion diagram of the non-linear FULL system with varying amplitudes and 75% of the maximum NSE value.	112
5.9	Numerical FRF for the FULL system with 25% NSE: (a) 1 layer and polynomial nonlinearity; (b) 1 layer and true nonlinearity; (c) 10 layers and polynomial nonlinearity; (d) 10 layers and true nonlinearity; (e) 20 layers and polynomial nonlinearity; (f) 20 layers and true nonlinearity.	115
5.10	Ground motion spectra: (a) Response spectra including the UHS and the mean response spectrum; (b) PSDs of all ground motion records and their average estimated with Welch's method.	117
5.11	Optimization surface plots for: (a) PI for the FULL system with 0% k_{Nmax} ; (b) PI for the FULL system with 25% k_{Nmax} ; (c) PI for the FULL system with 50% k_{Nmax} ; (d) PI for the FULL system with 99% k_{Nmax}	120
5.12	Time history analyses with $\epsilon = 0.95$ and various levels of NSE: (a) FULL system; (b) REDUCED system; (c) MINIMAL system.	122

5.13	Time history analyses with various ϵ and l values for a system with 75% NSE: (a) $\epsilon = 0.99$; (b) $\epsilon = 0.90$; (c) $\epsilon = 0.50$	124
6.1	Coupled foundation-tank system with two layers: (A) isometric view, (B) layout and (C) cross section.	132
6.2	(A) Configuration of a single unit cell equipped with steel wire ropes (measures in cm); (B) details of a single wire rope and (C) hysteretic loop of Bouc-Wen model.	133
6.3	Dispersion relation for an infinite stack of unit cells with the geometric properties of the two-layered foundation case. Figure from [31].	134
6.4	Apparent mass as a function of forcing frequency: (A) single and (B) double unit cell case.	134
6.5	Models of the Metafoundation for the two-layered case: (A) FMS; (B) CMS and (C) RMS.	136
6.6	Optimization surfaces of one-layered (A) CMS case and (B) RMS case.	141
6.7	Root mean square values of the (A) base shear, (B) interstory drift and (C) absolute acceleration of one-layered CMS for both PI_{dr} and PI_{acc}	144
6.8	Root mean square values of the tanks base shear for: (A) one-layered RMS; (B) two-layered RMS; (C) one-layered FMS; (D) and two-layered FMS.	145
6.9	(A) Hysteretic behaviour under cyclic shear loading (after Paolacci and Giannini [140]) and (B) typical hysteretic loop of a Bouc-Wen model.	148
6.10	Optimal surfaces in the nonlinear case: (A) one layered CMS and (B) two-layered CMS.	150
6.11	Hysteretic loops of one-layered CMS hysteretic damper -blue lines, $A = 1$, $\beta = 0.9$ and $\gamma = 0.1$ - and linear viscous damper -red lines, $\zeta_{1,1} = 0.2$ -: resonators equipped with (A) optimal and (B) minimum number of wire ropes.	150
6.12	Root-mean square values of the tank base shear for one-layered CMS: (A) $\beta = 0.9$ and $\gamma = 0.1$, (B) $\beta = 0.5$ and $\gamma = 0.5$ and (C) $\beta = 0.1$ and $\gamma = 0.9$	150
6.13	Time history results for a fixed base tank and CMS: (A) Maximum base shear; (B) Absolute acceleration of the impulsive mode; (C) Maximum displacement of wire ropes; (D) Maximum interstory drift.	151
6.14	$E_d^{non-lin} / E_d^{lin}$ ratio of dissipated energy by nonlinear hysteretic dampers and linear viscous dampers for the optimal cases of one-layered CMS.	152

List of Tables

2.1	Mechanical properties of materials	24
2.2	First impulsive eigenfrequency of broad-tank-foundation systems with various liquid heights	28
3.1	Material parameters	41
3.2	First impulsive eigenfrequencies of tank–foundation systems with various liquid levels	44
3.3	Parameter values for the analysis of two tank–foundation systems with various fluid levels	51
3.4	Set of EC 8 compatible ground motions for the site Priolo Gargallo (soil type B) with a return period of 2475 years	53
3.5	Seismic events for the experimental validation	63
4.1	Main characteristics of broad and slender tank.	71
4.2	Geometrical characteristics of each foundation layout.	73
4.3	List of natural accelerograms for OBE events.	74
4.4	List of natural accelerograms for SSE events.	75
4.5	Parameters of the KTCP filter.	83
4.6	Optimal parameters based on both PI and EDI for the slender tank.	86
4.7	Optimal parameters based on both PI and EDI for the broad tank.	87
5.1	Geometric properties of the various foundation setups.	99
5.2	Parameters for the discretized system.	104
5.3	List of ground motion records.	116
5.4	Results from the optimization for the relevant Metafoundation setups.	120
6.1	Optimal parameters of the CMS for both one and two-layered cases.	141
6.2	Optimal parameters of the RMS for both one and two-layered cases (frequency in Hz).	142

6.3	Optimal parameters of the FMS for both one and two-layered cases (frequency in Hz).	142
6.4	Geometric and mechanical properties of wire ropes.	148
6.5	Bouc-Wen Setups.	148